NASA TECHNICAL NOTE

NASA TN D-7518

NASA TN D-7518

THE EFFECT OF WIND-TUNNEL WALL INTERFERENCE ON THE PERFORMANCE OF A FAN-IN-WING VTOL MODEL

by Harry H. Heyson

Langley Research Center
Hampton, Va. 23665

NATIONAL AERONAUTICS AND SPACE ADMINISTRATION • WASHINGTON, D. C. • FEBRUARY 1974

1. Report No.	2. Government Accession No.	3. Recipient's Catalog No.
NASA TN D-7518		

4. Title and Subtitle	5. Report Date
THE EFFECT OF WIND-TUNNEL WALL INTERFERENCE ON THE PERFORMANCE OF A FAN-IN-WING VTOL MODEL	February 1974
	6. Performing Organization Code
7. Author(s)	8. Performing Organization Report No.
Harry H. Heyson	L-9202
	10. Work Unit No.
9. Performing Organization Name and Address	760-61-02-01
NASA Langley Research Center Hampton, Va. 23665	11. Contract or Grant No.
	13. Type of Report and Period Covered
12. Sponsoring Agency Name and Address	Technical Note
National Aeronautics and Space Administration Washington, D.C. 20546	14. Sponsoring Agency Code

15. Supplementary Notes

16. Abstract

A fan-in-wing model with a 1.07-m (42-in.) span was tested in seven different test sections with cross-sectional areas ranging from 2.2 m^2 to 265 m^2 (24 ft^2 to 2857 ft^2). The data from the different test sections are compared both with and without correction for wall interference. The results demonstrate that extreme care must be used in interpreting uncorrected VTOL data since the wall interference may be so large as to invalidate even trends in the data. The wall interference is particularly large at the tail, a result which is in agreement with recently published comparisons of flight and large-scale wind-tunnel data (NASA CR-2135) for a propeller-driven deflected-slipstream configuration. The data of the present investigation verify the wall-interference theory of NASA TR R-124 even under conditions of extreme interference. A method given by Tyler and Williamson in AGARD CP-91-71 yields reasonable estimates for the onset of Rae's minimum-speed limit.

The present investigation shows that the rules for choosing model sizes to produce negligible wall effects, as given by Cook and Hickey in NASA SP-116, are considerably in error and permit the use of excessively large models. Even simple momentum theory appears to yield more nearly correct performance estimates in transition flight than uncorrected wind-tunnel data when the model span approaches one-half of the tunnel width. The "fan-induced" lift indicated by a number of previous studies in which the model was of similar relative span appears to be largely the result of wall interference that was not accounted for in reducing the data.

17. Key Words (Suggested by Author(s))	18. Distribution Statement
Wind tunnels Wall interference Fan in wing VTOL	Unclassified – Unlimited STAR Category 11

19. Security Classif. (of this report)	20. Security Classif. (of this page)	21. No. of Pages	22. Price*
Unclassified	Unclassified	230	$5.75

*For sale by the National Technical Information Service, Springfield, Virginia 22151

CONTENTS

	Page
SUMMARY	1
INTRODUCTION	1
SYMBOLS	3
APPARATUS AND TESTS	6
Model	6
Model Instrumentation	7
Wind Tunnels	8
Procedure	13
Precision of Measurement	14
RESULTS AND DISCUSSION OF DATA FROM MODEL WITH FANS COVERED	15
Uncorrected Data	15
Considerations in Correcting Data	16
Procedure in Correcting Data	18
Corrections	20
Corrected Data	21
RESULTS AND DISCUSSION OF DATA FROM MODEL WITH FANS OPERATING	21
Uncorrected Data	21
Correcting the Data	33
Interference in Uncorrected Data	36
Corrected Data	37
Interference in Corrected Data	37
Maximum Model Size	37
CONCLUSIONS	38
APPENDIX A – JUSTIFICATION OF VORTEX-DENSITY CORRECTION FOR FANS AND JETS	40
APPENDIX B – FORTRAN PROGRAM FOR CORRECTING DATA FROM A FAN-IN-WING MODEL TESTED IN FOUR DIFFERENT TEST SECTIONS	41
REFERENCES	66
TABLES	70
FIGURES	72

THE EFFECT OF WIND-TUNNEL WALL INTERFERENCE ON THE PERFORMANCE OF A FAN-IN-WING VTOL MODEL

By Harry H. Heyson
Langley Research Center

SUMMARY

A fan-in-wing model with a 1.07-m (42-in.) span was tested in seven different test sections with cross-sectional areas ranging from 2.2 m^2 to 265 m^2 (24 ft^2 to 2857 ft^2). The data from the different test sections are compared both with and without correction for wall interference. The results demonstrate that extreme care must be used in interpreting uncorrected VTOL data since the wall interference may be so large as to invalidate even trends in the data. The wall interference is particularly large at the tail, a result which is in agreement with recently published comparisons of flight and large-scale wind-tunnel data (NASA CR-2135) for a propeller-driven deflected-slipstream configuration. The data of the present investigation verify the wall-interference theory of NASA TR R-124 even under conditions of extreme interference. A method given by Tyler and Williamson in AGARD CP-91-71 yields reasonable estimates for the onset of Rae's minimum-speed limit.

The present investigation shows that the rules for choosing model sizes to produce negligible wall effects, as given by Cook and Hickey in NASA SP-116, are considerably in error and permit the use of excessively large models. Even simple momentum theory appears to yield more nearly correct performance estimates in transition flight than uncorrected wind-tunnel data when the model span approaches one-half of the tunnel width. The "fan-induced" lift indicated by a number of previous studies in which the model was of similar relative span appears to be largely the result of wall interference that was not accounted for in reducing the data.

INTRODUCTION

Despite considerable theoretical study (e.g., refs. 1 to 6) of wind-tunnel interference for VTOL and STOL aircraft, it is not a general practice to correct all such data for wall effects. This failure to correct is due in part to conflicting reports of the efficacy of such corrections (e.g., refs. 7 and 8); it is due in part to some confusion between the effects of corrections and of the minimum-speed limits proposed by Rae (ref. 9); and finally, it is due in part to the rather considerable effort required to program corrections for data reduction when the programing may be significantly different for different types of model.

The magnitude of wall interference and the extent to which the data may be corrected for such interference become of paramount importance in the design of a new wind tunnel because the required test-section dimensions must be selected so that the data from the tunnel will be representative of the model operating in free air. Consequently, in connection with the design of a new full-scale subsonic wind tunnel (refs. 10 to 12), a major experimental study of wall effects was undertaken. This program was a joint effort of the Langley and Ames Research Centers of NASA. The model chosen was a simplified fan-in-wing aircraft differing from the model of reference 13 only in the addition of a large tail and a slight increase in wing-section thickness ratio. This model was chosen because it is considerably more complex, from a wall-effects viewpoint, than the models which have heretofore been used in V/STOL wall-effects investigations (e.g., refs. 8 and 14 to 18), and because the general type of configuration was representative of the configurations of reference 19 and therefore could provide an evaluation of the conclusions of reference 19. The model was tested, with and without smaller test-section inserts, in a 2.13- by 3.05-m (7- by 10-ft) wind tunnel at Ames as well as briefly in the 12.2- by 24.4-m (40- by 80-ft) wind tunnel at Ames. It was also tested with and without a test-section insert in the 9.14- by 18.3-m (30- by 60-ft) Langley full-scale wind tunnel.

The immediate objectives of the test program were twofold: First, since the tests conducted by Rae (ref. 9), which defined the problem of minimum-speed limits, were all conducted using relatively large single rotors, it was desired to examine the differences in these limits which might be caused by distributing much of the lift into two discrete highly loaded fans. Second, it was desired to obtain some experimental indication of the magnitude and correctability of the wall interference engendered by a model of this type. The approach used was to correct all the data to the maximum extent possible, and then to examine the differences in the data (both corrected and uncorrected) from tests under controlled conditions in the various test sections.

Examination of the data indicates that the first of the aforementioned objectives was only partially achieved. Some insight was obtained into the relative magnitude of the minimum-speed limits in different size test sections; however, the results are not adequate to distinguish any order of relative merit between the different cross-sectional shapes of the test sections. The second objective was met in a more satisfying manner. The data presented herein demonstrate the extent to which V/STOL data from different wind tunnels can be correlated, even in the face of extraordinarily large wall interference.

This wall-interference study is of particular interest since it demonstrates that, for V/STOL flight conditions, the interference may be of such magnitude that even the trends of the data may be incorrect. An example of correlation of wind-tunnel and flight-test data for an entirely different aircraft (ref. 20) is presented to demonstrate that this observation is also true for configurations totally different from that of the present investigation. Comparisons are made between the present work and previously published theoretically and experimentally chosen limits for V/STOL wind-tunnel testing (refs. 6 and 7).

In correcting wind-tunnel data of the nature of those presented herein, the biggest problem is the lack of uniformity over the model of the wall-induced interference (ref. 21). Some compensation must be made for the varying effective angles of attack and dynamic pressures over the different components of the model. Thus, in order to correct the data in a complete manner, it is necessary to have at least a rudimentary theoretical treatment of the performance of each component as affected by changes in velocity and angle of attack. In the present case, a simple momentum theory for the lifting fan in cross flow was used. This theoretical treatment, based largely on reference 22, is presented in its entirety in a separate paper (ref. 23). Throughout the present paper, the theoretical predictions of reference 23 are compared with the measured model performance as obtained both with and without wall interference.

Reference 13 has noted that a vortex-density correction is needed in applying the theory of references 2 and 3 to the correction of data obtained for fan-supported models. A justification of this vortex-density correction is presented in appendix A. A sample of the FORTRAN programs used in correcting the data obtained in the present investigation is presented as appendix B.

SYMBOLS

Because of the limited font of characters available in the automatic figure-plotting equipment, certain symbols may vary between the text and the figures. Where this variation occurs, the symbol used in the figures is shown parenthetically at the beginning of the definition.

A aspect ratio, b^2/S_W

A_L momentum area of VTOL elements

A_M momentum area of wing, $\frac{\pi}{4} b^2$

A_T cross-sectional area of wind-tunnel test section

b span of wing

C_D drag coefficient, D/qS_W or $D/q_c S_W$

C_L	lift coefficient, L/qS_W or L/q_cS_W
$C_{L,j}$	lift coefficient based on fan-area and fan-exit dynamic pressure, $\frac{L}{\frac{1}{2}\rho V_j^2 S_F}$
C_{L_α}	lift-curve slope of wing, $\partial C_L/\partial\alpha$, per rad
$C_{N,T}$	tail normal-force coefficient, N_T/qS_T or N_T/q_cS_T
c	chord
D	drag due to lift, total drag less drag at $\alpha = 0^o$
D_E	sum of D and D_{se}
D_{se}	drag equivalent to shaft power, P_s/V
d_e	equivalent fan diameter, $\sqrt{4S_F/\pi}$
h	height of fan exit above test-section floor
L	lift
N_T	tail normal force
P_s	shaft power
q	(Q) dynamic pressure of test-section flow, $\frac{\rho}{2}V^2$
q_c	(Q_C) corrected dynamic pressure at wing
q_F	(Q_F) corrected dynamic pressure at fans
q_T	(Q_T) corrected dynamic pressure at tail
R	body radius
S_F	fan area
S_T	tail area
S_W	wing area

T_S static thrust

V test-section, or forward, velocity

V_j fan-exit velocity in static thrust, $\sqrt{T_S/\rho S_F}$

w_0 vertical induced velocity in forward flight, positive upward

α angle of attack, angle between relative wind axis and longitudinal axis of model, positive nose up, deg

ΔD increment in fan external drag resulting from changes in α and V (see eq. (24))

Δi_F difference in $\Delta\alpha$ at wing and fans, $(\Delta\alpha)_F - (\Delta\alpha)_W$, deg except rad in equations (24) and (25)

Δi_T difference in $\Delta\alpha$ at wing and tail, $(\Delta\alpha)_T - (\Delta\alpha)_W$, deg

ΔL increment in fan lift resulting from changes in α and V (see eq. (25))

ΔL_i so-called "fan-induced" lift, total lift less the independent lifts of the fans and the model with the fans covered

Δu longitudinal component of wall-induced interference velocity, positive rearward

Δw vertical component of wall-induced interference, positive upward

$\Delta\alpha$ change in angle of attack caused by wall interference, referred to wing angle of attack unless otherwise subscripted, positive nose up, deg except rad in equations (13), (15), and (16)

δ_e elevator deflection angle, positive trailing-edge down, deg

$\delta_{u,D}$ interference factor for longitudinal interference due to drag

$\delta_{u,L}$ interference factor for longitudinal interference due to lift

$\delta_{w,D}$ interference factor for vertical interference due to drag

$\delta_{w,L}$ interference factor for vertical interference due to lift

ϵ downwash angle at tail, positive downward, deg

ρ mass density of air

χ wake skew angle, angle measured from vertical axis of test section to center of wake, positive rearward, deg

χ_e effective wake skew angle, deg

Subscripts:

c corrected

F fans

T tail

u uncorrected

W wing

APPARATUS AND TESTS

Model

The model used in this investigation is shown in figure 1 and pertinent dimensions are further detailed in tables I and II. The model consisted of a symmetrical streamline body 2.13 m (84 in.) long with a maximum diameter of 0.2 m (8 in.). A symmetrical tapered wing with a 1.07-m (42-in.) span was mounted at the midpoint of the body. The airfoil section at the wing tip was NACA 16-015 and the section increased in thickness to NACA 16-017 at the centerline of the body; straight-line fairings were used between these two stations.

Two commercially available 0.2-m (8-in.) tip-turbine-driven fans were mounted on centers spaced 0.56 m (22 in.) apart at the midchord position of the wing. The inlets to these fans were of the simple bellmouth type obtained by providing a reasonable radius at the intersection of the fan duct and the upper wing surface.

A slab tail with a 0.76-m (30-in.) span and a 0.32-m (12.5-in.) chord was mounted symmetrically so that its trailing edge was coincident with the rearmost end of the fuselage. This tail was installed during all tests for which the data are presented herein.

The model was mounted on a pivot at the midpoint of the fuselage and 6.67 cm $\left(2\frac{5}{8}\text{ in.}\right)$ below the centerline of the model. A linear actuator, installed between the mounting strut and a point farther rearward on the model, provided remote control of angle of attack.

Model Instrumentation

The model was designed to be operated on the normal external mechanical balances of the wind tunnels; thus, it was not necessary to provide a sting balance for measurement of the overall forces and moments. The mechanical balances involved are all of the simple platform type and have relatively poor resolution of moments for model forces of the magnitude encountered during the tests. The expected balance accuracy, together with some anticipated difficulty in setting precisely the same powered-lift flight conditions, precluded the possibility of obtaining accurate measurements of the effect of the tail on the moments by comparison of tail-on and tail-off tests. Consequently, the tail and tail-cone were mounted on the body by means of a commercial 1.9-cm-diameter (3/4-in.) six-component strain-gage balance. The primary measurement desired was the tail normal force, and the balance had a maximum load capability of 445 N (100 lb) for this component of force.

Numerous pressure and temperature transducers were provided in the independent pneumatic systems powering the two fans. The only measurement pertinent to the final results was the rotational speeds of the fans, for which magnetic pickups were provided in the fan casings. Considerable difficulty was experienced with this system because of 60-Hz pickup during the tests. The initial series of tests was actually conducted by setting the fan rotational speeds with a stroboscopic tachometer. For subsequent series of tests, a discriminator circuit was constructed to minimize the pickup problem, and magnetic tachometers with higher output were used. This aspect of the testing is discussed more completely in a later section of this paper.

Angle of attack was measured by an accelerometer-type transducer mounted within the model, except in the 12.2- by 24.4-m (40- by 80-ft) tunnel, where a selsyn indicator mounted at the actuator strut was used. Differences in the data-acquisition systems of the other two tunnels required the use of different transducers in each tunnel. In the smaller two tunnels, the accuracy of the overall system was approximately the same. In the largest tunnel the overall accuracy was somewhat less.

Wind Tunnels

<u>2.13- by 3.05-m (7- by 10-ft) tunnel.</u>- The smallest of the three tunnels used in this investigation was the Ames 7-foot by 10-foot Subsonic Wind Tunnel No. 2. This tunnel is described on pages 1-32 and 1-33 of reference 24. The model was mounted in the tunnel on a single unfaired strut (fig. 2). The pivot point at the top of the strut was on the centerline of the tunnel; thus, the model aerodynamic center was slightly above the tunnel centerline.

Air was supplied to the fans by means of two 5.1-cm-diameter (2-in.) hoses which were dressed closely to the front and back of the strut by means of guide rings. Below the floor of the tunnel, and above the balance frame, some slack was provided in the air lines to provide for the motion which occurred as a result of changes in angle of attack. An elaborate trapeze connection was provided between the balance frame and the main air supply. Tests of this system under pressure, with the model hoses blocked, indicated no measurable effect on the loads as seen by the balance.

Instrument leads were taped tightly to the sides of the strut and were connected to the data-acquisition system by means of a large hanging loop of wiring below the balance frame. The gap between the strut and the floor was closed to a minimum by specially trimmed sheet metal screwed to the floor of the tunnel.

Tunnel airspeed was measured by means of a pitot-static tube mounted from the ceiling of the tunnel. Corrections for position error are discussed in a later section of this paper. The tube was mounted 0.254 m (10 in.) below the tunnel ceiling, and the static-pressure holes of the tube were 1.33 m (52.5 in.) ahead of the model pivot point. (At zero angle of attack this location is 0.267 m (10.5 in.) ahead of the nose of the model.) The dynamic pressure measured by this tube was passed through a pressure transducer and then to both the data-acquisition system and a digital indicator, which was used as a speed reference during the tests.

Since this tunnel has continuous speed control, it had been hoped to maintain a close control over tunnel speed during each set of data points; however, this was not possible in practice. At high speed, blockage of the tunnel caused by the powerful variation of fan momentum drag with speed and angle of attack resulted in excessive time losses in attempting to set the tunnel speed precisely. At the lowest speeds, recirculation effects became so severe that the tunnel speed was found to lope; the pulsations in the tunnel flow were obvious even to the ear. Consequently, the tunnel speed was taken as the average of three readings, each of which in turn was averaged over a time of 1.25 seconds.

Tuft boards were placed on the floor of the tunnel for visual observations of the flow when recirculation began (refs. 9 and 13).

Inserts in 2.13- by 3.05-m (7- by 10-ft) tunnel.- In order to simulate still smaller test-section sizes, the insert technique of references 9, 13, 18, and 25 was used. Two rectangular test sections were simulated by means of two vertical walls (one of plywood and the other of transparent plastic to permit observation of the tufts) between which two horizontal surfaces were suspended to simulate the floor and ceiling of the small test sections. The entire assembly in each case was generously braced to insure stability and dimensional constancy.

The first of these simulated test sections had a width of 1.83 m (6 ft) and a height of 1.22 m (4 ft) providing a width-height ratio of 1.5. The second test section had a width of 2.24 m (88 in.) and a height of 1.12 m (44 in.) providing a width-height ratio of 2.0. A third test section was obtained by fitting the 2:1 insert internally with sheet metal ends which were rolled to a semicircular cross section; thus a flat-oval test section having a width-height ratio of 2.0 was provided. All these inserts were 3.66 m (12 ft) long. The model was centered longitudinally within each insert. Photographs of the model mounted in these test sections are given in figure 3.

The cross-sectional areas of the 1.5:1 rectangular insert and the 2:1 flat-oval insert were essentially identical with each other at 2.23 m^2 (24 ft^2). The 2:1 rectangular test section, with a cross-sectional area of 2.50 m^2 (26.89 ft^2), was approximately 12 percent larger in cross-sectional area. The choice of these sizes was not accidental. The dimensions of the 2:1 flat-oval test section were specifically chosen to represent the wing-span to tunnel-width ratios used in several Ames full-scale tunnel tests of fan and fan-in-wing models (e.g., refs. 26 to 32).

Speed measurement in the inserts was by means of the same pitot-static tube used in the basic wind tunnel. The longitudinal location of this pitot-static tube was constant, and in each insert the vertical location was adjusted so that the tube was 25.4 cm (10 in.) from the insert ceiling.

Each insert was generously tufted for visual flow observations; however, the curved sheet metal walls of the flat-oval section severely limited the field of view.

Compressed air to drive the fans was supplied from a large high-pressure storage tank. This air supply was adequate to drive the fans at nominal rotational speed of 10 000 and 12 000 rpm.

No evidence of any flow inclination was found in the data. Thus, the wind-tunnel stream angle was zero irrespective of the presence or absence of the inserts. Under these conditions, it was possible to set the model angle of attack directly to the desired values throughout the tests.

In any wind-tunnel wall-effects investigation the relative sizes of the test sections are of vital importance. A sketch illustrating the relative sizes is presented in figure 4.

12.2- by 24.4-m (40- by 80-ft) tunnel.- In order to obtain conditions essentially free of wall constraints, the model was tested briefly in the 12.2- by 24.4-m (40- by 80-ft) Ames full-scale tunnel. This wind tunnel is described in reference 24. The external balance of this tunnel was not designed to measure loads as small as those which were produced by the present model. In order to gain some increase in precision, the model was mounted with its span vertical (fig. 5) so that the lift could be measured by the side-force scales, which have a greater sensitivity than the lift scales.

The model was mounted on the same strut that was used in the tests conducted in the previously described tunnel; however, the mechanical arrangements did not allow the air hoses to be dressed closely to the strut. Instead, angled fittings were provided at the model and at the base of the strut. The required motion of the hoses with angle of attack was obtained by bending the supply hoses. As may be seen in figure 5, the resulting installation was substantially less clean than the installation in the smaller Ames tunnel.

A different pitch actuator was installed, and angle of attack was measured as a function of the actuator extension. The least division of the angle-of-attack indicator was 0.25°, and this reading was manually inserted into the data-acquisition system. A strain-gage balance was inserted into the actuator linkage in order to measure pitching moments; however, these measurements were invalidated by the omission of a static tare accounting for the moments imposed on the model by bending the air-supply hoses.

The discriminator circuit and large magnetic pickups were used in measuring the fan rotational speeds. This arrangement substantially reduced the amount of 60-Hz noise accepted by the counters; however, the static thrust measurements indicated that some spurious counts were still obtained. The counters were not connected directly to the data-acquisition system; the readings were manually inserted into the system.

The air supply in this tunnel was not adequate for continuous operation of the fans at 12 000 rpm. Therefore, the tests were conducted at 10 000 rpm and at the maximum available rotational speed, which tended to be on the order of 11 500 rpm.

Three different systems of tunnel flow-velocity measurement were employed. There were substantial disagreements in the data measured by the three systems. The staff of the tunnel provided their best estimates of the true velocities, and these values were punched into the data cards at a later date.

The tail-balance readings were recorded on a second data-acquisition system. This second system proved troublesome, with obviously mispunched cards being obtained even while recording zeros. It is believed that reasonably accurate readings were obtained during initial tests with the fans covered; however, the data obtained with the fans operating were so different from the data obtained in all the other test sections that they were rejected. Approximately half of the powered phase of the testing was complete when this system failed completely and no further tail data were obtained.

Initial tests with the fans covered indicated a very large stream-angle correction. Inasmuch as this tunnel is not equipped with flow-survey apparatus, it was not possible to obtain direct measurements of the flow inclination. Subsequent tests, with the model removed and the air hoses taped tangentially to the top of the strut, indicated that a large lift tare was also present in the data. No complete sequence of tare tests were conducted to obtain the precise magnitude of the tare. In analyzing the data, the stream angle and the lift and drag tares were obtained by finding those values that yielded the same performance as in all the other test sections when the fans were covered. These values were assumed to be unaltered by fan operation.

The stream angle obtained in the foregoing manner was significantly different from that presumed to exist during the conduct of the tests. Consequently, the maximum true angle of attack obtained in this tunnel was several degrees less than that obtained in the other tunnels.

The tests in this tunnel were conducted under the direction of Kenneth W. Mort, of the NASA Ames Research Center.

9.14- by 18.3-m (30- by 60-ft) tunnel.- The deficiencies inherent in the tests conducted in the Ames 12.2- by 24.4-m (40- by 80-ft) tunnel were such that the resulting data were too ambiguous to be accepted as defining the free-air characteristics of the model. Consequently, more complete tests were conducted in the 9.14- by 18.3-m (30- by 60-ft) Langley full-scale tunnel. This tunnel is described in reference 33. Some later information on the wind tunnel is presented in references 24 and 34.

The ground board normally used in the Langley full-scale tunnel was in place during these tests. The upper surface of this ground board is approximately 0.61 m (2 ft) above the lower edge of the jet boundary and thus reduces the cross-sectional area of the test section to 141.8 m^2 (1527 ft^2). By comparison, the model is very small; its wing area is less than one-half of 1 percent of the test-section cross-sectional area.

Because of the size of this tunnel, it was necessary to prepare a new mounting strut for the model. The new strut was designed so that the model was mounted vertically on the centerline of the active region of the tunnel (4.26 m (14 ft) above the ground board). As nearly as possible, the uppermost 1.07 m (3.5 ft) of the strut was identical with the strut used in the smaller tunnel. The end fitting on this strut, the hoses and their arrangement, and the angle-of-attack actuator were the same as those which were used in the smallest tunnel. A close-fitting fairing was installed around the strut starting 1.07 m (3.5 ft) below the model and continuing downward to meet the ground board. All hoses and electrical leads were dressed to the strut in, as closely as possible, the identical manner in which they were installed in the smaller tunnel. Photographs of the model installed in the tunnel are presented in figure 6.

The air-pressure lines were brought across the balance in a trapeze arrangement. Tests conducted under pressure with the hoses blocked at the model indicated no effect on the balance readings. The instrument leads were carried across the balance by means of a large hanging loop.

Prior to mounting the model on the strut, the region occupied by the model was surveyed with a pitot-static-pitch-yaw head. The dynamic pressure measured by this survey instrument was used to calibrate the velocity at the model as a function of static depression in the tunnel settling chamber; this static depression in turn was used to determine the tunnel velocity during the tests. The survey also disclosed the presence of a significant stream angle (approximately 0.7°) at the model location. The presence of this stream angle was confirmed later by the raw data from the symmetrical model when it was tested with the fans covered. The effects of this stream angle have been removed from all the data presented herein.

The Langley full-scale tunnel does not have continuous speed control throughout the velocity range covered in these tests; instead, it has some 24 discrete power settings, or "points." A number of these points appropriate to the prior tests in the smaller tunnel were selected. The actual velocity presented herein was determined from the average of no fewer than 10 samplings, spaced 1 second apart, of the static pressure.

In order to accommodate the different data-acquisition systems in this tunnel, it was necessary to use a different type of angle-of-attack transducer within the model. Again, the values presented result from the average of no fewer than 10 samplings of the transducer output.

Insert in 9.14- by 18.3-m (30- by 60-ft) tunnel.- It was desired to insure continuity of the test results between the tests conducted in the two wind-tunnel facilities. Consequently, a 2.13- by 3.05-m (7- by 10-ft) insert, 6.4 m (21 ft) long, was built up around the model in the Langley tunnel without disturbing the mounted model on the strut. The insert was fitted with a simple 15.2-cm-diameter (6-in.) semicircular sheet metal bellmouth inlet to discourage separation of the flow at the inlet.

The insert was constructed of 1.9-cm-thick (3/4-in.) plywood and was rigidly braced by angle iron to insure dimensional stability during the tests. It was supported by pipe columns and cable bracing so that the model pivot point was on the centerline of the insert, that is, in the same location as in the tests at the Ames Research Center, and so that it was centered longitudinally on the model. Photographs of this installation are presented in figure 7.

Within the insert, the gap at the floor of the tunnel was reduced to minimal size by means of closely trimmed sheet metal plates screwed to the floor. The fairing around the lower portion of the strut was sealed to the exterior of the insert.

The flow velocity within the insert was measured from the average of four sets of total- and static-pressure measurements. The probes for these measurements were located 45.7 cm (18 in.) behind the leading edge of the insert and 30.5 cm (12 in.) inward from the walls of the insert. Since no divergence was built into the insert, a small correction (approximately 4 percent) was made to the velocity in order to account for the difference in boundary-layer displacement thickness between the probe and the model locations.

It was not possible to survey the flow within the insert walls with the existing equipment in the Langley full-scale tunnel. Stream angle was determined by finding the angle which was required to reduce the lift of the symmetrical model with the fans covered to zero at an angle of attack of zero. In this regard, a root-mean-square average of such angles for all tunnel speeds was used. The resulting stream angle was approximately -0.2° and is accounted for in all data presented herein.

Air to power the fans was provided by a permanent compressor in the tunnel. It would have been desirable to maintain the same rotational speeds as were used in the earlier Ames tests. Unfortunately, the compressor proved inadequate in capacity for continuous operation at 12 000 rpm. Consequently, the tests at Langley were conducted at lower rotational speeds, 8000 and 10 000 rpm, which overlapped those in the other test sections.

All the tests in the Langley full-scale tunnel, as well as all the tests in the Ames 7-foot by 10-foot Subsonic Wind-Tunnel No. 2, were conducted under the personal supervision and direction of Frank A. Lazzeroni, of the U.S. Army Air Mobility R&D Laboratory, Ames Directorate.

Procedure

The same test procedure was used in all the tunnels and test-section inserts. First, the fans were started and brought to the required rotational speed. Generally, static thrust was measured, usually throughout the same angle-of-attack range as in the subsequent forward-flight tests. Then, the tunnel was started and brought to the desired velocity. Data were recorded in the following angle-of-attack sequence: 0°, -10°, -5°, 0°, 5°, 10°, and 16°. The tunnel speed was then altered to the next desired speed. Although the angle-of-attack sequence was constant, the progression of tunnel speeds was not constant. The sequence of speeds was often reversed so that the test commenced with the highest speed and ended with static thrust. Even more erratic velocity sequences were used in the Langley tunnel, where, because of a pole change in the motor-control system at approximately 48 knots, it was often more convenient to descend in velocity to that speed, drop to the smallest velocity, and then increase tunnel speed to obtain velocities up to 48 knots.

Data recording procedures differed in the three tunnel facilities because of differences in the data-acquisition systems. In the smallest tunnel, the data were obtained as three sets of time-averaged data (over a 1.25-second period) and were punched on cards for off-line reduction. In this tunnel, angle of attack was set manually and "dialed" into the data system manually. A similar set of two independent systems was used in the largest tunnel. In the Langley full-scale tunnel the data were obtained as at least 10 (and often 25) sets of samplings (with essentially no time averaging on each of the sets); the data were stored on magnetic tape for off-line processing. In this latter system, angle of attack was included as one of the directly recorded variables.

In each case, essentially no data were available during the actual testing. While this "blindness" may be a disadvantage during tests of a specific configuration, it is an advantage during tests of the present type because it eliminates any tendency to tinker with the model in order to obtain a preconceived result.

Precision of Measurement

Detailed examination of the data, together with the known capabilities of the external balances, indicates that the forces should be accurate to within the values shown in the following table:

Tunnel facility	Force					
	Lift		Drag		Tail normal force	
	N	lb	N	lb	N	lb
2.13 by 3.05 m (7 by 10 ft)	±8.9	±2.0	±2.2	±0.5	±4.4	±1.0
9.14 by 18.3 m (30 by 60 ft)	±13.3	±3.0	±4.4	±1.0	±4.4	±1.0
12.2 by 24.4 m (40 by 80 ft)	±22.2	±5.0	±22.2	±5.0	±4.4	±1.0

The values given for the 12.2- by 24.4-m (40- by 80-ft) tunnel include an allowance for the ambiguous nature of the stream angle and the tares.

It will be observed that these accuracies vary percentagewise according to the overall level of forces observed, and further that they will be reflected in the zeros for the data as well as in the data points themselves. As a proportionate point of reference for those figures in which the data have been nondimensionalized with respect to static thrust, it should be noted that the static thrust for the complete model ranges from about 196 N (44 lb) at a nominal speed of 8000 rpm to about 480 N (108 lb) at a nominal speed of 12 000 rpm.

In the Ames full-scale tunnel the dynamic pressure is believed accurate within 5 percent; angle of attack, to within 2.0°. In all the other test sections, dynamic pressure is believed accurate to within 1 percent and angle of attack to within 0.1°.

All data presented herein have been corrected for the effects of stream angle on the forces and the angle of attack, where such correction is appropriate. Where adequate rotational-speed data were recorded, the quantities V_j and T_S used in nondimensionalizing much of the data have been corrected for the actual rotational speed. Forces, where presented directly rather than as coefficients, have been corrected to standard density from the density at which the data were obtained.

Corrections for wall effects are discussed separately at appropriate points in the discussion of the results.

RESULTS AND DISCUSSION OF DATA FROM MODEL WITH FANS COVERED

Uncorrected Data

The uncorrected data for the model operating with the fans covered are presented in terms of lift, drag, and tail normal-force coefficients as a function of angle of attack in figure 8. Because of the small loads and the coarse sensitivity of the external balances employed, only the data from the highest dynamic pressure run in each test section are presented.

The strut used to mount the model during these tests was not faired, and a different length of this strut was exposed to the full dynamic pressure of the tunnel in each test section. No series of tare runs was made to determine the tare loads in the data; however, as noted earlier, the mounting arrangements near the model were as identical as possible during most of the tests. Consequently, an amount of drag equal to the entire drag of the model with fans covered at zero angle of attack has been removed from the data in this figure and in all subsequent figures. The resulting values of drag and drag coefficients may be considered to be approximately those due to lift.

The data for each coefficient, as obtained in the 9.14- by 18.3-m (30- by 60-ft) tunnel (where boundary interference is negligible due to the extremely small size of the model compared with the test section), were subjected to least-squares analysis. The resulting expressions for a quartic fit to the data are displayed as a curve on each figure.

It will be observed that even though the model was symmetrical, the data do not quite possess the expected symmetries and antisymmetries with angle of attack. This result is rational, for the rearmost portions of the model at positive angle of attack were immersed in a region of lowered dynamic pressure behind the mounting strut and were free of this region when at negative angle of attack. It is clear that under such conditions the emphasis placed on maintaining the mounting conditions as identical as possible in most of the test sections was entirely justified and necessary.

Considerations in Correcting Data

The data of figure 8 contain several types of boundary-induced interference. First, there is solid blockage. This interference is easily evaluated to a sufficient degree of accuracy from the compilation of studies presented in section 6:10 of reference 35. Next, there are the boundary-induced effects due to the presence of the lifting model within the tunnel. In the present case this last-named effect was obtained using the method of references 2 and 3 as implemented by the FORTRAN programs given in reference 36.

The use of references 2 and 3 presents two problems when the theory is applied to a model for which the lift may be zero. First, the momentum theory (refs. 2 and 22) used to obtain the wake skew angle appears to fail when the lift is negative. This difficulty is resolved by calculating the skew angle using the absolute value of the lift in the equations and subsequently choosing the proper quadrant for the wake according to whether the lift is positive or negative. The second problem is that the computer programs of reference 36 are arranged in such a manner that they yield the correct interference factors only when the wake skew angle is greater than -90° and less than or equal to 90° (that is, the wake cannot pass upward as it passes rearward). Some rules for treating the calculation by symmetries are presented in reference 5; however, in the present case, where the wake skew angles are only slightly greater than 90° (slightly upward), it is more convenient merely to extrapolate from the values calculated for the first quadrant.

The model was somewhat unusual in that the wing was closely coupled to an extraordinarily large tail. Furthermore, the tail had a greater aspect ratio than the wing (2.4 compared with 1.6), and thus would be expected to have a higher lift-curve slope than the wing. Under such conditions, it would be expected that the model would behave more nearly as a tandem-wing system than as a simple wing-tail combination; this expectation is confirmed by the nonlinear character of the lift-curve slope (fig. 8(a)). It is important to consider this tandem-wing-like character of the model in the corrections; that is, the effect of the interference at the tail must be considered not only with respect to tail normal force, but also with respect to the overall lift and drag of the model.

The appropriate interference factors for the wing due to its own presence may be obtained from the FORTRAN program given as appendix B of reference 36. It was assumed that the wing had an elliptic load distribution. Since the quarter chord of the model is displaced from the pivot point, both vertically and longitudinally, these interference factors will be a function of angle of attack by virtue of the different vertical location of the wing within the tunnel at each angle of attack. (See eq. (58) of ref. 3.) The effect of the presence of the tail and its loads on the tail itself is also significant and can be obtained from the same program; it is imperative that the location of the tail as a function of angle of attack be considered. Observe that this effect would have been difficult to consider if it had not been for the use of a tail balance to measure the tail loads. The interference factors at the tail due to the presence of the wing may be obtained from appendix D of reference 36. The interference at the wing due to the presence of the tail could be obtained from the same program (by considering the wing to be a canard tail); however, the rapid decrease of interference with distance upstream from the causative lifting element precludes any significant effect from this source and it may be ignored safely.

In the tests of the model installed in the inserts in the 2.13- by 3.05-m (7- by 10-ft) wind tunnel at the Ames Research Center, one other feature must be considered. This feature is the tunnel velocity measurement by means of a pitot-static tube near the nose of the model. At this location, the pitot-static tube is affected by the direct field of the model (both due to the body shape and to the lifting system) as well as by wall effects caused by the presence of the model. These effects must be evaluated in order to obtain the proper tunnel velocity to use in the interference calculations and in forming the corrected force coefficients.

The solid blockage at the pitot locations is caused primarily by the body because the body is the portion of the model closest to the pitot tube. The blockage is not the same as a classical blockage correction (ref. 35), since the classical blockage calculation is for the model location. In the present analysis, this blockage effect was approximated by setting up a calculation based on the use of a source and a sink to represent a Rankine ovoid (ref. 37, p. 208), and using the technique of reference 38 to obtain the strengths and spacing of these elements to produce an ovoid which, in free-air, has the same length and diameter as the fuselage. The ovoid was then reflected both horizontally and vertically to produce a pattern which represents the boundary conditions at the walls. The interference velocities at the pitot-static tube location can be obtained from this field of elemental sources and sinks.

It is the usual practice in such wall-effects calculations to omit the central image which represents the model itself on the basis that this is the portion to be measured and corrected. In the present calculations, the central image is retained since it is desired to include the direct field of the model as well as the blockage interference. The level of this correction is approximately 1 percent of the free-stream velocity.

The foregoing treatment was used in the present analysis; however, it does contain certain inadequacies. First, the existence of the images representing the boundary conditions at the wall results in an overall velocity at the model which is somewhat greater than the free-air condition for which the source and sink were chosen. Thus, the body for which the interference is obtained will be somewhat more slender than the desired body shape, and, furthermore, it will be slightly different in shape than a Rankine ovoid. These effects probably result in an underestimate of the actual interference. Second, the calculation method will produce a streamlined symmetrical body only at an angle of attack of zero. Thus, it is not possible to examine the effect of the angle of attack of the body on the calculated interference. Such effects would be expected to be large at positive angles of attack, where the nose approached more closely the pitot-static tube location; however, one would expect only smaller changes at negative angles of attack, where the model nose moved farther away from the tube. On an overall average basis, the actual effects of solid blockage at the pitot location probably are underestimated from the omission of angle-of-attack effects.

The wall interference at the pitot location can be obtained from appendix D of reference 36 by considering the pitot to be a canard tail of zero span. Considerable care must be exercised in choosing the tail length and height as a function of model angle of attack in order to retain the correct pitot location. The direct field of the lifting model is obtained by retaining the central image. This is accomplished most simply by altering the subroutine DLTAS given in appendix Q of reference 36. (Delete lines (Q13) and (Q67) through (Q105).)

Procedure in Correcting Data

The first step in correcting the data is to divide the loads between the wing and the tail. This is possible only because the present model was fitted with a tail balance. Then, the loads assigned to the wing are used to solve the momentum quartic (ref. 2 or 22) for V/w_0 and the wake skew angle χ. In those test sections where the tunnel velocity was measured near the model, the measured tunnel velocity is then corrected, and the corrected value is used to recompute V/w_0 and χ.

The value of χ obtained in this manner is the momentum-theory value and, as pointed out by reference 8, is not the value that should be used in wall-interference calculations. Because of wake roll-up, the wake vorticity will be concentrated at some higher location in the tunnel given by an effective average value of the skew angle χ_e. As discussed in references 6 and 39, the most appropriate choice for a simple wing is that given by

$$\tan \chi_e = \frac{\pi^2}{4} \tan \chi \qquad (1)$$

The values of the interference factors (previously obtained from ref. 36) are then interpolated to obtain the values corresponding to this value of χ_e. In this range of skew angles, the effect of χ_e on the interference factors for the effect on any element due to its own presence is small; thus, χ may be assumed to be 90^o when considering the effect of the tail on itself.

At this point the lift and drag of the wing and tail may be used to compute the individual vertical and horizontal increments of interference velocity separately at the wing and at the tail (eqs. (40) to (43) of ref. 2). At the wing, the total values of Δw and Δu are simply the sums of the respective components occasioned by the lift and drag of the wing; however, at the tail, the contributions of both the wing (which are different at the tail than at the wing) and the tail itself must be summed to obtain the total components of interference.

The total values of Δw and Δu are then used to obtain separately, at the wing and at the tail, the values of $\Delta\alpha$ and q_c/q by use of equations (48b) and (49b) of reference 2, which are

$$\Delta\alpha = \tan^{-1} \frac{\Delta w/V}{1 + \frac{\Delta u}{V}} \tag{2}$$

$$\frac{q_c}{q} = \left(1 + \frac{\Delta u}{V}\right)^2 + \left(\frac{\Delta w}{V}\right)^2 \tag{3}$$

The values of $\Delta\alpha$ and q_c/q at the wing are used as a first correction to the data; however, it is also necessary to account for the differences in $\Delta\alpha$ and q_c/q at the wing and the tail. These differences are conveniently expressed as

$$\Delta i_T = (\Delta\alpha)_T - (\Delta\alpha)_W \tag{4}$$

$$\frac{q_T}{q_c} = \frac{\left(\frac{q_c}{q}\right)_T}{\left(\frac{q_c}{q}\right)_W} \tag{5}$$

It will be noted that the difference in the two values of $\Delta\alpha$ is effectively a change in tail incidence (ref. 40), and q_T/q_c is an alteration in the effective dynamic-pressure ratio at the tail. If these effects were not removed from the data, the model would not be aerodynamically equivalent to the model under test.

The procedure used herein was to resolve the forces of the entire model around a new effective stream direction given by $\Delta\alpha$, where

$$(\alpha)_c = (\alpha)_u + \Delta\alpha \tag{6}$$

$$\left(C_L\right)_c = \frac{\left(C_L\right)_u \cos \Delta\alpha - \left(C_D\right)_u \sin \Delta\alpha}{q_c/q} \tag{7}$$

$$\left(C_D\right)_c = \frac{\left(C_D\right)_u \cos \Delta\alpha + \left(C_L\right)_u \sin \Delta\alpha}{q_c/q} \tag{8}$$

Next the tail forces as measured were resolved, and then the tail lift and drag were adjusted for Δi_t and q_T/q_c. This adjustment requires a knowledge of the lift-curve slope of the tail and the free-air dynamic-pressure ratio at the tail. It would be desirable to have test results for the tail in the presence of the body, but without the wing, as a guide in estimating these values. Unfortunately, the construction of the model did not allow for such tests; thus, the lift-curve slope was taken as 0.03 per degree (approximately the value given in fig. 5-5 of ref. 41) and the dynamic-pressure ratio at the tail was rather arbitrarily selected to be 0.9. A small correction to the induced drag of the tail was made to account for the difference in the measured and adjusted lift. A correction to the profile drag would be appropriate; however, insufficient data were available to make such an adjustment. In any event, such a profile-drag adjustment probably would be significant only if the tail were to stall during the test.

The foregoing adjustments were sufficient to provide the corrected values of $C_{N,T}$. As a final step, the differences in the lift and drag of the tail were applied as adjustment to the overall lift and drag of the model in order to obtain the final corrected values of C_L and C_D.

Corrections

The corrections obtained for the model with the fans covered are shown in figure 9. The dynamic pressure ratios differ from unity only by 2 or 3 percent and thus have only a comparatively small effect on the data. However, $\Delta\alpha$ and Δi_T assume significant proportions in the smallest test sections at large angles of attack.

One common rule of thumb in wind-tunnel testing (e.g., ref. 42) is that $\Delta\alpha$ should not exceed 2°. It is evident from figure 9(a) that $\Delta\alpha$ has assumed almost this value in the smaller inserts even with the fans covered, and that Δi_T (fig. 9(c)) is well in excess of 2°, yielding a total correction angle at the tail on the order of 4° (eq. (4)).

Corrected Data

After the application of corrections, the data for the model with the fans covered appear as shown in figure 10. The solid line shown in figure 10 is again a least-squares quartic faired through the data obtained in the 9.14- by 18.3-m (30- by 60-ft) tunnel.

On the basis of the force accuracies previously given and the dynamic pressures of the tests, the anticipated agreement should be on the order of 0.03 for C_L, 0.008 for C_D, and 0.03 for $C_{N,T}$. Examination of figure 10 indicates that the correlation between C_L and C_D is generally within these limits but that $C_{N,T}$ appears to be overcorrected to a somewhat greater extent than would be anticipated by a simple examination of the measurement accuracy at the highest values of lift.

One possible cause of the poorer correlation in the case of the tail normal-force coefficient could lie in the required estimates of the tail lift-curve slope and tail dynamic-pressure ratio. These estimates are far more critical in correcting tail normal force than in correcting the overall lift and drag of the model. Another possible cause could be the effect of the wall-induced velocities in relocating the wake to a higher position in the small test sections than in the large tunnel. References 43 and 44 have examined this latter effect theoretically. The maximum ratios of C_L/A encountered in the present test are on the order of 0.5. For such values of C_L/A, references 43 and 44 indicate that the correction to the tail should increase when the tail moves with the model. Such an effect would further degrade the present correlation. Finally, the assessment of test accuracy may be excessively optimistic since the value quoted represents only 1 percent of the full normal-force capability of the tail balance and considerable vibration and buffeting of the tail was obvious during the tests.

RESULTS AND DISCUSSION OF DATA FROM MODEL WITH FANS OPERATING

Uncorrected Data

Presentation of data.- In view of the difficulties experienced with the measurement of fan rotational speed during the tests, it is not possible to present the data directly for constant rotational speeds. Instead, the forward velocity has been nondimensionalized with respect to V_j, which is the fan efflux velocity in static thrust, defined from simple incompressible momentum theory as

$$V_j = \sqrt{\frac{T_S}{\rho S_F}} \tag{9}$$

Similarly, forces are presented only in nondimensional quantities, generally referenced either to the static thrust or to each other. The static thrust used in these nondimensionalizations is always the value obtained in the largest test section used in each series of tests. It is also measured at zero angle of attack. These two conditions insure that the value of static thrust used is the best available from the viewpoint of minimum flow recirculation in the tunnel during the measurement. Indeed, comparisons of the static-thrust data, with and without the insert, in the Langley full-scale tunnel, indicate that any errors caused by recirculation in the 2.13- by 3.05-m (7- by 10-ft) tunnel are within the accuracy of the data.

The uncorrected data in the form of lift, drag, and normal-force coefficients are presented in figures 11 to 13. They are presented in the form of the ratios of L/T_S, D/T_S, and D/L in figures 14 to 16. Finally, the ratio L/D_E (where D_E is the sum of the external drag and a drag equivalent to the power supplied to the fans (ref. 23)) is presented in figure 17.

For lift coefficients and the ratios of lift to static thrust, a line on the figures indicates the values which would be obtained if the lift were simply the direct sum of the vertical component of the fan static thrust and the lift of the wing with the fans covered. In a similar manner, the momentum-theory values of all the other parameters (with the exception of $C_{N,T}$, for which momentum theory is inappropriate) have been computed by means of the equations of reference 23, and these calculated values are compared with the corrected data.

When examining figure 17 it should be noted that no measurements adequate for the calculation of the power supplied directly to the fans were actually made. Indeed, in view of the small size and fairly low efficiency of the model fan turbines, such measurements of power would be meaningless in relation to flight hardware. Instead, the momentum-theory value of shaft power, as computed from reference 23, has been converted into an effective drag by means of the relationship

$$D_{se} = \frac{P_s}{V} \tag{10}$$

The values of D_{se} obtained from equation (10) have been added to both the experimental data and the theoretical curve. Although figure 17 presents no measured data that were not available in the preceding figures, it does serve the purpose of illustrating the effects of wall interference on the efficiency of this type of aircraft in transition.

Effect of wall interference on lift.- Figure 11 indicates clearly that at any constant angle of attack, the measured lift coefficient increases as the cross-sectional area of the test section decreases. The magnitude of this effect is disguised somewhat by the logarithmic scales and by the effect of the variation in dynamic pressure in computing the coefficient when a large part of the lift (from the fans) is essentially independent of forward speed. Figure 14 presents a truer picture of the influence of the walls by presenting the lift in the form of a ratio to the static thrust. Reference 23 has shown that the ratio L/T_S is proportional to a lift coefficient based on fan area and fan-exit velocity; that is

$$\frac{L}{T_S} = \frac{1}{2} C_{L,j} \tag{11}$$

In figure 14 the differences in the data, as measured in the various test sections, are demonstrated to represent very significant differences in lift. For example, at an angle of attack of zero (fig. 14(b)) and a speed of $V/V_j = 0.4$ (which would represent a speed near the high-speed end of transition), the data from the small inserts indicate that a lift of about 25 percent more than the static thrust would be obtained; the data from the moderately larger 2.13- by 3.05-m (7- by 10-ft) test section would indicate that the gain in lift would be only 10 percent; and the data from the largest test section indicate that a small loss in lift would be encountered. Indeed, the data from the largest test section indicate that this model would have a loss of lift (from that expected from a simple addition of lift components) for all angles of attack and for all forward speeds less than $V/V_j = 0.5$. This speed range encompasses the entire feasible transition range of lifting fans with modern pressure ratios.

Reference 7 presents a set of charts which define relative proportions between model and test section which were believed to yield negligible wall effects at a speed of 30 knots. Figure 18 shows the degree to which the present tests meet these size limits. Only the highest and the lowest disk loadings encountered are shown. The test conditions include points between these two disk loadings. In particular, the present tests in the 1.12- by 2.24-m (44- by 88-in.) insert meet these limits at least as well as many of the tests reported in references 26 to 32. In the 2.13- by 3.05-m (7- by 10-ft) tunnel, the size of the present model falls well within the size limitations of reference 7. In contrast, the data in figure 14 clearly indicate unacceptably large overestimates of "fan-induced" lift in these test sections. Therefore, it must be concluded that the size limits proposed by reference 7 are not valid for configurations such as that of the present investigation; indeed, since there is nothing very unusual about this configuration except the relative size of the tail, it would be presumed that these size limits are equally inapplicable to other configurations as well.

Reference 7 attempts to limit its conclusions to conditions for which the overall drag of the model is trimmed. This limitation to zero net drag is based upon the theoretical results of reference 2, which the authors of reference 7 claim to be incorrect and even in the wrong direction. In fact, reference 2 was misinterpreted in arriving at the limitation to zero net drag. As will become clear in the subsequent discussion of correcting the present fan-in-wing data, each element of the aircraft must be considered individually. Thus, the fans, except for a few isolated conditions, always have a drag; also, the wing always has an induced drag. The addition of a centered jet exhausting directly rearward ($\chi = 90^o$) could balance the drag of the model under any condition; however, the thrusting jet would contribute nothing to the interference at the model $\left(\text{from ref. 2, } \delta_{u,L} = \delta_{w,D} = \delta_{u,D} = 0, \text{ and } \delta_{w,L} \text{ has no effect since the lift of the thrusting jet would be zero}\right)$. Consequently, the limitation to trimmed drag in reference 7 is meaningless.

The comparisons between flight and wind-tunnel data given in reference 7 have already been discussed in reference 39, which shows that the conclusions of reference 7 were based upon faulty comparisons between flight and wind tunnel. Such an error should have been anticipated, since one of the conclusions was that both Glauert's corrections and those of reference 2 were in the wrong direction. Since both Glauert and reference 2 predict upwash interference in a closed tunnel, this result of reference 7 could only be obtained if a downwash interference was produced by the walls. Such a result is physically impossible for an overall correction in a closed tunnel. Indeed, references 4 and 39 have already demonstrated that the calculated flow of reference 2 is in the correct direction.

Since the only guide in choosing model sizes for the fan-in-wing tests of references 26 to 32 has been the set of limits given in reference 7, the data shown in figures 14 and 18 should lead to serious concern regarding the highly favorable "fan-induced" lift reported as one of the main advantages to the fan-in-wing configuration in those studies which have produced and correlated uncorrected wind-tunnel data (e.g., refs. 19 and 26 to 32). One such correlation (from ref. 19) is presented in figure 19, where the "fan-induced" lift is correlated as a function of the ratio of fan area to wing area.

The present model has a ratio of fan area to wing area of 0.094 and, as may be seen in figure 14, has a "fan-induced" lift in the 1.12- by 2.24-m (44- by 88-in.) flat-oval insert which lies very near the lower boundary of the correlation region. This value does not really correspond to the other data in figure 19 because all those data were obtained with models having either no tail or a small tail; whereas the present model has an extremely large tail which carries a significant download (fig. 13) under almost all conditions. It is easily shown from the definition of $C_{N,T}$ and V_j that

$$\frac{N_T}{T_S} = \frac{1}{2} C_{N,T} \frac{S_T}{S_F}\left(\frac{V}{V_j}\right)^2 \tag{12}$$

The value of $C_{N,T}$ at $\alpha = 0^{\circ}$ and $V/V_j = 0.4$ is obtained from figure 13(b) as -0.53; S_T/S_F is 3.73; thus, from equation (12) the ratio N_T/T_S is equal to -0.16 for the conditions of figure 19. Removing the tail load from the data of figure 14 increases ΔL_i $\left(= L - T_S\right)$ from 0.25 to 0.41, which is near the upper edge of the correlation band of reference 19. (See fig. 19.) On the other hand, in the largest test section, $\Delta L_i/T_S$ is negative for the complete model at this value of V/V_j.

The slope of the correlation band of reference 19 which is reproduced in figure 19 deserves some comment. It is obvious in examining the data points of figure 19 that a band of the same width, drawn parallel to the abscissa, and thus indicating total independence from the ratio S_F/S_W, would have encompassed a larger number of data points than the band which was drawn. In either event, the major exceptions to the correlation band are those configurations in which the fans are displaced far from the center of pressure of the wing. Such aircraft would be unflyable as VTOL configurations without the provision of additional fans to provide moment balance.

Since reference 7 presents several different criteria upon which to scale wind-tunnel tests for wall interference, it is advisable to perform a first-order analysis in order to determine which parameters really are significant. For this first-order analysis, examine the zero-angle-of-attack case, for which the wing of the present model would have no lift in free air. Then assume that the horizontal components of wall-induced interference have only a second-order effect and that $\Delta\alpha$ is sufficiently small to let $\Delta\alpha \approx \tan \Delta\alpha$. Under these assumptions, following references 1 to 3,

$$\Delta\alpha = \frac{\Delta w}{V} = \left(\delta_{w,L} + \frac{D}{L} \delta_{w,D}\right)\frac{S_F}{A_T} \frac{w_0}{V} \tag{13}$$

where $\Delta\alpha$ is in radians and where $\delta_{w,L}$ and $\delta_{w,D}$ are calculated for the fans.

From reference 23, momentum theory shows that for the fans at $\alpha = 0$,

$$\left.\begin{aligned} w_0 &= w_h = -V_j \\ \frac{D}{L} &= \frac{V}{V_j} \end{aligned}\right\} \tag{14}$$

Substitution of equations (14) into equation (13) yields

$$\Delta\alpha = -\left(\delta_{w,L} + \frac{V}{V_j}\,\delta_{w,D}\right)\frac{S_F}{A_T}\,\frac{1}{V/V_j} \tag{15}$$

Observe that both $\delta_{w,L}$ and $\delta_{w,D}$ are negative in a closed tunnel; thus, $\Delta\alpha$ will be positive (upwash). Reference 23 shows that the lift of the fan is virtually insensitive to angle of attack for angles near zero; therefore, the increase in lift will be essentially all on the wing. This increase in lift may be written as

$$\Delta L = \Delta\alpha C_{L_\alpha} q S_W \tag{16}$$

Substitute equation (16) into equation (15) to obtain

$$\Delta L = -\left(\delta_{w,L} + \frac{V}{V_j}\,\delta_{w,D}\right)\frac{\rho}{2}\,C_{L_\alpha} V^2 S_W\,\frac{S_F}{A_T}\,\frac{1}{V/V_j} \tag{17}$$

Divide both sides of equation (17) by $T_S = \rho S_F V_j^{\,2}$ to yield

$$\frac{\Delta L}{T_S} = -\left(\delta_{w,L} + \frac{V}{V_j}\,\delta_{w,D}\right)\frac{C_{L_\alpha}}{2}\,\frac{S_W}{A_T}\,\frac{V}{V_j} \tag{18}$$

Consider the product $C_{L_\alpha} S_W$ in equation (18). Since $C_{L_\alpha} = \frac{2\pi A}{A + 2}$, this product may be rewritten as

$$C_{L_\alpha} S_W = \frac{2\pi A}{A + 2}\,S_W = \frac{2\pi\,\frac{b^2}{S_W}\,S_W}{A + 2} = 2\pi\,\frac{b^2}{A + 2} \tag{19}$$

Finally, substitute equation (19) into equation (18) to yield

$$\frac{\Delta L}{T_S} = -\left(\delta_{w,L} + \frac{V}{V_j}\,\delta_{w,D}\right)\frac{\pi}{A + 2}\,\frac{b^2}{A_T}\,\frac{V}{V_j} \tag{20}$$

which is the wall-induced lift.

Observe that the only term of equation (20) which explicitly involves the model dimensions is b^2/A_T. For test sections having approximately the same width-height ratios (in the present case, from 1.4 to 2.0), b^2/A_T will be approximately proportional to the square of the ratio of the wing span to the test-section width. The ratio of fan area to test-section cross-sectional area is completely immaterial.

One more significant point is evident in the preceding analysis. It is generally believed that wall effects are greatest at low speeds. For a constant model configuration and for data presented in terms of coefficients based on free-stream dynamic pressure, wall effects are greatest at low speed. (Note that $\Delta C_L = \Delta\alpha C_{L_\alpha}$ and, from eq. (15), that $\Delta\alpha$ has a $1/V$ component.) On the other hand, again for a constant model configuration, when the data are presented in terms of forces or force ratios, equation (20) clearly shows that the greatest effect of wall interference will be at high speed. This conclusion is confirmed by the data presented in figure 14.

It is obvious that the present results from the small insert lead to a gross overestimate of "fan-induced" lift. The correlation with the data presented in reference 19 indicates that the data presented therein also include substantial overestimates of "fan-induced" lift which would not be obtained in flight. (Observe that, with two exceptions, the models of ref. 19 have essentially the same span-to-width ratio as the present model in the smallest inserts. Of the two exceptions, one is anomalous because of its thin delta wing; the second was notable for producing the smallest "fan-induced" lift of any of the models of ref. 19.) Further, the model of reference 19 in which the fans are behind the trailing edge of the wing would be expected to show a far smaller "fan-induced" lift than indicated in figure 19, and, similarly, the model with the fans well forward of the wing would be expected to show far greater "fan-induced" losses than indicated. In either of these two cases, the results would be affected substantially by provision of the additional fans required for moment control in the VTOL mode. This latter effect is evident in figure 19 when these two configurations are combined into one. (See the appendix of ref. 23 for a further discussion of the effect of fan location on mutual interference.) Irrespective, however, of whether or not VTOL moment control is feasible for the configurations of reference 19, it is obvious that all the data of that paper contain a large increment of wall-induced, rather than "fan-induced," interference. The "good" configurations will be far less "good" in free air; the "poor" configurations will be even worse in free air.

It will be observed that there are differences in notation between the present paper and reference 19. In the present paper, ΔL_i is defined (at $\alpha = 0^o$) as $L - T_S$ since T_S is equal to the thrust in forward flight according to ideal momentum theory (ref. 23). Similarly, V_j is defined (see Symbols) as the fan efflux velocity in static thrust. In reference 19, ΔL_i is defined as total lift, less any wing lift (which is zero at $\alpha = 0^o$ in the present tests), less the thrust in forward flight as measured by rakes in the fan exit; and V_j is defined in relation to this measured thrust.

Because of the square root involved in determining V_j from the thrust, as well as the relatively flat character of L/T_S near $V/V_j = 0.4$ and $\alpha = 0^o$ (the conditions chosen by ref. 19; see fig. 14(b)), there will be little effect of the difference in definition of V_j. The difference in definition of ΔL_i has a more serious effect. In practice, because of inlet efficiency, the actual value of thrust in forward flight will be somewhat less than the theoretical value of T_S. Figure 6 of reference 32 indicates that at V/V_j of 0.4, a loss of 10 to 15 percent of T_S may be expected for a typical lift-fan model. For complete comparability, this loss should be added to the present results; that is, in figure 19 the values of $\Delta L_i/T_S$ should be about 0.1 to 0.15 greater than indicated therein for the present model. Thus, the effect of wall interference on the data of reference 19 may be even greater than indicated by the data shown in figure 19.

Effect of wall interference on drag.- The drag of the model also increases as the tunnel size decreases (figs. 12 and 15); however, the increases in drag are not commensurate with the increases in lift. Indeed, at the lower angles of attack, the increases in drag are minimal. The disparity between the increases in lift and drag may be seen more clearly in figure 16, which presents the external drag-lift ratio for the model. At all angles of attack, D/L is greater in the larger test sections, thus indicating poorer efficiency.

The apparent gain in efficiency in the smallest test sections is retained even when the data are presented in terms of L/D_E (fig. 17). For example, at $V/V_j = 0.4$ and at $\alpha = 0^o$ (fig. 17(b)), L/D_E as measured in the smallest test sections is approximately 25 percent greater than the same values measured in the largest test sections. Thus, wall effects are sufficient to indicate a 25-percent decrease in the power required to fly in the transition speed range.

The values of L/D_E shown in figure 17 appear at first glance to be remarkably small. They are confirmed however by the momentum theory presented in reference 23. This confirmation is demonstrated by the theoretical curves (from ref. 23) given in figure 17. They are further confirmed by calculations made using the measured shaft powers given in reference 45, as well as by the extraordinary fuel consumption in low-speed flight found in design studies of fan-supported aircraft (ref. 46).

Effect of wall interference on tail normal force.- The uncorrected measurements of tail normal force, as a function of V/V_j, are shown in figure 13. At low speed, the trends shown for the various test sections are observed to scatter. This effect is probably due to Rae's limit (refs. 4, 9, 13, and 18), and it will be discussed in the next section.

At the higher speeds and for angles of attack less than 10° (figs. 13(a) to 13(c)), the observed tail normal-force coefficient is essentially independent of the test-section size or shape. As the angle of attack becomes greater, the data from the various test sections show greater differences (fig. 13(e)), with the tail normal force becoming more positive as the test-section size decreases.

Even constancy in tail normal-force coefficient would indicate a serious degree of wall interference since, in free air, the increased lift (shown in fig. 14) in the small sections would increase the downwash at the tail, reduce the tail angle of attack, and result in a more negative tail normal-force coefficient. However, the data of figure 13 indicate that the wall-induced interference at the tail is of sufficient magnitude to negate, or even to reverse, the trend that would be expected with increased lift.

Wall-induced effects at the tail, of course, are not confined to this configuration. Large wall effects have also been noted in comparing large-scale wind-tunnel and flight data; for example, consider the comparison of flight-test data and uncorrected wind-tunnel test data (Ames full-scale tunnel test 388) presented in reference 20 for a YOV-10 aircraft fitted with a rotating-cylinder flap. Serious differences were found in maximum lift and the angle of attack at which it was obtained; however, by far the greatest disagreement between wind tunnel and flight was with regard to the effects at the tail.

Figure 20 shows these differences (as presented in ref. 20) in terms of the elevator angle required to trim the aircraft as a function of forward speed. The uncorrected wind-tunnel data indicate positive speed stability with the stick moving rearward (the elevator moving trailing edge upward) as the speed decreases; the elevator is 20° trailing edge up when 55 knots is reached. In contrast, the flight data indicate a speed instability; the elevator angle is always in the opposite sense (trailing edge down); and at 55 knots the elevator angle is 13° trailing edge down. The total disagreement between tunnel and flight at 55 knots is 33°, and this disagreement is in the same direction as that indicated in figure 13.

The trends shown in figure 20 are given further import by the flight-test data when extended to slightly lower speeds (fig. 21). Here the speed instability became more dramatic, and the minimum speed in many cases was determined by the speed at which the elevator contacted the limit of travel in the trailing-edge-down direction and not by maximum lift. Needless to say, under such circumstances, the pilot finds himself in somewhat compromised circumstances because he has no control left for any unanticipated maneuvering requirement. The point here, of course, is that not even full-scale wind-tunnel tests of the actual aircraft gave any indication that the pilot would find himself in these circumstances because wall effects were not properly accounted for in the data reduction.

It is noted that the YOV-10 with the rotating-cylinder flap, as tested in the tunnel, also fell well within the boundaries of reference 7, which, according to that paper, would indicate negligible wall effects (fig. 22). This evidence confirms the previous conclusion that the testing boundaries of reference 7 are erroneous.

The opinion is sometimes voiced that wind-tunnel interference does not affect the trends shown by the data, or, as expressed in reference 47 (p. 7-1): "Informative results, even when the model lifting system spans 2/3 to 3/4 of the wind tunnel test section width, will still be obtained." Neither the model of the present investigation, nor the aircraft of reference 20, approached so great a size relative to the test section; and, in each case, the wall interference was so great that even the trends shown by the data were in the opposite direction from "free air" results at low speed. Such results clearly show that extreme caution must be used when interpreting uncorrected wind-tunnel data.

Effect of test-section size on Rae's limit.- The separately instrumented tail was installed on the model in the hope that measurements of tail normal force would provide a sensitive indication of the onset of the recirculation which results in Rae's minimum-speed limit (ref. 9). This procedure was chosen because of the dramatic alterations in tail lift which were observed behind a rotor in reference 18.

Although the tail normal-force-coefficient data presented in figure 13 do show marked effects as a function of tunnel configuration at low forward speed, effects as definitive as those of reference 18 were not always observed. One reason may be the magnitude of the wall interference in the present tests. This aspect of the problem will be discussed in subsequent sections of the present paper. A second reason is that the tail on this model, as may be seen by comparisons between the individual parts of figure 13, has very nearly zero tail effectiveness $\left(\text{that is, } \frac{d\epsilon}{d\alpha} \approx 1, \text{ so that } 1 - \frac{d\epsilon}{d\alpha} \approx 0\right)$ until the highest angle of attack (16^o) is reached. At $\alpha = 16^o$, the tail normal-force coefficient suddenly turns upward as the speed is reduced in the small test sections. In the small inserts, $C_{N,T}$ departs from the trends shown in the data from the 9.14- by 18.3-m (30- by 60-ft) tunnel at a value of V/V_j below 0.38; a similar departure may be observed in the data from the 2.13- by 3.05-m (7- by 10-ft) tunnel at a value of V/V_j below about 0.2. The values correspond approximately to conditions at which visual tuft observations indicated substantial flow reversal on the floor; furthermore, the values are roughly in proportion to the height of the various test sections, as might be expected from the correlation rules presented in references 6, 9, and 21. Unfortunately, those rules are expressed in terms of the momentum wake angle. Since the momentum wake angle for the fan is always along its axis and is actually negative for the data of figure 13(e), those rules cannot apply to the present case.

Tyler and Williamson (refs. 48 and 49) have conducted a systematic program to determine minimum-speed test limits for jet lifting systems. Their results indicate incipient stagnation (near $\alpha = 0^{o}$) on the floor of the test section when

$$\frac{V}{V_j} = 1.59 \frac{d_e}{h} \tag{21}$$

for single and tandem-paired jets, and when

$$\frac{V}{V_j} = 1.31 \frac{d_e}{h} \tag{22}$$

for a laterally paired system of two jets spaced 4.3 nozzle diameters apart. The spacing of the two fan nozzles in the present model is considerably closer (2.75 diameters); nevertheless, using equation (22) yields $V/V_j = 0.67$ for the two 1.12- by 2.24-m (44- by 88-in.) test sections; $V/V_j = 0.62$ for the 1.22- by 1.83-m (4- by 6-ft) test section; and $V/V_j = 0.39$ for the 2.13- by 3.05-m (7- by 10-ft) test section. The corresponding values for the largest test section are below the smallest velocities at which tests were run.

To define the point of incipient stagnation and to define the point at which the data will be affected are two different things, as is noted in reference 49. Tyler and Williamson suggest that test speeds as small as 55 percent of the speed for incipient stagnation may be acceptable for single jets and 65 percent of this speed may be acceptable for widely spaced lateral pairs of jets. If the values obtained in the preceding paragraph are reduced by a multiplying factor of 0.6 (an average of 0.55 and 0.65), they will be observed to agree closely with the previously noted points of figure 13(e). Therefore, it would appear that the Tyler and Williamson relations (eqs. (21) and (22)) provide a reasonable means of estimating the minimum speed for wind-tunnel testing of jet- and fan-supported models.

The value observed for the degradation of data due to recirculation in the 1.12- by 2.24-in. (44- by 88-in.) flat-oval test section was about $V/V_j = 0.38$, and that obtained from equation (22) reduced by 40 percent was 0.40. Not only the correlation between these values is of interest; their magnitude is significant in itself. Observe that the correlation of "fan-induced" lift in reference 19 was obtained at $V/V_j = 0.4$. It is entirely possible that some of the data upon which reference 19 is based are suspect because of recirculation effects, since the model to tunnel-size ratios in those data are comparable with those obtained in the present small flat-oval insert. Furthermore, at 30 knots, it is clear that much of the data used to prepare the testing limits defined in reference 7 were obtained for flow conditions which were unrepresentative of flight in free air because of flow breakdown induced by the model in the wind tunnel.

Two primary requirements exist in planning wind-tunnel tests. One is simulation of the aircraft, and, given a drawing of the aircraft, it is simple to produce a reasonable model of it. Equally important, however, is that the basic free-air flow must also be simulated. At speeds less than Rae's limit, a powerful cylindrical sheet of vorticity is formed ahead of the intersection of the wake on the floor (refs. 4, 13, 18, and 39). This sheet ultimately extends across the floor and up the sides of the test section. Except in ground effect, no equivalent vortex formation exists in actual flight. Under such conditions, the flow in the test section does not simulate free air and almost any result may be obtained.

It is particularly important to realize that the existence of the basic alteration of the flow does not depend upon the presence, or the absence, of a tail on the model. The flow alteration is caused by the presence within the walls of the main lifting system. Indeed, the models used by Rae (ref. 9) when he discovered this effect had no tails; neither did the models used by Tyler and Williamson (refs. 48 and 49).

Comparison of simple momentum theory with experimental results.- Reference 23 develops a simple incompressible-flow momentum theory for the fan-in-wing configuration based upon the assumption that there is no mutual interference between the fans and the wing. Momentum theory, by itself, is incapable of calculating the actual lift of the model, since the lift depends intimately on the local angles of attack of the wing and of the fan blades. However, once the lift is given, momentum theory is capable of estimating the remaining performance items. Momentum theory, obviously, also is incapable of predicting the tail normal-force coefficient because this coefficient depends upon a detailed calculation of the flow field in the vicinity of the tail.

In the present case, it is assumed (following ref. 23) that the thrust of the fan is unaltered by forward speed or angle of attack. This assumption is verified by figure 6 of reference 32, which shows that the actual thrust for a typical lift-fan model (at V/V_j as great as 0.6) is only 10 or 15 percent less than the static thrust. When the normal component of static thrust is added to the lift of the wing with covered, inoperative fans, the results previously presented in figures 11 and 14 are obtained. Evidently, at high speed, significant fan-wing interaction effects are present; however, throughout the usable transition speed range $\left(0 \leqq V/V_j < 0.5\right)$, the assumption of zero interaction yields values close to the observed total lift. The differences in notation between reference 19 and the present paper have no effect herein, since both theory and experiment are presented in the identical manner.

All the remaining curves in figures 12 and 15 to 17 follow directly from the equations of reference 23 once the lifts are assumed. It will be observed that, for transition speeds, the observed performance is predicted more closely by even this simple momentum theory than by the data from the small inserts. Note that the model in the present investigation spanned only a little less than half the width of the smallest inserts. This relative size is essentially the same as that used in references 26 to 32, and a similar result may be implied to be true for those tests as well.

Correcting the Data

Considerations in correcting the data.- Correcting the data with the fans operating follows the same general procedure described earlier for the data with the fans covered. Obviously, the procedure is complicated to a degree in accommodating the presence of the fans. In this case, the interference factors are obtained from appendices O and P of reference 36.* The previously discussed modifications to subroutine DLTAS (appendix Q of ref. 36) were used to obtain the interference factors at the pitot-static tube location. The solid blockage factors are identical with those used when the fans were covered. Since there was no independent measurement of the thrust of each of the fans, there is no alternative but to deal with them simultaneously. Therefore, the appropriate interference factors for the pair of fans are the average of those for the fan due to its own presence and those for the fan due to the presence of the other fan. In all cases, slight changes to the programs of reference 36 allowed data cards containing the interference factors to be punched automatically as they were calculated. These cards were used as input data to the data correction program to be discussed shortly. This procedure eliminates the possibility of errors in transcription when preparing the input to the correction program.

Reference 36 offers choices of wing load distribution and rotor-disk load distribution. In the absence of definitive measurements to the contrary, an elliptic load distribution was chosen for the wing. In order to ascertain the degree to which this choice might affect the corrections, the data were also reduced using the interference factors for a uniform load distribution; no significant effect was found for this model, perhaps because of the magnitude of the corrections. Because of the large central boss in the fans, the disk load distribution over the faces of the fans is not uniform. Consequently, the triangular disk load distribution was taken as being more nearly representative of the actual fan load distribution. In any event, the fans were so small compared with the test-section dimensions that little effect of this choice should be evident.

---

*Three known errors exist in the programs given in reference 36. Two of these affect the work contained herein. The following lines should be corrected to read as follows:

```
805 XDELTA(L1)=XDELTA(L1)+DELTA(L1)*XLOAD(N1)                (E 79)
    SUML=0.063052                                            (P 113)
    SUML=0.252208                                            (P 136)
```

The first problem is to divide the measured loads between the elements which produce them. The tail presents no problem since it was mounted on its own strain-gage balance; however, there was no balance to separate the independent forces of the wing and fans when they were operating in unison. In the absence of specific information, the wing was assumed to produce the same lift and drag as it did when the fans were covered. Thus, the fan lift and drag are assumed to be the main balance readings, less the measured tail loads, and less the aforementioned assumed lift and drag of the wing. Then the fan lift and drag thus obtained were used to solve the momentum quartic and to calculate the fan wake skew angle χ and the fan velocity ratio V/w_0. The resulting values of χ were within 2^o or 3^o of being equal to $-\alpha$, as they should be (ref. 23). For the fans, it is more appropriate to use the effective skew angle

$$\chi_e = \frac{90^o + \chi}{2} \tag{23}$$

as given in references 8 and 39. For the wing and for the tail, the effective skew angle was assumed to be 90^o. In the face of the powerful downwash field generated by the fans, the use of the momentum quartic given in references 2 and 22 is not strictly applicable because it would be necessary to include the local effective downwash angle in the vector diagram defining χ. In any event, the use of $\chi = 90^o$ for the wing and the tail is a great simplification in the calculation.

At this point, everything is in hand to compute the average interference velocity components over the wing, over the tail, and at the pitot tube. Observe that the fans now contribute substantially to the interference velocities at each location.

Reference 13 has noted that it is necessary to apply a vortex-density correction to the theoretical interference factors when applying them to ducted fans. This correction was used in the present calculations. A justification of the vortex-density correction is presented in appendix A.

The first step in applying corrections to the data from the smaller Ames tunnel is to correct the pitot-static tube reading of tunnel velocity. The forces that were charged to the wing are directly dependent on dynamic pressure; thus, it is necessary at this point to return to the original division of loads and redo that division with the corrected dynamic pressure, and then repeat all the steps to this point.

The calculation now proceeds as before, correcting the overall performance to the corrected flight condition at the wing and then adjusting the tail loads to account for the substantially different wall-induced interference at the tail location. Despite the fact that the fans are mounted within the wing planform, there is a significant difference in the average wall-induced interference over the full span of the wing and the similar average over the faces of the fans. It is necessary to remove this difference by adjustments to the fan lift and drag. The adjustment is accomplished by the use of the following equations from reference 23:

$$\Delta D = T_S\left[\left(\frac{\Delta V}{V_j}\right)_F + \Delta i_F \cos \alpha\right] \tag{24}$$

$$\Delta L = -T_S\, \Delta i_F \sin \alpha \tag{25}$$

where Δi_F is in radians. It will be observed from figure 15 that an α-dependent multiplying factor, generally greater than 1.0, could have been applied legitimately to equation (24) (that is, the actual drag of the fans is generally greater than the momentum-theory value). This was not done; equation (24) was used directly as given above.

Corrections at zero tunnel velocity are particularly suspect. As noted in reference 8, a hovering condition in the tunnel leads to an interference which is a pure upwash. Proceeding in a formal manner, this upwash is equivalent to change in angle of attack of 90°. While true in a sense, it is more rational to consider the model to be at the same angle of attack, but with a rate of sink equal to the upwash velocity. The corrections to the data then would depend upon the effect of a rate of sink. Unfortunately, sufficient data are not present to make such a correction for this model. Furthermore, at zero speed, the test conditions always violate Rae's minimum-speed limit (ref. 9).

In view of the foregoing observations, no attempt has been made herein to correct data obtained at zero velocity. When such points are shown in the corrected data, they are identical with the uncorrected data, and they are presented only to preserve the continuity of the data set.

Computer program.- Appendix B presents one of the computer programs used in correcting the data obtained in the present investigation. Because of differences in the measurement of fan rotational speed, it was necessary to write slightly different programs for the two separate sets of tests in the Ames tunnel. The absence of a stream-angle correction in that tunnel provides one simplification in that it was possible to compute the interference factors specifically for the angles of attack which were used; thus, only a single interpolation against χ_e is required to obtain the proper factors for each data point. The presence of a small stream angle in the Langley 2.13- by 3.05-m (7- by 10-ft) insert was accommodated by means of a double interpolation against both χ and α in a third modified version of the computer program.

The program of appendix B is substantially more complex than would normally be required because it simultaneously treats four different test sections. This feature requires considerably more storage and additional steps (which increase running time) than would a program written for a single test section. Nevertheless, in the Langley Computer Complex, the program requires only 54000_8 ($\approx 22\ 500_{10}$) storage locations for compilation, 46000_8 ($\approx 19\ 500_{10}$) storage locations to run, and completely corrects more than 360 data points in about 30 seconds (including compilation time) at a cost of only $7. The storage lengths, the time, and the cost obviously would be different in almost any other computer; however, it also is obvious that only minimal costs and computer capabilities are required to fully correct data for wall effects even for a fairly complex model.

The program of appendix B produces several files of output data and a sequence of punched-card sets for subsequent plotting of the data. In sequence, the written files present the interference factors used in the correction routines, the uncorrected data together with a preliminary breakdown of the division of loads (in the Langley insert, the presence of a stream angle requires interpolation in order to obtain this file), a point-by-point listing of the corrected data, a listing of the corrected data at fixed angles of attack obtained by interpolation of the previous listing, an interpolated listing of the corrections themselves at a series of fixed corrected angles of attack, and finally a listing of the corrections according to the uncorrected angles of attack. Punched-card decks of the last four listings are provided for subsequent automatic plotting of the data.

The data herein are presented as a function of forward speed. If it is desired to obtain polar plots of the performance at fixed speeds, an interpolation against V/V_j would be required. The addition of one more interpolation should not present any significant difficulty.

Interference in Uncorrected Data

The corrections in the uncorrected data of figures 13 to 17, as calculated from the foregoing considerations, are presented in figures 23 to 28. The corrections are distinguished by their enormous magnitude, which far exceeds the more reasonable values suggested as the maximum practical limits in references 6 and 42. Depending upon α and V/V_j, the average interference angle $\Delta\alpha$ at the wing varies from about $2\frac{1}{2}^{\circ}$ to over 14° in the smaller inserts (fig. 23). Similarly, the effective dynamic pressure at the wing is reduced by 5 to 22 percent (fig. 24). The effective tail incidence in the smaller inserts is increased by from 5° to 12° (fig. 25) and the dynamic pressure at the tail varies from 1.15 to almost 3 times that at the wing (fig. 26). In the small inserts, even the fans are operating at effective angles of attack as much as 7° more than the wing in which they were mounted (fig. 27). Only the ratios of the dynamic pressures at the fans to those at the wing remain relatively small (fig. 28). The wall interference in the 2.13- by 3.05-m

(7- by 10-ft) test section is generally of a lesser magnitude, although, even in that test section, $\Delta\alpha$ and Δi_T (figs. 23 and 25) tend to be larger than would be desirable.

It is noticeable that the values for Rae's limit, which were obtained earlier, were for speeds so low that a prudent investigator would have discontinued testing long before this limit was a serious concern. This result is in accordance with the results of reference 6, which show that Rae's limit is of primary concern only for those models which are very small with respect to the test-section size. In all other cases, the magnitude of the wall-induced distortions of flow over the model are the controlling factors in choosing the maximum permissible model size.

Corrected Data

It is obvious from the magnitude of the indicated corrections (figs. 23 to 28) that perfect correlation of the data from all the test sections cannot be expected. Nevertheless, the corrected data show remarkably improved agreement (figs. 29 to 35). This agreement is poorest at those speeds previously determined to be less than Rae's limit $\left(V/V_j \approx 0.38 \text{ in the smallest test sections}\right)$. It is also somewhat poorer in the smaller inserts than in the more moderately sized 2.13- by 3.05-m (7- by 10-ft) test section. (See particularly fig. 33(a).) On the other hand, considering the magnitude of the required corrections, the data presented in figures 29 to 35 are an impressive verification of wall-interference theory (refs. 1 to 6).

Interference in Corrected Data

It is obvious that the angular range of model settings in figures 29 to 35 differs from that in figures 11 to 17 because the geometric angle of attack in figures 11 to 17 has been decreased by $\Delta\alpha$ to obtain the corrected values of α in figures 29 to 35. Since the wall-induced interference increases as the lift and drag increase, and since these forces increase with α, the corrections are somewhat less in figures 29 to 35 than in figures 11 to 17. For completeness, figures 36 to 41 have been prepared to indicate the magnitude of the corrections that are actually present in the corrected data. Although slightly less than the values presented earlier, the corrections in the final data are still extremely large.

Maximum Model Size

It is clear from the data presented in this paper that the model was so large in relation to the small inserts that the corrections were excessive. At low speeds, the model was excessively large in the 2.14- by 3.05-m (7- by 10-ft) test section as well. It would appear that prudent model sizing would have led to a model having a span of about a quarter of the test-section width.

A similar conclusion as to an appropriate model size would have been reached by examining the charts of reference 6. The overall corrections $(\Delta\alpha$ and $q_c/q)$ and the wall-induced tail incidence (Δi_T) are about the same in those charts as were found herein; however, the charts of reference 6 fail totally to indicate the magnitude of the wall-induced dynamic-pressure ratio (q_T/q_c) at the tail. Such a discrepancy is understandable. The charts of reference 6 are based on the assumption of a winglike model having a uniformly loaded span and a single, blended wake; these assumptions are grossly violated by the present fan-in-wing model. Thus, in using reference 6 to size models of unusual VTOL configurations which do not approximate the assumptions of that paper, it is best to err on the safe side by selecting a model size even smaller than indicated therein.

It will be observed that nonuniformities in wall-induced interference decrease more rapidly (ref. 6) with decreases in span (in a given tunnel) than do the overall corrections, which are roughly proportional to the square of the span. Thus, a small model does not require the same rigor in applying corrections as is required for a large-span model. Furthermore, considerably more confidence in the final results is justified when the model is small enough to require only minimal correction to the data.

While the present model should have been about half its present size, in the smallest insert, this conclusion should not be extended to indicate that all VTOL models should span about one-quarter of the test-section width. The allowable size of a VTOL or STOL model will depend upon the configuration, upon the minimum speed for which useful data are required, and upon the degree of correction applied to the data. Reference 6 should be some help in this regard; however, the only real safety will be found in correcting, as fully as possible, all wind-tunnel data as a standard practice. As noted earlier, the additional computing cost is minor in comparison with the total cost of a wind-tunnel investigation.

CONCLUSIONS

The results of this investigation of wind-tunnel wall interference on the performance of a fan-in-wing model are as follows:

1. Extreme caution must be used in interpreting uncorrected wind-tunnel data obtained at low speeds. Unless the model is extremely small in relation to the test-section size, the wall interference can be so large that even the trends in the data may be opposite to those which would be obtained in flight.

2. Wall-induced interference is particularly large at the model tail. This result confirms recently published (NASA CR-2135) conclusions based on the correlation of flight and wind-tunnel data for a YOV-10 aircraft.

3. The theory of wall interference for VTOL and STOL models, presented in NASA TR R-124 and subsequent papers, has been verified under conditions of extreme wall interference.

4. The rules for choosing model sizes to produce negligible wall effects, as given by Cook and Hickey in NASA SP-116 (also in AGARD Rep. 520), appear to be considerably in error and to permit the use of models which are significantly too large for the tunnel.

5. The method presented by Tyler and Williamson in AGARD CP-91-71 yields reasonable estimates of the onset of Rae's minimum-speed limit for jet- and fan-supported models; however, for reasonably large models, wall interference becomes so great that testing should be discontinued at a speed significantly greater than Rae's limit.

6. The "fan-induced" lift indicated by a number of previous investigations appears to be largely the result of wind-tunnel wall interference which was not accounted for in reducing the data. The uncorrected results obtained herein, when the model spanned almost half of the tunnel width, fall directly on a previously published correlation of "fan-induced" lift (Hickey and Cook, AGARD CP-22, paper No. 15); however, the increase in lift for the model under conditions which approach testing in free air was small or negative for the actual transition speed range.

7. The simple incompressible-flow momentum theory presented in NASA TN D-7498 appears to yield reasonable estimates of fan-in-wing performance in transition flight; indeed, the theoretical predictions are more accurate than uncorrected wind-tunnel test data in which the model span is approximately half of the tunnel width.

Langley Research Center,
National Aeronautics and Space Administration,
Hampton, Va., December 12, 1973.

APPENDIX A

JUSTIFICATION OF VORTEX-DENSITY CORRECTION FOR FANS AND JETS

The theoretical treatment of wall interference for VTOL-STOL aircraft (refs. 1, 2, and 5) sets up the inclined wake of the aircraft in free air as a doublet string extending from the aircraft to infinity. If the model is small, this doublet string might represent a rotor or a lifting fan or a jet. Indeed, the relationship between the doublet strength and the induced velocity was obtained directly from an earlier analysis of a rotor wake in the wind tunnel (ref. 50). The basis of the relationship was the doublet strength required to match the vorticity along the edge of the vortex cylinder comprising the wake.

Now, if one considers a vortex cylinder cutting through an otherwise unbounded flow, and then takes the line integral of $\overline{V} \cdot d\bar{s}$ (where $\overline{V}$ is the total vectorial velocity and $\bar{s}$ the path length), the eventual result is that the vorticity along the edge of the cylinder is precisely equal to the velocity jump across the cylinder. Unfortunately, integration, by means of the Biot-Savart law, of all the vorticity in the wake, leads to a velocity only one-half this great at the origin of the cylinder. In order to obtain the correct velocity at the end of the cylinder, it is necessary to double the vorticity. Since the corrections for wall interference depend upon the velocity w_0, which is the mean vertical induced velocity, it appears appropriate to take the corrections due to the fan as being twice as great as those of references 1 to 3. The changes need not be made in the interference factors, but can be made most simply by doubling the wall-induced interference components caused by the presence of the fans.

This effect was first noted in reference 13 and the vortex-density correction was used both in that paper and in the present analysis. The results of both papers appear to justify its use.

It will be observed that no similar correction is required for rotors or propellers. In those configurations, the induced velocity at the origin of the wake <u>should</u> be equal to one-half the vortex density.

APPENDIX B

FORTRAN PROGRAM FOR CORRECTING DATA FROM A FAN-IN-WING MODEL TESTED IN FOUR DIFFERENT TEST SECTIONS

THIS PROGRAM WAS WRITTEN IN CDC FORTRAN, VERSION 2.1, TO RUN ON THE CDC 6000 SERIES COMPUTERS IN THE LANGLEY RESEARCH CENTER COMPUTER COMPLEX. MINOR MODIFICATIONS MAY BE NECESSARY PRIOR TO USE IN OTHER COMPUTERS. A DESCRIPTION OF THIS PROGRAM IS GIVEN IN THE TEXT OF THIS PAPER. A COMPLETE LISTING OF THE INTERFERENCE FACTORS USED IS INCLUDED. EACH LINE IS CODED AT THE END BY THE ANGLE OF ATTACK FOR WHICH THE FACTORS WERE COMPUTED, AN INTEGER CODE SPECIFYING THE TEST SECTION, AND THE CODE WORD DESCRIBED WITHIN THE PROGRAM. THESE INTERFERENCE FACTORS WERE OBTAINED USING THE COMPUTER PROGRAMS OF NASA TM X-1740 (REF 36). CERTAIN ERRORS IN THAT REFERENCE ARE DISCUSSED IN THE TEXT.

THE SUBROUTINE DISCOT IS INCLUDED FOR COMPLETENESS. THIS IS A RELATIVELY STANDARD SINGLE OR DOUBLE INTERPOLATION ROUTINE. IT, OR ITS EQUIVALENT, WILL BE FOUND IN MOST COMPUTER SYSTEM LIBRARIES.

```
      PROGRAM AARL6A (INPUT,OUTPUT,TAPE5=INPUT,TAPE6=OUTPUT,TAPE1,TAPE3,
     1  TAPE4,PUNCH)
C
C                TUNNEL     CODE
C          ITUN=1  IS 44X88 INCH WITH ROUND ENDS
C          ITUN=2  IS 44X88 INCH WITH RECTANGULAR ENDS
C          ITUN=3  IS 48X72 INCH WITH RECTANGULAR ENDS
C          ITUN=4  IS  7X10 FOOT TUNNEL
C
C       FORTRAN WORDS REPRESENTING INTERFERENCE FACTORS ARE ALL CODED BY
C       THE LAST FOUR CHARACTERS OF THE WORD.  STARTING FROM THE RIGHT-
C       HAND SIDE OF THE WORD, THE FIRST CHARACTER REPRESENTS THE ELEMENT
C       ACTED UPON AND THE SECOND CHARACTER THE ELEMENT WHICH CAUSES THE
C       WALL INTERFERENCE, WHERE:  W=WING; F=FANS; T=TAIL; AND P=PITOT.
C       THE NEXT TWO CHARACTERS ARE THE SUBSCRIPTS OF THE INTERFERENCE
C       FACTORS AS DEFINED IN NASA TR R-124.  VARIOUS PREFIXES ARE
C       APPENDED TO THESE CODE LETTERS TO DISTINGUISH SPECFIC CHOSEN
C       VALUES.
C
      REAL LOTS
      DIMENSION WLFF(4,6,8),ULFF(4,6,8),WDFF(4,6,8),UDFF(4,6,8),
     1 WLWF(4,6),ULWF(4,6),WLWW(4,6),ULWW(4,6),WLFW(4,6,8),ULFW(4,6,8),
     2 WDFW(4,6,8),UDFW(4,6,8),WLFT(4,6,8),ULFT(4,6,8),WDFT(4,6,8),
     3 UDFT(4,6,8),WLWT(4,6),ULWT(4,6),WLTT(4,6),ULTT(4,6),ANAME(28)
      DIMENSION CWLFF(8),CULFF(8),CWDFF(8),CUDFF(8),CWLFW(8),CULFW(8),
     1  CWDFW(8),CUDFW(8),CWLFT(8),CULFT(8),CWDFT(8),CUDFT(8)
      DIMENSION TDALPF(6),TDALPT(6),TQOQF(6),TQOQT(6),TDVOVJ(6),TALP(6),
     1 TQ(6),TDALPW(6),TQOQW(6),TQC(6),TALPC(6),TCNC(6),TLIFT(6),SLT(6),
     2 TVOVJ(6),TLOTS(6),TDOL(6),A(5),TQOQJ(6),EPSILON(4),BDT(6),BLT(6),
     3 CHI(8),AT(4),SLAT(4,6),SDAT(4,6),JTUN(4),JTYPE(3),SLAT1(6),
     4 SLAT2(6),SLAT3(6),SLAT4(6),SDAT1(6),SDAT2(6),SDAT3(6),SDAT4(6),
     5 UOVPIT(4),WOVPIT(4)
```

```
      DIMENSION WLFP(4,6,8),ULFP(4,6,8),WDFP(4,6,8),UDFP(4,6,8),        (B 16)
     1   WLWP(4,6),ULWP(4,6),WDWP(4,6),UDWP(4,6),CWLFP(8),CULFP(8),     (B 17)
     2   CWDFP(8),CUDFP(8)                                              (B 18)
C
C      NOTE THAT WLFP,ULFP,WDFP,UDFP,WLWP,ULWP,WDWP, AND UDWP ARE ALL
C      COMPUTED RETAINING THE N=M=0 TERMS IN THE WALL-EFFECTS CALCULA-
C      TION.  THUS, THEY CONTAIN THE DIRECT EFFECT OF THE MODEL FLOW
C      FIELD AS WELL AS THE WALL EFFECTS AT THE PITOT LOCATION.
C
      DATA (A(I),I=1,5)/-5.,0.,5.,10.,16./                              (B 19)
      DATA (AT(I),I=1,4)/24.004,26.889,24.,70./                         (B 20)
      DATA (CHI(I),I=1,8)/20.,30.,40.,50.,60.,70.,80.,90./              (B 21)
      DATA (JTUN(I),I=1,4)/10H2-1 ROUND ,10H2-1 RECT.  ,10H 1.5-1    ,  (B 22)
     1  10H  7X10       /                                               (B 23)
      DATA (JTYPE(I),I=1,3)/10H WT TARE   ,10H AERO TARE,10H  DATA    / (B 24)
      DATA (EPSILON(I),I=1,4)/.02705,.02445,.02565,.00716/              (B 25)
C
C      UOVPIT AND WOVPIT ARE THE SOLID BLOCKAGE EFFECTS (INCLUDING THE
C      DIRECT MODEL FIELD) OF THE BODY AT THE PITOT LOCATION.  THESE ARE
C      COMPUTED FROM A SOURCE AND SINK SPACED SO AS TO PRODUCE IN FREE
C      AIR A RANKINE OVOID OF THE SAME LENGTH AND DIAMETER AS THE MODEL
C      FUSELAGE.  IN THE TUNNEL THE BODY WILL BE SOMEWHAT SLENDERER
C      AND THE CALCULATED BLOCKAGE WILL BE SOMEWHAT UNDERESTIMATED.
C
      DATA (UOVPIT(I),I=1,4)/-.00672,-.00707,-.00443,0.00035/           (B 26)
      DATA (WOVPIT(I),I=1,4)/2*0.00685,0.00622,0.00191/                 (B 27)
C
C      STATIC WEIGHT TARE DATA
C
      DATA (BDT(I),I=1,6)/-1.7383,-0.8929,-0.0238,0.8546,1.7515,2.7357/ (B 28)
      DATA (BLT(I),I=1,6)/0.1566,0.0113,0.0081,0.0197,0.0835,0.3732/    (B 29)
      DATA (SLT(I),I=1,6)/0.1999,-0.0750,0.2250,0.1000,0.0333,0.0374/   (B 30)
C
C      AERODYNAMIC TARE DATA
C
      DATA (SLAT1(I),I=1,6)/-.477,-.200,.026,.258,.518,.897/            (B 31)
      DATA (SLAT2(I),I=1,6)/-.482,-.207,.021,.251,.523,.902/            (B 32)
      DATA (SLAT3(I),I=1,6)/-.433,-.179,.036,.256,.508,.882/            (B 33)
      DATA (SLAT4(I),I=1,6)/-.390,-.185,.010,.205,.420,.697/            (B 34)
      DATA (SDAT1(I),I=1,6)/.198,.152,.137,.144,.178,.273/              (B 35)
      DATA (SDAT2(I),I=1,6)/.197,.153,.138,.146,.179,.274/              (B 36)
      DATA (SDAT3(I),I=1,6)/.182,.140,.128,.135,.169,.258/              (B 37)
      DATA (SDAT4(I),I=1,6)/.208,.164,.151,.155,.182,.246/              (B 38)
      DO 6  I=1,6                                                       (B 39)
      SLAT(1,I)=SLAT1(I)                                                (B 40)
      SLAT(2,I)=SLAT2(I)                                                (B 41)
      SLAT(3,I)=SLAT3(I)                                                (B 42)
      SLAT(4,I)=SLAT4(I)                                                (B 43)
      SDAT(1,I)=SDAT1(I)                                                (B 44)
      SDAT(2,I)=SDAT2(I)                                                (B 45)
      SDAT(3,I)=SDAT3(I)                                                (B 46)
    6 SDAT(4,I)=SDAT4(I)                                                (B 47)
      PI=3.14159265358979                                               (B 48)
      RAD=PI/180.                                                       (B 49)
      SW=7.41125                                                        (B 50)
      ST=2.6042                                                         (B 51)
      SF=2.*PI/9.                                                       (B 52)
      REWIND 1                                                          (B 53)
      REWIND 3                                                          (B 54)
      REWIND 4                                                          (B 55)
```

APPENDIX B

```
C
C       READ IN INTERFERENCE FACTORS
C
      WRITE (6,120)                                                     (B  56)
      READ (5,2024)  WINGLOG                                            (B  57)
      WRITE (6,2025)  WINGLOG                                           (B  58)
      DO 20  ITUN=1,4                                                   (B  59)
      WRITE (6,127) JTUN(ITUN)                                          (B  60)
      DO 20  IALPHA=1,6                                                 (B  61)
      READ (5,121) (WLFF(ITUN,IALPHA,ICHI),ICHI=1,8),ANAME(1)           (B  62)
      IF (EOF,5)  999,22                                                (B  63)
   22 READ (5,121) (ULFF(ITUN,IALPHA,ICHI),ICHI=1,8),ANAME(2)           (B  64)
      READ (5,121) (WDFF(ITUN,IALPHA,ICHI),ICHI=1,8),ANAME(3)           (B  65)
      READ (5,121) (UDFF(ITUN,IALPHA,ICHI),ICHI=1,8),ANAME(4)           (B  66)
      READ (5,122)  WLWF(ITUN,IALPHA),ANAME(5)                          (B  67)
      READ (5,122)  ULWF(ITUN,IALPHA),ANAME(6)                          (B  68)
      READ (5,2022)                                                     (B  69)
      READ (5,2022)                                                     (B  70)
      READ (5,122)  WLWW(ITUN,IALPHA),ANAME(7)                          (B  71)
      READ (5,122)  ULWW(ITUN,IALPHA),ANAME(8)                          (B  72)
      READ (5,2022)                                                     (B  73)
      READ (5,2022)                                                     (B  74)
      READ (5,121)  (WLFW(ITUN,IALPHA,ICHI),ICHI=1,8),ANAME(9)          (B  75)
      READ (5,121)  (ULFW(ITUN,IALPHA,ICHI),ICHI=1,8),ANAME(10)         (B  76)
      READ (5,121)  (WDFW(ITUN,IALPHA,ICHI),ICHI=1,8),ANAME(11)         (B  77)
      READ (5,121)  (UDFW(ITUN,IALPHA,ICHI),ICHI=1,8),ANAME(12)         (B  78)
      READ (5,121)  (WLFT(ITUN,IALPHA,ICHI),ICHI=1,8),ANAME(13)         (B  79)
      READ (5,121)  (ULFT(ITUN,IALPHA,ICHI),ICHI=1,8),ANAME(14)         (B  80)
      READ (5,121)  (WDFT(ITUN,IALPHA,ICHI),ICHI=1,8),ANAME(15)         (B  81)
      READ (5,121)  (UDFT(ITUN,IALPHA,ICHI),ICHI=1,8),ANAME(16)         (B  82)
      READ (5,122)  (WLWT(ITUN,IALPHA),ANAME(17))                       (B  83)
      READ (5,122)  (ULWT(ITUN,IALPHA),ANAME(18))                       (B  84)
      READ (5,2022)                                                     (B  85)
      READ (5,2022)                                                     (B  86)
      READ (5,122)  (WLTT(ITUN,IALPHA),ANAME(19))                       (B  87)
      READ (5,122)  (ULTT(ITUN,IALPHA),ANAME(20))                       (B  88)
      READ (5,2022)                                                     (B  89)
      READ (5,2022)                                                     (B  90)
      READ (5,121)  (WLFP(ITUN,IALPHA,ICHI),ICHI=1,8),ANAME(21)         (B  91)
      READ (5,121)  (ULFP(ITUN,IALPHA,ICHI),ICHI=1,8),ANAME(22)         (B  92)
      READ (5,121)  (WDFP(ITUN,IALPHA,ICHI),ICHI=1,8),ANAME(23)         (B  93)
      READ (5,121)  (UDFP(ITUN,IALPHA,ICHI),ICHI=1,8),ANAME(24)         (B  94)
      READ (5,122)  (WLWP(ITUN,IALPHA),ANAME(25))                       (B  95)
      READ (5,122)  (ULWP(ITUN,IALPHA),ANAME(26))                       (B  96)
      READ (5,122)  (WDWP(ITUN,IALPHA),ANAME(27))                       (B  97)
      READ (5,122)  (UDWP(ITUN,IALPHA),ANAME(28))                       (B  98)
C
C       WRITE OUT INTERFERENCE FACTORS
C
      WRITE (6,123) (CHI(I),I=1,8)                                      (B  99)
      WRITE (6,123) (WLFF(ITUN,IALPHA,ICHI),ICHI=1,8),ANAME(1)          (B 100)
      WRITE (6,123) (ULFF(ITUN,IALPHA,ICHI),ICHI=1,8),ANAME(2)          (B 101)
      WRITE (6,123) (WDFF(ITUN,IALPHA,ICHI),ICHI=1,8),ANAME(3)          (B 102)
      WRITE (6,123) (UDFF(ITUN,IALPHA,ICHI),ICHI=1,8),ANAME(4)          (B 103)
      WRITE (6,124) (WLWF(ITUN,IALPHA),ANAME(5))                        (B 104)
      WRITE (6,124) (ULWF(ITUN,IALPHA),ANAME(6))                        (B 105)
      WRITE (6,124) (WLWW(ITUN,IALPHA),ANAME(7))                        (B 106)
      WRITE (6,124) (ULWW(ITUN,IALPHA),ANAME(8))                        (B 107)
      WRITE (6,123) (WLFW(ITUN,IALPHA,ICHI),ICHI=1,8),ANAME(9)          (B 108)
      WRITE (6,123) (ULFW(ITUN,IALPHA,ICHI),ICHI=1,8),ANAME(10)         (B 109)
```

```
      WRITE (6,123) (WDFW(ITUN,IALPHA,ICHI),ICHI=1,8),ANAME(11)              (B 110)
      WRITE (6,123) (UDFW(ITUN,IALPHA,ICHI),ICHI=1,8),ANAME(12)              (B 111)
      WRITE (6,123) (WLFT(ITUN,IALPHA,ICHI),ICHI=1,8),ANAME(13)              (B 112)
      WRITE (6,123) (ULFT(ITUN,IALPHA,ICHI),ICHI=1,8),ANAME(14)              (B 113)
      WRITE (6,123) (WDFT(ITUN,IALPHA,ICHI),ICHI=1,8),ANAME(15)              (B 114)
      WRITE (6,123) (UDFT(ITUN,IALPHA,ICHI),ICHI=1,8),ANAME(16)              (B 115)
      WRITE (6,124)  WLWT(ITUN,IALPHA),ANAME(17)                             (B 116)
      WRITE (6,124)  ULWT(ITUN,IALPHA),ANAME(18)                             (B 117)
      WRITE (6,124)  WLTT(ITUN,IALPHA),ANAME(19)                             (B 118)
      WRITE (6,124)  ULTT(ITUN,IALPHA),ANAME(20)                             (B 119)
      WRITE (6,123) (WLFP(ITUN,IALPHA,ICHI),ICHI=1,8),ANAME(21)              (B 120)
      WRITE (6,123) (ULFP(ITUN,IALPHA,ICHI),ICHI=1,8),ANAME(22)              (B 121)
      WRITE (6,123) (WDFP(ITUN,IALPHA,ICHI),ICHI=1,8),ANAME(23)              (B 122)
      WRITE (6,123) (UDFP(ITUN,IALPHA,ICHI),ICHI=1,8),ANAME(24)              (B 123)
      WRITE (6,124) (WLWP(ITUN,IALPHA),ANAME(25))                            (B 124)
      WRITE (6,124) (ULWP(ITUN,IALPHA),ANAME(26))                            (B 125)
      WRITE (6,124) (WDWP(ITUN,IALPHA),ANAME(27))                            (B 126)
      WRITE (6,124) (UDWP(ITUN,IALPHA),ANAME(28))                            (B 127)
      WRITE (6,2022)                                                         (B 128)
   20 CONTINUE                                                               (B 129)
      WRITE (6,110)                                                          (B 130)
      LINE=0                                                                 (B 131)
C
C        READ IN TEST DATA
C
    1 READ (5,100) IRUN,IRPM,ITUN,ITYPE,IFRAME,Q,BALDRAG,BALLIFT,SCLDRAG     (B 132)
     1   ,SCLLIFT,ALPHA,RPM,DENSITY                                          (B 133)
      IF (EOF,5)  998,2                                                      (B 134)
C
C        NOTE THAT PITOT MEASUREMENT OF TUNNEL VELOCITY IS CORRECTED ON
C        THE FIRST PASS THROUGH THE INTERFERENCE CALCULATIONS.  ON THE
C        SECOND PASS, THE LOADS ARE REDIVIDED ACCORDING TO THE CORRECTED
C        PITOT READING AND ALL THE CORRECTIONS ARE CALCULATED.
C
    2 ITRIP=1                                                                (B 135)
      AQ=Q                                                                   (B 136)
      I=1                                                                    (B 137)
      IF (ALPHA.GT.-6.)  I=2                                                 (B 138)
      IF (ALPHA.GT.-1.)  I=3                                                 (B 139)
      IF (ALPHA.GT.4.)  I=4                                                  (B 140)
      IF (ALPHA.GT.9.)  I=5                                                  (B 141)
      IF (ALPHA.GT.15.)  I=6                                                 (B 142)
      LINE=LINE+3                                                            (B 143)
      IF (LINE.LE.40)  GO TO 75                                              (B 144)
      LINE=0                                                                 (B 145)
      WRITE (6,110)                                                          (B 146)
C
C        SUBTRACT OUT WEIGHT TARES
C
   75 BALDRAG=BALDRAG-BDT(I)                                                 (B 147)
      BALLIFT=BALLIFT-BLT(I)                                                 (B 148)
      SCLLIFT=SCLLIFT-SLT(I)                                                 (B 149)
C
C        DIVISION OF FORCES BETWEEN WING, FANS, AND TAIL
C
      IF (ITYPE-2)  1,1,5                                                    (B 150)
    5 TL=SCLLIFT-BALLIFT*COS(ALPHA*RAD)+ BALDRAG*SIN(ALPHA*RAD)              (B 151)
      TD=SCLDRAG-BALLIFT*SIN(ALPHA*RAD)- BALDRAG*COS(ALPHA*RAD)              (B 152)
      FL=SCLLIFT-SLAT(ITUN,I)*Q*SW                                           (B 153)
      FD=SCLDRAG-SDAT(ITUN,I)*Q*SW                                           (B 154)
```

```
      CN=BALLIFT/(Q*ST)                                                  (B 155)
      CA=BALDRAG/(Q*ST)                                                  (B 156)
      IF (ITRIP.EQ.2)  GO TO 42                                          (B 157)
C
C      WRITE OUT UNCORRECTED DATA
C
      WRITE (6,111) JTUN(ITUN),IRUN,IFRAME,IRPM,ALPHA,Q,SCLLIFT,SCLDRAG,  (B 158)
     1 CN,CA,TL,TD,FL,FD                                                 (B 159)
      IF (IRPM.EQ.0 )  GO TO 1000                                        (B 160)
      IF (IRPM.EQ.8 )  TSTATIC=40.2                                      (B 161)
      IF (IRPM.EQ.10)  TSTATIC=66.3                                      (B 162)
      IF (IRPM.EQ.12)  TSTATIC=95.0                                      (B 163)
      QJ=TSTATIC/(2.*SF)                                                 (B 164)
      IF (Q.LE.0.)  Q=10E-10                                             (B 165)
      QOQJ=Q/QJ                                                          (B 166)
      VOVJ=SQRT(QOQJ)                                                    (B 167)
      VOVJUN=VOVJ                                                        (B 168)
      TOTS=(SCLLIFT/TSTATIC)*(0.002378/DENSITY)                          (B 169)
      DOL=(SCLDRAG-SDAT(ITUN,3)*Q*SW)/SCLLIFT                            (B 170)
      WRITE (6,1001)  QOQJ,VOVJ,TOTS,DOL                                 (B 171)
      RPM=1000.*FLOAT(IRPM)                                              (B 172)
      CL=SCLLIFT/(Q*SW)                                                  (B 173)
      ISIZE=3                                                            (B 174)
      IF (Q.LT.0.8)  Q=CL=CN=VOVJ=QOQJ=0.                                (B 175)
C
C      PUNCH CARDS FOR SUBSEQUENT PLOTTING OF UNCORRECTED DATA.
C
      PUNCH 2023,  IRUN,IFRAME,RPM,ALPHA,Q,SCLLIFT,CL,CN,QOQJ,VOVJ,DOL,  (B 176)
     1  TOTS,ITUN,ISIZE                                                  (B 177)
 1000 CONTINUE                                                           (B 178)
C
C      ELIMINATE STATIC THRUST POINTS FROM THE DATA TO BE CORRECTED.
C
      IF (Q.LE.0.8)  GO TO 1                                             (B 179)
C
C     CORRECT FOR SOLID BLOCKAGE
C
   42 QFAC=(1.0+EPSILON(ITUN))**2                                        (B 180)
      Q=AQ*QFAC                                                          (B 181)
      CLW=SLAT(ITUN,I)/QFAC                                              (B 182)
      CDW=SDAT(ITUN,I)/QFAC                                              (B 183)
      CDO=SDAT(ITUN,3)/QFAC                                              (B 184)
      CN=CN/QFAC                                                         (B 185)
      CA=CA/QFAC                                                         (B 186)
C
C      SOLVE MOMENTUM QUARTIC FOR SKEW ANGLE AND VELOCITY RATIO.
C
      XT=0.                                                              (B 187)
      DELTX=0.01                                                         (B 188)
      AX=-1.                                                             (B 189)
      IF (CL)  1,44,45                                                   (B 190)
   45 DOL=FD/FL                                                          (B 191)
      VWH=-SQRT(2.*Q*SF/FL)                                              (B 192)
   46 X=XT+DELTX                                                         (B 193)
      XT=X                                                               (B 194)
      IF (XT.GT.1.02)  GO TO 51                                          (B 195)
      IF (XT.LT.-0.01)  GO TO 52                                         (B 196)
      X=(1.0+DOL*DOL)*X*X*X*X+2.0*DOL*VWH*X*X*X+VWH*VWH*X*X-1.0          (B 197)
      IF (ABS(X).LT.0.000001)  GO TO 47                                  (B 198)
      IF (X/AX)  48,47,49                                                (B 199)
```

```
   48 DELTX=-0.5*DELTX                                                  (B 200)
   49 AX=X                                                              (B 201)
      GO TO 46                                                          (B 202)
   47 WWH=XT                                                            (B 203)
      VWO=VWH/WWH                                                       (B 204)
      TANCHI=-VWO-DOL                                                   (B 205)
      CHIM=ATAN(TANCHI)/RAD                                             (B 206)
      CHIEFF=45.0+CHIM/2.                                               (B 207)
      GO TO 53                                                          (B 208)
   44 CHIM=CHIEFF=90.                                                   (B 209)
      VWO=10E10                                                         (B 210)
      GO TO 53                                                          (B 211)
   51 WRITE (6,151)  IRUN, IFRAME                                       (B 212)
      GO TO 1                                                           (B 213)
   52 WRITE (6,152)  IRUN, IFRAME                                       (B 214)
      GO TO 1                                                           (B 215)
C
C       SELECT TABLES OF INTERFERENCE FACTORS FOR APPROPRIATE TUNNEL.
C
   53 DO 60  ICHI=1,8                                                   (B 216)
      CWLFP(ICHI)=WLFP(ITUN,I,ICHI)                                     (B 217)
      CULFP(ICHI)=ULFP(ITUN,I,ICHI)                                     (B 218)
      CWDFP(ICHI)=WDFP(ITUN,I,ICHI)                                     (B 219)
      CUDFP(ICHI)=UDFP(ITUN,I,ICHI)                                     (B 220)
      IF (ITRIP.EQ.1)  GO TO 60                                         (B 221)
      CWLFF(ICHI)=WLFF(ITUN,I,ICHI)                                     (B 222)
      CULFF(ICHI)=ULFF(ITUN,I,ICHI)                                     (B 223)
      CWDFF(ICHI)=WDFF(ITUN,I,ICHI)                                     (B 224)
      CUDFF(ICHI)=UDFF(ITUN,I,ICHI)                                     (B 225)
      CWLFW(ICHI)=WLFW(ITUN,I,ICHI)                                     (B 226)
      CULFW(ICHI)=ULFW(ITUN,I,ICHI)                                     (B 227)
      CWDFW(ICHI)=WDFW(ITUN,I,ICHI)                                     (B 228)
      CUDFW(ICHI)=UDFW(ITUN,I,ICHI)                                     (B 229)
      CWLFT(ICHI)=WLFT(ITUN,I,ICHI)                                     (B 230)
      CULFT(ICHI)=ULFT(ITUN,I,ICHI)                                     (B 231)
      CWDFT(ICHI)=WDFT(ITUN,I,ICHI)                                     (B 232)
   60 CUDFT(ICHI)=UDFT(ITUN,I,ICHI)                                     (B 233)
C
C       INTERPOLATE FOR CHI EFF IN TABLES OF INTERFERENCE FACTORS
C
      CALL DISCOT  (CHIEFF,CHIEFF,CHI,CWLFP,CWLFP,-030,8,0,DWLFP)       (B 234)
      CALL DISCOT  (CHIEFF,CHIEFF,CHI,CULFP,CULFP,-030,8,0,DULFP)       (B 235)
      CALL DISCOT  (CHIEFF,CHIEFF,CHI,CWDFP,CWDFP,-030,8,0,DWDFP)       (B 236)
      CALL DISCOT  (CHIEFF,CHIEFF,CHI,CUDFP,CUDFP,-030,8,0,DUDFP)       (B 237)
      IF (ITRIP.EQ.1)  GO TO 39                                         (B 238)
      CALL DISCOT (CHIEFF,CHIEFF,CHI,CWLFF,CWLFF,-030,8,0,DWLFF)        (B 239)
      CALL DISCOT (CHIEFF,CHIEFF,CHI,CULFF,CULFF,-030,8,0,DULFF)        (B 240)
      CALL DISCOT (CHIEFF,CHIEFF,CHI,CWDFF,CWDFF,-030,8,0,DWDFF)        (B 241)
      CALL DISCOT (CHIEFF,CHIEFF,CHI,CUDFF,CUDFF,-030,8,0,DUDFF)        (B 242)
      CALL DISCOT (CHIEFF,CHIEFF,CHI,CWLFW,CWLFW,-030,8,0,DWLFW)        (B 243)
      CALL DISCOT (CHIEFF,CHIEFF,CHI,CULFW,CULFW,-030,8,0,DULFW)        (B 244)
      CALL DISCOT (CHIEFF,CHIEFF,CHI,CWDFW,CWDFW,-030,8,0,DWDFW)        (B 245)
      CALL DISCOT (CHIEFF,CHIEFF,CHI,CUDFW,CUDFW,-030,8,0,DUDFW)        (B 246)
      CALL DISCOT (CHIEFF,CHIEFF,CHI,CWLFT,CWLFT,-030,8,0,DWLFT)        (B 247)
      CALL DISCOT (CHIEFF,CHIEFF,CHI,CULFT,CULFT,-030,8,0,DULFT)        (B 248)
      CALL DISCOT (CHIEFF,CHIEFF,CHI,CWDFT,CWDFT,-030,8,0,DWDFT)        (B 249)
      CALL DISCOT (CHIEFF,CHIEFF,CHI,CUDFT,CUDFT,-030,8,0,DUDFT)        (B 250)
```

```
C
C        CORRECT TUNNEL PITOT MEASUREMENT FOR WALL EFFECTS
C
   39 DWP=2.*DWLFP*SF/(AT(ITUN)*VWO)+2.*DWDFP*SF*DOL/(AT(ITUN)*VWO)        (B 251)
     1     +WLWP(ITUN,I)*CLW*(-0.25)*SW/AT(ITUN)                           (B 252)
      DUP=2.*DULFP*SF/(AT(ITUN)*VWO)+2.*DUDFP*SF*DOL/(AT(ITUN)*VWO)        (B 253)
     1     +ULWP(ITUN,I)*CLW*(-0.25)*SW/AT(ITUN)                           (B 254)
      DWP=DWP+WOVPIT(ITUN)                                                 (B 255)
      DUP=DUP+UOVPIT(ITUN)                                                 (B 256)
      QFACT=DWP*DWP+(1.+DUP)*(1.+DUP)                                      (B 257)
      IF (ITRIP.EQ.1)  QFACTOR=QFACT                                       (B 258)
      Q=AQ/QFACT                                                           (B 259)
      IF (ITRIP.EQ.2)  GO TO 40                                            (B 260)
      ITRIP=2                                                              (B 261)
      GO TO 5                                                              (B 262)
   40 VWO=VWO*SQRT(QFACTOR/QFACT)                                          (B 263)
      CLW=CLW*QFACT/QFACTOR                                                (B 264)
      CDO=CDO*QFACT/QFACTOR                                                (B 265)
      CN =CN *QFACT/QFACTOR                                                (B 266)
C
C        FIND INTERFERENCE VELOCITY RATIOS
C
      DWF=2.*DWLFF*SF/(AT(ITUN)*VWO)+2.*DWDFF*SF*DOL/(AT(ITUN)*VWO)        (B 267)
     1     +WLWF(ITUN,I)*CLW*SW*(-0.25)/AT(ITUN)                           (B 268)
      DUF=2.*DULFF*SF/(AT(ITUN)*VWO)+2.*DUDFF*SF*DOL/(AT(ITUN)*VWO)        (B 269)
     1     +ULWF(ITUN,I)*CLW*SW*(-0.25)/AT(ITUN)                           (B 270)
      DWW=2.*DWLFW*SF/(AT(ITUN)*VWO)+2.*DWDFW*SF*DOL/(AT(ITUN)*VWO)        (B 271)
     1     +WLWW(ITUN,I)*CLW*SW*(-0.25)/AT(ITUN)                           (B 272)
      DUW=2.*DULFW*SF/(AT(ITUN)*VWO)+2.*DUDFW*SF*DOL/(AT(ITUN)*VWO)        (B 273)
     1     +ULWW(ITUN,I)*CLW*SW*(-0.25)/AT(ITUN)                           (B 274)
      DWT=2.*DWLFT*SF/(AT(ITUN)*VWO)+2.*DWDFT*SF*DOL/(AT(ITUN)*VWO)        (B 275)
     1     +WLWT(ITUN,I)*CLW*SW*(-0.25)/AT(ITUN)                           (B 276)
     2      +WLTT(ITUN,I)*CN*ST*(-0.25)/AT(ITUN)                           (B 277)
      DUT=2.*DULFT*SF/(AT(ITUN)*VWO)+2.*DUDFT*SF*DOL/(AT(ITUN)*VWO)        (B 278)
     1     +ULWT(ITUN,I)*CLW*SW*(-0.25)/AT(ITUN)                           (B 279)
     2      +ULTT(ITUN,I)*CN*ST*(-0.25)/AT(ITUN)                           (B 280)
C
C        CALCULATE CORRECTIONS
C
      TANALPF=DWF/(1.+DUF)                                                 (B 281)
      TANALPW=DWW/(1.+DUW)                                                 (B 282)
      TANALPT=DWT/(1.+DUT)                                                 (B 283)
      DALPF=ATAN(TANALPF)/RAD                                              (B 284)
      DALPW=ATAN(TANALPW)/RAD                                              (B 285)
      DALPT=ATAN(TANALPT)/RAD                                              (B 286)
      QOQF=DWF*DWF+(1.+DUF)**2                                             (B 287)
      QOQW=DWW*DWW+(1.+DUW)**2                                             (B 288)
      QOQT=DWT*DWT+(1.+DUT)**2                                             (B 289)
      ALPCF=ALPHA+DALPF                                                    (B 290)
      ALPCW=ALPHA+DALPW                                                    (B 291)
      ALPTC=ALPHA+DALPT                                                    (B 292)
      QCF=Q*QOQF                                                           (B 293)
      QCW=Q*QOQW                                                           (B 294)
      QCT=Q*QOQT                                                           (B 295)
      SLIFTC=SCLLIFT*COS(DALPW*RAD)-(SCLDRAG-CDO*Q*SW)*SIN(DALPW*RAD)      (B 296)
      SDRAGC=SCLLIFT*SIN(DALPW*RAD)+(SCLDRAG-CDO*Q*SW)*COS(DALPW*RAD)      (B 297)
      CNTC=CN/QOQT                                                         (B 298)
```

```
C
C     ADJUST FOR DIFFERENCES IN CORRECTIONS AT WING, FANS, AND TAIL
C     ASSUME A TAIL EFFICIENCY FACTOR (QT/Q) OF 0.9
C
      DDALPT=DALPT-DALPW
      CNTCA=(CNTC-0.030*DDALPT*0.9)
      TOTL=SLIFTC        -CN*ST*Q  *COS(ALPHA*RAD)
     1    +CNTCA*QCW*ST*COS(ALPHA*RAD)
      CDIUN=CN*CN/(PI*2.40)
      CDIC=CNTCA*CNTCA/(PI*2.40)
      SDRAGC=SDRAGC-CDIUN*Q*ST+CDIC*QCW*ST
      DDAFW=DALPF-DALPW
      TSTATIC=40.2
      IF (IRPM.EQ.10)  TSTATIC=66.3
      IF (IRPM.EQ.12)  TSTATIC=95.0
      QJ=TSTATIC/(2.*SF)
      QOQJ=QCW/QJ
      QOQJF=QCF/QJ
      VOVJ=SQRT(QOQJ)
      VOVJF=SQRT(QOQJF)
      DVOVJ=VOVJF-VOVJ
      SA=SIN(ALPCW*RAD)
      CA=COS(ALPCW*RAD)
      TOTL=TOTL+TSTATIC*DDAFW*RAD*SA
      SDRAGC=SDRAGC-TSTATIC*(DVOVJ+DDAFW*RAD*CA)
      TOTDOL=SDRAGC/TOTL
C
C     STORE CORRECTED VALUES ON TAPE 1 AND CORRECTIONS ON TAPE 4
C
      WRITE (1)     ITUN ,IRUN,IFRAME,IRPM,ALPHA,Q,CHIM,DALPF,QOQF,
     1  DALPW,QOQW,DALPT,QOQT,QCW,ALPCW,CNTCA,TOTL,TOTDOL,DENSITY
      WRITE (4)  ITUN,IRUN,ALPHA,ALPCW,DALPW,DALPF,DALPT,QOQW,QOQF,
     1  QOQT,VOVJ,DVOVJ,VOVJUN
      GO TO 1
  998 ENDFILE 1
      REWIND 1
      ENDFILE 4
      REWIND 4
      WRITE (6,125)
C
C     WRITE OUT CORRECTED VALUES FROM TAPE 1
C
      LINE=0
      DO 61  K=1,1000
      READ (1)      ITUN ,IRUN,IFRAME,IRPM,ALPHA,Q,CHIM,DALPF,QOQF,
     1  DALPW,QOQW,DALPT,QOQT,QCW,ALPCW,CNTCA,TOTL,TOTDOL,DENSITY
      IF (EOF,1)  999,62
   62 WRITE (6,126) JTUN(ITUN),IRUN,IFRAME,IRPM,ALPHA,Q,CHIM,DALPF,
     1  QOQF,DALPW,QOQW,DALPT,QOQT,QCW,ALPCW,CNTCA,TOTL
C
C     NONDIMENSIONALIZE CORRECTED VALUES.
C
      IF (IRPM.EQ.0 )  GO TO 1002
      IF (IRPM.EQ.8 )  TSTATIC=40.2
      IF (IRPM.EQ.10)  TSTATIC=66.3
      IF (IRPM.EQ.12)  TSTATIC=95.0
      QJ=TSTATIC/(2.*SF)
      QOQJ=QCW/QJ
      VOVJ=SQRT(QOQJ)
      TOTS=(TOTL/TSTATIC)*(0.002378/DENSITY)
```

```
      WRITE (6,1001)  QOQJ,VOVJ,TOTS,TOTDOL
C
C      STORE CORRECTED NONDIMENSIONAL VALUES ON TAPE 3
C
      WRITE (3) ITUN,IRUN,IRPM,ALPHA,Q,DALPW,QOQW,QCW,ALPCW,CNTCA,TOTL,
     1 QOQJ,VOVJ,TOTS,TOTDOL
      LINE=LINE+3
 1002 CONTINUE
      IF (LINE.LT.40)  GO TO 61
      LINE=0
      WRITE (6,125)
   61 CONTINUE
  999 ENDFILE 3
      REWIND 3
C
C      INTERPOLATE DATA ON TAPE 3 TO OBTAIN CORRECTED VALUES AT FIXED
C      CORRECTED ANGLES OF ATTACK.
C
      WRITE (6,2020)
      LINE=0
 2003 DO 2001  I=1,6
      READ (3)  ITUN,IRUN,IRPM,TALP(I),TQ(I),TDALPW(I),TQOQW(I),TQC(I),
     1 TALPC(I),TCNC(I),TLIFT(I),TQOQJ(I),TVOVJ(I),TLOTS(I),TDOL(I)
      IF (EOF,3) 9999,2001
 2001 CONTINUE
      DO 2002  I=1,5
      IF (I.EQ.1.AND.TALPC(1).GT.-4.5)  GO TO 2002
      IF (I.EQ.1.AND.TALPC(1).GT.-4.5)  LINE=LINE+1
      AA=A(I)
      CALL DISCOT (AA,AA,TALPC,TALP,TALP,-010,6,0,AUN)
      CALL DISCOT (AA,AA,TALPC,TQ,TQ,-010,6,0,QUN)
      CALL DISCOT (AA,AA,TALPC,TDALPW,TDALPW,-010,6,0,DALW)
      CALL DISCOT (AA,AA,TALPC,TQOQW,TQOQW,-010,6,0,QOQ)
      CALL DISCOT (AA,AA,TALPC,TQC,TQC,-010,6,0,QC)
      CALL DISCOT (AA,AA,TALPC,TCNC,TCNC,-010,6,0,CNC)
      CALL DISCOT (AA,AA,TALPC,TLIFT,TLIFT,-010,6,0,TLFT)
      CALL DISCOT (AA,AA,TALPC,TQOQJ,TQOQJ,-010,6,0,QOQJ)
      CALL DISCOT (AA,AA,TALPC,TVOVJ,TVOVJ,-010,6,0,VOVJ)
      CALL DISCOT (AA,AA,TALPC,TLOTS,TLOTS,-010,6,0,LOTS)
      CALL DISCOT (AA,AA,TALPC,TDOL,TDOL,-010,6,0,DL)
      DOTS=DL*LOTS
C
C      WRITE OUT, AND PUNCH FOR SUBSEQUENT PLOTTING, THE CORRECTED
C      NONDIMENSIONAL VALUES.
C
      WRITE (6,2021)  JTUN(ITUN),IRUN,IRPM,AA,QC,QOQJ,VOVJ,TLFT,LOTS,
     1 CNC,DL,DOTS,AUN,QUN,DALW,QOQ
      RPM=1000.*FLOAT(IRPM)
      CL=TLFT/(QC*SW)
      ISIZE=1
      PUNCH 2023,   IRUN,IRUN,RPM,AA,QC,TLFT,CL,CNC,QOQJ,VOVJ,DL,LOTS,
     1 ITUN,ISIZE
      LINE=LINE+1
      IF (LINE.LT.35)  GO TO 2002
      LINE=0
      WRITE (6,2020)
 2002 CONTINUE
      WRITE (6,2022)
      GO TO 2003
 9999 WRITE (6,3000)
```

```
      WRITE (6,3008)                                                   (B 395)
      ICOR=1                                                           (B 396)
      LINE=0                                                           (B 397)
C
C       INTERPOLATE DATA ON TAPE 4 TO OBTAIN VALUES OF CORRECTION ANGLES
C       AND VELOCITY RATIOS AT FIXED CORRECTEC ANGLES OF ATTACK.
C
 3003 DO 3001  I=1,6                                                   (B 398)
      READ (4) ITUN,IRUN,TALP(I),TALPC(I),TDALPW(I),TDALPF(I),TDALPT(I), (B 399)
     1 TQOQW(I),TQOQF(I),TQOQT(I),TVOVJ(I),TDVOVJ(I),VOVJUN            (B 400)
      IF (EOF,4)  3002,3001                                            (B 401)
 3001 CONTINUE                                                         (B 402)
      DO 3004  I=1,5                                                   (B 403)
      AA=A(I)                                                          (B 404)
      CALL DISCOT (AA,AA,TALPC,TALP,TALP,-010,6,0,AUN)                 (B 405)
      CALL DISCOT (AA,AA,TALPC,TDALPW,TDALPW,-010,6,0,DALW)            (B 406)
      CALL DISCOT (AA,AA,TALPC,TDALPF,TDALPF,-010,6,0,DALF)            (B 407)
      CALL DISCOT (AA,AA,TALPC,TDALPT,TDALPT,-010,6,0,DALT)            (B 408)
      CALL DISCOT (AA,AA,TALPC,TQOQW,TQOQW,-010,6,0,TQW)               (B 409)
      CALL DISCOT (AA,AA,TALPC,TQOQF,TQOQF,-010,6,0,TQF)               (B 410)
      CALL DISCOT (AA,AA,TALPC,TQOQT,TQOQT,-010,6,0,TQT)               (B 411)
      CALL DISCOT (AA,AA,TALPC,TVOVJ,TVOVJ,-010,6,0,VOVJ)              (B 412)
      CALL DISCOT (AA,AA,TALPC,TDVOVJ,TDVOVJ,-010,6,0,DVOVJ)           (B 413)
      DIT=DALT-DALW                                                    (B 414)
      DIF=DALF-DALW                                                    (B 415)
      QTOQC=TQT/TQW                                                    (B 416)
      QFOQC=TQF/TQW                                                    (B 417)
      LINE=LINE+1                                                      (B 418)
C
C       WRITE OUT, AND PUNCH FOR SUBSEQUENT PLOTTING, THE CORRECTION
C       ANGLES AND VELOCITY RATIOS.
C
      WRITE (6,3005)  JTUN(ITUN),IRUN,AA,AUN,VOVJ,DALW,DIT,DIF,TQW,    (B 419)
     1  QTOQC,QFOQC,DVOVJ                                              (B 420)
      PUNCH 3006,  IRUN,AA,VOVJ,DALW,DIT,DIF,TQW,QTOQC,QFOQC,DVOVJ,    (B 421)
     1  ITUN,ICOR                                                      (B 422)
 3004 CONTINUE                                                         (B 423)
      WRITE (6,3007)                                                   (B 424)
      LINE=LINE+1                                                      (B 425)
      IF (LINE.LT.36)  GO TO 3003                                      (B 426)
      GO TO 9999                                                       (B 427)
C
C       WRITE OUT, AND PUNCH FOR SUBSEQUENT PLOTTING, THE CORRECTION
C       ANGLES AND VELOCITY RATIOS IN THE UNCORRECTED DATA.
C
 3002 REWIND 4                                                         (B 428)
      ICOR=3                                                           (B 429)
 3011 WRITE (6,3009)                                                   (B 430)
      WRITE (6,3008)                                                   (B 431)
      LINE=0                                                           (B 432)
 3014 DO 3010  I=1,6                                                   (B 433)
      PEAD (4)  ITUN,IRUN,ALPHA,ALPCW,DALPW,DALPF,DALPT,QOQW,QOQF,     (B 434)
     1  QOQT,VOVJ,DVOVJ,VOVJUN                                         (B 435)
      IF (EOF,4)  3012,3013                                            (B 436)
 3013 DIT=DALPT-DALPW                                                  (B 437)
      DIF=DALPF-DALPW                                                  (B 438)
      QTOQC=QOQT/QOQW                                                  (B 439)
      QFOQC=QOQF/QOQW                                                  (B 440)
```

```
      LINE=LINE+1
      WRITE (6,3005)  JTUN(ITUN),IRUN,ALPCW,ALPHA,VOVJ,DALPW,DIT,DIF,
     1  QOQW,QTOQC,QFOQC,DVOVJ
      PUNCH 3006,   IRUN,ALPHA,VOVJUN,DALPW,DIT,DIF,QOQW,QTOQC,QFOQC,
     1  DVOVJ,ITUN,ICOR
 3010 CONTINUE
      WRITE (6,3007)
      LINE=LINE+1
      IF (LINE.LT.35)  GO TO 3014
      GO TO 3011
 3012 STOP
C
C       FORMATS
C
  100 FORMAT (2I2,2I1,I4,F5.2,5F6.2,F7.1,F8.6)
  110 FORMAT (1H1/  37X*FAN-IN-WING TESTS IN AMES 7X10 TUNNEL (AARL TEST
     1 NO. 6)*//4X*TUNNEL   RUN FRAME    RPM*5X*ALPHA*4X*Q*6X*L*8X*D*
     2 5X*CN(T)   CA(T)*4X*L(WB)*4X*D(WB)*5X*L(F)*5X*D(F)*2X/)
  111 FORMAT (2X,A10,2X,I2,I6,I4*,000*F7.1,F7.2,2F9.3,2F8.4,4F9.3,F8.2)
  120 FORMAT (1H1//30X*INTERFERENCE FACTORS*)
  121 FORMAT (8F7.4,16X,A8)
  122 FORMAT (49X,F7.4,16X,A8)
  123 FORMAT (8F10.4,5X,A10)
  124 FORMAT (70X,F10.4,5X,A10)
  125 FORMAT (1H1//50X*CORRECTED DATA*//4X*TUNNEL   RUN FRAME    RPM*5X
     1 *ALPHA*4X*Q*3X*CHI  DALPF   QOQF  DALPW   QOQW  DALPT   QOQT*
     2     4X*QCW  ALPC(W)*4X*CNTC    TOT L*/)
  126 FORMAT (2X,A10,I4,I6,I4*,000*F7.1,2F7.2,3(F7.2,F7.4)
     1     ,F7.2,F8.2,F9.4,F8.2)
  127 FORMAT (//35X,A10//)
  151 FORMAT (10X*RUN *I2*, FRAME *I4* FAILS, WWH TOO GREAT*)
  152 FORMAT (10X*RUN *I2*, FRAME *I4* FAILS, WWH TOO SMALL*)
  153 FORMAT (20X*CHI =*F6.2*, CHI E =*F6.2*, V/WO =*F8.2*, D/L =*F8.4)
 1001 FORMAT (10X*Q/QJ = *F8.4*, V/VJ = *F8.4 *, L/TS = *F8.4*, D/L = *
     1  F6.3/)
 2020 FORMAT (1H1//49X*INTERPOLATED CORRECTED VALUES*//12X*TUNNEL*5X*RUN
     1*2X*RPM*2X*ALPHA C*3X*QC*3X*Q/QJ*2X*V/VJ*2X*LIFT*4X*L/TS*3X*CNTC*
     23X*D/L*3X*D/TS*2X*ALPHA*4X*Q*4X*D ALP*2X*QC/Q*/)
 2021 FORMAT (10X,A10,I6,I3*000*2F7.2,2F6.4,F7.2,2F7.3,F6.3,F7.3,F6.2,
     1  2F7.2,F8.4)
 2022 FORMAT ()
 2023 FORMAT (I3,I4,F5.0,3F6.2,2F7.4,4F6.4,2I1)
 2024 FORMAT (A8)
 2025 FORMAT (/30X,A8* WING LOADING*)
 3000 FORMAT (1H1//43X*CORRECTICNS ACCORDING TO CORRECTED ALPHAS*/)
 3005 FORMAT (4X,A10,I7,2F10.2,F10.4,3F10.2,4F10.4)
 3006 FORMAT (I3,9F8.4,2I1)
 3007 FORMAT ()
 3008 FORMAT (6X*TUNNEL*6X*RUN*4X*ALPHAC*4X*ALPHAU*6X*V/VJ*4X*D ALPW*
     1 6X*D IT*6X*D IF*5X*QC/QW*5X*QT/QC*5X*QF/QC*3X*D VF/VJ*/)
 3009 FORMAT (1H1//42X*CORRECTIONS ACCORDING TO UNCORRECTED ALPHAS*/)
      END
```

```
      SUBROUTINE DISCOT (XA,ZA,TABX,TABY,TABZ,NC,NY,NZ,ANS)
      DIMENSION TABX(2),TABY(2),TABZ(2)
      DIMENSION NPX(8),NPY(8),YY(8)
      CALL UNS (NC,IA,IDX,IDZ,IMS)
      IF (NZ-1)   5,5,10
    5 CALL DISSER (XA,TABX(1),1,NY,IDX,NN)
      NNN=IDX+1
      CALL LAGRAN (XA,TABX(NN),TABY(NN),NNN,ANS)
      GOTO 70
   10 ZARG=ZA
      IP1X=IDX+1
      IP1Z=IDZ+1
      IF (IA)   15,25,15
   15 IF (ZARG-TABZ(NZ))   25,25,20
   20 ZARG=TABZ(NZ)
   25 CALL DISSER (ZARG,TABZ(1),1,NZ,IDZ,NPZ)
      NX=NY/NZ
      NPZL=NPZ+IDZ
      I=1
      IF (IMS)   30,30,40
   30 CALL DISSER (XA,TABX(1),1,NX,IDX,NPX(1))
      DO 35 JJ=NPZ,NPZL
      NPY(I)=(JJ-1)*NX+NPX(1)
      NPX(I)=NPX(1)
   35 I=I+1
      GOTO 50
   40 DO 45 JJ=NPZ,NPZL
      IS=(JJ-1)*NX+1
      CALL DISSER (XA,TABX(1),IS,NX,IDX,NPX(I))
      NPY(I)=NPX(I)
   45 I=I+1
   50 DO 55 LL=1,IP1Z
      NLOC=NPX(LL)
      NLOCY=NPY(LL)
   55 CALL LAGRAN(XA,TABX(NLOC),TABY(NLOCY),IP1X,YY(LL))
      CALL LAGRAN (ZARG,TABZ(NPZ),YY(1),IP1Z,ANS)
   70 RETURN
      END


      SUBROUTINE UNS (IC,IA,IDX,IDZ,IMS)
      IF (IC)   5,5,10
    5 IMS=1
      NC=-IC
      GOTO 15
   10 IMS=0
      NC=IC
   15 IF (NC-100)   20,25,25
   20 IA=0
      GOTO 30
   25 IA=1
      NC=NC-100
   30 IDX=NC/10
      IDZ=NC-IDX*10
      RETURN
      END
```

APPENDIX B

```
      SUBROUTINE DISSER (XA,TAB,I,NX,ID,NPX)
      DIMENSION TAB(2)
      NPT=ID+1
      NPB=NPT/2
      NPU=NPT-NPB
      IF (NX-NPT)   10,5,10
    5 NPX=I
      RETURN
   10 NLOW=I+NPB
      NUPP=I+NX-(NPU+1)
      DO 15 II=NLOW,NUPP
      NLOC=II
      IF (TAB(II)-XA)   15,20,20
   15 CONTINUE
      NPX=NUPP-NPB+1
      RETURN
   20 NL=NLOC-NPB
      NU=NL+ID
      DO 25 JJ=NL,NU
      NDIS=JJ
      IF (TAB(JJ)-TAB(JJ+1))   25,30,25
   25 CONTINUE
      NPX=NL
      RETURN
   30 IF (TAB(NDIS)-XA)   40,35,35
   35 NPX=NDIS-ID
      RETURN
   40 NPX=NDIS+1
      RETURN
      END
```

```
      SUBROUTINE LAGRAN (XA,X,Y,N,ANS)
      DIMENSION X(2),Y(2)
      SUM=0.0
      DO 3 I=1,N
      PROD=Y(I)
      DO 2 J=1,N
      A=X(I)-X(J)
      IF (A)   1,2,1
    1 B=(XA-X(J))/A
      PROD=PROD*B
    2 CONTINUE
    3 SUM=SUM+PROD
      ANS=SUM
      RETURN
      END
```

APPENDIX B

INTERFERENCE FACTORS

ELLIPTIC WING LOADING

2-1 ROUND

ALPHA = -10

20.0000	30.0000	40.0000	50.0000	60.0000	70.0000	80.0000	90.0000	CHI
-1.0118	-.8363	-.6547	-.5091	-.4268	-.4055	-.4103	-.4063	-101WLFF
.3881	.4843	.4934	.4245	.3048	.1654	.0271	-.0776	-101ULFF
-.7516	-.5460	-.3678	-.2319	-.1354	-.0619	.0069	.0776	-101WDFF
.0556	.1213	.1216	.0855	.0416	.0091	-.0046	0.0000	-101UDFF
							-.6552	-101WLWF
							-.0592	-101ULWF
							-.5024	-101WLWW
							-.0383	-101ULWW
-.7751	-.5925	-.4447	-.3449	-.2951	-.2843	-.2873	-.2821	-101WLFW
.4994	.5029	.4490	.3578	.2483	.1350	.0260	-.0508	-101ULFW
-.5651	-.3865	-.2553	-.1644	-.1011	-.0510	-.0027	.0469	-101WDFW
.3149	.3108	.2749	.2303	.1914	.1655	.1542	.1563	-101UDFW
-.4772	-.6266	-.7998	-.9492	-.9402	-.8037	-.8332	-.9208	-101WLFT
-.2087	-.1603	-.0490	.1622	.4217	.4299	.1956	-.0264	-101ULFT
-.4997	-.5371	-.5528	-.5183	-.3967	-.2341	-.1020	.0437	-101WDFT
-.8894	-.8167	-.7219	-.6086	-.5218	-.5373	-.5874	-.6020	-101UDFT
							-1.1440	-101WLWT
							.0035	-101ULWT
							-.5791	-101WLTT
							-.4450	-101ULTT
-.0338	-.0327	-.0322	-.0324	-.0329	-.0335	-.0335	-.0339	-101WLFP
-.0428	-.0408	-.0397	-.0394	-.0395	-.0395	-.0370	-.0083	-101ULFP
-.0910	-.0812	-.0729	-.0657	-.0591	-.0526	-.0466	-.0405	-101WDFP
.8766	.8740	.8715	.8694	.8677	.8668	.8666	.8674	-101UDFP
							-.0684	-101WLWP
							-.0408	-101ULWP
							-.0493	-101WDWP
							1.1376	-101UDWP

ALPHA = -5

20.0000	30.0000	40.0000	50.0000	60.0000	70.0000	80.0000	90.0000	CHI
-1.0023	-.8370	-.6550	-.5092	-.4270	-.4059	-.4107	-.4064	-51WLFF
.3865	.4835	.4929	.4238	.3037	.1642	.0258	-.0788	-51ULFF
-.7506	-.5452	-.3667	-.2307	-.1342	-.0608	.0081	.0788	-51WDFF
.0537	.1212	.1208	.0848	.0410	.0087	-.0048	0.0000	-51UDFF
							-.6602	-51WLWF
							-.0758	-51ULWF
							-.5048	-51WLWW
							-.0688	-51ULWW
-.7623	-.5879	-.4451	-.3475	-.2978	-.2860	-.2876	-.2811	-51WLFW
.4752	.4811	.4311	.3435	.2363	.1237	.0146	-.0620	-51ULFW
-.5397	-.3676	-.2399	-.1504	-.0875	-.0376	.0106	.0600	-51WDFW
.2954	.2959	.2647	.2240	.1879	.1641	.1548	.1588	-51UDFW
-.5010	-.6778	-.8915	-1.0795	-1.0384	-.8222	-.8215	-.8819	-51WLFT
-.2785	-.2400	-.1262	.1221	.4447	.4445	.2019	-.0140	-51ULFT
-.5362	-.5918	-.6258	-.5992	-.4545	-.2621	-.1215	.0225	-51WDFT
-.9360	-.8614	-.7557	-.6181	-.5066	-.5245	-.5773	-.5932	-51UDWT
							-1.1188	-51WLWT
							.0084	-51ULWT
							-.4932	-51WLTT
							-.2463	-51ULTT
-.0335	-.0323	-.0318	-.0319	-.0325	-.0331	-.0330	-.0334	-51WLFP
-.0403	-.0403	-.0392	-.0389	-.0390	-.0389	-.0363	-.0076	-51ULFP
-.0903	-.0805	-.0724	-.0653	-.0588	-.0525	-.0464	-.0404	-51WDFP
.8764	.8737	.8711	.8689	.8672	.8661	.8659	.8665	-51UDFP
							-.0673	-51WLWP
							-.0394	-51ULWP
							-.0492	-51WDWP
							1.1361	-51UDWP

APPENDIX B

ALPHA = 0

20.0000	30.0000	40.0000	50.0000	60.0000	70.0000	80.0000	90.0000	CHI
-.9887	-.8382	-.6555	-.5093	-.4270	-.4061	-.4108	-.4065	01WLFF
.3858	.4837	.4933	.4238	.3035	.1638	.0254	-.0792	01ULFF
-.7513	-.5455	-.3666	-.2304	-.1338	-.0604	.0084	.0792	01WDFF
.0529	.1201	.1208	.0847	.0388	.0086	-.0048	0.0000	01UDFF
							-.6642	01WLWF
							-.0917	01ULWF
							-.5079	01WLWW
							-.0990	01ULWW
-.7520	-.5851	-.4468	-.3509	-.3011	-.2884	-.2887	-.2808	01WLFW
.4528	.4611	.4150	.3307	.2255	.1133	.0040	-.0727	01ULFW
-.5171	-.3507	-.2259	-.1376	-.0749	-.0249	.0233	.0727	01WDFW
.2763	.2812	.2545	.2173	.1838	.1620	.1544	.1603	01UDFW
-.5261	-.7369	-1.0049	-1.2490	-1.1605	-.8497	-.8191	-.8525	01WLFT
-.3580	-.3335	-.2187	.0809	.4898	.4662	.2108	-.0015	01ULFT
-.5773	-.6556	-.7143	-.7000	-.5229	-.2936	-.1424	.0015	01WDFT
-.9922	-.9170	-.7994	-.6298	-.4860	-.5115	-.5686	-.5861	01UDFT
							-1.0952	01WLWT
							.0132	01ULWT
							-.4489	01WLTT
							-.0934	01ULTT
-.0330	-.0319	-.0314	-.0315	-.0320	-.0326	-.0325	-.0328	01WLFP
-.0417	-.0397	-.0387	-.0383	-.0384	-.0383	-.0357	-.0070	01ULFP
-.0895	-.0799	-.0719	-.0648	-.0584	-.0523	-.0462	-.0404	01WDFP
.8761	.8733	.8707	.8683	.8665	.8654	.8651	.8656	01UDFP
							-.0662	01WLWP
							-.0382	01ULWP
							-.0492	01WDWP
							1.1345	01UDWP

ALPHA = 5

20.0000	30.0000	40.0000	50.0000	60.0000	70.0000	80.0000	90.0000	CHI
-1.0162	-.8400	-.6562	-.5093	-.4570	-.4060	-.4108	-.4064	51WLFF
.3860	.4849	.4947	.4248	.3040	.1642	.0258	-.0788	51ULFF
-.7536	-.5471	-.3675	-.2308	-.1343	-.0608	.0080	.0788	51WDFF
.0532	.1210	.1217	.0852	.0411	.0087	-.0048	0.0000	51UDFF
							-.6671	51WLWF
							-.1069	51ULWF
							-.5117	51WLWW
							-.1287	51ULWW
-.7442	-.5840	-.4496	-.3552	-.3051	-.2914	-.2905	-.2815	51WLFW
.4320	.4430	.4005	.3194	.2159	.1040	-.0058	-.0828	51ULFW
-.4972	-.3359	-.2135	-.1259	-.0633	-.0131	.0352	.0847	51WDFW
.2574	.2666	.2441	.2102	.1790	.1590	.1530	.1606	51UDFW
-.5518	-.8048	-1.1464	-1.4726	-1.3066	-.8848	-.8254	-.8320	51WLFT
-.4506	-.4467	-.3341	.0381	.5656	.4948	.2226	.0113	51ULFT
-.6235	-.7301	-.8227	-.8280	-.6030	-.3286	-.1652	-.0198	51WDFT
-1.0606	-.9872	-.8567	-.6434	-.4570	-.4979	-.5610	-.5807	51UDFT
							-1.0729	51WLWT
							.0181	51ULWT
							-.4369	51WLTT
							.0409	51ULTT
-.0326	-.0314	-.0309	-.0310	-.0315	-.0321	-.0319	-.0323	51WLFP
-.0411	-.0391	-.0381	-.0377	-.0378	-.0376	-.0351	-.0063	51ULFP
-.0888	-.0793	-.0714	-.0645	-.0582	-.0521	-.0461	-.0404	51WDFP
.8758	.8729	.8701	.8677	.8658	.8646	.8642	.8646	51UDFP
							-.0652	51WLWP
							-.0369	51ULWP
							-.0493	51WDWP
							1.1328	51UDWP

APPENDIX B

ALPHA = 10

20.0000	30.0000	40.0000	50.0000	60.0000	70.0000	80.0000	90.0000	CHI
-1.0196	-.8422	-.6569	-.5092	-.4266	-.4056	-.4105	-.4063	101WLFF
.3871	.4872	.4971	.4266	.3053	.1654	.0270	-.0776	101ULFF
-.6830	-.5499	-.3692	-.2321	-.1355	-.0620	.0068	.0776	101WDFF
.0546	.1229	.1233	.0863	.0417	.0091	-.0046	0.0000	101UDFF
							-.6687	101WLWF
							-.1213	101ULWF
							-.5160	101WLWW
							-.1579	101ULWW
-.7385	-.5844	-.4535	-.3602	-.3098	-.2950	-.2931	-.2829	101WLFW
.4129	.4265	.3877	.3096	.2076	.0957	-.0147	-.0922	101ULFW
-.4800	-.3230	-.2026	-.1155	-.0527	-.0023	.0464	.0962	101WDFW
.2389	.2522	.2336	.2027	.1736	.1551	.1506	.1598	101UDFW
-.5771	-.8825	-1.3255	-1.7749	-1.4724	-.9266	-.8399	-.8202	101WLFT
-.5604	-.5871	-.4841	-.0044	.6840	.5301	.2378	.0247	101ULFT
-.6750	-.8173	-.9576	-.9946	-.6948	-.3680	-.1904	-.0420	101WDFT
-1.1445	-1.0768	-.9333	-.6581	-.4158	-.4837	-.5545	-.5769	101UDFT
							-1.0523	101WLWT
							.0234	101ULWT
							-.4547	101WLTT
							.1767	101ULTT
-.0321	-.0309	-.0305	-.0306	-.0311	-.0316	-.0314	-.0318	101WLFP
-.0404	-.0385	-.0374	-.0371	-.0372	-.0370	-.0344	-.0057	101ULFP
-.0881	-.0787	-.0709	-.0641	-.0579	-.0520	-.0461	-.0404	101WDFP
.8753	.8723	.8695	.8670	.8651	.8638	.8633	.8636	101UDFP
							-.0642	101WLWP
							-.0358	101ULWP
							-.0495	101WDWP
							1.1311	101UDWP

ALPHA = 16

20.0000	30.0000	40.0000	50.0000	60.0000	70.0000	80.0000	90.0000	CHI
-1.0249	-.8454	-.6581	-.5090	-.4260	-.4050	-.4100	-.4060	161WLFF
.3896	.4912	.5011	.4299	.3080	.1678	.0296	-.0751	161ULFF
-.7639	-.5547	-.3726	-.2348	-.1379	-.0644	.0044	.0751	161WDFF
.0578	.1265	.1263	.0883	.0427	.0100	-.0042	0.0000	161UDFF
							-.6689	161WLWF
							-.1374	161ULWF
							-.5219	161WLWW
							-.1919	161ULWW
-.7344	-.5869	-.4596	-.3672	-.3161	-.3002	-.2971	-.2858	161WLFW
.3921	.4091	.3745	.2998	.1994	.0873	-.0241	-.1026	161ULFW
-.4629	-.3104	-.1918	-.1049	-.0416	.0094	.0586	.1089	161WDFW
.2170	.2350	.2208	.1931	.1662	.1492	.1463	.1572	161UDFW
-.6040	-.9897	-1.6116	-2.3032	-1.6787	-.9850	-.8686	-.8179	161WLFT
-.7229	-.8075	-.7369	-.0439	.9005	.5804	.2609	.0421	161ULFT
-.7436	-.9418	-1.1686	-1.2737	-.8174	-.4212	-.2246	-.0707	161WDFT
-1.2716	-1.2202	-1.0644	-.6723	-.3438	-.4657	-.5481	-.5747	161UDFT
							-1.0308	161WLWT
							.0306	161ULWT
							-.5208	161WLTT
							.3715	161ULTT
-.0315	-.0304	-.0299	-.0300	-.0305	-.0310	-.0308	-.0312	161WLFP
-.0396	-.0377	-.0367	-.0363	-.0364	-.0362	-.0337	-.0051	161ULFP
-.0873	-.0781	-.0705	-.0638	-.0577	-.0519	-.0461	-.0405	161WDFP
.8746	.8716	.8686	.8661	.8640	.8627	.8621	.8622	161UDFP
							-.0630	161WLWP
							-.0345	161ULWP
							-.0498	161WDWP
							1.1288	161UDWP

APPENDIX B

2-1 RECT.

ALPHA = -10

20.0000	30.0000	40.0000	50.0000	60.0000	70.0000	80.0000	90.0000	CHI
-1.1143	-.9164	-.7110	-.5449	-.4485	-.4196	-.4207	-.4160	-102WLFF
.4351	.5430	.5535	.4768	.3431	.1876	.0330	-.0862	-102ULFF
-.8233	-.5931	-.3939	-.2426	-.1365	-.0577	.0138	.0862	-102WDFF
.1121	.1757	.1666	.1173	.0598	.0162	-.0038	0.0000	-102UDFF
							-.6718	-102WLWF
							-.0650	-102ULWF
							-.5064	-102WLWW
							-.0430	-102ULWW
-.8488	-.6433	-.4761	-.3620	-.3030	-.2872	-.2877	-.2820	-102WLFW
.5600	.5641	.5039	.4020	.2795	.1528	.0306	-.0574	-102ULFW
-.6131	-.4137	-.2679	-.1678	-.0993	-.0469	.0020	.0515	-102WDFW
.3806	.3654	.3157	.2571	.2060	.1709	.1545	.1561	-102UDFW
-.5264	-.6925	-.8845	-1.0485	-1.0325	-.8689	-.8874	-.9808	-102WLFT
-.2366	-.1826	-.0583	.1779	.4686	.4794	.2213	-.0276	-102ULFT
-.5531	-.5940	-.6104	-.5705	-.4328	-.2498	-.1047	.0504	-102WDFT
-.9040	-.8245	-.7202	-.5956	-.5015	-.5234	-.5853	-.6042	-102UDFT
							-1.2103	-102WLWT
							.0055	-102ULWT
							-.6270	-102WLTT
							-.4956	-102ULTT
-.0362	-.0349	-.0344	-.0345	-.0350	-.0357	-.0356	-.0363	-102WLFP
-.0465	-.0443	-.0431	-.0426	-.0427	-.0425	-.0399	-.0093	-102ULFP
-.0973	-.0866	-.0777	-.0699	-.0629	-.0561	-.0495	-.0431	-102WDFP
.9045	.9003	.8967	.8937	.8915	.8903	.8904	.8916	-102UDFP
							-.0733	-102WLWP
							-.0448	-102ULWP
							-.0524	-102WDWP
							1.1750	-102UDWP

ALPHA = -5

20.0000	30.0000	40.0000	50.0000	60.0000	70.0000	80.0000	90.0000	CHI
-1.1147	-.9171	-.7112	-.5450	-.4487	-.4284	-.4210	-.4161	-52WLFF
.4333	.5451	.5529	.4759	.3419	.1863	.0317	-.0875	-52ULFF
-.8223	-.5922	-.3926	-.2413	-.1352	-.0564	.0151	.0875	-52WDFF
.1100	.1745	.1658	.1165	.0591	.0156	-.0041	0.0000	-52UDFF
							-.6775	-52WLWF
							-.0837	-52ULWF
							-.5096	-52WLWW
							-.0764	-52ULWW
-.8346	-.6383	-.4768	-.3651	-.3062	-.2893	-.2883	-.2811	-52WLFW
.5332	.5399	.4842	.3863	.2665	.1407	.0185	-.0693	-52ULFW
-.5847	-.3926	-.2507	-.1522	-.0842	-.0319	.0169	.0663	-52WDFW
.3585	.3486	.3042	.2500	.2020	.1693	.1551	.1588	-52UDFW
-.5522	-.7488	-.9859	-1.1927	-1.1399	-.8856	-.8685	-.9314	-52WLFT
-.3140	-.2710	-.1437	.1341	.4955	.4965	.2277	-.0150	-52ULFT
-.5937	-.6549	-.6918	-.6604	-.4966	-.2802	-.1259	.0263	-52WDFT
-.9555	-.8737	-.7572	-.6053	-.4835	-.5085	-.5738	-.5940	-52UDFT
							-1.1739	-52WLWT
							.0097	-52ULWT
							-.5258	-52WLTT
							-.2741	-52ULTT
-.0358	-.0345	-.0339	-.0340	-.0346	-.0352	-.0351	-.0357	-52WLFP
-.0459	.0437	-.0425	-.0421	-.0421	-.0419	-.0392	-.0085	-52ULFP
-.0965	-.0859	-.0771	-.0694	-.0625	-.0558	-.0493	-.0430	-52WDFP
.9041	.8999	.8961	.8930	.8908	.8896	.8896	.8906	-52UDFP
							-.0721	-52WLWP
							-.0433	-52ULWP
							-.0523	-52WDWP
							1.1733	-52UDWP

APPENDIX B

ALPHA = 0

20.0000	30.0000	40.0000	50.0000	60.0000	70.0000	80.0000	90.0000	CHI
-1.1164	-.9185	-.7118	-.5450	-.4487	-.4200	-.4211	-.4162	02WLFF
.4325	.5424	.5534	.4760	.3417	.1659	.0312	-.0880	02ULFF
-.8231	-.5926	-.3925	-.2409	-.1347	-.0560	.0156	.0880	02WDFF
.1091	.1744	.1658	.1164	.0589	.0156	-.0041	0.0000	02UDFF
							-.6823	02WLWF
							-.1016	02ULWF
							-.5137	02WLWW
							-.1094	02ULWW
-.8233	-.6354	-.4789	-.3692	-.3102	-.2922	-.2898	-.2811	02WLFW
.5082	.5177	.4663	.3723	.2548	.1296	.0073	-.0806	02ULFW
-.5595	-.3738	-.2352	-.1379	-.0701	-.0178	.0312	.0806	02WDFW
.3371	.3321	.2928	.2426	.1976	.1670	.1547	.1603	02UDFW
-.5797	-.8142	-1.1120	-1.3813	-1.2749	-.9136	-.8621	-.8952	02WLFT
-.4021	-.3748	-.2462	.0892	.5473	.5215	.2370	-.0024	02ULFT
-.6396	-.7262	-.7906	-.7730	-.5727	-.3148	-.1491	.0024	02WDFT
-1.0178	-.9352	-.8052	-.6174	-.4596	-.4936	-.5642	-.5861	02UDFT
							-1.1432	02WLWT
							.0136	02ULWT
							-.4729	02WLTT
							-.1045	02ULTT
-.0353	-.0340	-.0335	-.0336	-.0341	-.0346	-.0345	-.0351	02WLFP
-.0453	-.0431	-.0419	-.0414	-.0414	-.0412	-.0385	-.0078	02ULFP
-.0956	-.0852	-.0765	-.0690	-.0621	-.0556	-.0491	-.0429	02WDFP
.9036	.8993	.8955	.8923	.8900	.8887	.8886	.8896	02UDFP
							-.0709	02WLWP
							-.0419	02ULWP
							-.0523	02WDWP
							1.1714	02UDWP

ALPHA = 5

20.0000	30.0000	40.0000	50.0000	60.0000	70.0000	80.0000	90.0000	CHI
-1.1191	-.9204	-.7125	-.5449	-.4486	-.4200	-.4211	-.4161	52WLFF
.4327	.5438	.5550	.4771	.3423	.1863	.0316	-.0875	52ULFF
-.8256	-.5943	-.3935	-.2414	-.1352	-.0564	.0151	.0875	52WDFF
.1095	.1754	.1668	.1170	.0592	.0158	-.0041	0.0000	52UDFF
							-.6860	52WLWF
							-.1188	52ULWF
							-.5187	52WLWW
							-.1420	52ULWW
-.8147	-.6343	-.4823	-.3742	-.3150	-.2959	-.2920	-.2820	52WLFW
.4851	.4975	.4503	.3599	.2444	.1196	-.0031	-.0913	52ULFW
-.5373	-.3573	-.2213	-.1248	-.0571	-.0046	.0446	.0942	52WDFW
.3161	.3160	.2814	.2349	.1925	.1638	.1533	.1608	52UDFW
-.6081	-.8899	-1.2700	-1.6312	-1.4376	-.9516	-.8677	-.8714	52WLFT
-.5047	-.5004	-.3743	.0426	.6336	.5545	.2495	.0105	52ULFT
-.6914	-.8096	-.9120	-.9163	-.6622	-.3540	-.1747	-.0218	52WDFT
-1.0936	-1.0129	-.8645	-.6318	-.4265	-.4783	-.5561	-.5803	52UDFT
							-1.1181	52WLWT
							.0176	52ULWT
							-.4583	52WLTT
							.0439	52ULTT
-.0348	-.0335	-.0330	-.0331	-.0336	-.0341	-.0340	-.0346	52WLFP
-.0446	-.0424	-.0412	-.0408	-.0408	-.0405	-.0378	-.0072	52ULFP
-.0948	-.0846	-.0760	-.0686	-.0618	-.0554	-.0490	-.0429	52WDFP
.9031	.8987	.8948	.8916	.8892	.8878	.8876	.8884	52UDFP
							-.0698	52WLWP
							-.0405	52ULWP
							-.0524	52WDWP
							1.1694	52UDWP

APPENDIX B

ALPHA = 10

20.0000	30.0000	40.0000	50.0000	60.0000	70.0000	80.0000	90.0000	CHI
-1.1230	-.9229	-.7134	-.5449	-.4482	-.4196	-.4208	-.4160	102WLFF
.4340	.5463	.5576	.4791	.3438	.1876	.0330	-.0862	102ULFF
-.8298	-.5974	-.3954	-.2429	-.1365	-.0577	.0138	.0862	102WDFF
.1111	.1775	.1686	.1182	.0600	.0162	-.0038	0.0000	102UDFF
							-.6884	102WLWF
							-.1351	102ULWF
							-.5244	102WLWW
							-.1740	102ULWW
-.8086	-.6351	-.4869	-.3801	-.3205	-.3002	-.2951	-.2838	102WLFW
.4638	.4793	.4361	.3491	.2355	.1108	-.0125	-.1012	102ULFW
-.5182	-.3430	-.2092	-.1133	-.0453	.0076	.0572	.1071	102WDFW
.2956	.3002	.2700	.2269	.1868	.1599	.1509	.1600	102UDFW
-.6364	-.9770	-1.4706	-1.9698	-1.6234	-.9986	-.8851	-.8601	102WLFT
-.6268	-.6566	-.5412	-.0037	.7676	.5949	.2657	.0242	102ULFT
-.7493	-.9074	-1.0632	-1.1031	-.7653	-.3983	-.2033	-.0469	102WDFT
-1.1868	-1.1125	-.9536	-.6476	-.3800	-.4625	-.5495	-.5766	102UDFT
							-1.0986	102WLWT
							.0221	102ULWT
							-.4795	102WLTT
							.1941	102ULTT
-.0343	-.0330	-.0325	-.0326	-.0330	-.0336	-.0334	-.0340	102WLFP
-.0439	-.0417	-.0405	-.0401	-.0401	-.0398	-.0371	-.0065	102ULFP
-.0941	-.0840	-.0755	-.0682	-.0615	-.0552	-.0490	-.0429	102WDFP
.9024	.8980	.8940	.8907	.8882	.8868	.8865	.8872	102UDFP
							-.0687	102WLWP
							-.0393	102ULWP
							-.0526	102WDWP
							1.1673	102UDWP

ALPHA = 16

20.0000	30.0000	40.0000	50.0000	60.0000	70.0000	80.0000	90.0000	CHI
-1.1289	-.9266	-.7146	-.5447	-.4475	-.4189	-.4203	-.4156	162WLFF
.4368	.5508	.5621	.4828	.3467	.1904	.0398	-.0834	162ULFF
-.8372	-.6028	-.3992	-.2458	-.1392	-.0604	.0111	.0834	162WDFF
.1146	.1815	.1718	.1205	.0615	.0172	-.0032	0.0000	162UDFF
							-.6895	162WLWF
							-.1533	162ULWF
							-.5320	162WLWW
							-.2114	162ULWW
-.8043	-.6382	-.4940	-.3882	-.3279	-.3064	-.2999	-.2873	162WLFW
.4405	.4600	.4215	.3384	.2267	.1020	-.0224	-.1122	162ULFW
-.4992	-.3290	-.1971	-.1013	-.0328	.0208	.0710	.1215	162WDFW
.2716	.2816	.2563	.2169	.1792	.1540	.1466	.1576	162UDFW
-.6671	-1.0976	-1.7918	-2.5625	-1.8559	-1.0666	-.9217	-.8630	162WLFT
-.8076	-.9022	-.8229	-.0463	1.0117	.6520	.2905	.0420	162ULFT
-.8266	-1.0475	-1.3002	-1.4164	-.9035	-.4589	-.2426	-.0792	162WDFT
-1.3284	-1.2722	-1.0997	-.6630	-.2993	-.4432	-.5436	-.5751	162UDFT
							-1.0835	162WLWT
							.0284	162ULWT
							-.5578	162WLTT
							.4104	162ULTT
-.0336	-.0324	-.0319	-.0319	-.0324	-.0329	-.0328	-.0334	162WLFP
-.0429	-.0408	-.0397	-.0392	-.0392	-.0390	-.0363	-.0058	162ULFP
-.0932	-.0833	-.0750	-.0679	-.0613	-.0551	-.0490	-.0430	162WDFP
.9015	.8970	.8930	.8896	.8870	.8855	.8851	.8857	162UDFP
							-.0675	162WLWP
							-.0379	162ULWP
							-.0530	162WDWP
							1.1647	162UDWP

APPENDIX B

1.5-1

ALPHA = -10

20.0000	30.0000	40.0000	50.0000	60.0000	70.0000	80.0000	90.0000	CHI
-.9307	-.8193	-.6189	-.4954	-.4301	-.4205	-.4325	-.4308	-103WLFF
.3435	.4276	.4341	.3721	.2661	.1442	.0248	-.0635	-103ULFF
-.7085	-.5263	-.3673	-.2445	-.1548	-.0826	-.0115	.0635	-103WDFF
-.0104	.0605	.0724	.0516	.0231	.0028	-.0045	0.0000	-103UDFF
							-.6806	-103WLWF
							-.0507	-103ULWF
							-.5458	-103WLWW
							-.0304	-103ULWW
-.7394	-.5771	-.4461	-.3594	-.3194	-.3161	-.3243	-.3208	-103WLFW
.4381	.4449	.3989	.3183	.2212	.1212	.0258	-.0403	-103ULFW
-.5604	-.3969	-.2744	-.1870	-.1233	-.0699	-.0161	.0401	-103WDFW
.2299	.2429	.2244	.1956	.1699	.1533	.1465	.1483	-103UDFW
-.4928	-.6343	-.7894	-.9028	-.8638	-.7591	-.8089	-.8868	-103WLFT
-.1834	-.1284	-.0114	.1906	.3968	.3631	.1518	-.0357	-103ULFT
-.4854	-.5201	-.5295	-.4856	-.3638	-.2197	-.0977	.0438	-103WDFT
-.8742	-.7985	-.7024	-.5945	.5231	-.5395	-.5747	-.5824	-103UDFT
							-1.1251	-103WLWT
							-.0106	-103ULWT
							-.5329	-103WLTT
							-.3457	-103ULTT
-.0395	-.0384	-.0381	-.0386	-.0395	-.0406	-.0408	-.0410	-103WLFP
-.0566	-.0542	-.0531	-.0530	-.0536	-.0542	-.0524	-.0264	-103ULFP
-.0971	-.0858	-.0762	-.0678	-.0600	-.0525	-.0450	-.0376	-103WDFP
.8465	.8485	.8497	.8507	.8518	.8533	.8555	.8586	-103UDFP
							-.0797	-103WLWP
							-.0704	-103ULWP
							-.0470	-103WDWP
							1.1224	-103UDWP

ALPHA = -5

20.0000	30.0000	40.0000	50.0000	60.0000	70.0000	80.0000	90.0000	CHI
-.9310	-.7771	-.6192	-.4956	-.4304	-.4209	-.4328	-.4309	-53WLFF
.3422	.4268	.4336	.3714	.2651	.1432	.0238	-.0645	-53ULFF
-.7077	-.5255	-.3664	-.2436	-.1538	-.0817	-.0105	.0645	-53WDFF
-.0119	.0595	.0717	.0510	.0226	.0025	-.0047	0.0000	-53UDFF
							-.6844	-53WLWF
							-.0638	-53ULWF
							-.5471	-53WLWW
							-.0562	-53ULWW
-.7272	-.5721	-.4455	-.3608	-.3210	-.3170	-.3242	-.3198	-53WLFW
.4182	.4265	.3836	.3060	.2106	.1110	.0154	-.0506	-53ULFW
-.5387	-.3809	-.2615	-.1755	-.1124	-.0592	-.0056	.0505	-53WDFW
.2140	.2306	.2159	.1902	.1666	.1520	.1470	.1505	-53UDFW
-.5203	-.6888	-.8804	-1.0197	-.9418	-.7792	-.8088	-.8652	-53WLFT
-.2483	-.1992	-.0736	.1686	.4220	.3761	.1611	-.0204	-53ULFT
-.5236	-.5758	-.6008	-.5596	-.4140	-.2469	-.1175	.0243	-53WDFT
-.9171	-.8381	-.7295	-.5982	-.5090	-.5291	-.5662	-.5757	-53UDFT
							-1.1175	-53WLWT
							-.0017	-53ULWT
							-.4767	-53WLTT
							-.1954	-53ULTT
-.0391	-.0360	-.0377	-.0381	-.0390	-.0401	-.0403	-.0404	-53WLFP
-.0560	-.0536	-.0525	-.0524	-.0530	-.0535	-.0516	-.0256	-53ULFP
-.0963	-.0850	-.0756	-.0672	-.0596	-.0521	-.0447	-.0375	-53WDFP
.8467	.8485	.8496	.8504	.8514	.8529	.8549	.8579	-53UDFP
							-.0785	-53WLWP
							-.0688	-53ULWP
							-.0468	-53WDWP
							1.1211	-53UDWP

APPENDIX B

ALPHA = 0

20.0000	30.0000	40.0000	50.0000	60.0000	70.0000	80.0000	90.0000	CHI
-.9322	-.7781	-.6196	-.4957	-.4305	-.4210	-.4329	-.4310	03WLFF
.3415	.4269	.4339	.3714	.2649	.1428	.0234	-.0648	03ULFF
-.7082	-.5258	-.3663	-.2434	-.1536	-.0814	-.0102	.0648	03WDFF
-.0127	.0593	.0716	.0509	.0224	.0023	-.0047	0.0000	03UDFF
							-.6871	03WLWF
							-.0763	03ULWF
							-.5489	03WLWW
							-.0815	03ULWW
-.7173	-.5686	-.4460	-.3628	-.3231	-.3184	-.3248	-.3194	03WLFW
.3991	.4095	.3697	.2949	.2011	.1017	.0057	-.0604	03ULFW
-.5193	-.3666	-.2499	-.1650	-.1022	-.0491	.0044	.0604	03WDFW
.1981	.2182	.2070	.1843	.1630	.1499	.1464	.1517	03UDFW
-.5507	-.7530	-.9938	-1.1693	-1.0344	-.8047	-.8129	-.8470	03WLFT
-.3228	-.2827	-.1472	.1507	.4643	.3938	.1723	-.0051	03ULFT
-.5674	-.6409	-.6871	-.6500	-.4711	-.2761	-.1377	.0051	03WDFT
-.9690	-.8873	-.7639	-.6013	-.4903	-.5182	-.5584	-.5699	03UDFT
							-1.1049	03WLWT
							.0070	03ULWT
							-.4481	03WLTT
							-.0737	03ULTT
-.0387	-.0376	-.0373	-.0377	-.0386	-.0395	-.0397	-.0399	03WLFP
-.0553	-.0529	-.0518	-.0517	-.0523	-.0527	-.0509	-.0248	03ULFP
-.0955	-.0844	-.0750	-.0668	-.0592	-.0519	-.0446	-.0374	03WDFP
.8468	.8484	.8494	.8501	.8510	.8523	.8542	.8571	03UDFP
							-.0774	03WLWP
							-.0673	03ULWP
							-.0467	03WDWP
							1.1198	03UDWP

ALPHA = 5

20.0000	30.0000	40.0000	50.0000	60.0000	70.0000	80.0000	90.0000	CHI
-.9341	-.7743	-.6201	-.4957	-.4305	-.4200	-.4329	-.4309	53WLFF
.3417	.4279	.4350	.3721	.2653	.1431	.0237	-.0645	53ULFF
-.7100	-.5271	-.3670	-.2438	-.1539	-.0818	-.0105	.0645	53WDFF
-.0124	.0600	.0722	.0512	.0226	.0025	-.0047	0.0000	53UDFF
							-.6886	53WLWF
							-.0881	53ULWF
							-.5510	53WLWW
							-.1064	53ULWW
-.7093	-.5666	-.4474	-.3656	-.3258	-.3204	-.3259	-.3198	53WLFW
.3816	.3940	.3572	.2850	.1926	.0933	-.0032	-.0697	53ULFW
-.5022	-.3540	-.2396	-.1555	-.0929	-.0398	.0138	.0698	53WDFW
.1823	.2057	.1980	.1779	.1586	.1470	.1450	.1518	53UDFW
-.5837	-.8289	-1.1365	-1.3623	-1.1392	-.8342	-.8201	-.8314	53WLFT
-.4100	-.3838	-.2373	.1400	.5291	.4164	.1859	.0104	53ULFT
-.6170	-.7177	-.7929	-.7622	-.5351	-.3074	-.1588	-.0143	53WDFT
-1.0324	-.9492	-.8081	-.6024	-.4650	-.5066	-.5509	-.5649	53UDFT
							-1.0867	53WLWT
							.0158	53ULWT
							-.4406	53WLTT
							.0360	53ULTT
-.0382	-.0371	-.0368	-.0372	-.0380	-.0390	-.0392	-.0393	53WLFP
-.0546	-.0522	-.0511	-.0510	-.0515	-.0520	-.0501	-.0241	53ULFP
-.0947	-.0837	-.0745	-.0663	-.0589	-.0516	-.0444	-.0374	53WDFP
.8467	.8482	.8491	.8497	.8505	.8517	.8534	.8562	53UDFP
							-.0763	53WLWP
							-.0658	53ULWP
							-.0468	53WDWP
							1.1182	53UDWP

ALPHA = 10

20.0000	30.0000	40.0000	50.0000	60.0000	70.0000	80.0000	90.0000	CHI
-.9367	-.7811	-.6707	-.4956	-.4302	-.4208	-.4328	-.4301	103WLFF
.3426	.4297	.4368	.3735	.2664	.1441	.0247	-.0635	103ULFF
-.7130	-.5293	-.3685	-.2449	-.1549	-.0828	-.0115	.0635	103WDFF
-.0113	.0615	.0735	.0521	.0231	.0026	-.0045	0.0000	103UDFF
							-.6889	103WLWF
							-.0992	103ULWF
							-.5535	103WLWW
							-.1307	103ULWW
-.7032	-.5658	-.4497	-.3690	-.3290	-.3229	-.3276	-.3208	103WLFW
.3655	.3800	.3462	.2765	.1852	.0858	-.0114	-.0783	103ULFW
-.4874	-.3432	-.2306	-.1471	-.0845	-.0313	.0224	.0786	103WDFW
.1066	.1932	.1886	.1711	.1534	.1432	.1425	.1508	103UDFW
-.6192	-.9189	-1.3197	-1.6148	-1.2510	-.8664	-.8298	-.8183	103WLFT
-.5143	-.5095	-.3516	.1441	.6224	.4439	.2022	.0264	103ULFT
-.6731	-.8089	-.9252	-.9037	-.6053	-.3409	-.1810	-.0345	103WDFT
-1.1105	-1.0281	-.8655	-.5981	-.4310	-.4940	-.5438	-.5608	103UDFT
							-1.0633	103WLWT
							.0249	103ULWT
							-.4522	103WLTT
							.1467	103ULTT
-.0377	-.0366	-.0363	-.0367	-.0375	-.0385	-.0386	-.0387	103WLFP
-.0538	-.0514	-.0504	-.0502	-.0507	-.0512	-.0493	-.0233	103ULFP
-.0939	-.0831	-.0740	-.0660	-.0586	-.0515	-.0444	-.0374	103WDFP
.8466	.8480	.8487	.8492	.8499	.8509	.8526	.8552	103UDFP
							-.0752	103WLWP
							-.0644	103ULWP
							-.0469	103WDWP
							1.1166	103UDWP

ALPHA = 16

20.0000	30.0000	40.0000	50.0000	60.0000	70.0000	80.0000	90.0000	CHI
-.9408	-.7836	-.6215	-.4954	-.4297	-.4202	-.4323	-.4306	163WLFF
.3446	.4329	.4400	.3762	.2686	.1463	.0269	-.0614	163ULFF
-.7183	-.5332	-.3698	-.2471	-.1570	-.0848	-.0136	.0614	163WDFF
-.0086	.0644	.0759	.0538	.0242	.0035	-.0042	0.0000	163UDFF
							-.6875	163WLWF
							-.1114	163ULWF
							-.5569	163WLWW
							-.1588	163ULWW
-.6981	-.5666	-.4537	-.3738	-.3334	-.3265	-.3306	-.3231	163WLFW
.3478	.3651	.3348	.2679	.1779	.0781	-.0201	-.0879	163ULFW
-.4727	-.3325	-.2216	-.1385	-.0757	-.0223	.0317	.0883	163WDFW
.1477	.1781	.1771	.1622	.1463	.1374	.1381	.1480	163UDFW
-.6640	-1.0508	-1.6188	-2.0318	-1.3796	-.9080	-.8448	-.8069	163WLFT
-.6702	-.7075	-.5375	.1924	.7780	.4835	.2260	.0467	163ULFT
-.7503	-.9426	-1.1345	-1.1289	-.6948	-.3846	-.2100	-.0604	163WDFT
-1.2297	-1.1544	-.9602	-.5760	-.3758	-.4774	-.5356	-.5568	163UDFT
							-1.0307	163WLWT
							.0367	163ULWT
							-.4954	163WLTT
							.2999	163ULTT
-.0371	-.0360	-.0357	-.0360	-.0369	-.0378	-.0379	-.0381	163WLFP
-.0527	-.0505	-.0494	-.0493	-.0498	-.0502	-.0483	-.0225	163ULFP
-.0931	-.0824	-.0735	-.0656	-.0583	-.0513	-.0443	-.0375	163WDFP
.8464	.8476	.8481	.8485	.8491	.8500	.8515	.8540	163UDFP
							-.0740	163WLWP
							-.0628	163ULWP
							-.0472	163WDWP
							1.1145	163UDWP

APPENDIX B

7X10

ALPHA = -10

20.0000	30.0000	40.0000	50.0000	60.0000	70.0000	80.0000	90.0000	CHI
-1.1129	-.9093	-.7039	-.5446	-.4580	-.4396	-.4519	-.4403	-104WLFF
.4294	.5293	.5312	.4527	.3291	.1947	.0673	-.0298	-104ULFF
-.8990	-.6676	-.4672	-.3150	-.2071	-.1252	-.0491	.0298	-104WDFF
.0860	.1539	.1489	.1058	.0567	.0209	.0030	0.0000	-104UDFF
							-.6545	-104WLWF
							-.0208	-104ULWF
							-.5698	-104WLWW
							-.0069	-104ULWW
-.9765	-.7615	-.5768	-.4484	-.3844	-.3738	-.3851	-.3871	-104WLFW
.5157	.5522	.5104	.4163	.2984	.1784	.0661	-.0173	-104ULFW
-.7923	-.5698	-.3963	-.2718	-.1841	-.1158	-.0508	.0165	-104WDFW
.2454	.2647	.2335	.1836	.1372	.1050	.0882	.0840	-104UDFW
-.9957	-1.1313	-1.1673	-1.0441	-.8348	-.7314	-.7523	-.7852	-104WLFT
-.1746	.0105	.2513	.4525	.4697	.3104	.1111	-.0534	-104ULFT
-.8538	-.8389	-.7383	-.5544	-.3517	-.1976	-.0729	.0585	-104WDFT
-.7428	-.5701	-.4082	-.3109	-.3118	-.3602	-.3911	-.3950	-104UDFT
							-1.0301	-104WLWT
							-.0422	-104ULWT
							-.4987	-104WLTT
							-.1713	-104ULTT
-.0688	-.0709	-.0761	-.0828	-.0910	-.1001	-.1081	-.1143	-104WLFP
-.2841	-.2795	-.2808	-.2876	-.2991	-.3132	-.3243	-.3058	-104ULFP
-.2217	-.1966	-.1748	-.1551	-.1366	-.1182	-.0992	-.0794	-104WDFP
.6975	.7454	.7873	.8261	.8645	.9050	.9495	.9991	-104UDFP
							-.1811	-104WLWP
							-.5131	-104ULWP
							-.1314	-104WDWP
							1.2980	-104UDWP

ALPHA = -5

20.0000	30.0000	40.0000	50.0000	60.0000	70.0000	80.0000	90.0000	CHI
-1.1126	-.9317	-.7038	-.5445	-.4581	-.4397	-.4495	-.4552	-54WLFF
.4286	.5287	.5307	.4521	.3284	.1941	.0666	-.0305	-54ULFF
-.8981	-.6668	-.4664	-.3143	-.2065	-.1246	-.0484	.0305	-54WDFF
.0850	.1532	.1483	.1053	.0563	.0207	.0029	0.0000	-54UDFF
							-.6564	-54WLWF
							-.0293	-54ULWF
							-.5708	-54WLWW
							-.0228	-54ULWW
-.9263	-.7542	-.5742	-.4482	-.3849	-.3742	-.3851	-.3867	-54WLFW
.5008	.5380	.4987	.4073	.2913	.1720	.0597	-.0236	-54ULFW
-.7731	-.5564	-.3864	-.2636	-.1767	-.1087	-.0440	.0232	-54WDFW
.2333	.2548	.2265	.1793	.1347	.1039	.0881	.0851	-54UDFW
-1.0703	-1.2331	-1.2740	-1.1166	-.8616	-.7377	-.7503	-.7749	-54WLFT
-.2289	-.0202	.2610	.4936	.5052	.3308	.1296	-.0329	-54ULFT
-.9365	-.9331	-.8257	-.6163	-.3892	-.2244	-.0960	.0354	-54WDFT
-.7786	-.5854	-.3994	-.2895	-.2959	-.3521	-.3868	-.3940	-54UDFT
							-1.0236	-54WLWT
							-.0253	-54ULWT
							-.4769	-54WLTT
							-.0997	-54ULTT
-.0668	-.0708	-.0760	-.0825	-.0906	-.0996	-.1075	-.1136	-54WLFP
-.2825	-.2778	-.2791	-.2835	-.2971	-.3110	-.3218	-.3031	-54ULFP
-.2202	-.1952	-.1735	-.1539	-.1355	-.1172	-.0983	-.0786	-54WDFP
.6996	.7471	.7887	.8272	.8653	.9054	.9496	.9987	-54UDFP
							-.1799	-54WLWP
							-.5084	-54ULWP
							-.1299	-54WDWP
							1.2974	-54UDWP

APPENDIX B

ALPHA = 0

20.0000	30.0000	40.0000	50.0000	60.0000	70.0000	80.0000	90.0000	CHI
-1.1130	-.9045	-.7039	-.5445	-.4581	-.4396	-.4521	-.4552	04WLFF
.4283	.5287	.5307	.4520	.3282	.1939	.0664	-.0307	04ULFF
-.8981	-.6668	-.4663	-.3141	-.2062	-.1244	-.0483	.0307	04WDFF
.0847	.1531	.1482	.1052	.0562	.0206	.0028	0.0000	04UDFF
							-.6577	04WLWF
							-.0374	04ULWF
							-.5721	04WLWW
							-.0383	04ULWW
-.9501	-.7484	-.5727	-.4487	-.3859	-.3750	-.3856	-.3868	04WLFW
.4865	.5246	.4880	.3993	.2849	.1662	.0537	-.0296	04ULFW
-.7559	-.5445	-.3775	-.2562	-.1695	-.1022	-.0376	.0296	04WDFW
.2211	.2449	.2195	.1747	.1319	.1023	.0876	.0855	04UDFW
-1.1610	-1.3568	-1.4012	-1.1980	-.8902	-.7461	-.7500	-.7660	04WLFT
-.2906	-.0524	.2790	.5463	.5452	.3522	.1484	-.0127	04ULFT
-1.0327	-1.0427	-.9255	-.6835	-.4280	-.2516	-.1190	.0127	04WDFT
-.8195	-.6011	-.3853	-.2621	-.2773	-.3427	-.3814	-.3919	04UDFT
							-1.0158	04WLWT
							-.0087	04ULWT
							-.4648	04WLTT
							-.0330	04ULTT
-.0667	-.0707	-.0757	-.0822	-.0902	-.0991	-.1069	-.1128	04WLFP
-.2807	-.2760	-.2772	-.2837	-.2949	-.3086	-.3191	-.3003	04ULFP
-.2187	-.1938	-.1722	-.1527	-.1344	-.1162	-.0974	-.0779	04WDFP
.7016	.7487	.7899	.8281	.8659	.9056	.9493	.9981	04UDFP
							-.1787	04WLWP
							-.5036	04ULWP
							-.1285	04WDWP
							1.2963	04UDWP

ALPHA = 5

20.0000	30.0000	40.0000	50.0000	60.0000	70.0000	80.0000	90.0000	CHI
-1.1141	-.9103	-.7042	-.5445	-.4581	-.4396	-.4521	-.4552	54WLFF
.4284	.5292	.5313	.4524	.3285	.1941	.0666	-.0305	54ULFF
-.8992	-.6675	-.4667	-.3144	-.2065	-.1247	-.0485	.0305	54WDFF
.0849	.1535	.1486	.1054	.0563	.0207	.0029	0.0000	54UDFF
							-.6584	54WLWF
							-.0449	54ULWF
							-.5736	54WLWW
							-.0534	54ULWW
-.9397	-.7439	-.5720	-.4498	-.3873	-.3761	-.3864	-.3875	54WLFW
.4729	.5122	.4782	.3921	.2793	.1610	.0483	-.0352	54ULFW
-.7408	-.5341	-.3698	-.2497	-.1638	-.0962	-.0316	.0356	54WDFW
.2090	.2351	.2125	.1700	.1288	.1002	.0864	.0854	54UDFW
-1.2714	-1.5072	-1.5515	-1.2865	-.9195	-.7563	-.7513	-.7584	54WLFT
-.3611	-.0853	.3092	.6133	.5900	.3746	.1678	.0074	54ULFT
-1.1457	-1.1716	-1.0398	-.7557	-.4680	-.2794	-.1422	-.0099	54WDFT
-.8664	-.6164	-.3639	-.2273	-.2556	-.3317	-.3749	-.3889	54UDFT
							-1.0068	54WLWT
							.0078	54ULWT
							-.4615	54WLTT
							.0316	54ULTT
-.0666	-.0705	-.0754	-.0819	-.0897	-.0985	-.1061	-.1120	54WLFP
-.2786	-.2739	-.2750	-.2815	-.2925	-.3060	-.3164	-.2975	54ULFP
-.2172	-.1925	-.1710	-.1516	-.1334	-.1153	-.0967	-.0773	54WDFP
.7034	.7501	.7909	.8288	.8662	.9056	.9489	.9971	54UDFP
							-.1773	54WLWP
							-.4987	54ULWP
							-.1272	54WDWP
							1.2947	54UDWP

APPENDIX B

ALPHA = 10

20.0000	30.0000	40.0000	50.0000	60.0000	70.0000	80.0000	90.0000	CHI
-1.1158	-.9114	-.7047	-.5446	-.4580	-.4397	-.4520	-.4630	104WLFF
.4291	.5304	.5325	.4533	.3292	.1947	.0673	-.0298	104ULFF
-.9012	-.6690	-.4677	-.3151	-.2072	-.1253	-.0501	.0298	104WDFF
.0857	.1545	.1494	.1060	.0567	.0209	.0030	0.0000	104UDFF
							-.6584	104WLWF
							-.0520	104ULWF
							-.5754	104WLWW
							-.0679	104ULWW
-.9312	-.7408	-.5724	-.4515	-.3892	-.3777	-.3876	-.3885	104WLFW
.4600	.5008	.4695	.3859	.2746	.1565	.0435	-.0404	104ULFW
-.7277	-.5252	-.3633	-.2441	-.1584	-.0909	-.0262	.0412	104WDFW
.1926	.2254	.2055	.1651	.1253	.0977	.0847	.0845	104UDFW
-1.4067	-1.6910	-1.7274	-1.3794	-.9479	-.7680	-.7540	-.7524	104WLFT
-.4419	-.1170	.3572	.6971	.6392	.3989	.1880	.0277	104ULFT
-1.2797	-1.3244	-1.1704	-.8322	-.5089	-.3081	-.1659	-.0327	104WDFT
-.9203	-.6300	-.3321	-.1839	-.2308	-.3192	-.3673	-.3849	104UDFT
							-.9967	104WLWT
							.0246	104ULWT
							-.4668	104WLTT
							.0964	104ULTT
-.0664	-.0702	-.0751	-.0814	-.0892	-.0978	-.1054	-.1111	104WLFP
-.2764	-.2716	-.2727	-.2791	-.2895	-.3033	-.3136	-.2946	104ULFP
-.2158	-.1912	-.1698	-.1505	-.1324	-.1145	-.0960	-.0767	104WDFP
.7051	.7514	.7918	.8292	.8663	.9053	.9481	.9959	104UDFP
							-.1759	104WLWP
							-.4939	104ULWP
							-.1261	104WDWP
							1.2927	104UDWP

ALPHA = 16

20.0000	30.0000	40.0000	50.0000	60.0000	70.0000	80.0000	90.0000	CHI
-1.1186	-.9132	-.7055	-.5447	-.4578	-.4394	-.4518	-.4550	164WLFF
.4306	.5325	.5345	.4551	.3307	.1961	.0686	-.0285	164ULFF
-.9048	-.6717	-.4697	-.3167	-.2085	-.1266	-.0504	.0285	164WDFF
.0875	.1564	.1511	.1072	.0575	.0214	.0032	0.0000	164UDFF
							-.6574	164WLWF
							-.0596	164ULWF
							-.5777	164WLWW
							-.0845	164ULWW
-.9231	-.7388	-.5739	-.4543	-.3919	-.3801	-.3899	-.3905	164WLFW
.4455	.4884	.4604	.3797	.2699	.1520	.0384	-.0460	164ULFW
-.7145	-.5166	-.3569	-.2385	-.1529	-.0853	-.0204	.0472	164WDFW
.1826	.2139	.1971	.1591	.1208	.0941	.0819	.0827	164UDFW
-1.6116	-1.9668	-1.9741	-1.4897	-.9786	-.7832	-.7590	-.7472	164WLFT
-.5551	-.1486	.4496	.8228	.7031	.4300	.2138	.0527	164ULFT
-1.4766	-1.5474	-1.3506	-.9274	-.5589	-.3440	-.1954	-.0609	164WDFT
-.9957	-.6408	-.2739	-.1187	-.1972	-.3021	-.3567	-.3789	164UDFT
							-.9835	164WLWT
							.0435	164ULWT
							-.4848	164WLTT
							.1778	164ULTT
-.0661	-.0698	-.0746	-.0808	-.0885	-.0970	-.1044	-.1101	164WLFP
-.2734	-.2687	-.2697	-.2760	-.2867	-.3000	-.3102	-.2912	164ULFP
-.2141	-.1897	-.1685	-.1494	-.1314	-.1136	-.0952	-.0762	164WDFP
.7069	.7526	.7925	.8295	.8661	.9046	.9469	.9942	164UDFP
							-.1742	164WLWP
							-.4881	164ULWP
							-.1251	164WDWP
							1.2898	164UDWP

REFERENCES

1. Heyson, Harry H.: Wind-Tunnel Wall Interference and Ground Effect for VTOL-STOL Aircraft. J. Amer. Helicopter Soc., vol. 6, no. 1, Jan. 1961, pp. 1-9.

2. Heyson, Harry H.: Linearized Theory of Wind-Tunnel Jet-Boundary Corrections and Ground Effect for VTOL-STOL Aircraft. NASA TR R-124, 1962.

3. Heyson, Harry H.: Use of Superposition in Digital Computers To Obtain Wind-Tunnel Interference Factors for Arbitrary Configurations, With Particular Reference to V/STOL Models. NASA TR R-302, 1969.

4. Heyson, Harry H.: Theoretical Study of Conditions Limiting V/STOL Testing in Wind Tunnels With Solid Floor. NASA TN D-5819, 1970.

5. Heyson, Harry H.: General Theory of Wall Interference for Static Stability Tests in Closed Rectangular Test Sections and in Ground Effect. NASA TR R-364, 1971.

6. Heyson, Harry H.: Rapid Estimation of Wind-Tunnel Corrections With Application to Wind-Tunnel and Model Design. NASA TN D-6416, 1971.

7. Cook, Woodrow L.; and Hickey, David H.: Comparison of Wind-Tunnel and Flight Test Aerodynamic Data in the Transition-Flight Speed Range for Five V/STOL Aircraft. Conference on V/STOL and STOL Aircraft, NASA SP-116, 1966, pp. 447-467. (Also available as AGARD Rep. 520, 1965.)

8. Heyson, Harry H.; and Grunwald, Kalman J.: Wind-Tunnel Boundary Interference for V/STOL Testing. Conference on V/STOL and STOL Aircraft, NASA SP-116, 1966, pp. 409-434.

9. Rae, William H., Jr.: Limits on Minimum-Speed V/STOL Wind-Tunnel Tests. J. Aircraft, vol. 4, no. 3, May-June 1967, pp. 249-254.

10. Kelly, Mark W.; Mort, Kenneth W.; and Hickey, David H.: Full-Scale Subsonic Wind Tunnel Requirements and Design Studies. NASA TM X-62,184, 1972.

11. Elson, Benjamin M.: New Tunnel Could Cut V/STOL Costs. Aviat. Week & Space Technol., vol. 97, no. 18, Oct. 30, 1972, pp. 54-56.

12. Kelly, Mark W.: Meeting the Challenge of Advanced Helicopters. Vertiflite, vol. 19, no. 2, Mar./Apr. 1973, pp. 4-8.

13. Lazzeroni, F. A.; and Carr, L. W.: Problems Associated With Wind Tunnel Tests of High Disk Loading Systems at Low Forward Speeds. Proceedings Third CAL/AVLABS Symposium, Aerodynamics of Rotary Wing and V/STOL Aircraft, Vol. II, June 1969.

14. Lee, Jerry Louis: An Experimental Investigation of the Use of Test Section Inserts as a Device To Verify Theoretical Wall Corrections for a Lifting Rotor Centered in a Closed Rectangular Test Section. M.S. Thesis, Univ. of Washington, Aug. 20, 1964.

15. Davenport, Edwin E.; and Kuhn, Richard E.: Wind-Tunnel-Wall Effects and Scale Effects on a VTOL Configuration With a Fan Mounted in the Fuselage. NASA TN D-2560, 1965.

16. Grunwald, Kalman J.: Experimental Study of Wind-Tunnel Wall Effects and Wall Corrections for a General-Research V/STOL Tilt-Wing Model With Flap. NASA TN D-2887, 1965.

17. South, P.: Measurements of the Influence of Mixed Boundaries on the Aerodynamic Characteristics of a V/STOL Wind-Tunnel Model. Fluid Dynamics of Rotor and Fan Supported Aircraft at Subsonic Speeds, AGARD CP No. 22, Sept. 1967, pp. 25-1 – 25-15.

18. Rae, William H., Jr.; and Shindo, Shojiro: Comments on V/STOL Wind Tunnel Data at Low Forward Speeds. Proceedings Third CAL/AVLABS Symposium, Aerodynamics of Rotary Wing and V/STOL Aircraft, Vol. II, June 1969.

19. Hickey, David H.; and Cook, Woodrow L.: Aerodynamics of V/STOL Aircraft Powered by Lift Fans. Fluid Dynamics of Rotor and Fan Supported Aircraft at Subsonic Speeds, AGARD CP No. 22, Sept. 1967, pp. 15-1 – 15-17.

20. Cichy, D. R.; Harris, J. W.; and MacKay, J. K.: Flight Tests of a Rotating Cylinder Flap on a North American Rockwell YOV-10 Aircraft. NASA CR-2135, 1972.

21. Heyson, Harry H.: Wind-Tunnel Wall Effects at Extreme Force Coefficients. Ann. N.Y. Acad. Sci., vol. 154, art. 2, Nov. 22, 1968, pp. 1074-1093.

22. Heyson, Harry H.: Nomographic Solution of the Momentum Equation for VTOL-STOL Aircraft. NASA TN D-814, 1961. (Also available as V/STOL Momentum Equation, Space/Aeronaut., vol. 38, no. 2, July 1972, pp. B-18 – B-20.)

23. Heyson, Harry H.: Theoretical and Experimental Investigation of the Performance of a Fan-in-Wing VTOL Configuration. NASA TN D-7498, 1973.

24. Pirrello, C. J.; Hardin, R. D.; Heckart, M. V.; and Brown, K. R.: An Inventory of Aeronautical Ground Research Facilities. Vol. I – Wind Tunnels. NASA CR-1874, 1971.

25. Ganzer, Victor M.; and Rae, William H., Jr.: An Experimental Investigation of the Effect of Wind Tunnel Walls on the Aerodynamic Performance of a Helicopter Rotor. NASA TN D-415, 1960.

26. Aoyagi, Kiyoshi; Hickey, David H.; and DeSavigney, Richard A.: Aerodynamic Characteristics of a Large-Scale Model With a High Disk-Loading Lifting Fan Mounted in the Fuselage. NASA TN D-775, 1961.

27. Hickey, David H.; and Hall, Leo P.: Aerodynamic Characteristics of a Large-Scale Model With Two High Disk-Loading Fans Mounted in the Wing. NASA TN D-1650, 1963.

28. Kirk, Jerry V.; Hickey, David H.; and Hall, Leo P.: Aerodynamic Characteristics of a Full-Scale Fan-in-Wing Model Including Results in Ground Effect With Nose-Fan Pitch Control. NASA TN D-2368, 1964.

29. Hall, Leo P.; Hickey, David H.; and Kirk, Jerry V.: Aerodynamic Characteristics of a Large-Scale V/STOL Transport Model With Lift and Lift-Cruise Fans. NASA TN D-4092, 1967.

30. Kirk, Jerry V.; Hodder, Brent K.; and Hall, Leo P.: Large-Scale Wind-Tunnel Investigation of a V/STOL Transport Model With Wing-Mounted Lift Fans and Fuselage-Mounted Lift-Cruise Engines for Propulsion. NASA TN D-4233, 1967.

31. Dickinson, Stanley O.; Hall, Leo P.; and Hodder, Brent K.: Aerodynamic Characteristics of a Large-Scale V/STOL Transport Model With Tandem Lift Fans Mounted at Mid-Semispan of the Wing. NASA TN D-6234, 1971.

32. Kirk, Jerry V.; Hall, Leo P.; and Hodder, Brent K.: Aerodynamics of Lift Fan V/STOL Aircraft. AIAA Paper No. 71-981, Oct. 1971.

33. DeFrance, Smith J.: The N.A.C.A. Full-Scale Wind Tunnel. NACA Rep. 459, 1933.

34. Schaefer, William T., Jr.: Characteristics of Major Active Wind Tunnels at the Langley Research Center. NASA TM X-1130, 1965.

35. Pope, Alan; and Harper, John J.: Low-Speed Wind Tunnel Testing. John Wiley & Sons, Inc., c.1966.

36. Heyson, Harry H.: FORTRAN Programs for Calculating Wind-Tunnel Boundary Interference. NASA TM X-1740, 1969.

37. Durand, W. F.: Fluid Mechanics, Part I. Vol. 1 of Aerodynamic Theory, William Frederick Durand, ed., Julius Springer (Berlin), 1934, pp. 105-223.

38. Pope, Alan: Basic Wing and Airfoil Theory. First ed., McGraw-Hill Book Co., Inc., 1951, pp. 41-45.

39. Heyson, Harry H.: The Flow Throughout a Wind Tunnel Containing a Rotor With a Sharply Deflected Wake. Proceedings Third CAL/AVLABS Symposium, Aerodynamics of Rotary Wing and V/STOL Aircraft, Vol. II, June 1969.

40. Heyson, Harry H.: Equations for the Application of Wind-Tunnel Wall Corrections to Pitching Moments Caused by the Tail of an Aircraft Model. NASA TN D-3738, 1966.

41. Perkins, Courtland D.; and Hage, Robert E.: Airplane Performance Stability and Control. John Wiley & Sons, Inc., c.1949, pp. 186, 221.

42. Anscombe, A.; and Williams, J.: Some Comments on High-Lift Testing in Wind Tunnels With Particular Reference to Jet-Blowing Models. AGARD Rep. 63, Aug. 1956.

43. Joppa, Robert G.: Wall Interference Effects in Wind-Tunnel Testing of STOL Aircraft. J. Aircraft, vol. 6, no. 3, May-June 1969, pp. 209-214.

44. Joppa, Robert G.: Wind-Tunnel Interference Factors for High-Lift Wings in Closed Wind Tunnels. NASA CR-2191, 1973.

45. Schaub, Uwe W.; and Bassett, Robert W.: Flow Distortion and Performance Measurements on a 12" Fan-in-Wing Model for a Range of Forward Speeds and Angle of Attack Settings. Inlets and Nozzles for Aerospace Engines, AGARD-CP-91-71, Dec. 1971, pp. 17-1 – 17-12.

46. Deckert, Wallace H.; and Evans, Robert C.: NASA Lift Fan Transport Technology Status. [Preprint] 720856, Soc. Automot. Eng., Oct. 1972.

47. Harris, Franklin D.: Aerodynamic and Dynamic Rotary Wing Model Testing in Wind Tunnels and Other Facilities. Helicopter Aerodynamics and Dynamics, AGARD-LS-63, 1973, pp. 7-1 – 7-62.

48. Tyler, R. A.; and Williamson, R. G.: Experience With the NRC 10 Ft. × 20 Ft. V/STOL Propulsion Tunnel – Some Practical Aspects of V/STOL Engine Model Testing. Can. Aeronaut. & Space J., vol. 18, no. 7, Sept. 1972, pp. 191-199.

49. Tyler, R. A.; and Williamson, R. G.: Wind-Tunnel Testing of V/STOL Engine Models – Some Observed Flow Interaction and Tunnel Effects. Inlets and Nozzles for Aerospace Engines, AGARD-CP-91-71, Dec. 1971, pp. 8-1 – 8-12.

50. Heyson, Harry H.: Jet-Boundary Corrections for Lifting Rotors Centered in Rectangular Wind Tunnels. NASA TR R-71, 1960.

TABLE I.- AIRFOIL ORDINATES

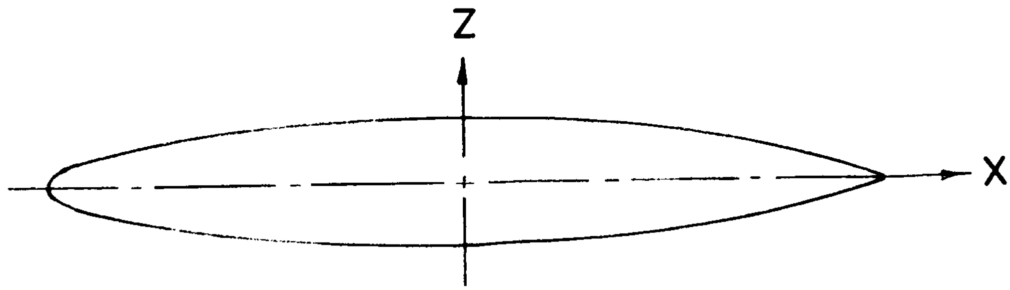

NACA 16-015				Modified NACA 16-017			
Tip sta.: c = 45.72 cm (18.00 in.)				¢ Sta.: c = 83.414 cm (32.84 in.)			
X		±Z		X		±Z	
cm	in.	cm	in.	cm	in.	cm	in.
-22.860	-9.000	0	0	-41.707	-16.42	0	0
-22.288	-8.775	.739	.291	-40.640	-16.00	1.521	.599
-21.717	-8.550	1.031	.406	-39.624	-15.60	2.126	.837
-20.574	-8.100	1.435	.565	-37.567	-14.79	2.957	1.164
-19.431	-7.650	1.732	.682	-35.458	-13.96	3.571	1.406
-18.288	-7.200	1.976	.778	-33.350	-13.13	4.074	1.604
-16.002	-6.300	2.362	.930	-29.210	-11.50	4.862	1.914
-13.716	-5.400	2.664	1.049	-25.019	-9.85	5.497	2.164
-9.144	-3.600	3.096	1.219	-16.688	-6.57	6.386	2.514
-4.572	-1.800	3.345	1.317	-8.331	-3.28	6.896	2.715
0	0	3.429	1.350	0	0	7.069	2.783
4.572	1.800	3.335	1.313	8.331	3.28	6.876	2.707
9.144	3.600	3.012	1.186	16.688	6.57	6.208	2.444
13.716	5.400	2.400	.945	25.019	9.85	4.945	1.947
18.288	7.200	1.438	.566	33.350	13.13	2.967	1.168
20.574	8.100	.808	.318	37.567	14.79	1.651	.650
22.860	9.000	.069	.027	41.707	16.42	.142	.056
L.E. radius: 0.503 cm (0.198 in.)				L.E. radius: 0.917 cm (0.361 in.)			

TABLE II.- FUSELAGE ORDINATES

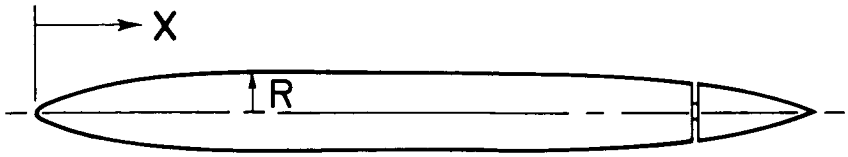

X		R	
cm	in.	cm	in.
0	0	0	0
1.70	.67	2.18	.86
3.38	1.33	3.05	1.20
6.78	2.67	4.24	1.67
10.16	4.00	5.13	2.02
13.54	5.33	5.87	2.31
20.32	8.00	7.01	2.76
27.10	10.67	7.90	3.11
40.64	16.00	9.17	3.61
54.18	21.33	9.40	3.70
67.74	26.67	10.16	4.00
↓	↓	↓	↓
145.62	57.33	10.16	4.00
159.18	62.67	9.88	3.89
172.72	68.00	8.92	3.51
186.26	73.33	7.11	2.80
199.82	78.67	4.27	1.68
206.58	81.33	2.39	.94
213.36	84.00	.20	.08
Nose radius: 1.50 cm (0.59 in.)			

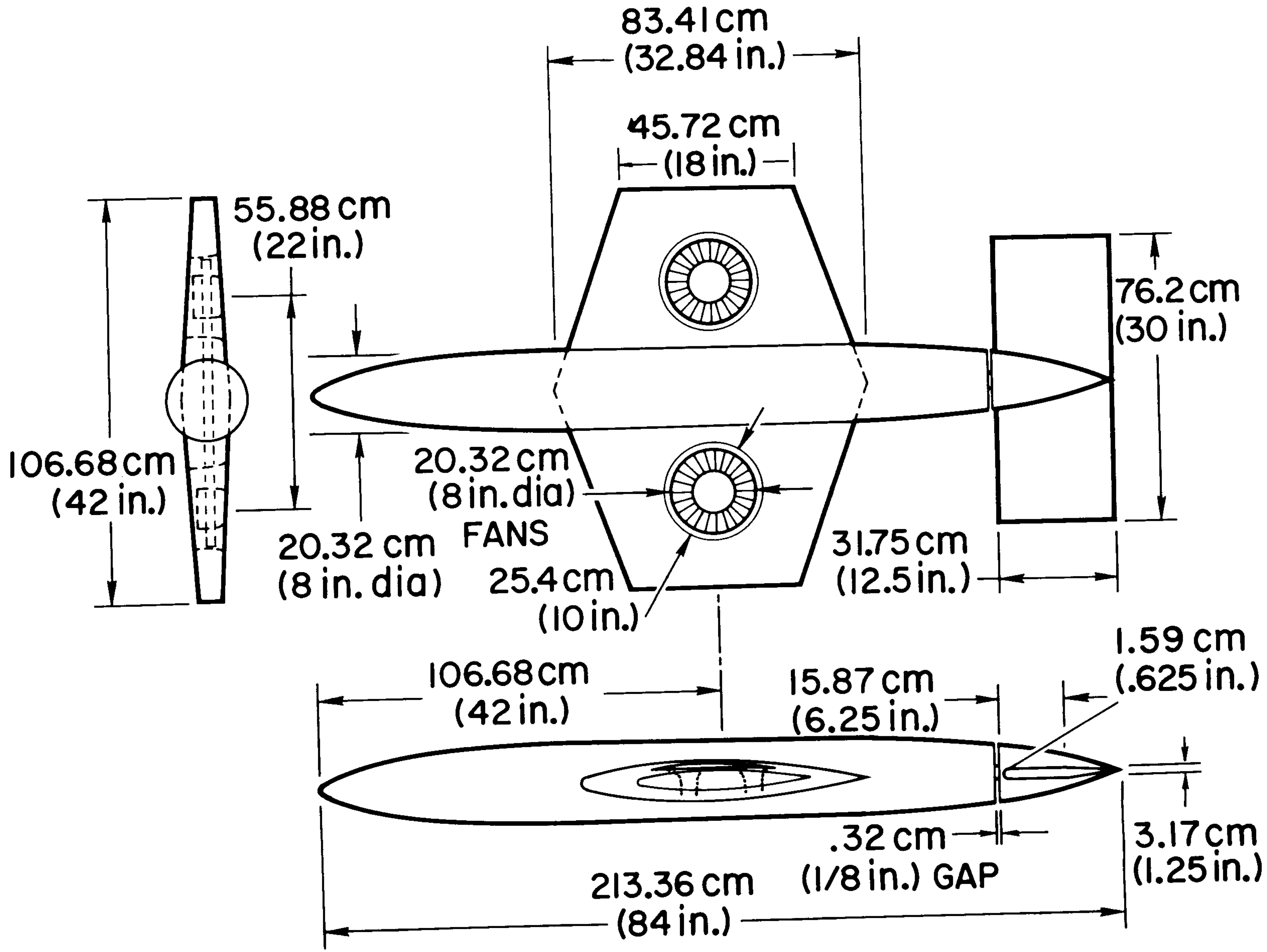

Figure 1.- Dimensioned drawing of model.

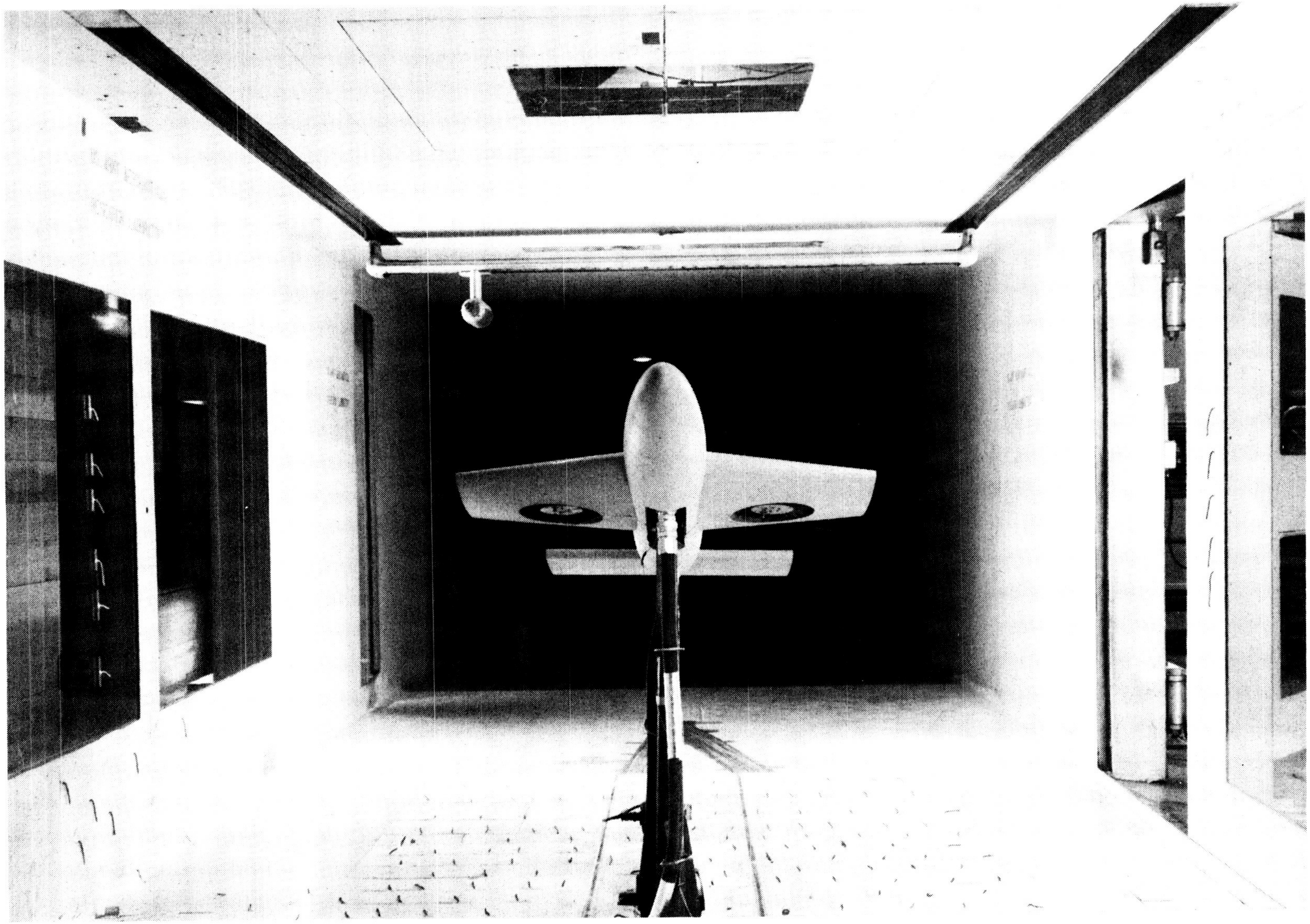

Figure 2.- Fan-in-wing model mounted in Ames 2.13- by 3.05-m (7- by 10-ft) wind tunnel.

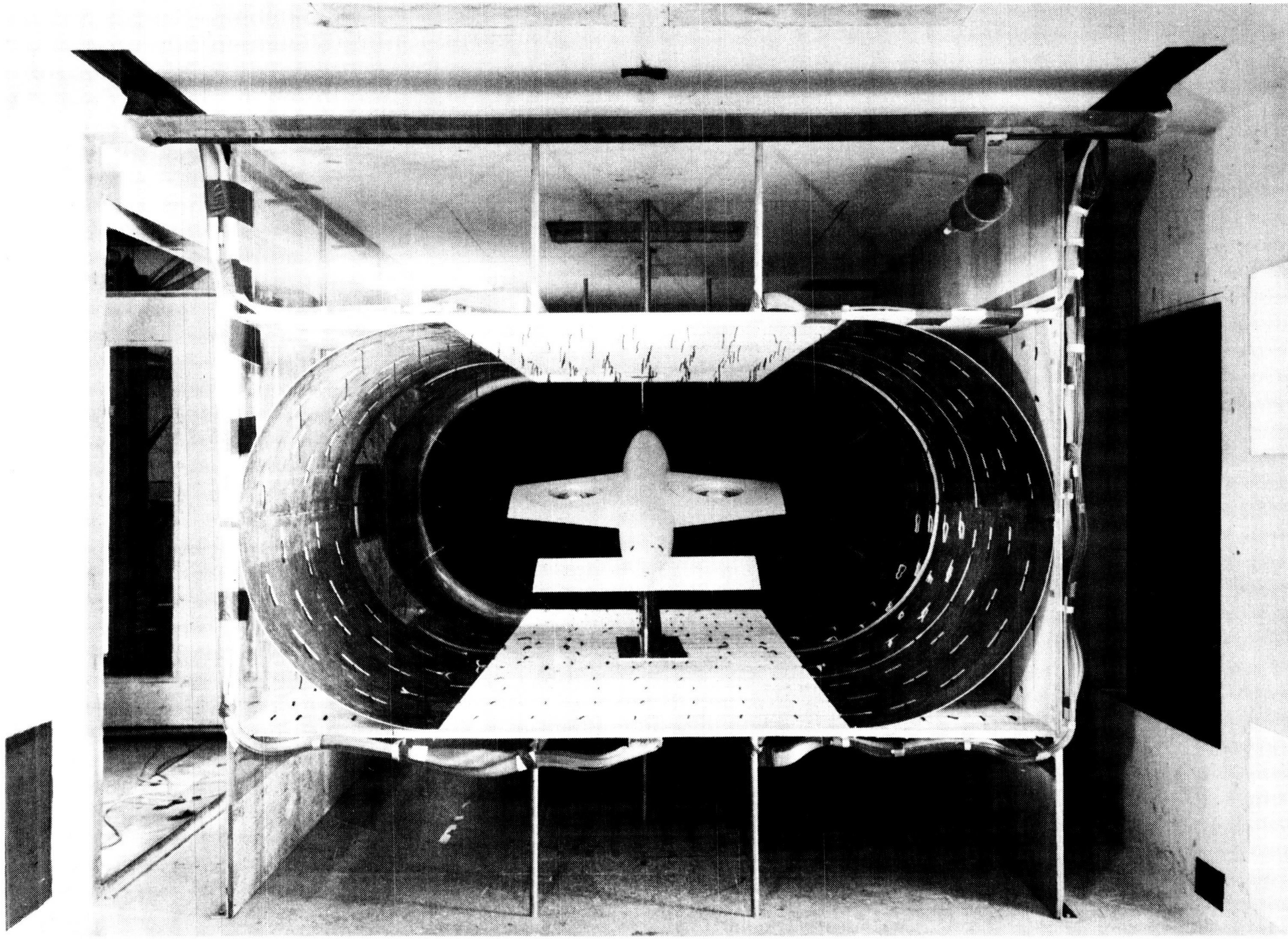

(a) 1.12- by 2.24-m (44- by 88-in.) flat-oval test section.

Figure 3.- Fan-in-wing model mounted in inserts in Ames 2.13- by 3.05-m (7- by 10-ft) wind tunnel.

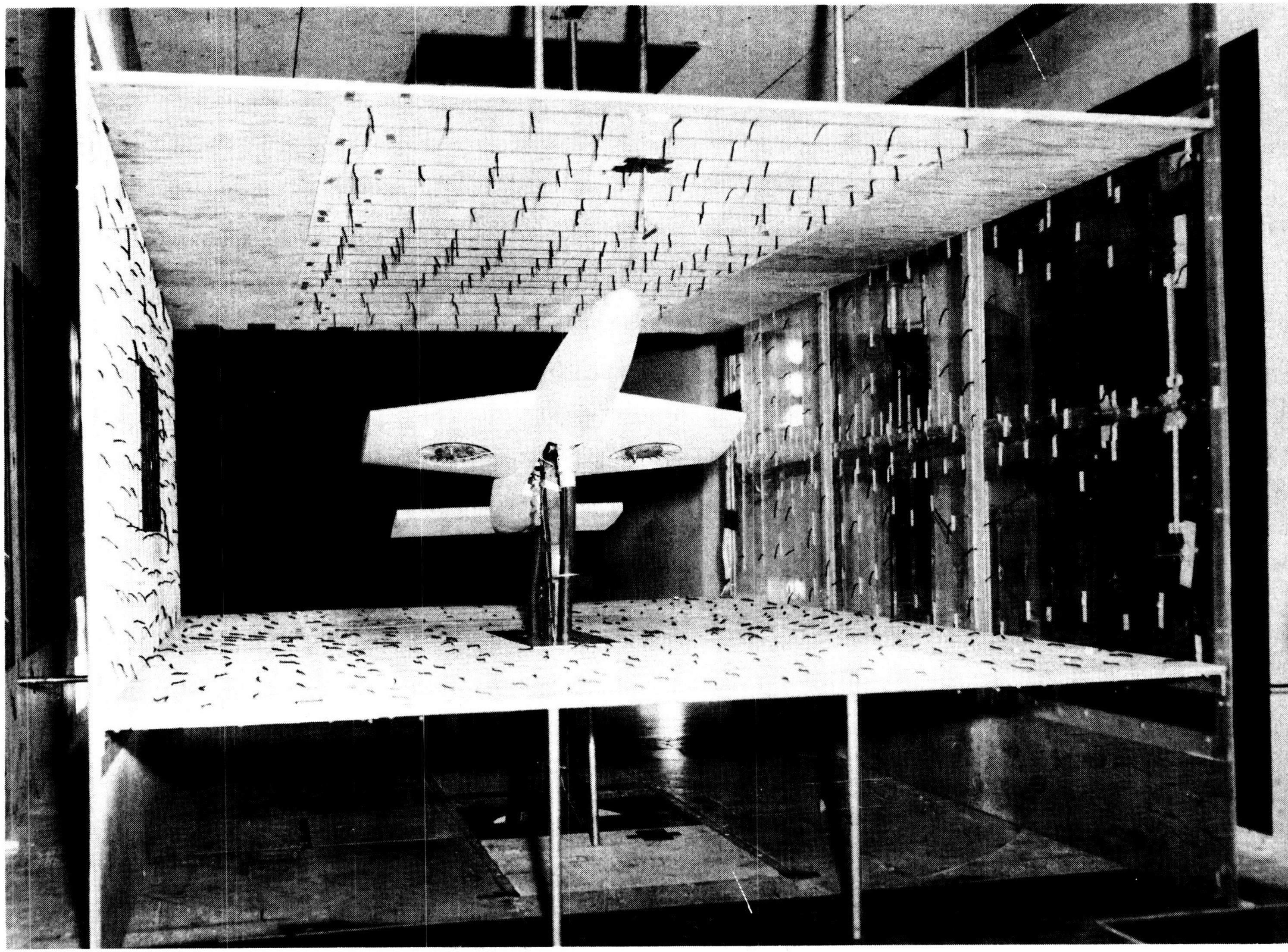

(b) 1.12- by 2.24-m (44- by 88-in.) rectangular test section.

Figure 3.- Continued.

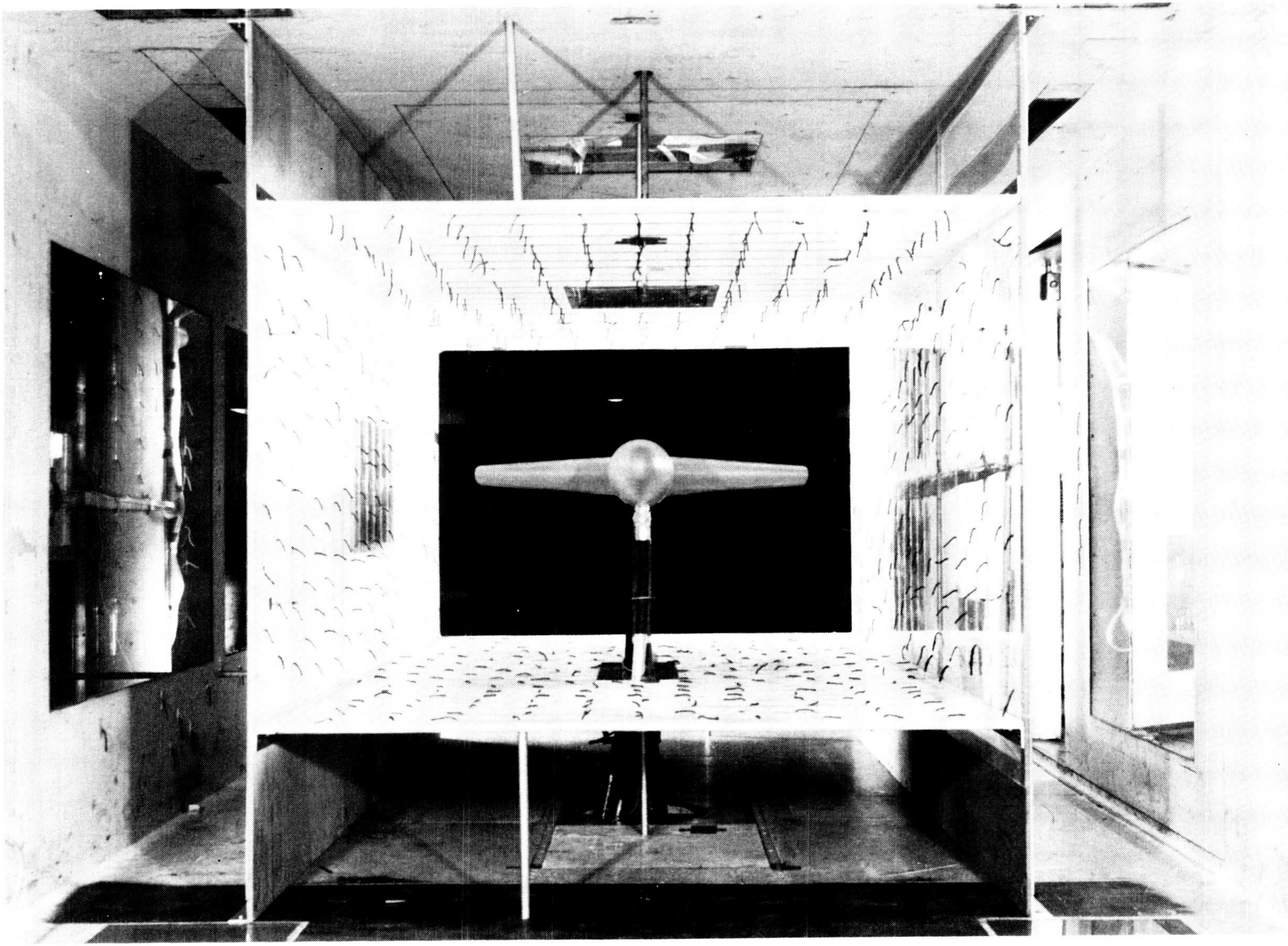

(c) 1.22- by 1.83-m (4- by 6-ft) rectangular test section.

Figure 3.- Concluded.

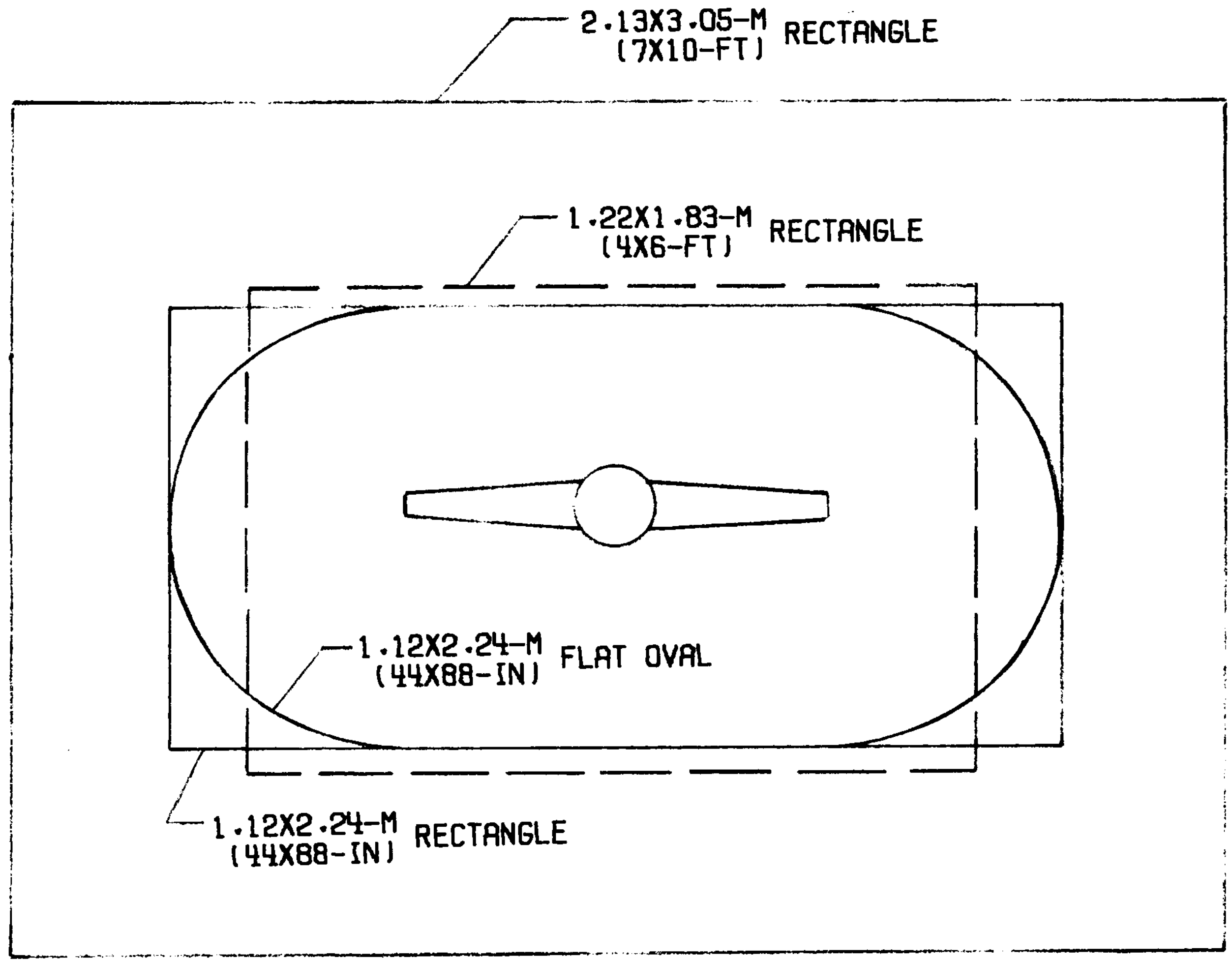

Figure 4.- Relative size of test sections with respect to model. Langley full-scale tunnel has been omitted because of its vastly greater size. (See fig. 5 for relative size of Ames full-scale tunnel and fig. 6 for relative size of Langley full-scale tunnel.)

A-72-1215

(a) Overall view.

Figure 5.- Fan-in-wing model mounted in Ames 12.2- by 24.4-m (40- by 80- ft) tunnel.

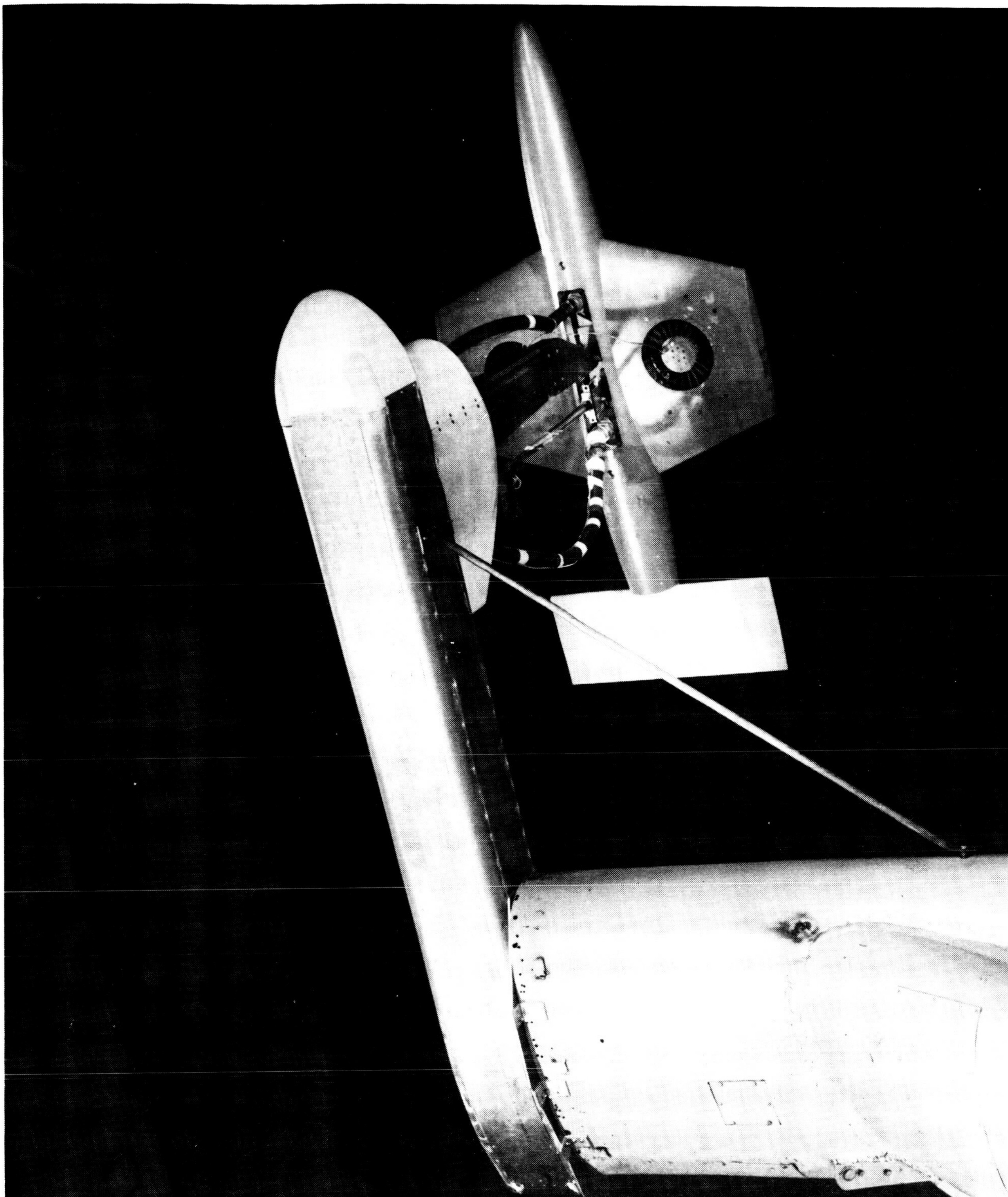

A-72-1216

(b) View from "below" model.

Figure 5.- Continued.

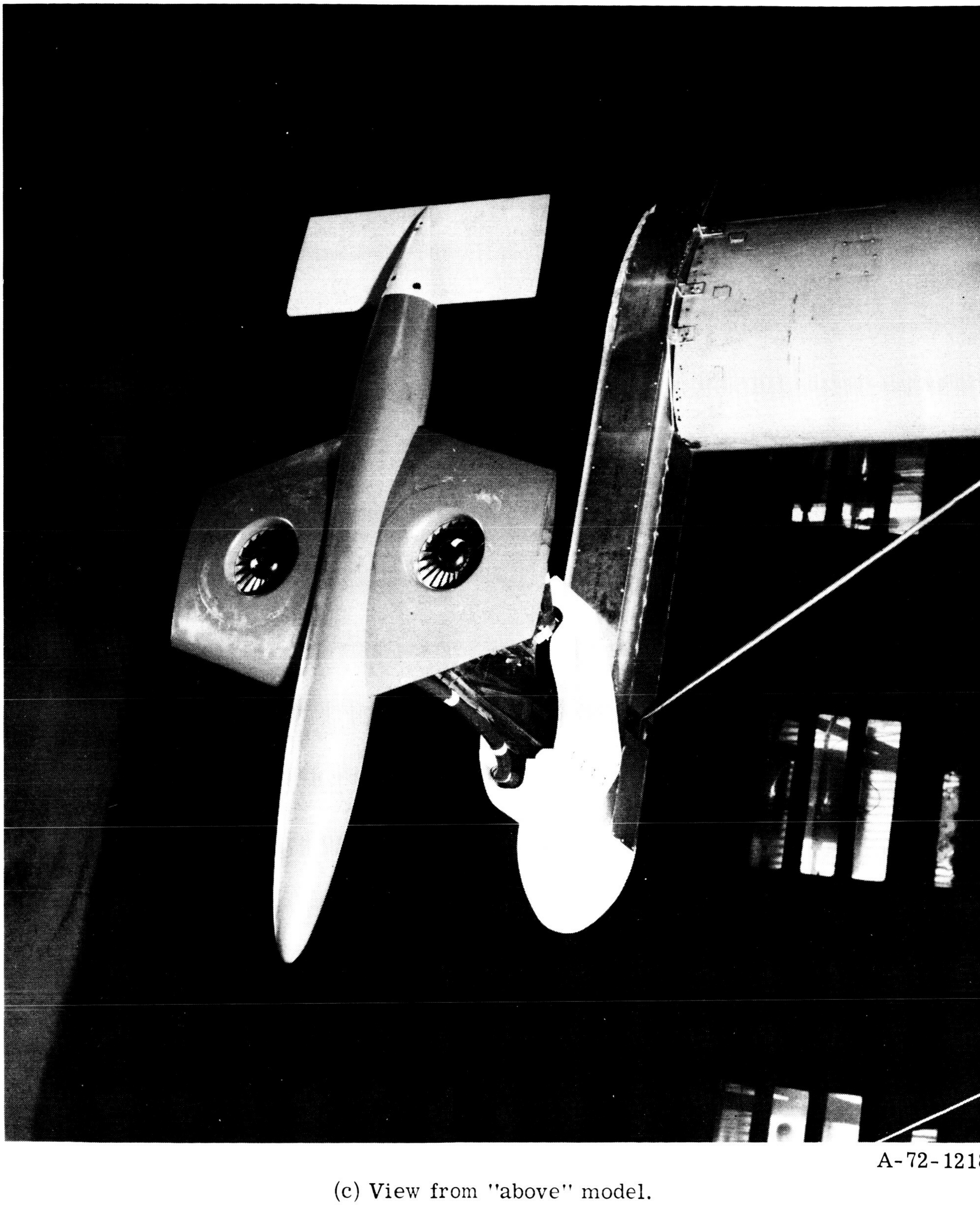

A-72-1218

(c) View from "above" model.

Figure 5.- Concluded.

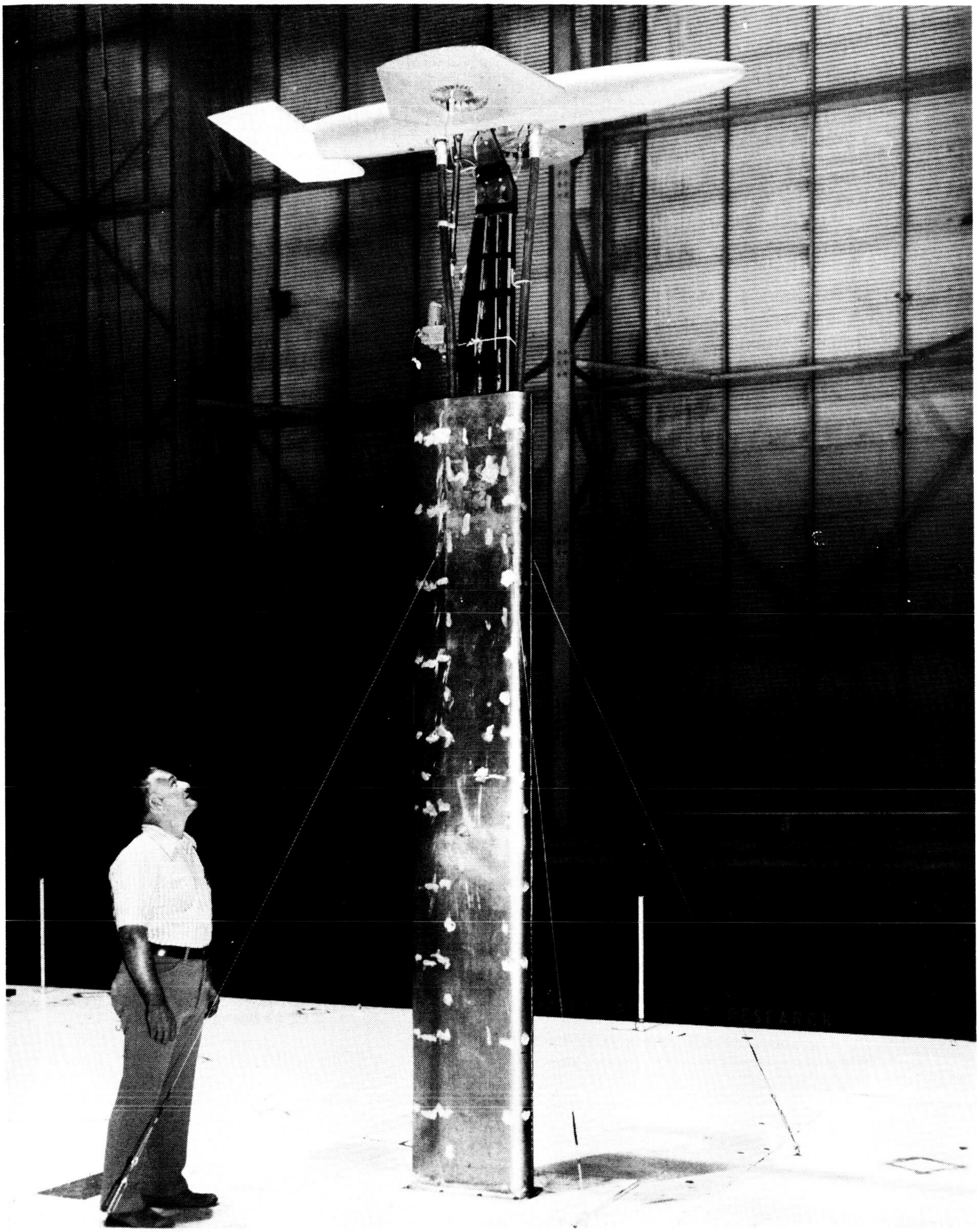

L-72-2844

(a) Near view.

Figure 6.- Fan-in-wing model mounted in 9.14- by 18.3-m (30- by 60-ft) Langley full-scale tunnel.

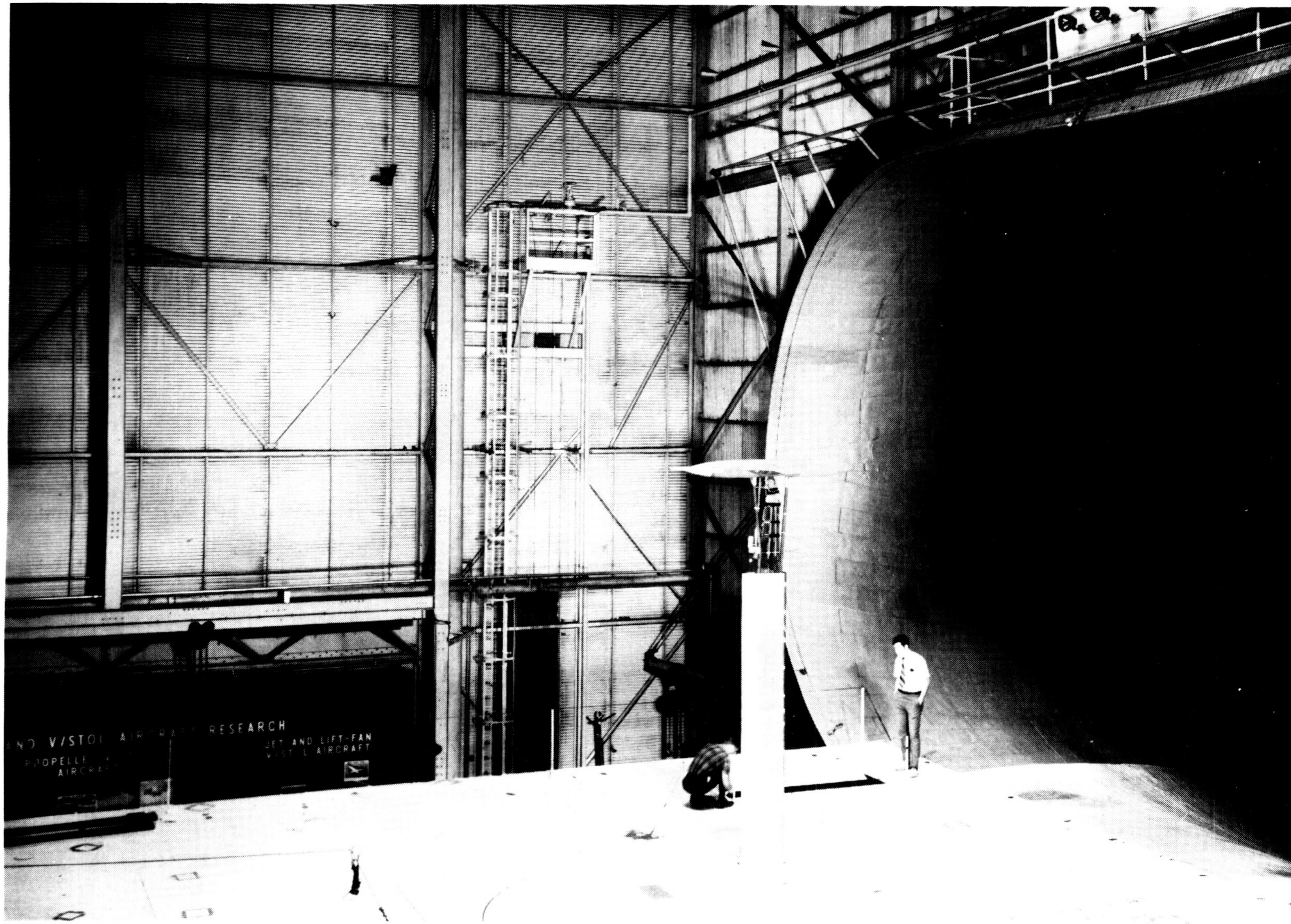

L-72-2843

(b) Distant view.

Figure 6.- Concluded.

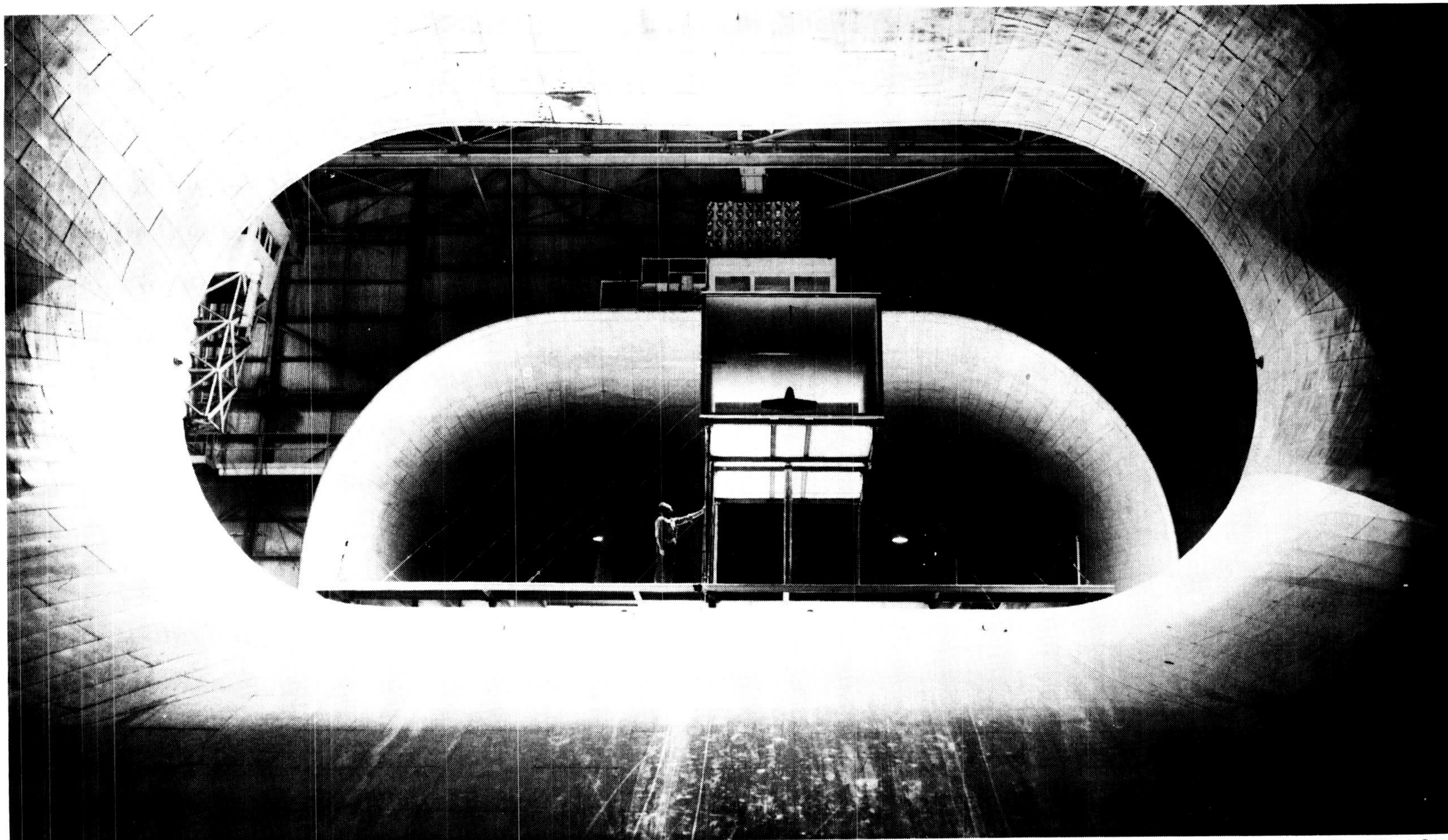

L-72-2873

(a) Front view.

Figure 7.- Fan-in-wing model mounted in 2.13- by 3.05-m (7- by 10-ft) insert in Langley full-scale tunnel.

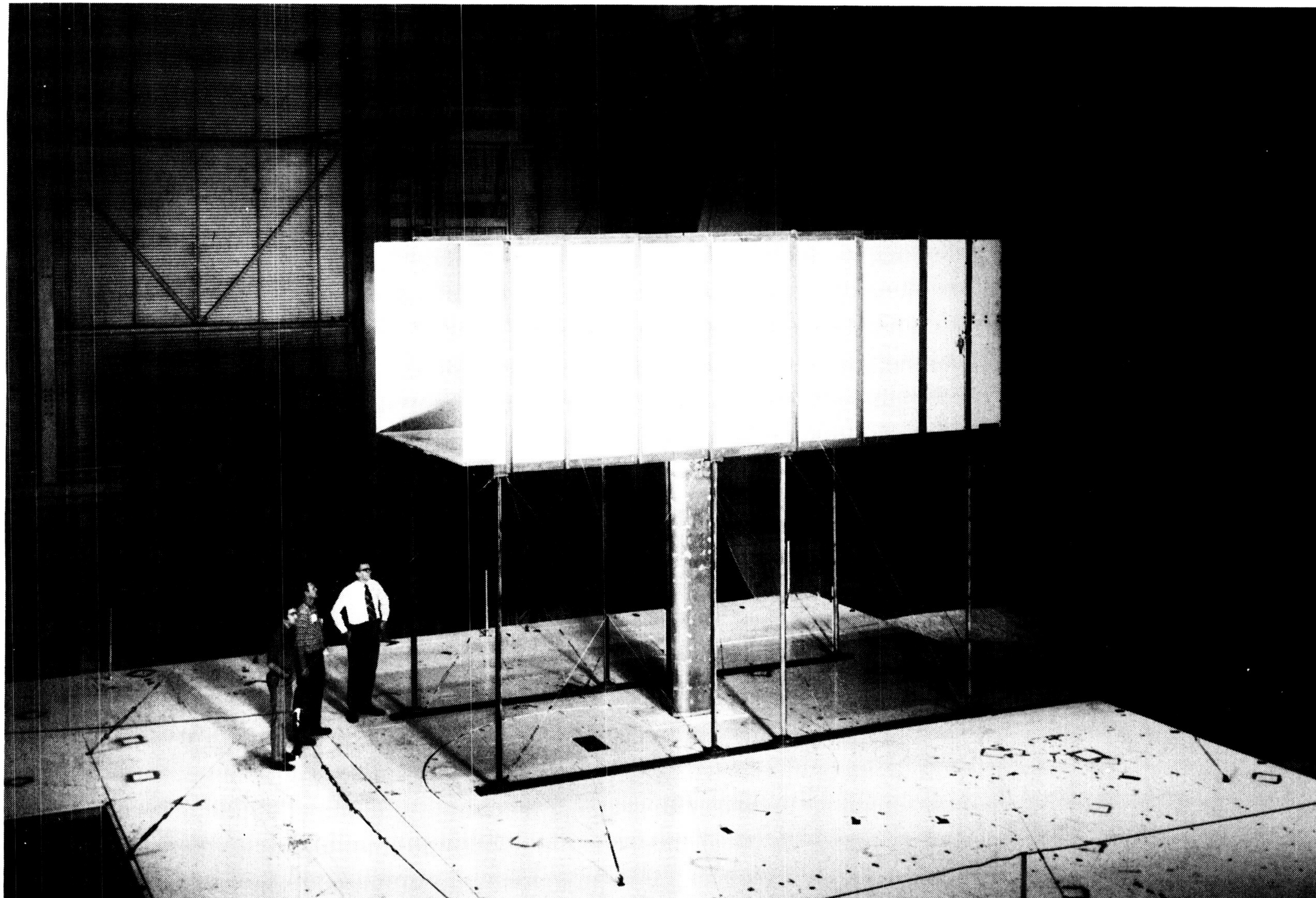

L-72-2872

(b) Side view.

Figure 7.- Continued.

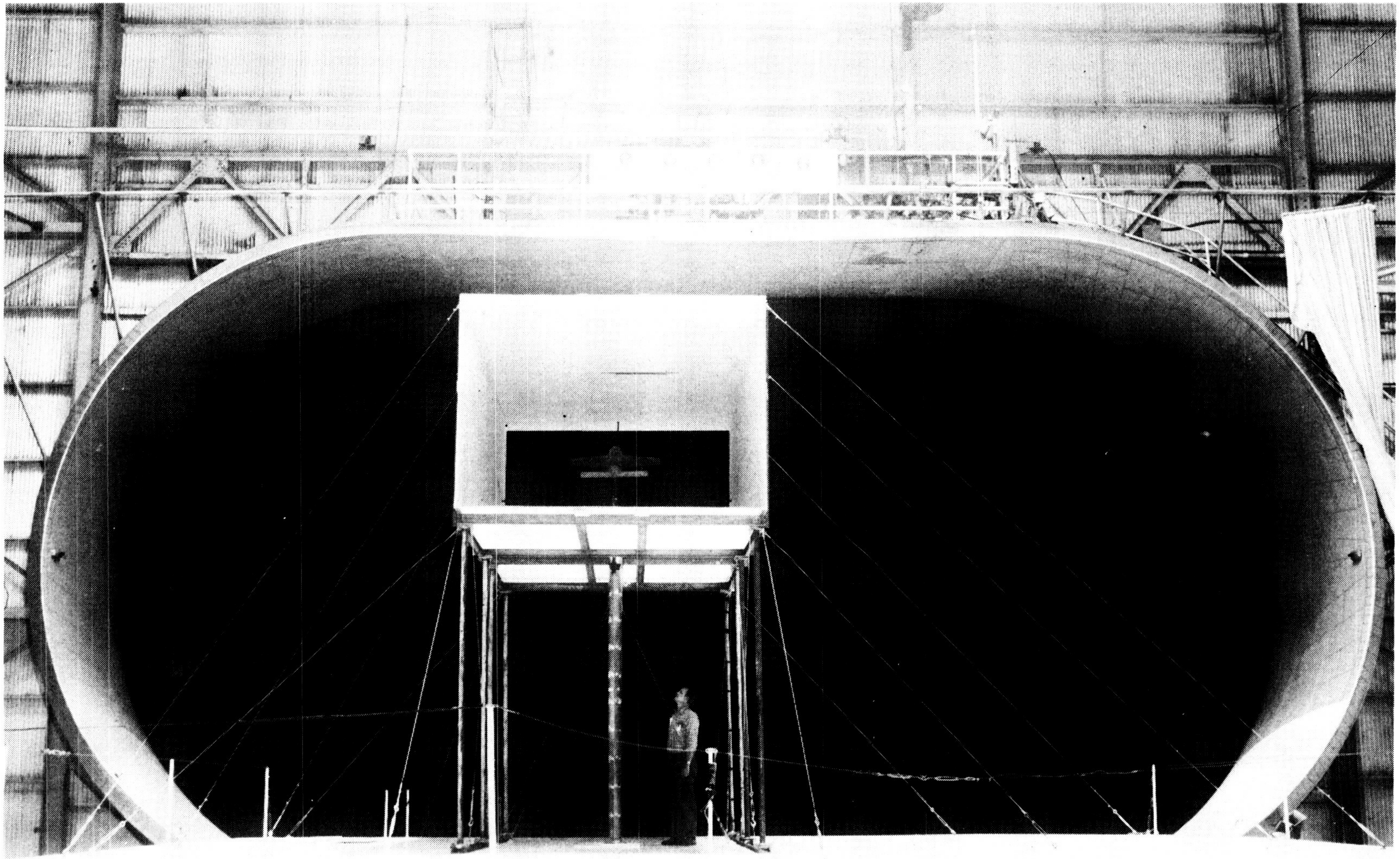

L-72-2874

(c) Rear view.

Figure 7.- Concluded.

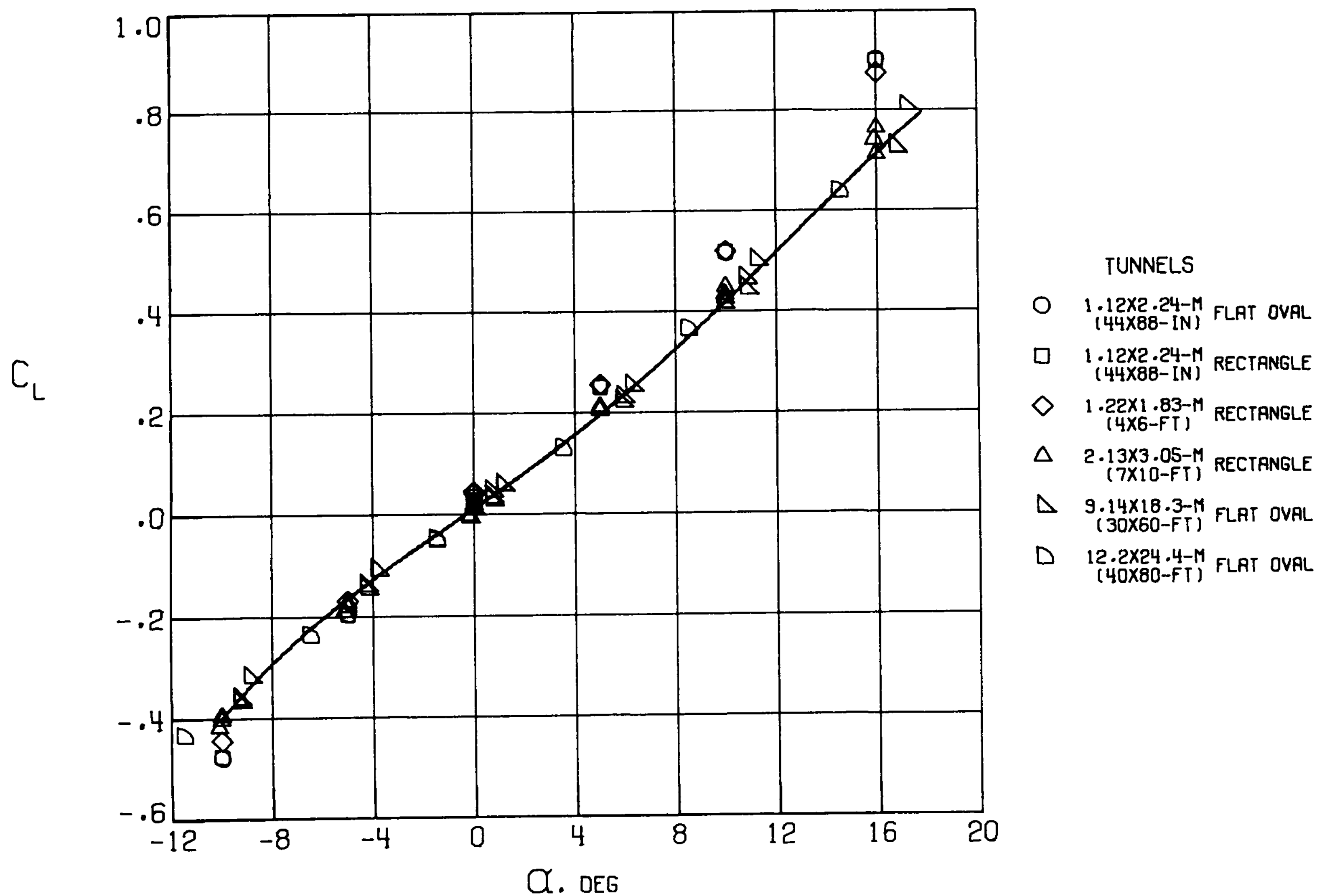

(a) C_L.

Figure 8.- Uncorrected data for the model with the fans covered in several different test sections. The drag of the model at zero angle of attack has been removed from the data. The solid curve is a least-squares quartic faired through the data from the 9.14- by 18.3-m (30- by 60-ft) tunnel.

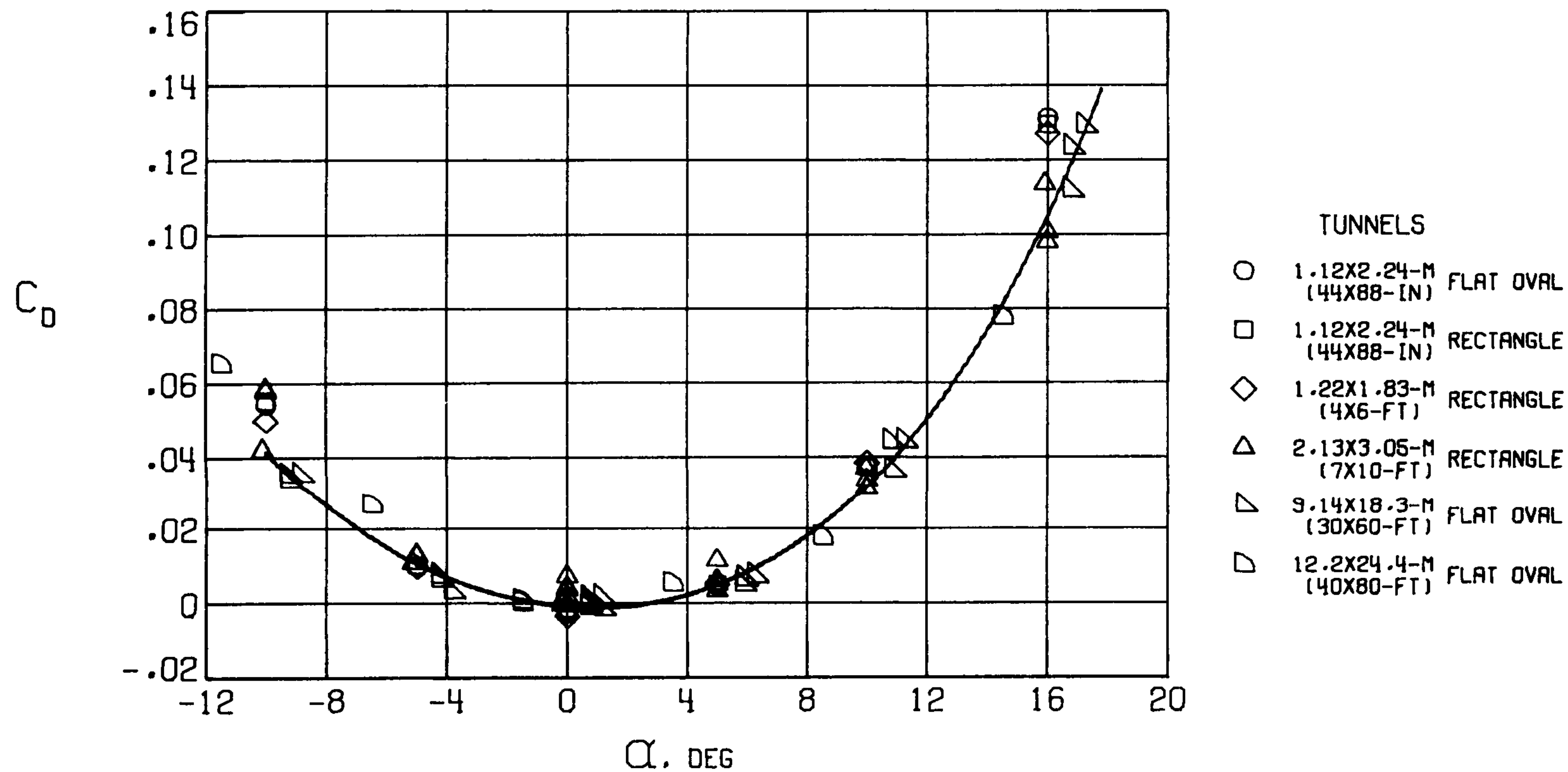

(b) C_D.

Figure 8.- Continued.

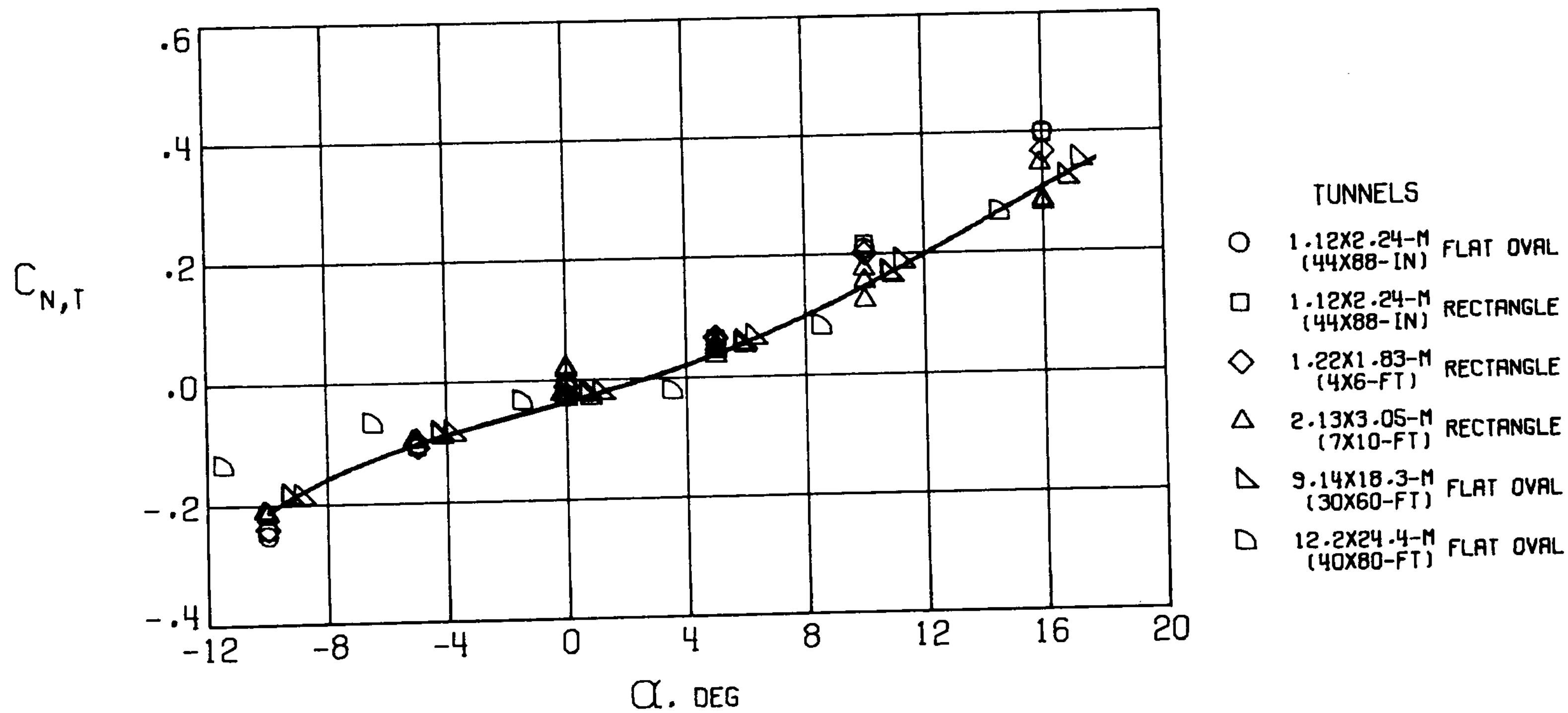

(c) $C_{N,T}$.

Figure 8.- Concluded.

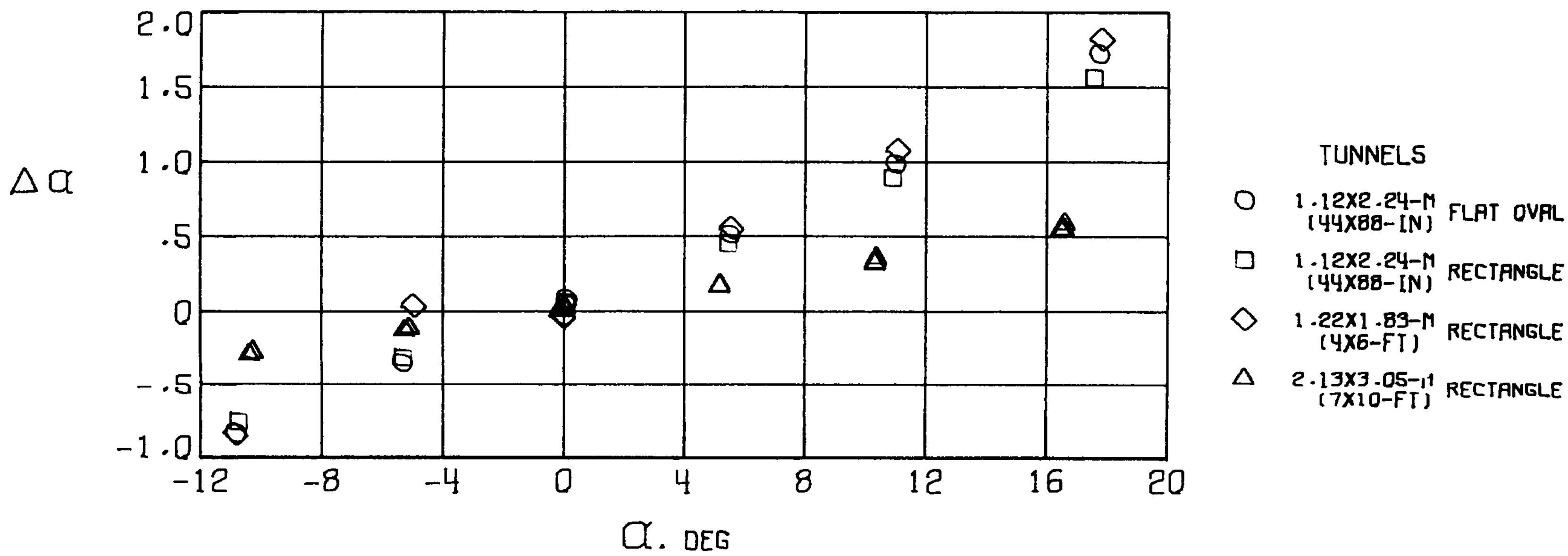

(a) $\Delta\alpha$.

Figure 9.- Calculated corrections for the model with the fans covered in several different test sections.

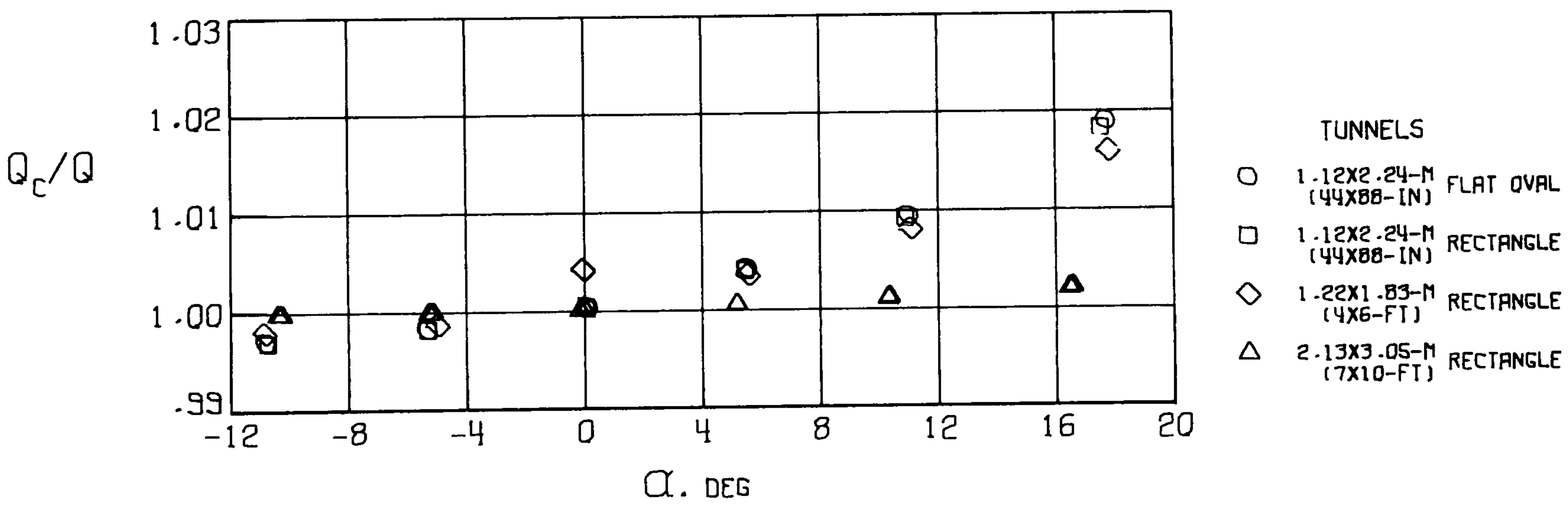

(b) q_c/q.

Figure 9.- Continued.

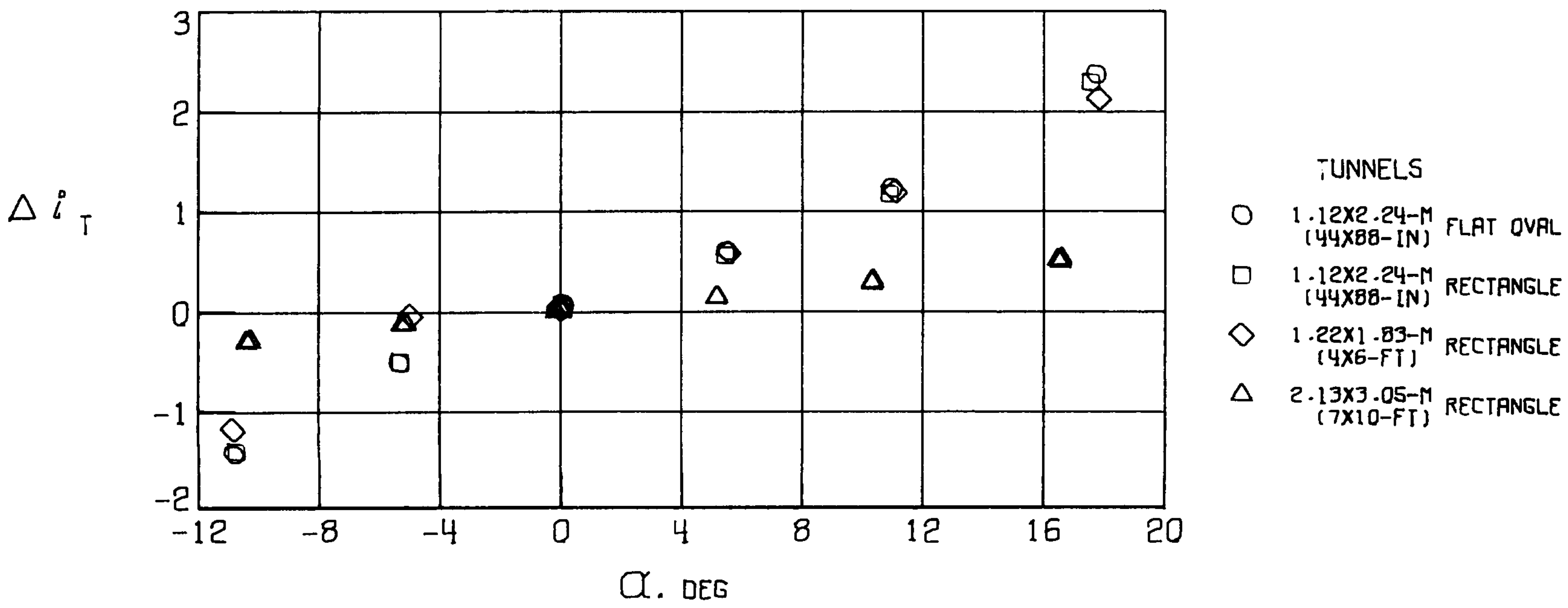

(c) Δi_T.

Figure 9.- Continued.

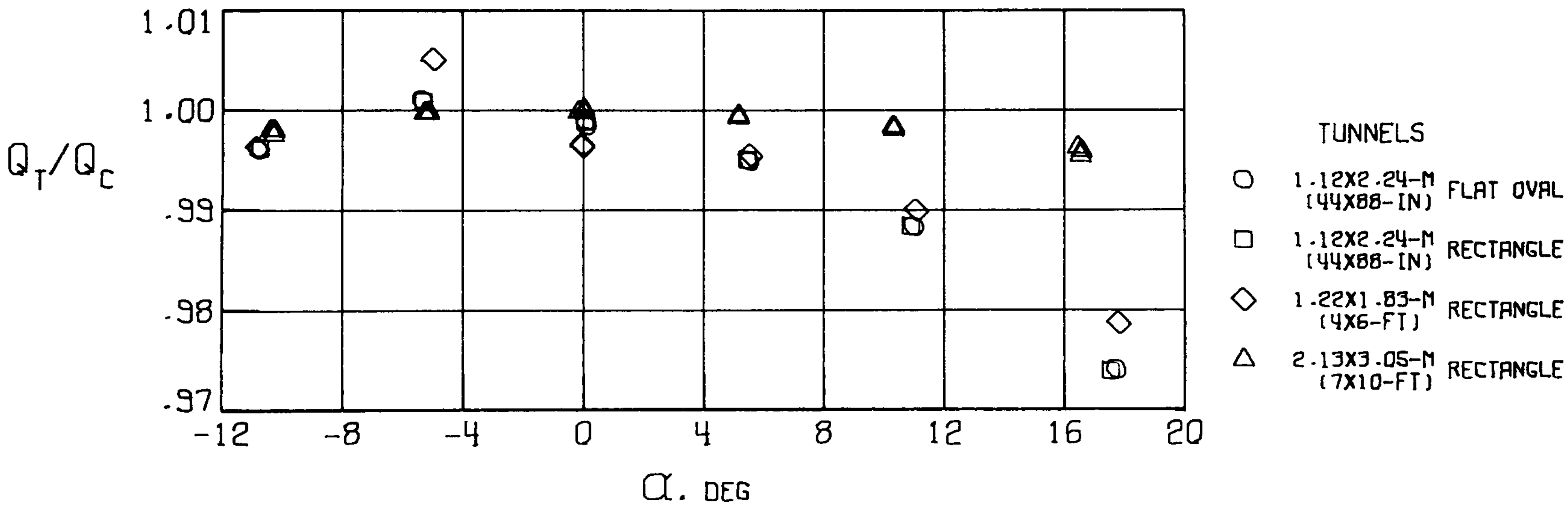

(d) q_T/q_c.

Figure 9.- Concluded.

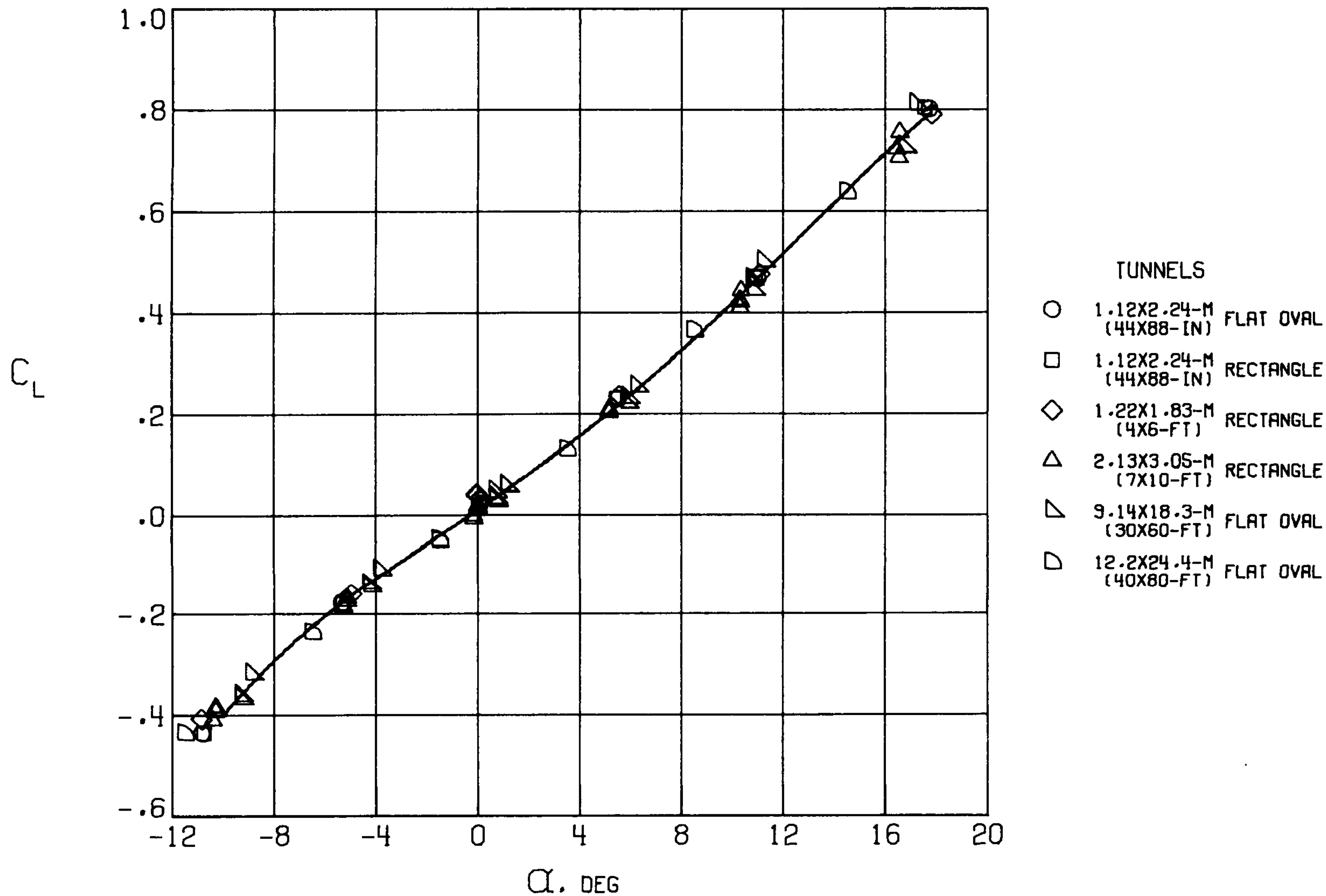

(a) C_L.

Figure 10.- Corrected data for the model with the fans covered in several different test sections. The drag of the model at zero angle of attack has been removed from the data. The solid curve is a least-squares quartic faired through the data from the 9.14- by 18.3-m (30- by 60-ft) tunnel.

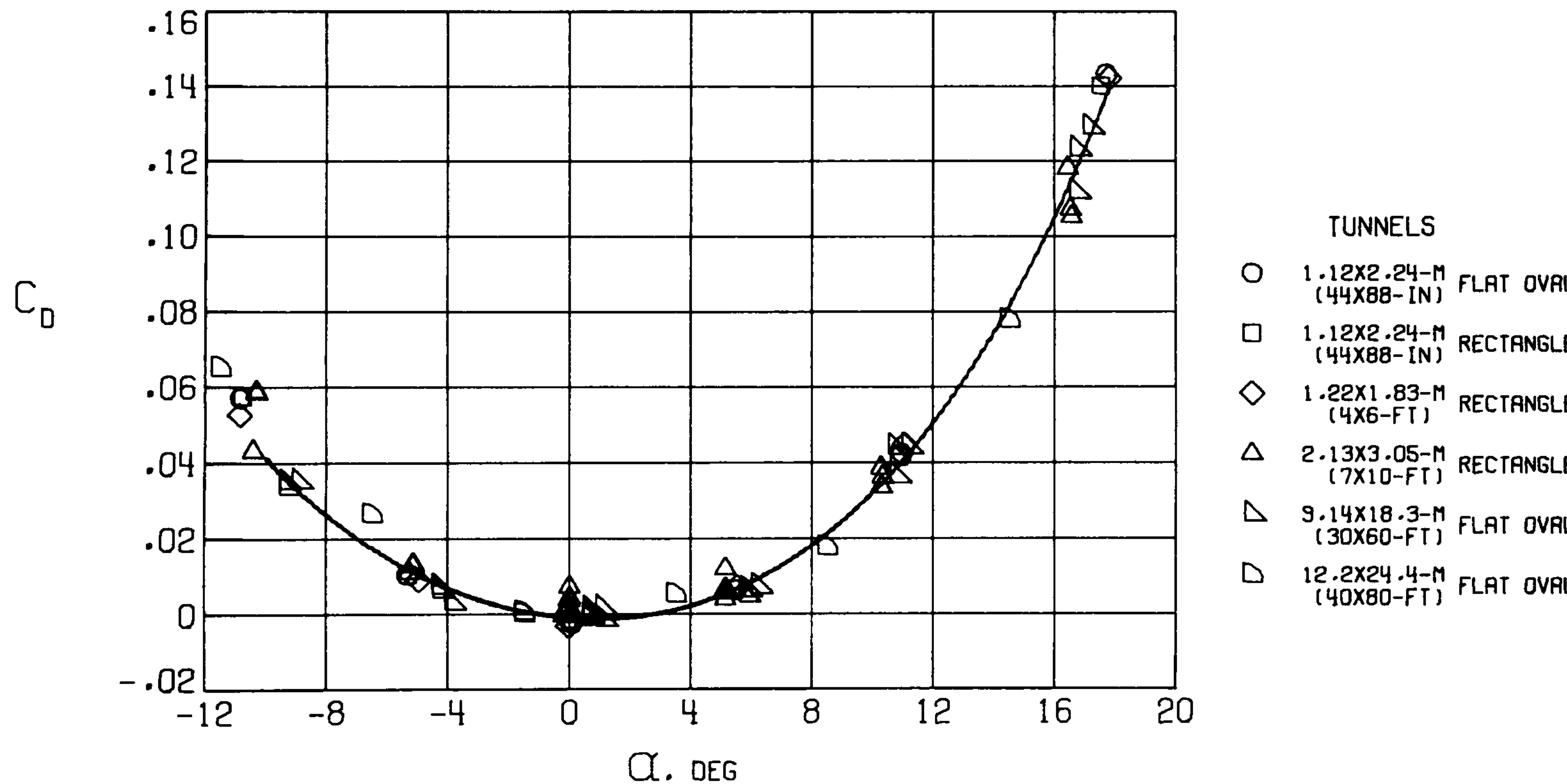

(b) C_D.

Figure 10.- Continued.

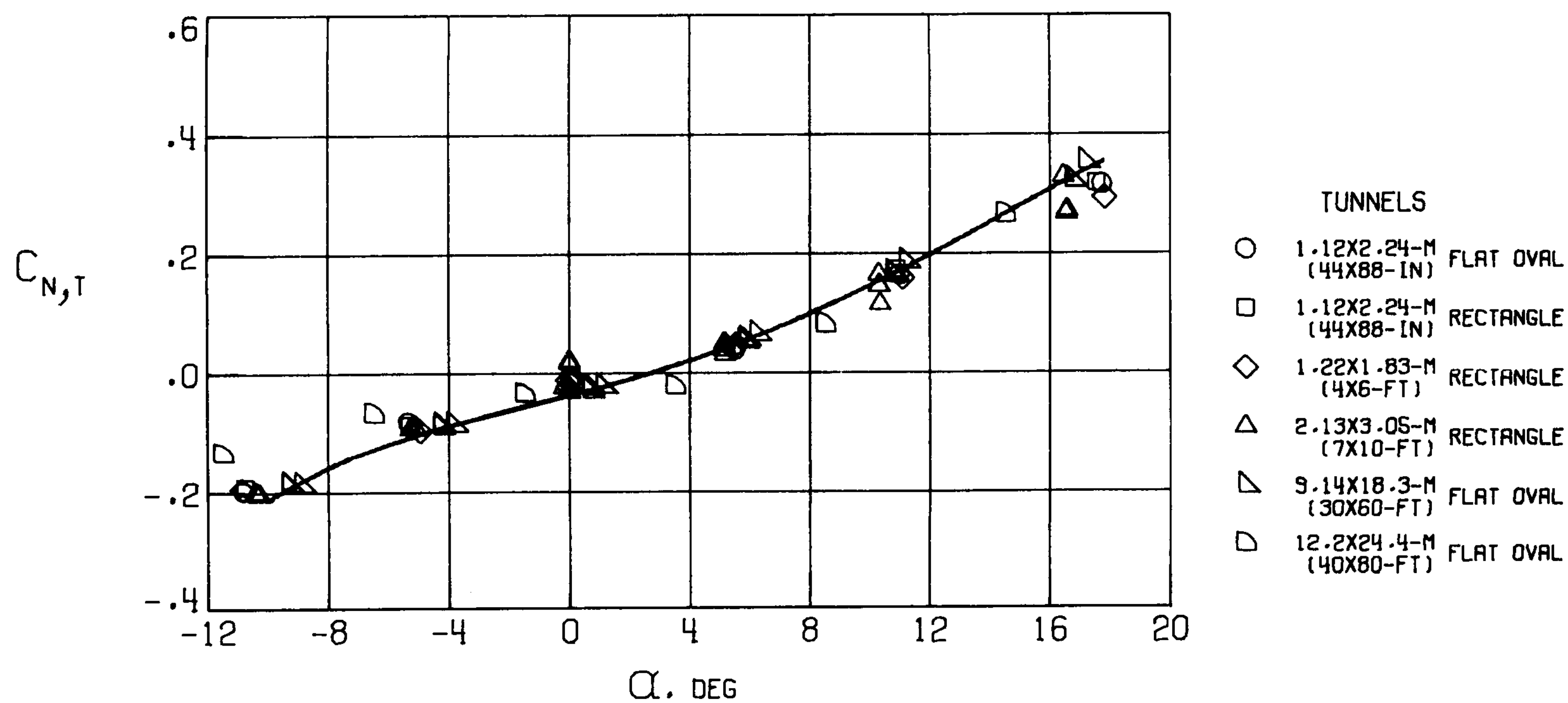

(c) $C_{N,T}$.

Figure 10.- Concluded.

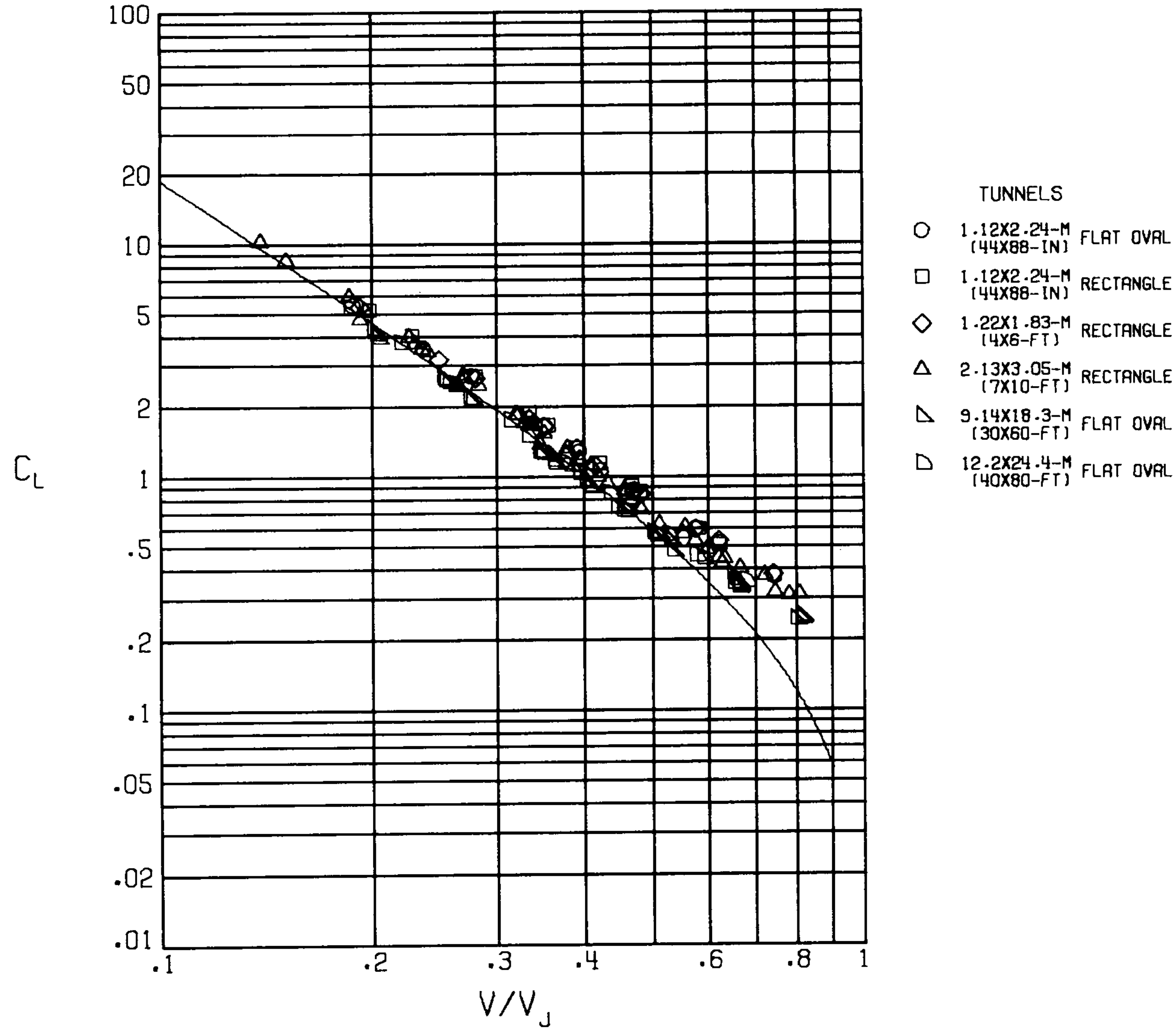

(a) $\alpha = -5^{\circ}$.

Figure 11.- Uncorrected values of lift coefficient as a function of V/V_j. The solid curve represents the sum of the vertical component of the static thrust and the lift of the wing expressed in coefficient form. It is assumed that there is no interference between the wing and the fans.

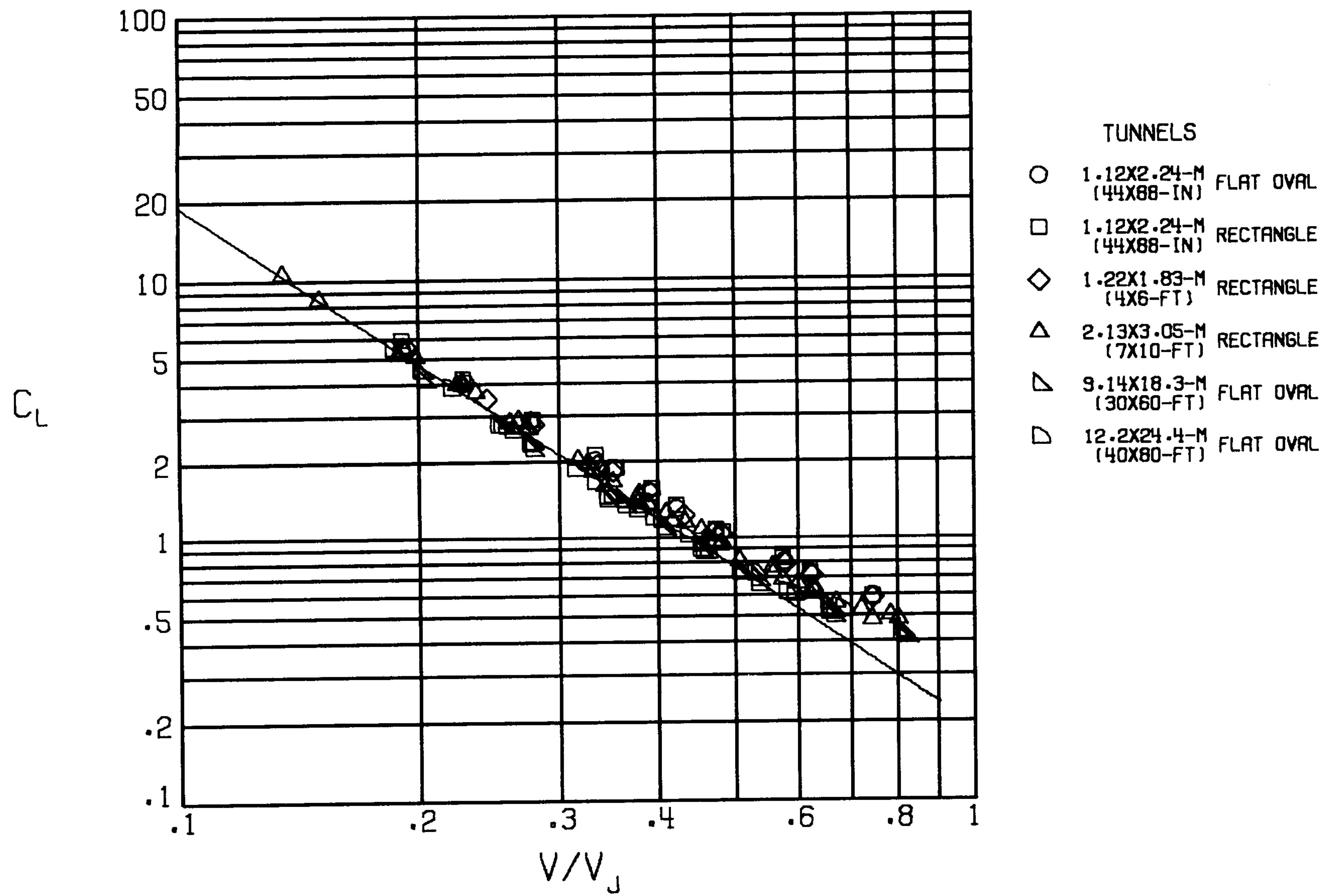

(b) $\alpha = 0^{\circ}$.

Figure 11.- Continued.

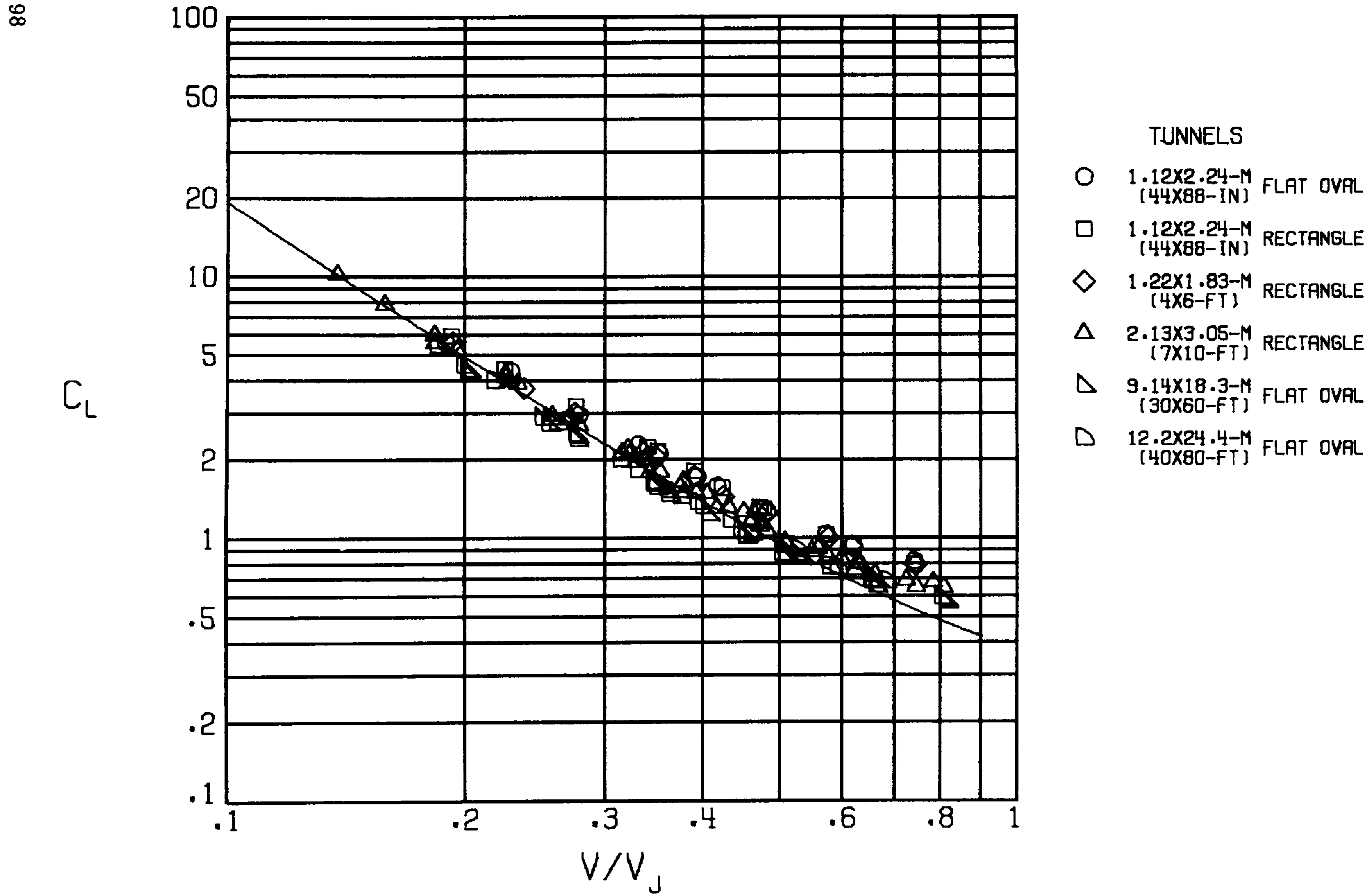

(c) $\alpha = 5^{o}$.

Figure 11.- Continued.

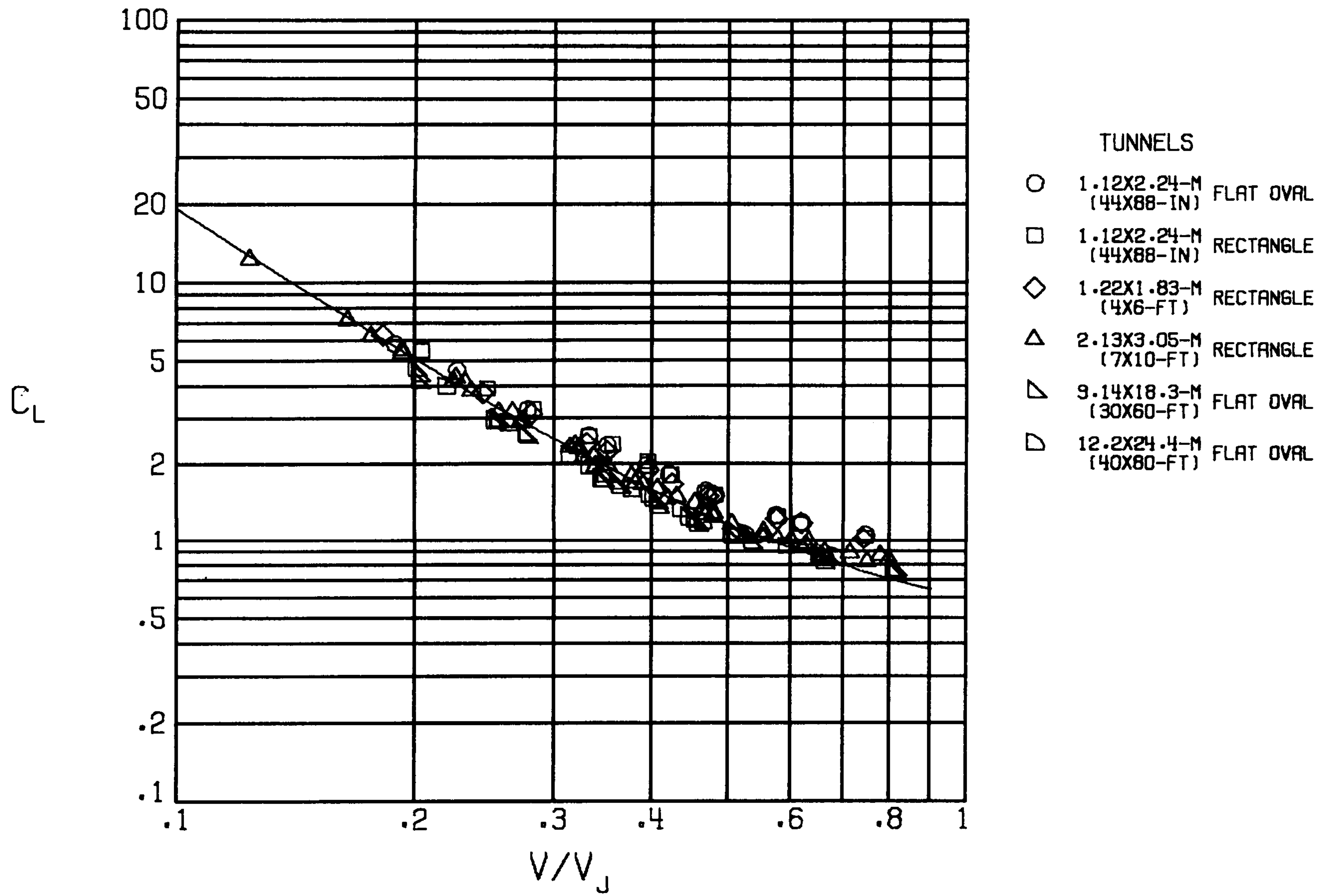

(d) $\alpha = 10^{o}$.

Figure 11.- Continued.

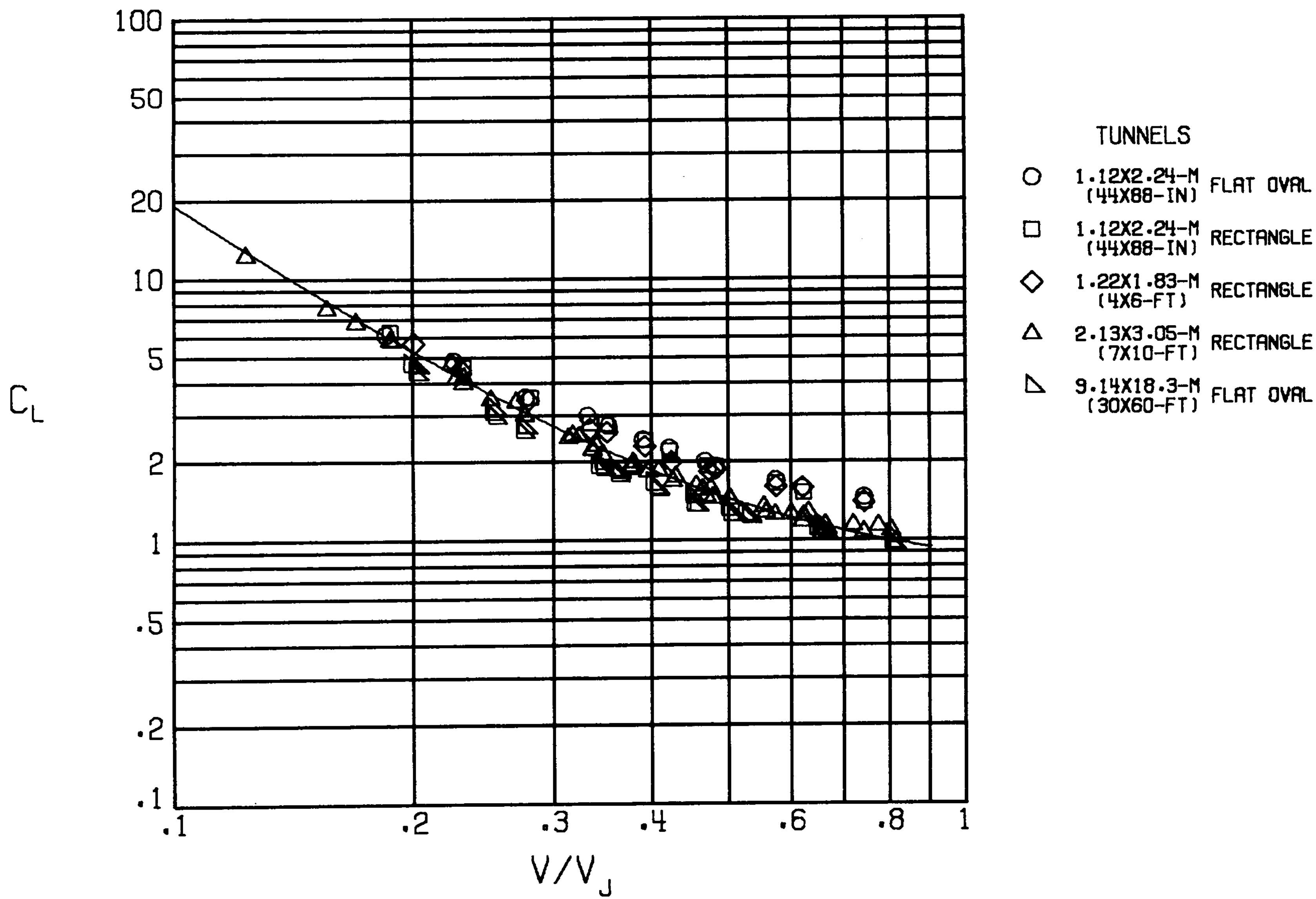

(e) $\alpha = 16^o$.

Figure 11.- Concluded.

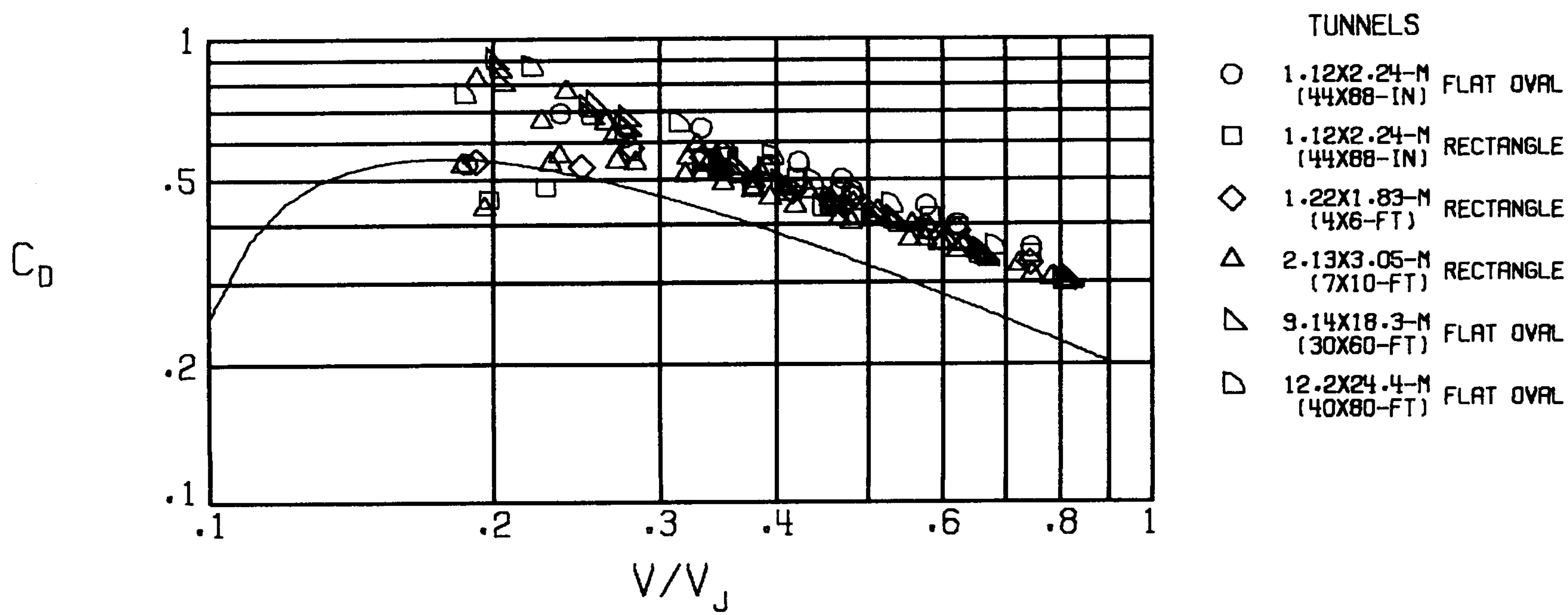

(a) $\alpha = -5^{\circ}$.

Figure 12.- Uncorrected values of drag coefficient as a function of V/V_j. The solid curve represents the sum of the momentum-theory value of fan drag and the drag of the wing expressed in coefficient form. It is assumed that there is no interference between the wing and the fans.

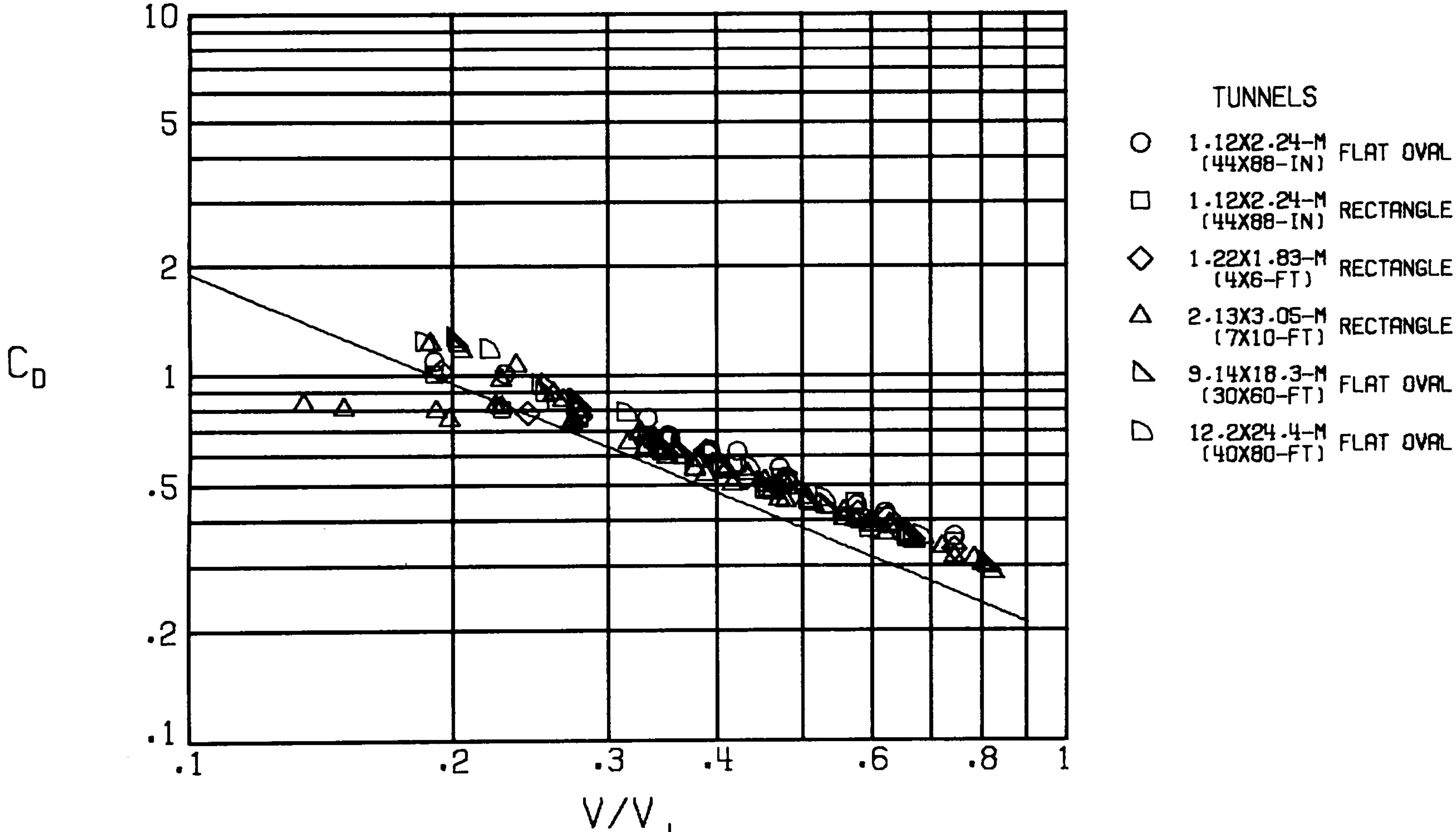

(b) $\alpha = 0^{o}$.

Figure 12.- Continued.

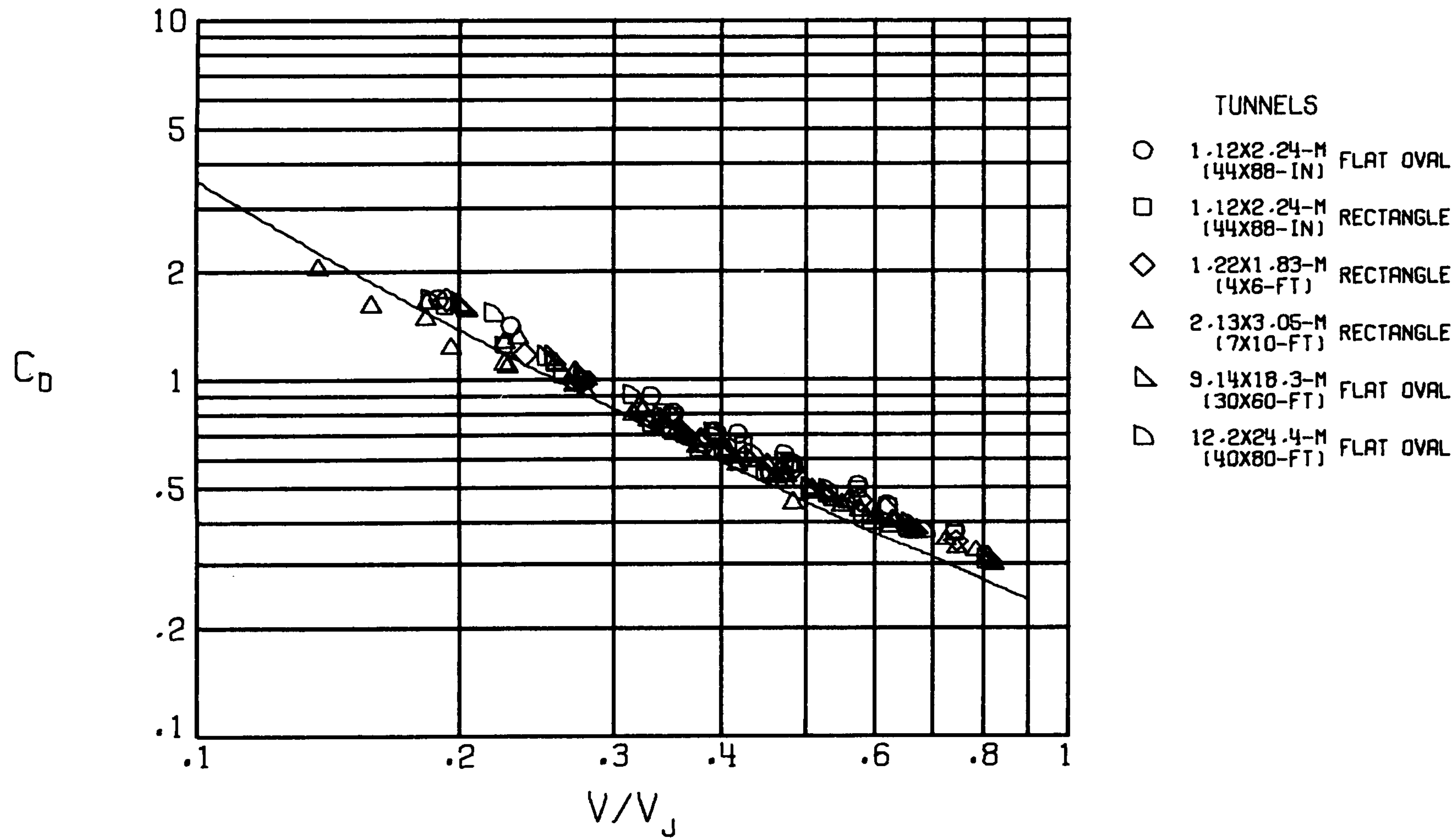

(c) $\alpha = 5^{o}$.

Figure 12.- Continued.

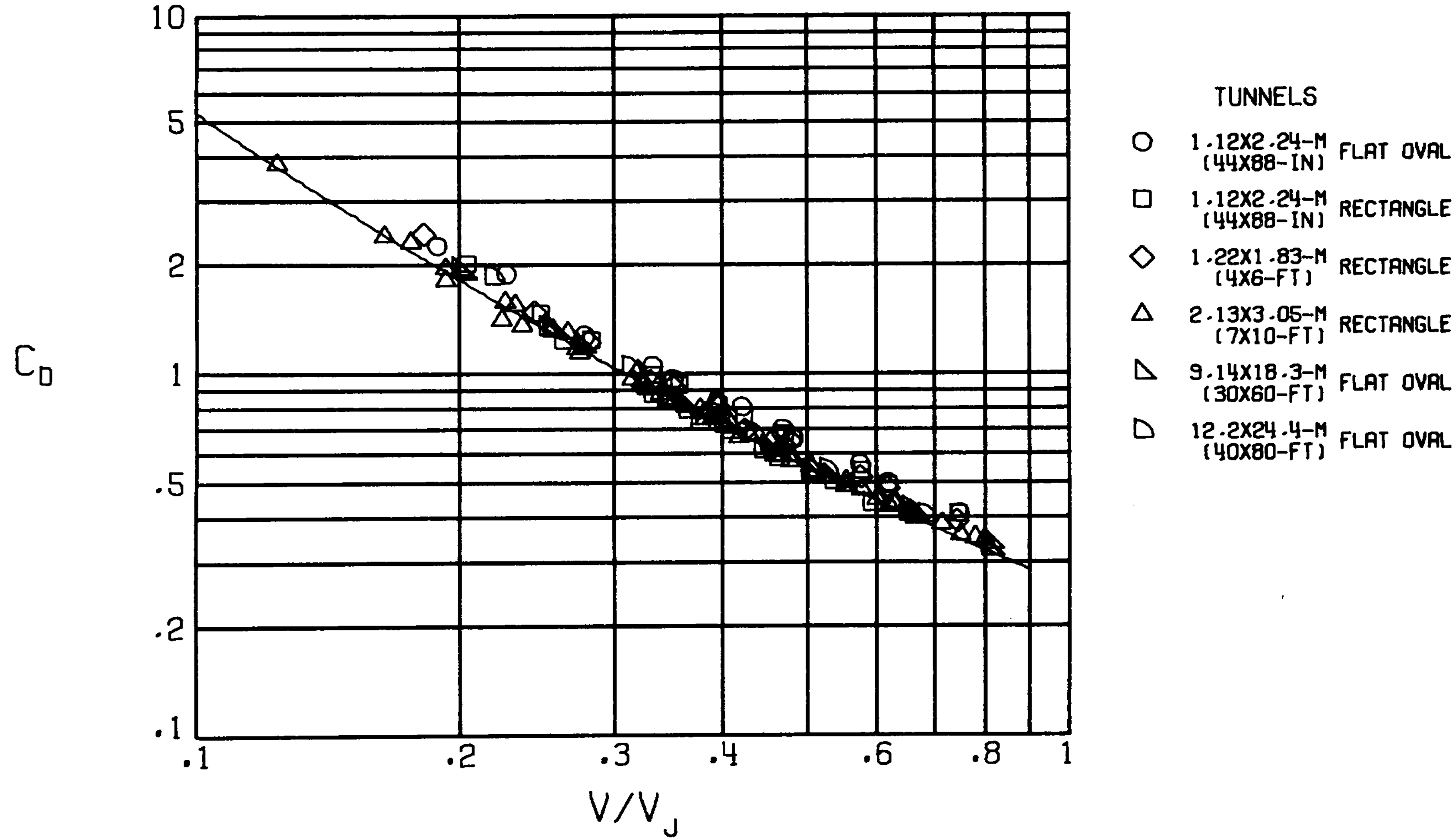

(d) $\alpha = 10^{o}$.

Figure 12.- Continued.

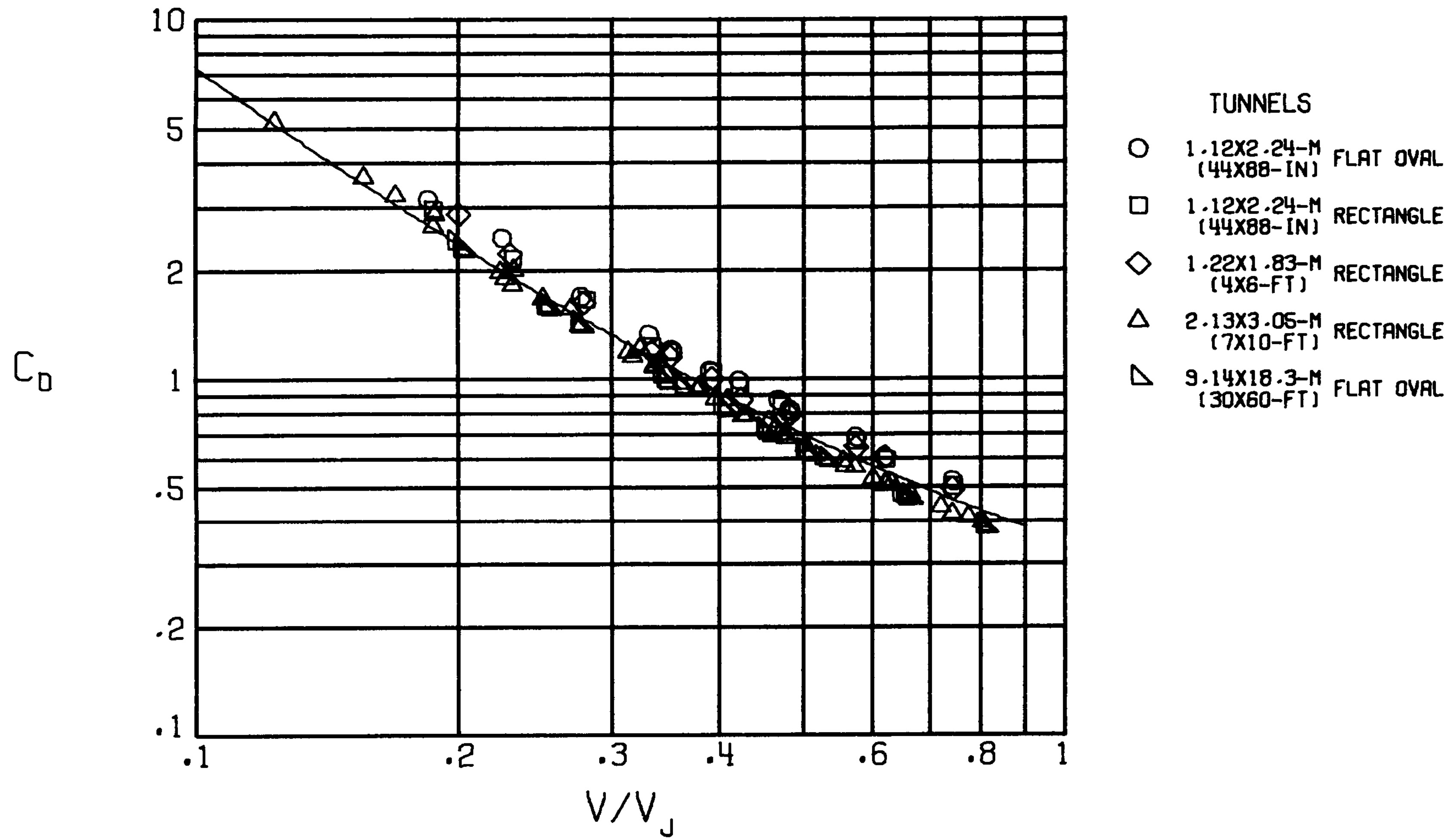

(e) $\alpha = 16^{o}$.

Figure 12.- Concluded.

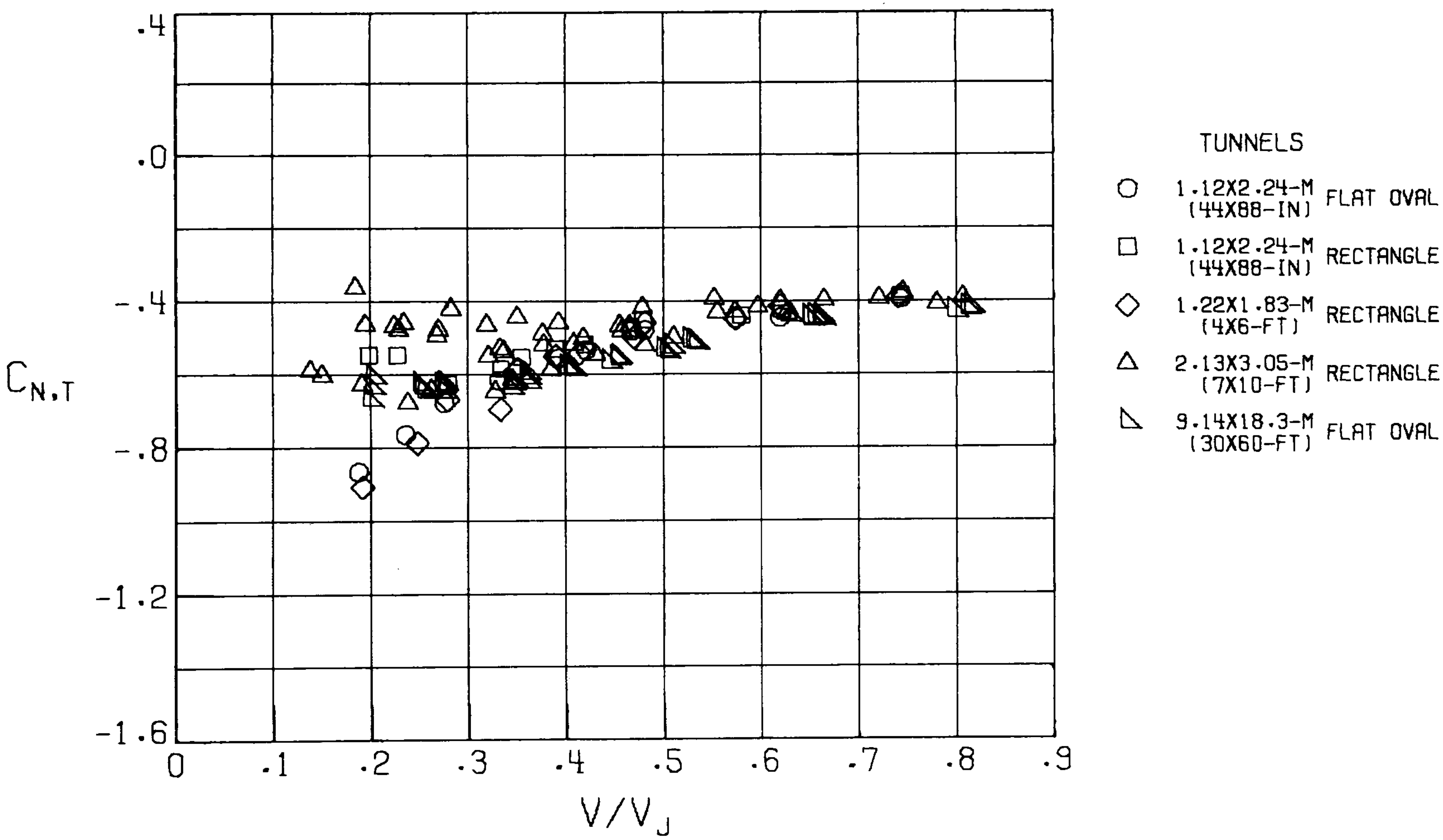

(a) $\alpha = -5^{o}$.

Figure 13.- Uncorrected values of tail normal-force coefficient as a function of V/V_j.

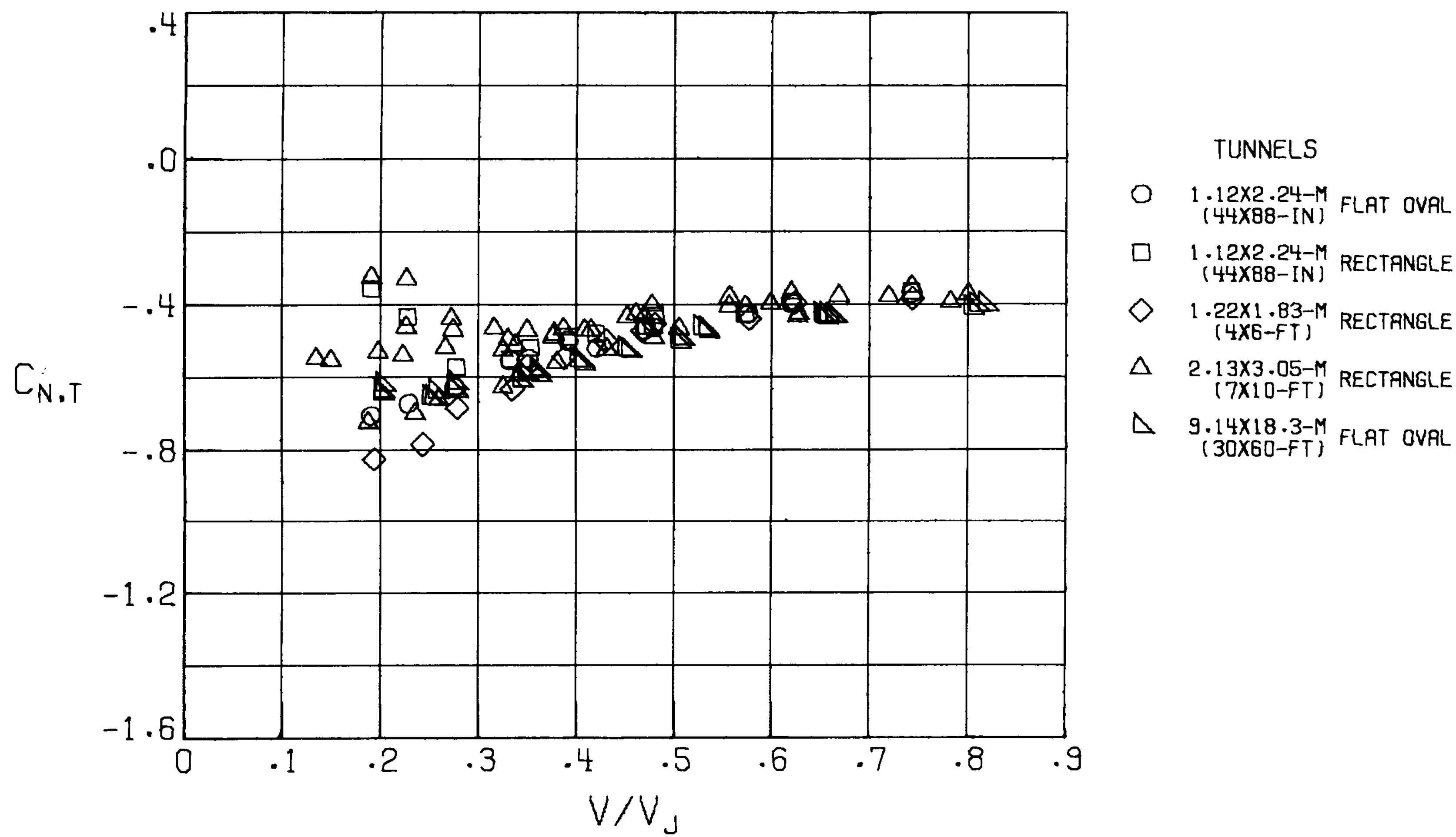

(b) $\alpha = 0^{o}$.

Figure 13.- Continued.

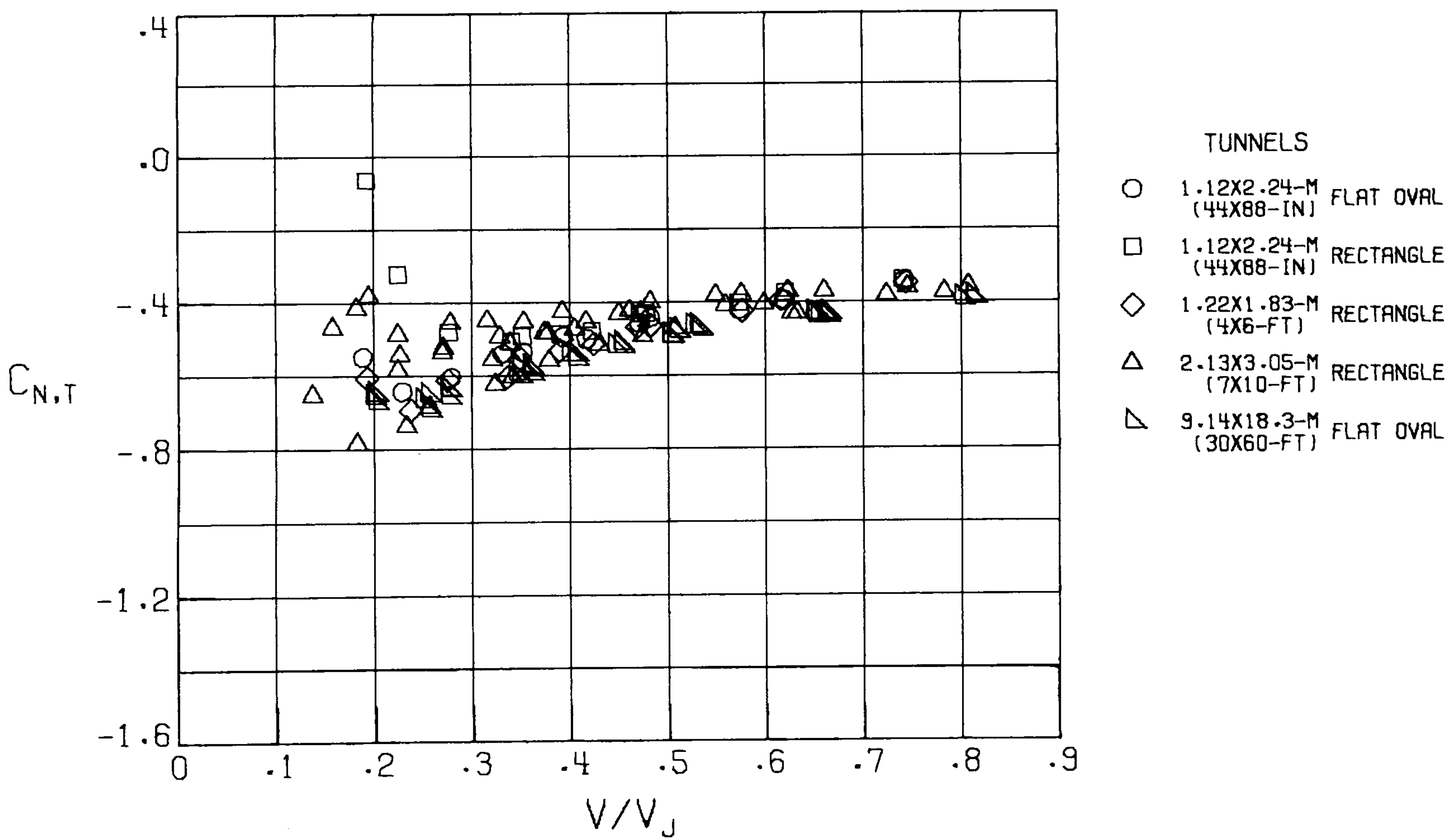

(c) $\alpha = 5^{o}$.

Figure 13.- Continued.

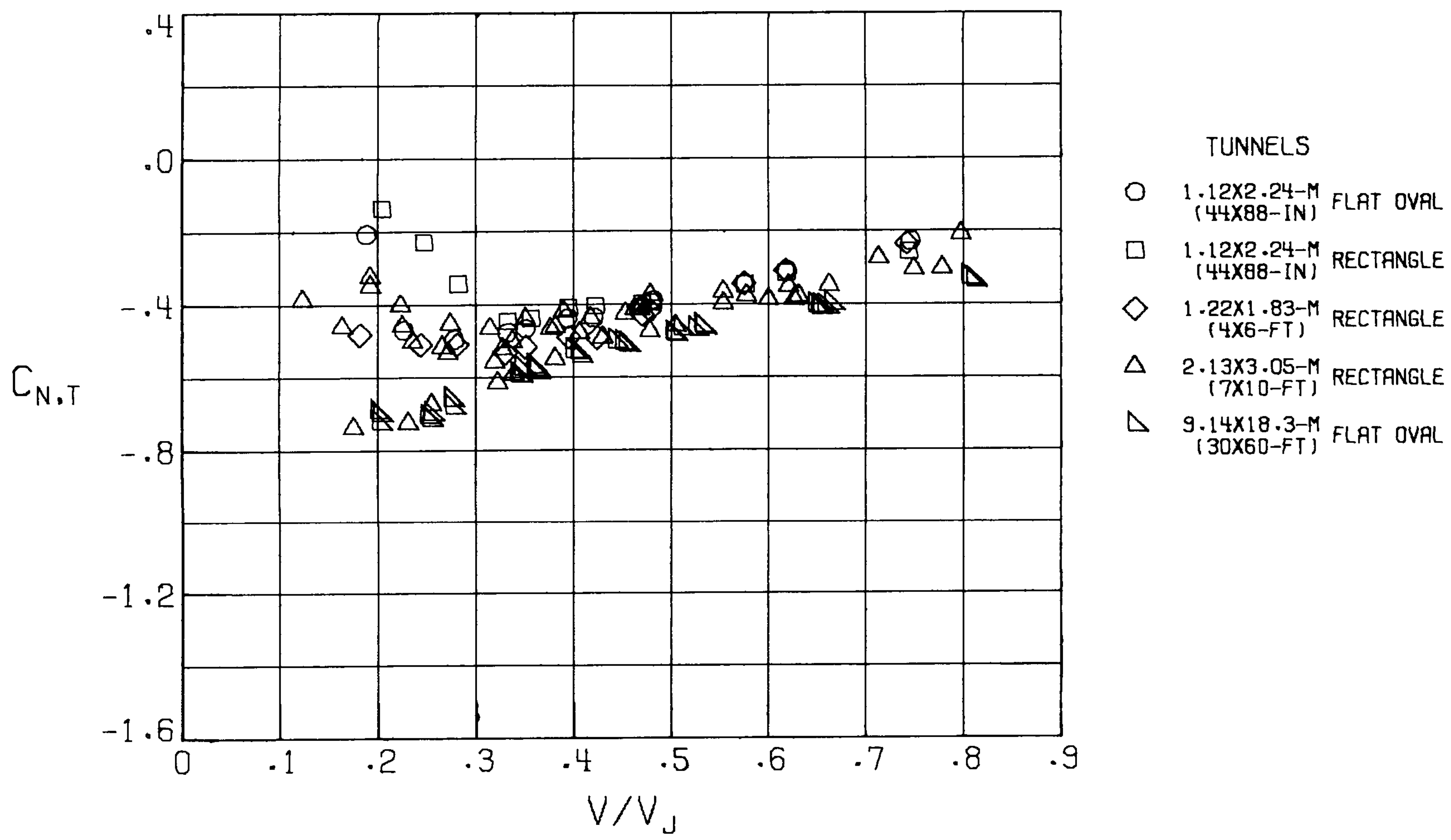

(d) $\alpha = 10^{\circ}$.

Figure 13.- Continued.

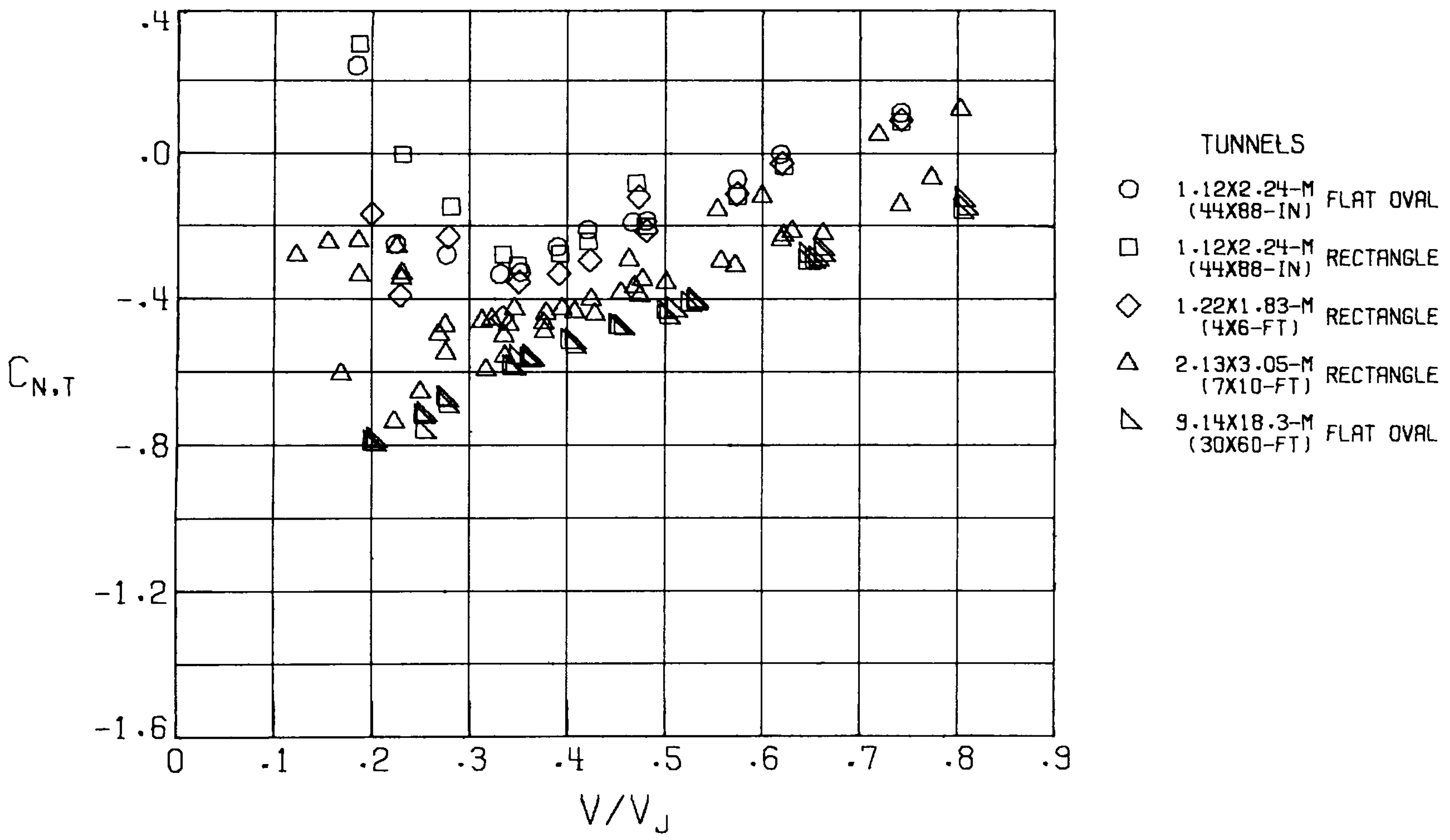

(e) $\alpha = 16^{o}$.

Figure 13.- Concluded.

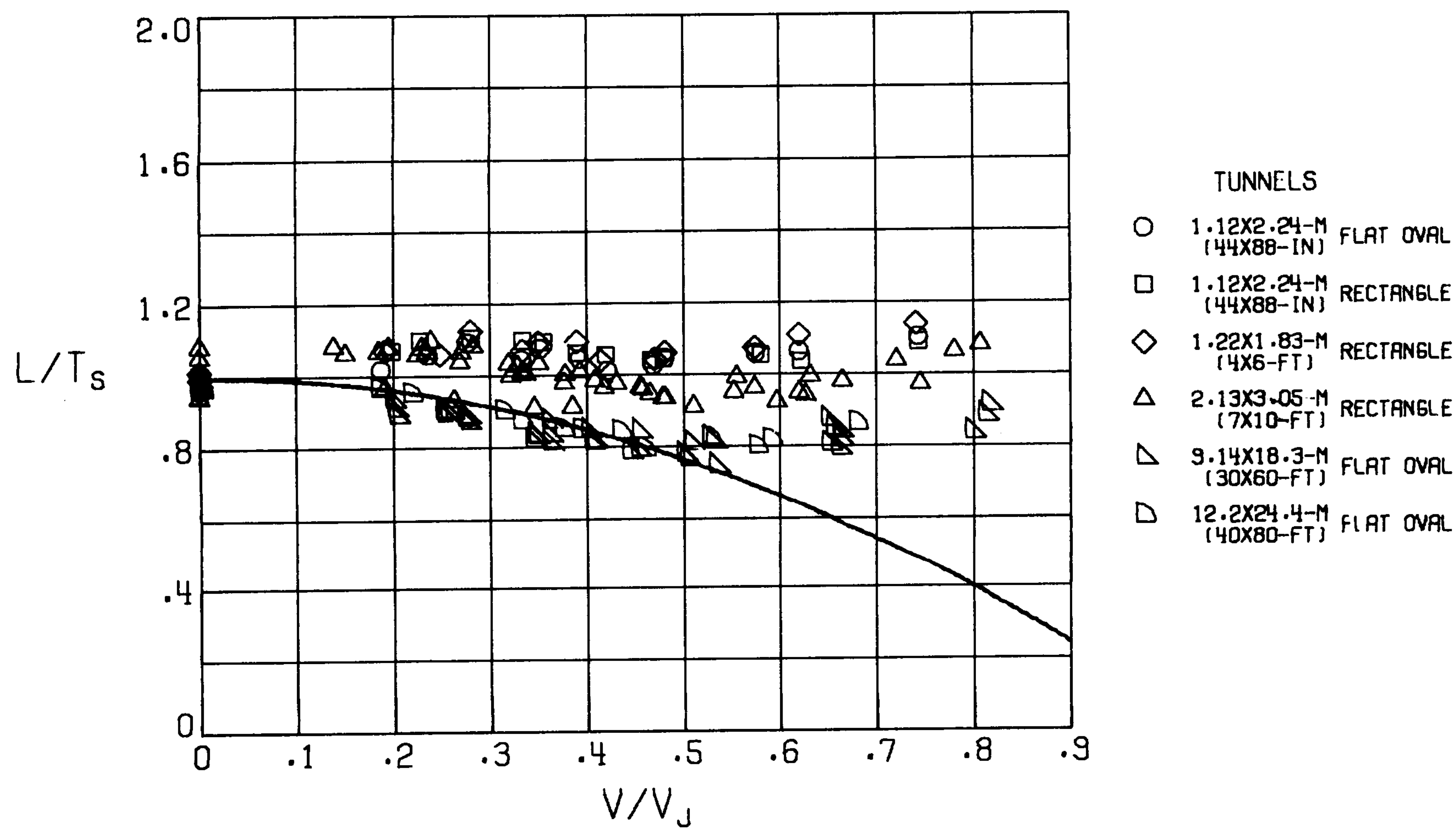

(a) $\alpha = -5^{o}$.

Figure 14.- Uncorrected values of ratios of lift to static thrust as a function of V/V_j. The curve is the sum of the vertical component of static thrust and the lift of the wing. It is assumed that there is no interference between the fans and the wing.

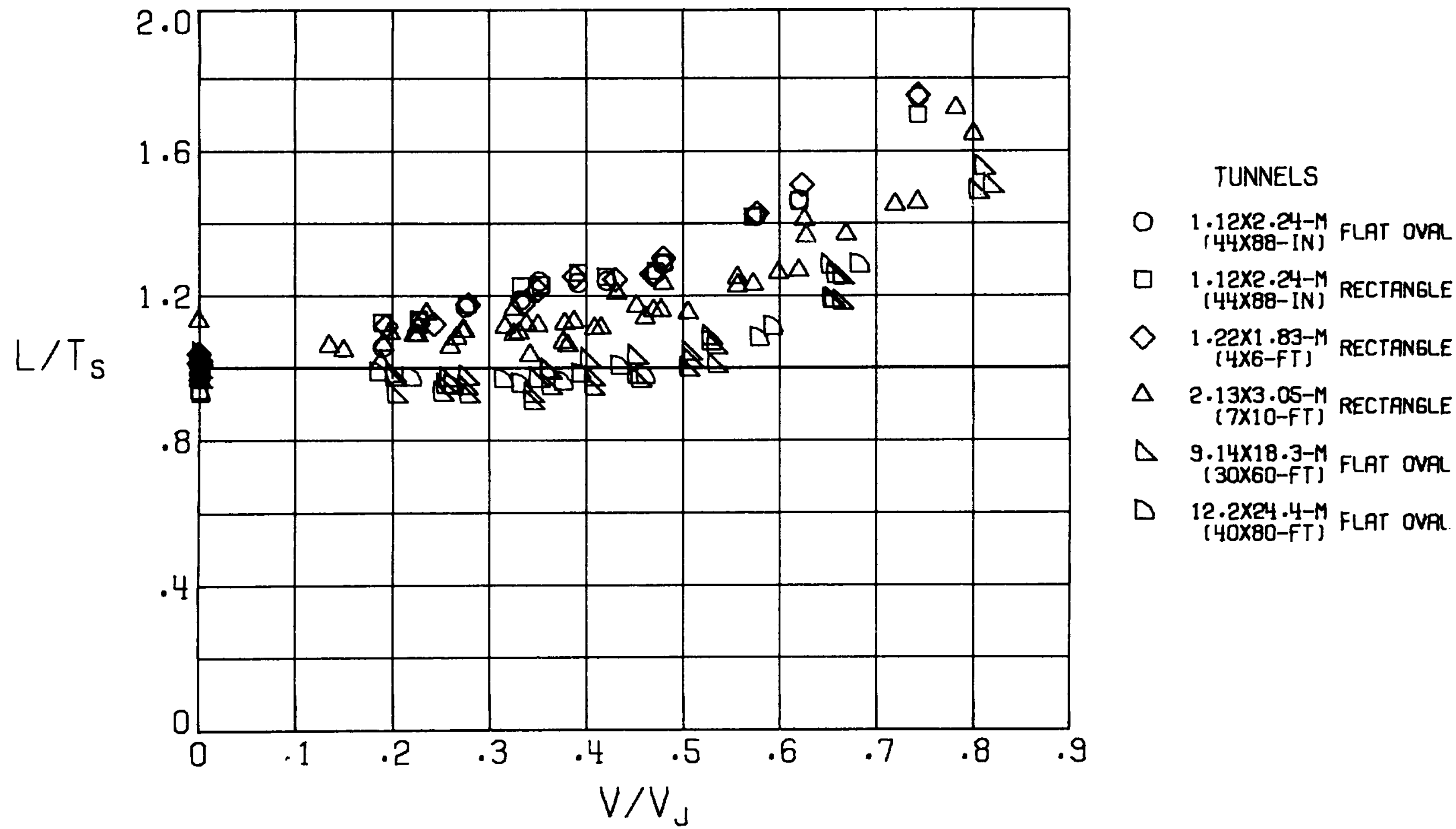

(b) $\alpha = 0^{o}$.

Figure 14.- Continued.

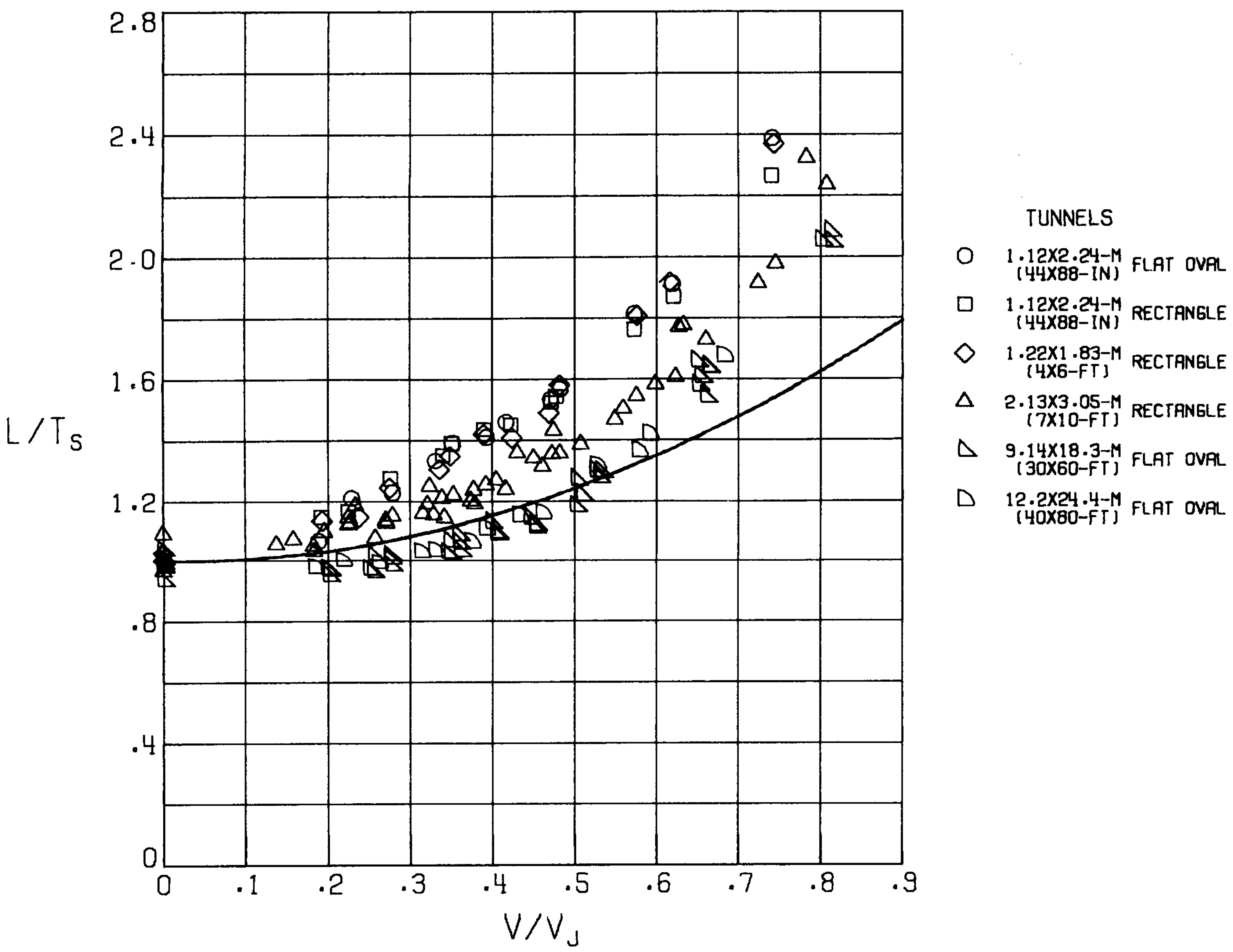

(c) $\alpha = 5^{o}$.

Figure 14.- Continued.

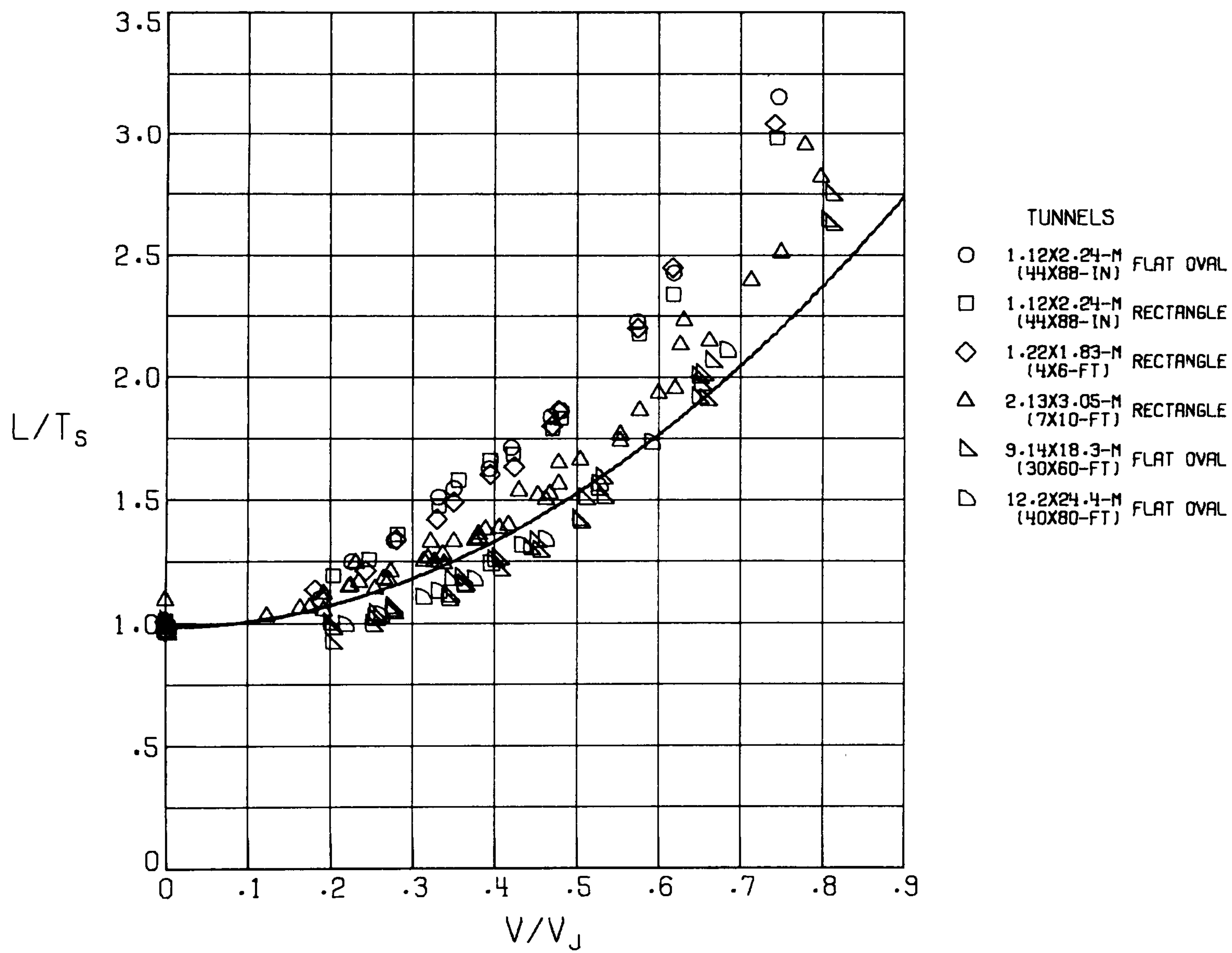

(d) $\alpha = 10^{o}$.

Figure 14.- Continued.

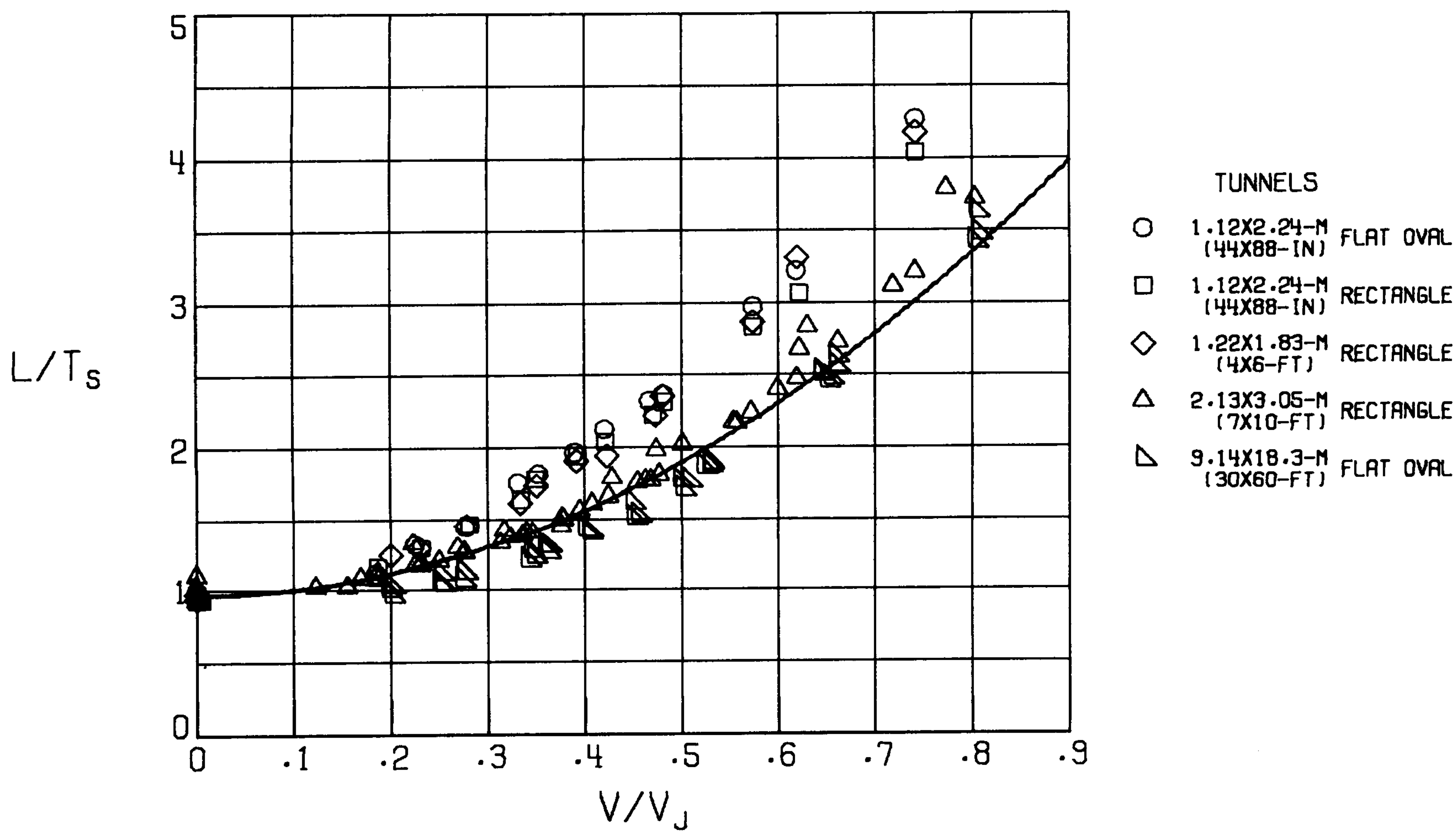

(e) $\alpha = 16^{o}$.

Figure 14.- Concluded.

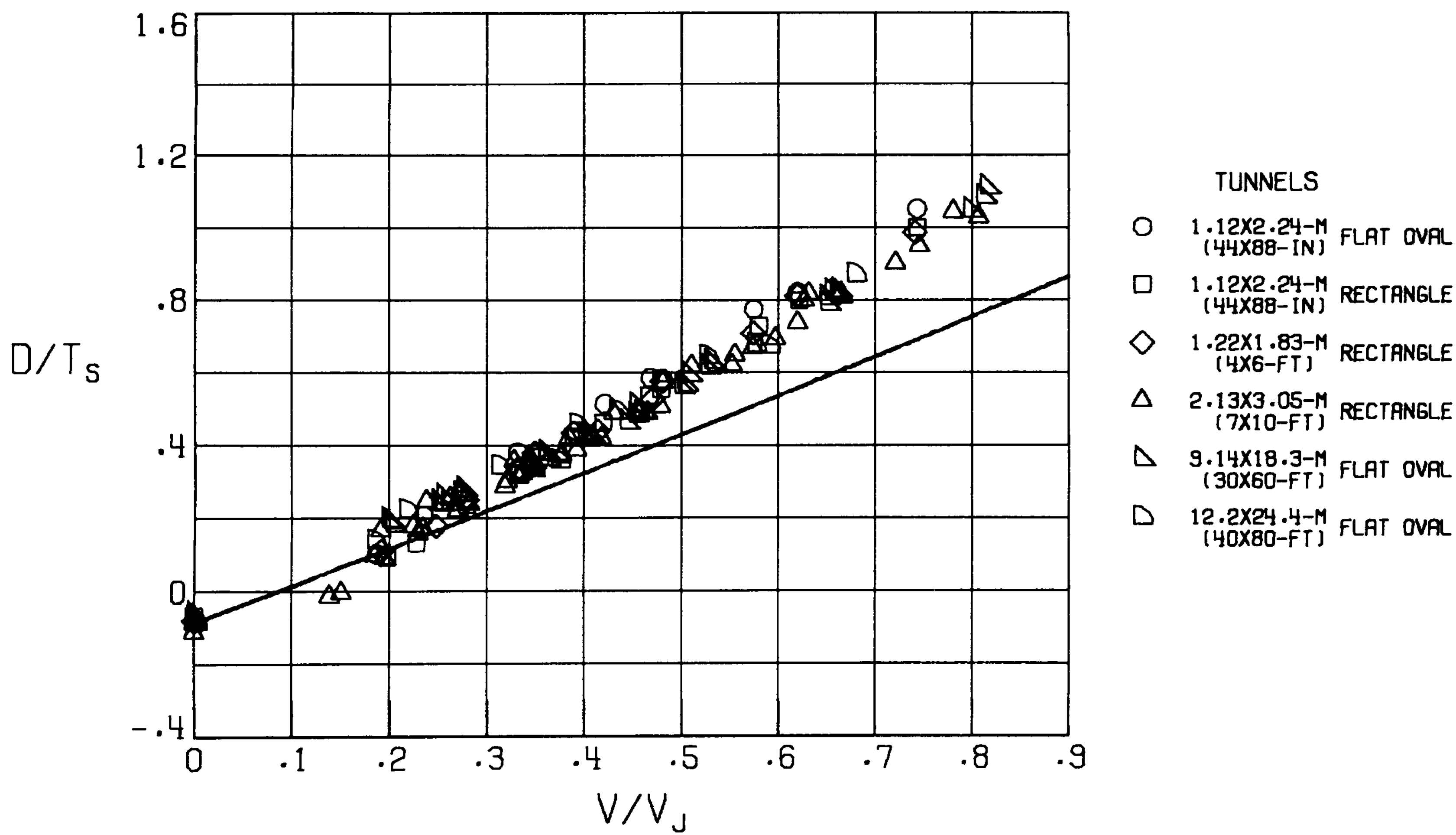

(a) $\alpha = -5^{\circ}$.

Figure 15.- Uncorrected values of ratios of drag to static thrust as a function of V/V_j. The curve is calculated from the momentum-theory values of the fan forces and the lift and drag of the wing. It is assumed that there is no interference between the fans and the wing.

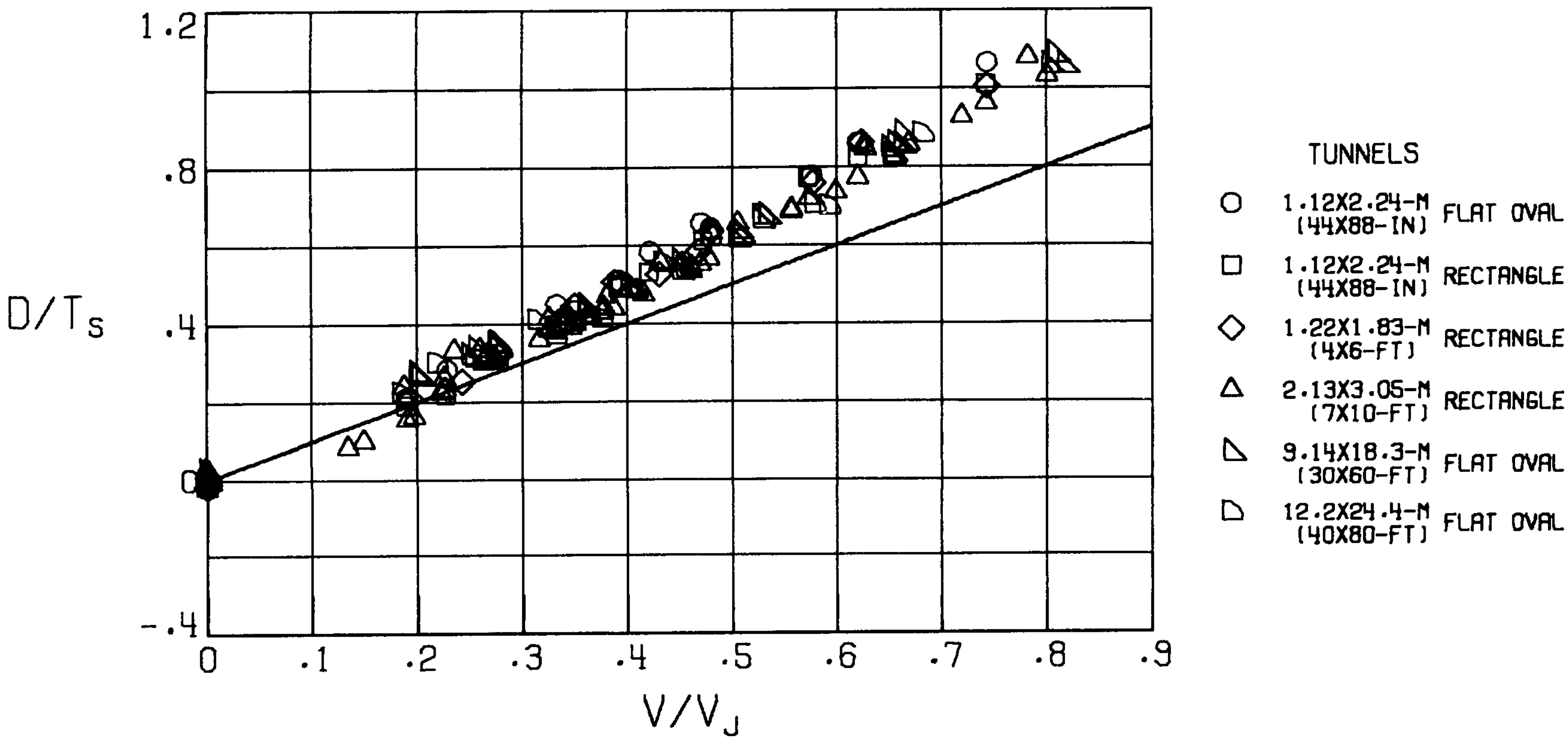

(b) $\alpha = 0^{\circ}$.

Figure 15.- Continued.

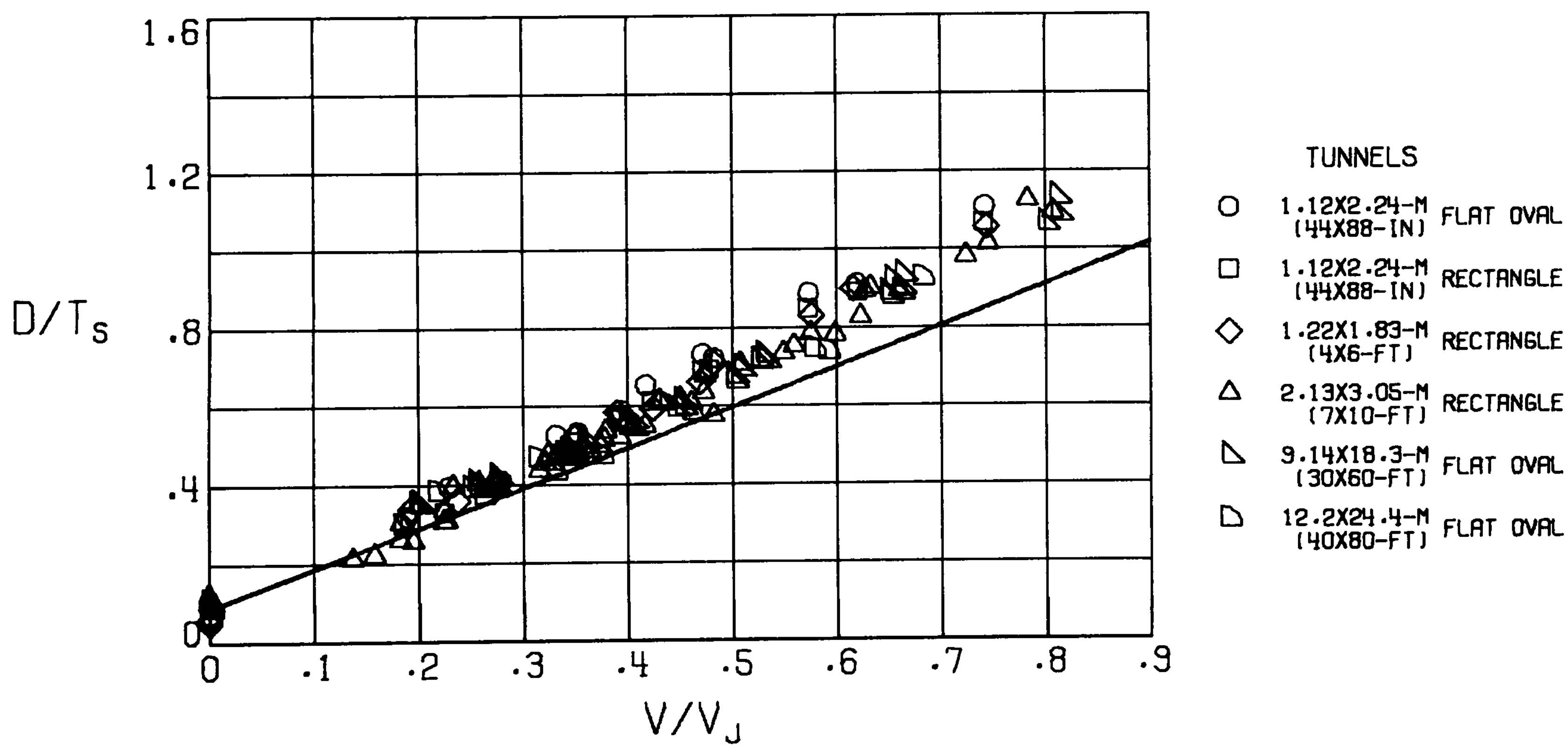

(c) $\alpha = 5^{o}$.

Figure 15.- Continued.

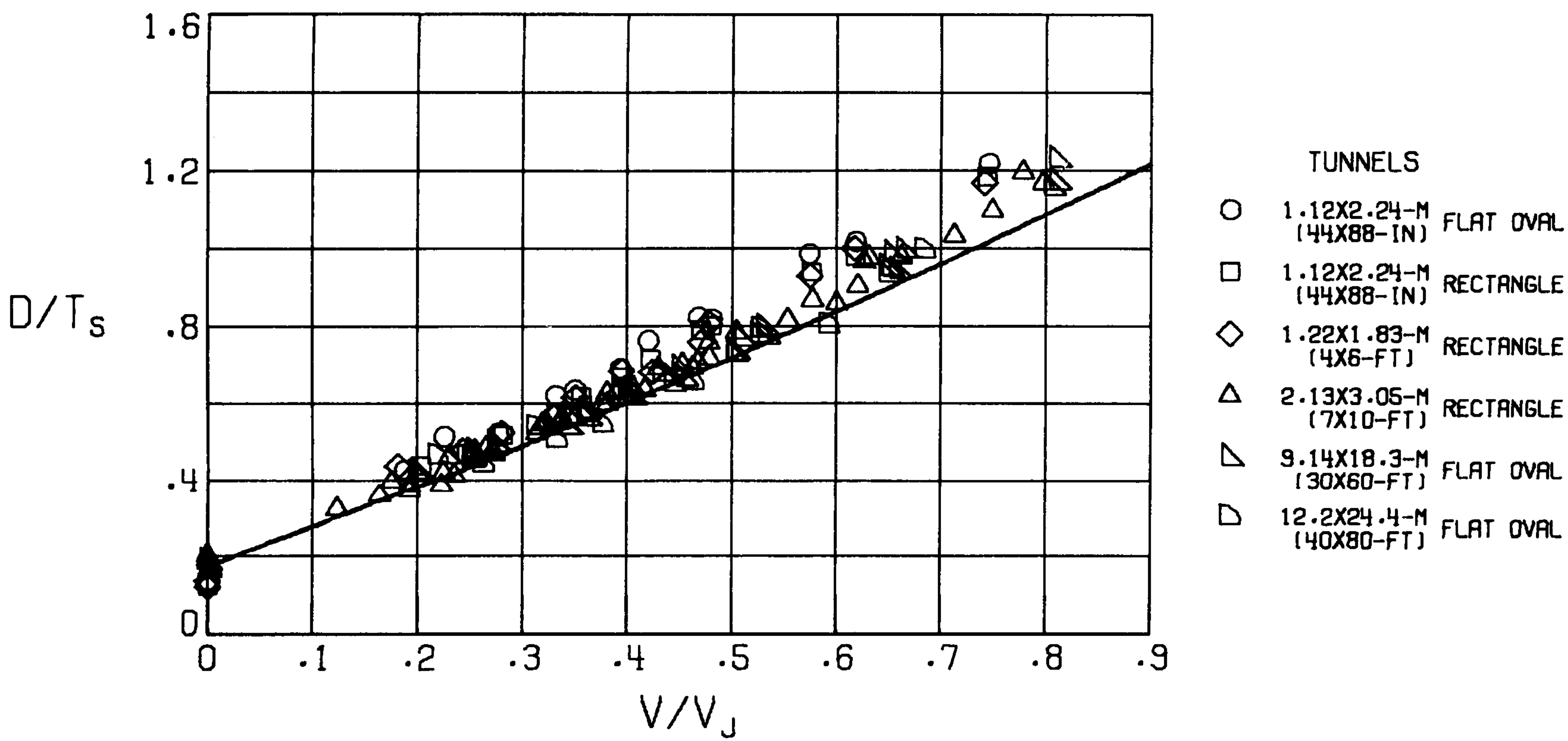

(d) $\alpha = 10^{o}$.

Figure 15.- Continued.

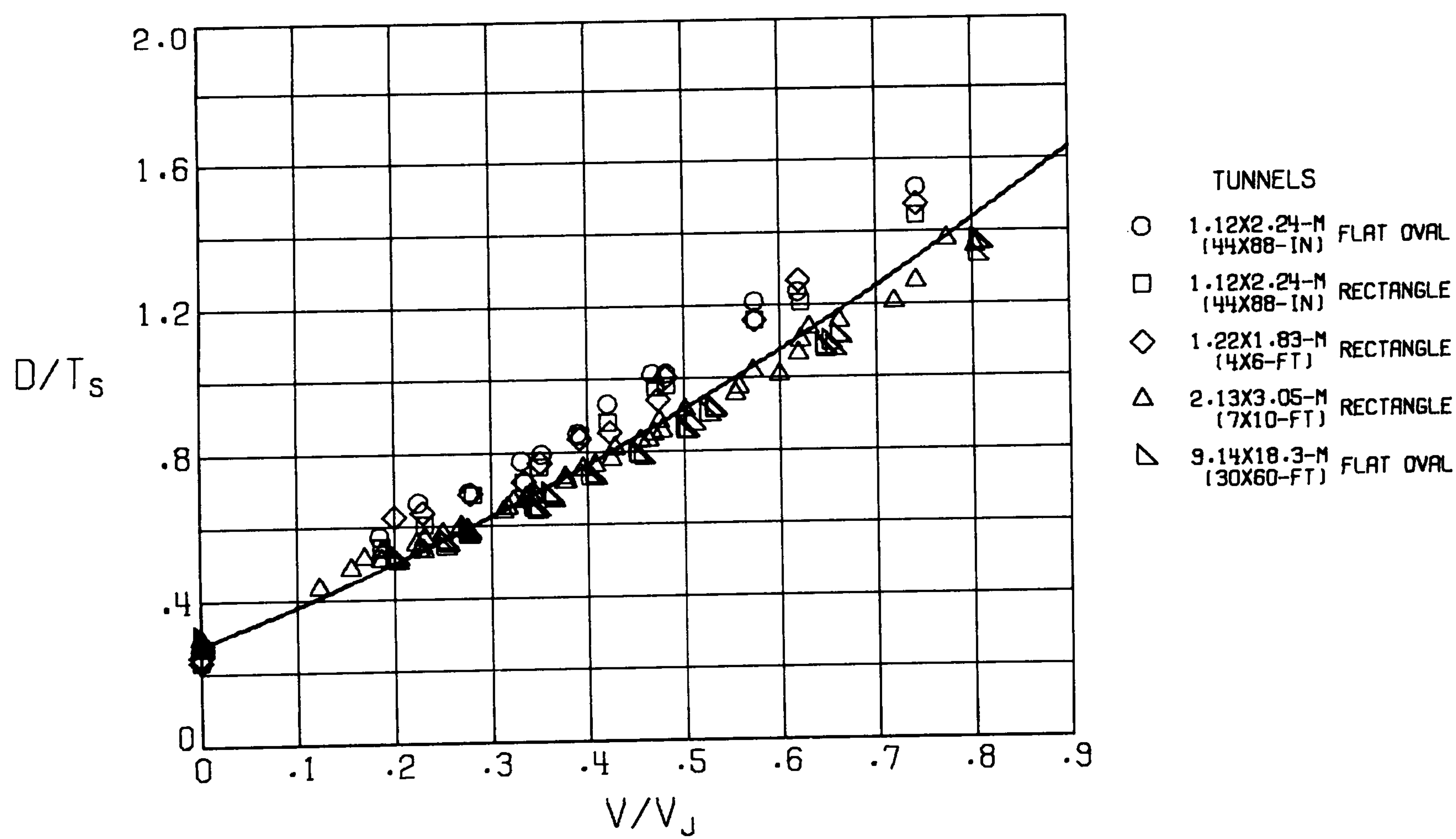

(e) $\alpha = 16^{o}$.

Figure 15.- Concluded.

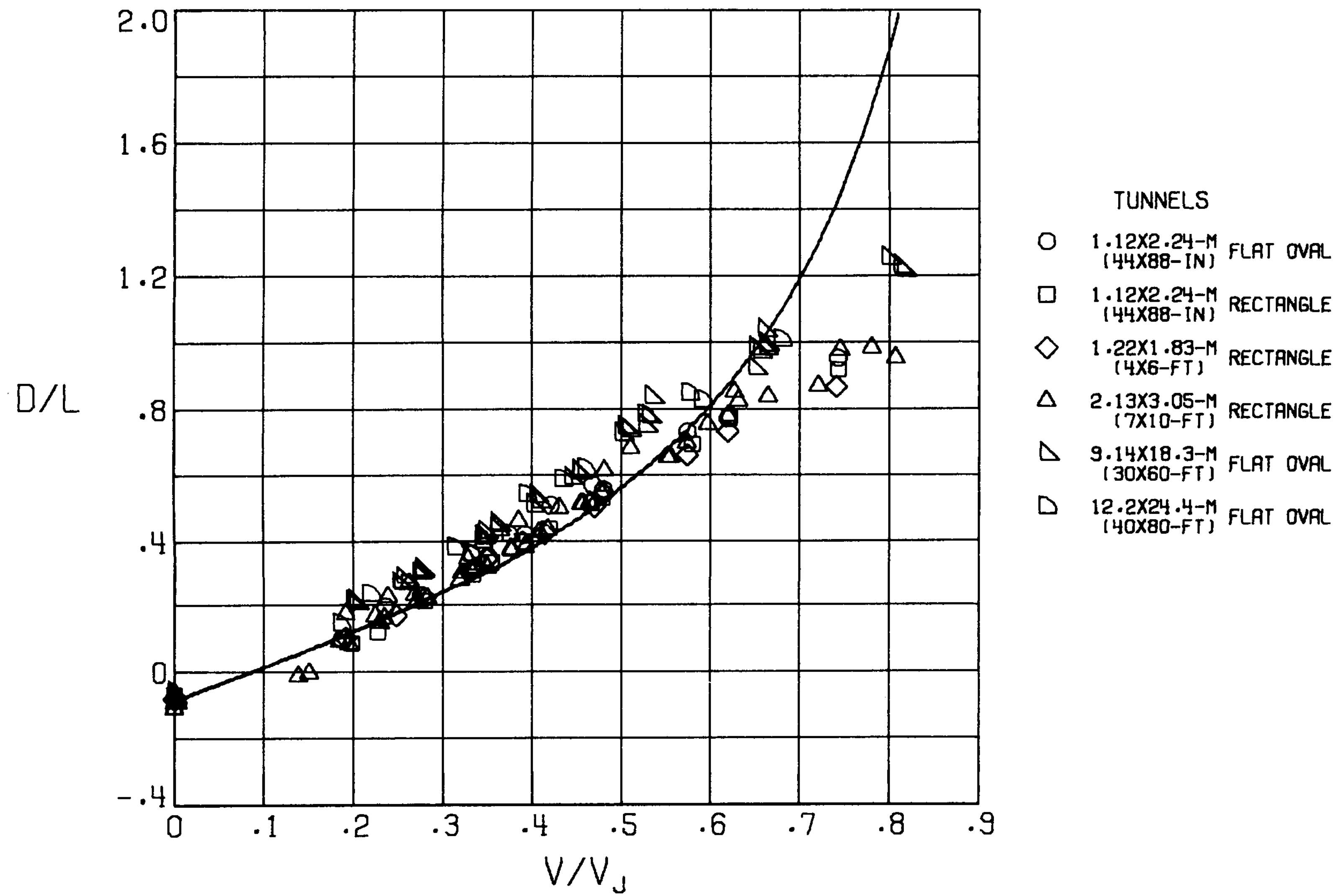

(a) $\alpha = -5^{\circ}$.

Figure 16.- Uncorrected values of external drag-lift ratios as a function of V/V_j. The curve is calculated from the momentum-theory values of the fan forces and the lift and drag of the wing. It is assumed that there is no interference between the fans and the wing.

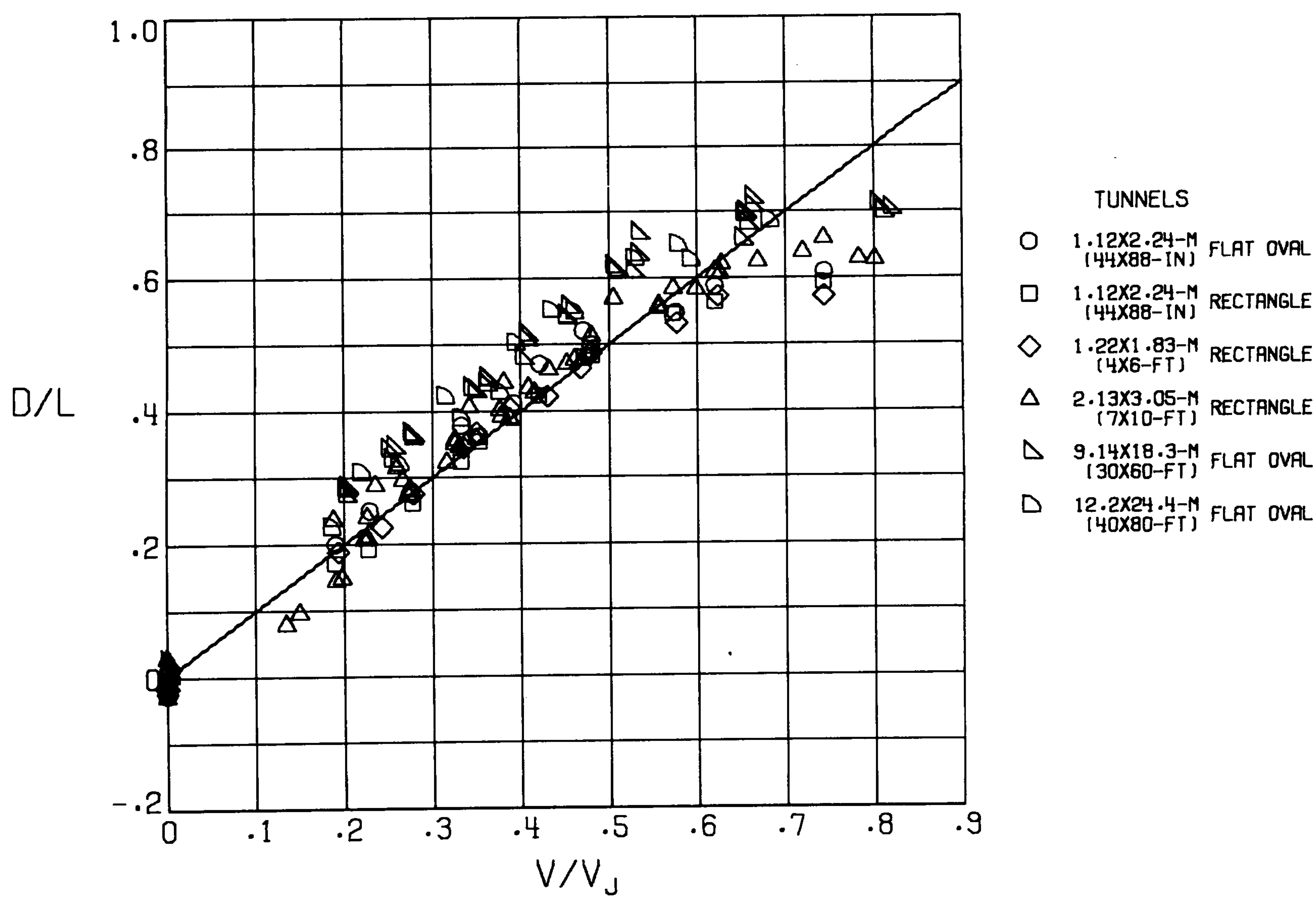

(b) $\alpha = 0^{o}$.

Figure 16.- Continued.

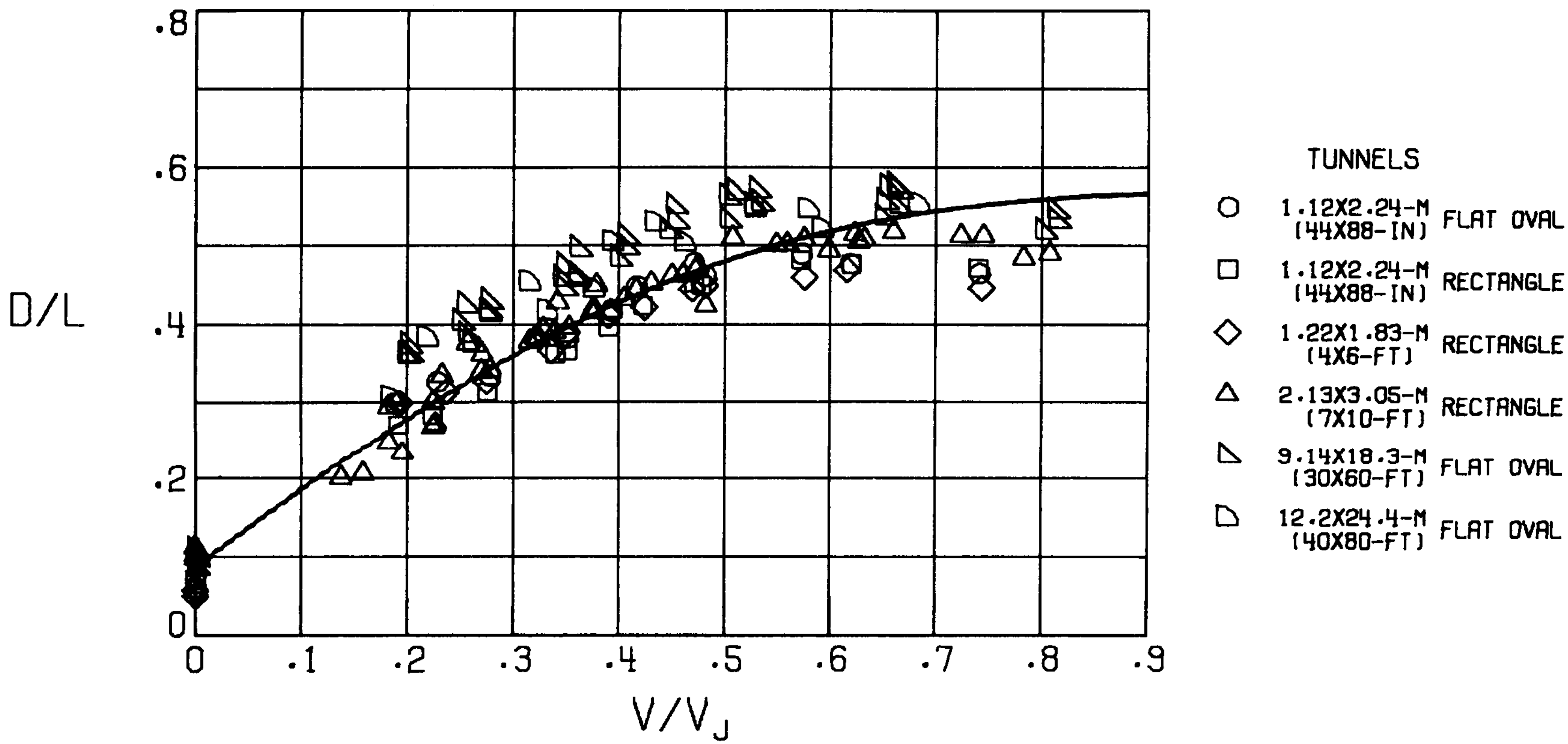

(c) $\alpha = 5^{o}$.

Figure 16.- Continued.

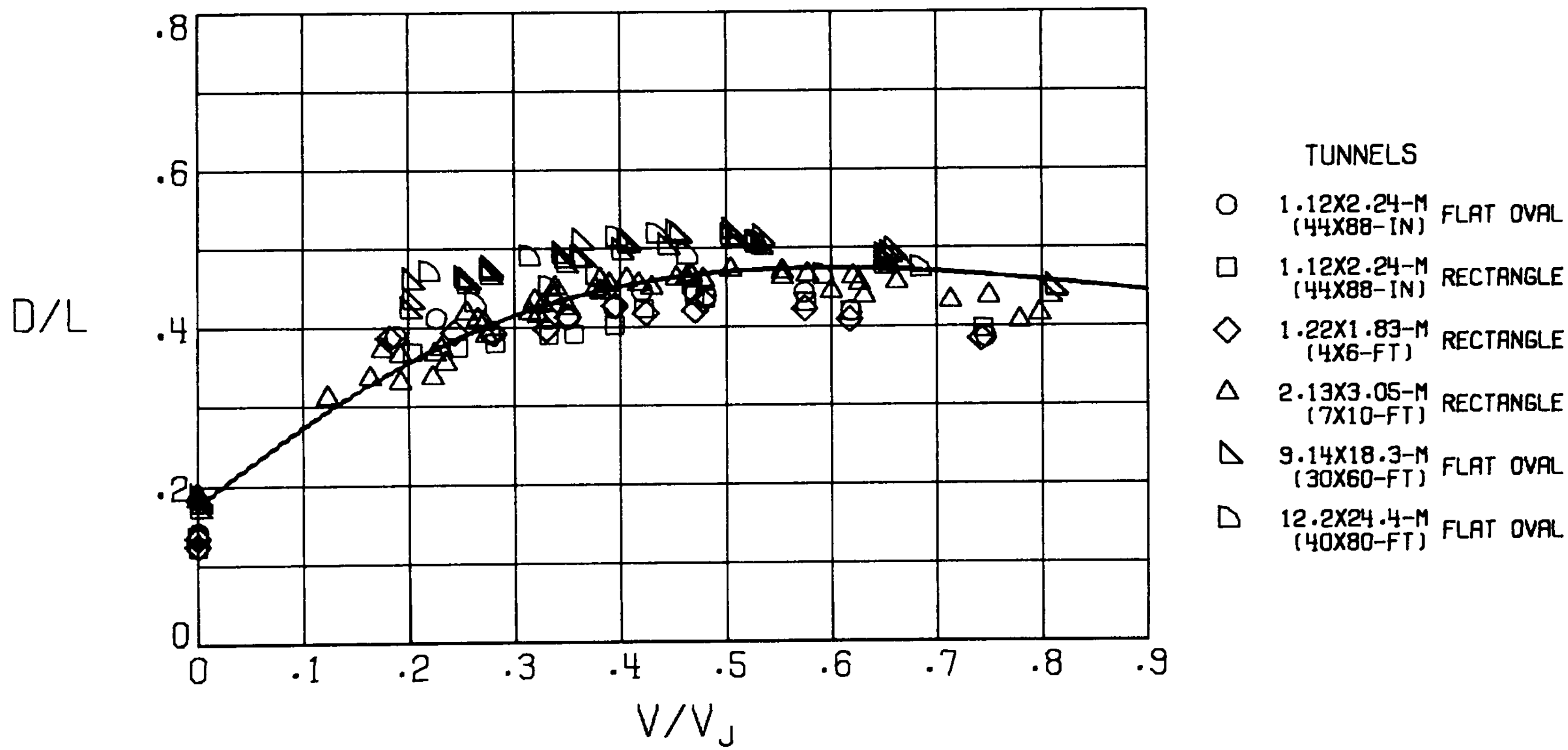

(d) $\alpha = 10^{\circ}$.

Figure 16.- Continued.

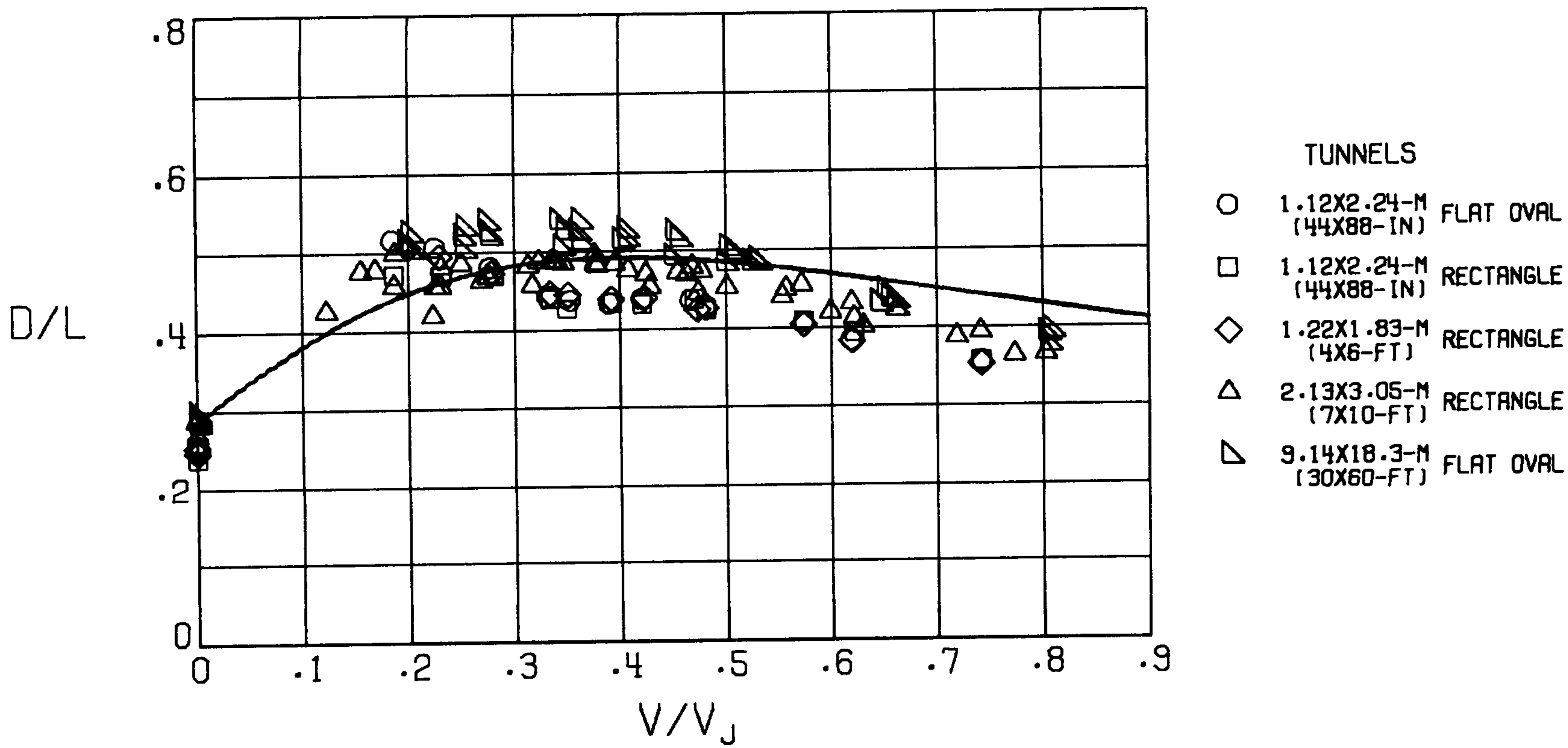

(e) $\alpha = 16^{o}$.

Figure 16.- Concluded.

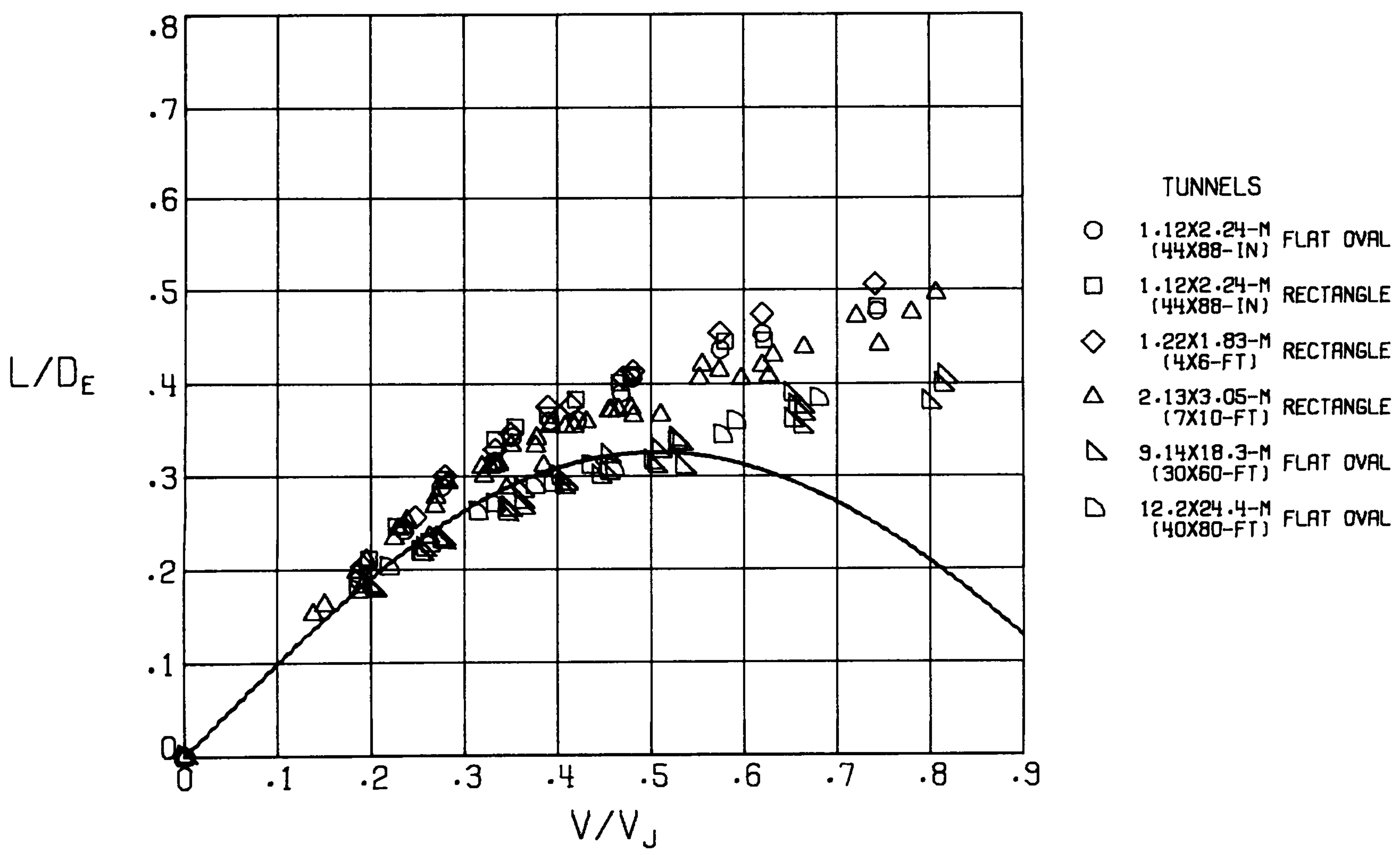

(a) $\alpha = -5^{o}$.

Figure 17.- Uncorrected values of equivalent lift-drag ratios as a function of V/V_j. The curve is calculated from the momentum-theory values of the fan lift, drag, and shaft power together with the lift and drag of the wing. It is assumed that there is no interference between the fans and the wing.

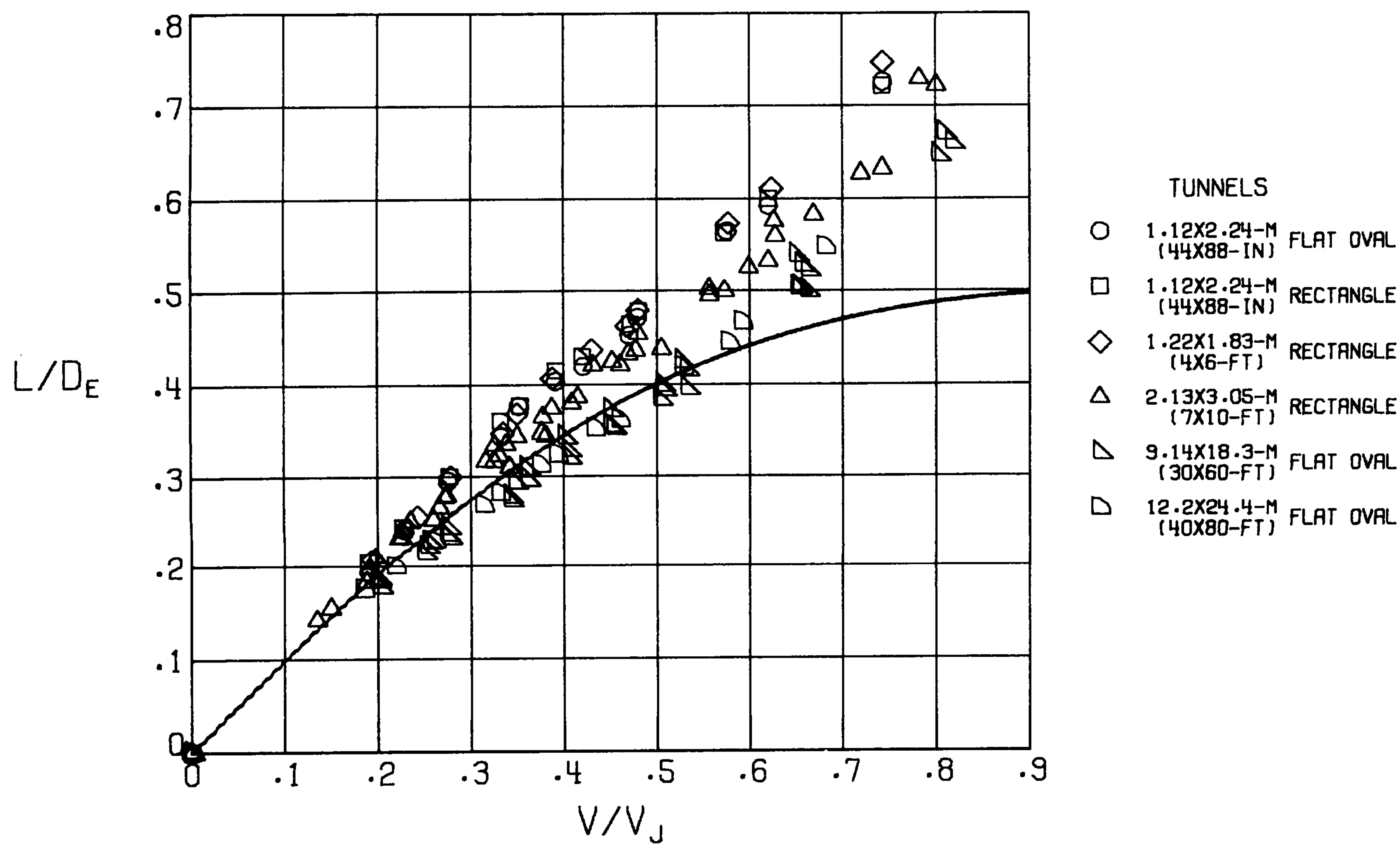

(b) $\alpha = 0^{\circ}$.

Figure 17.- Continued.

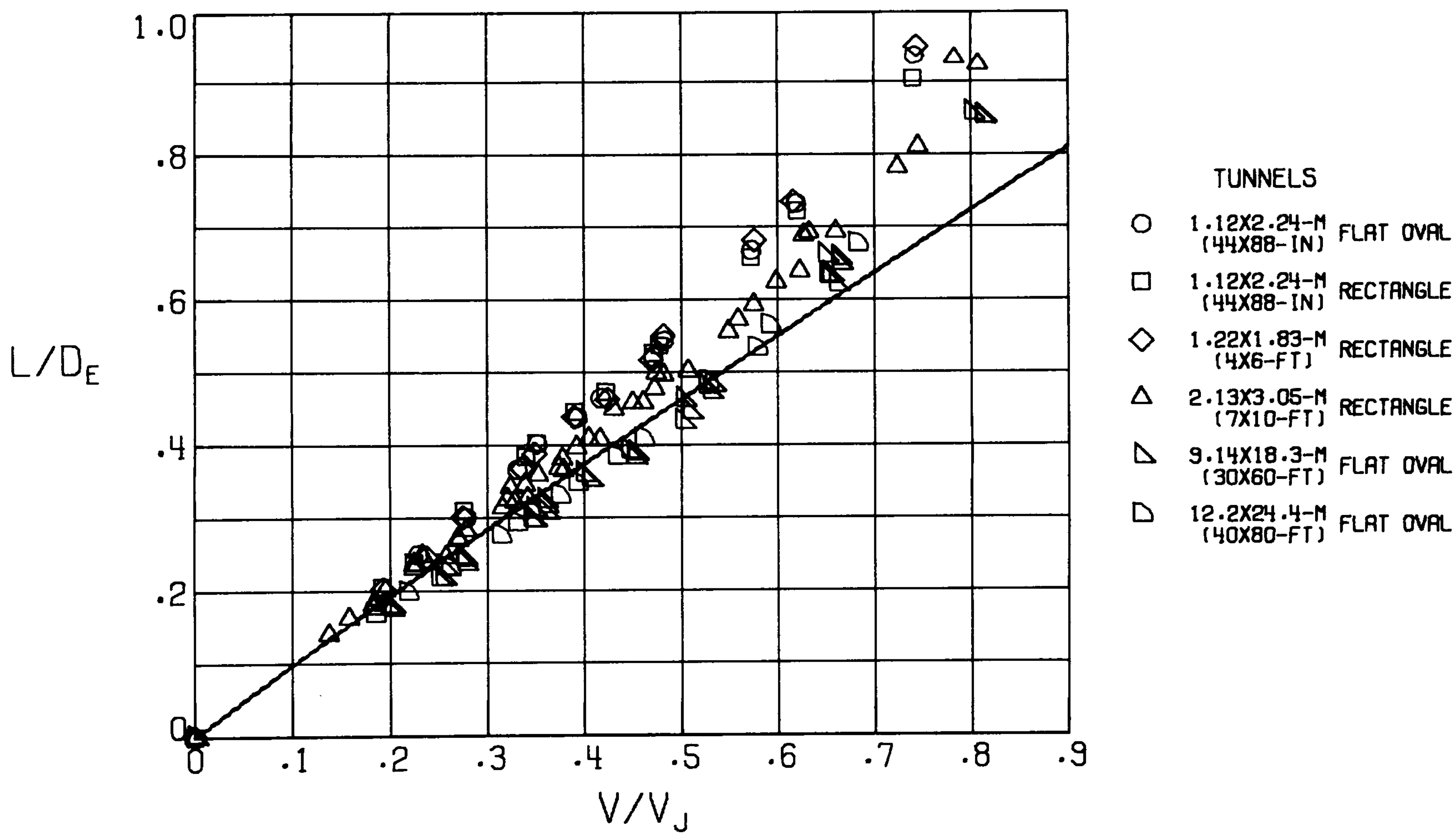

(c) $\alpha = 5^{\circ}$.

Figure 17.- Continued.

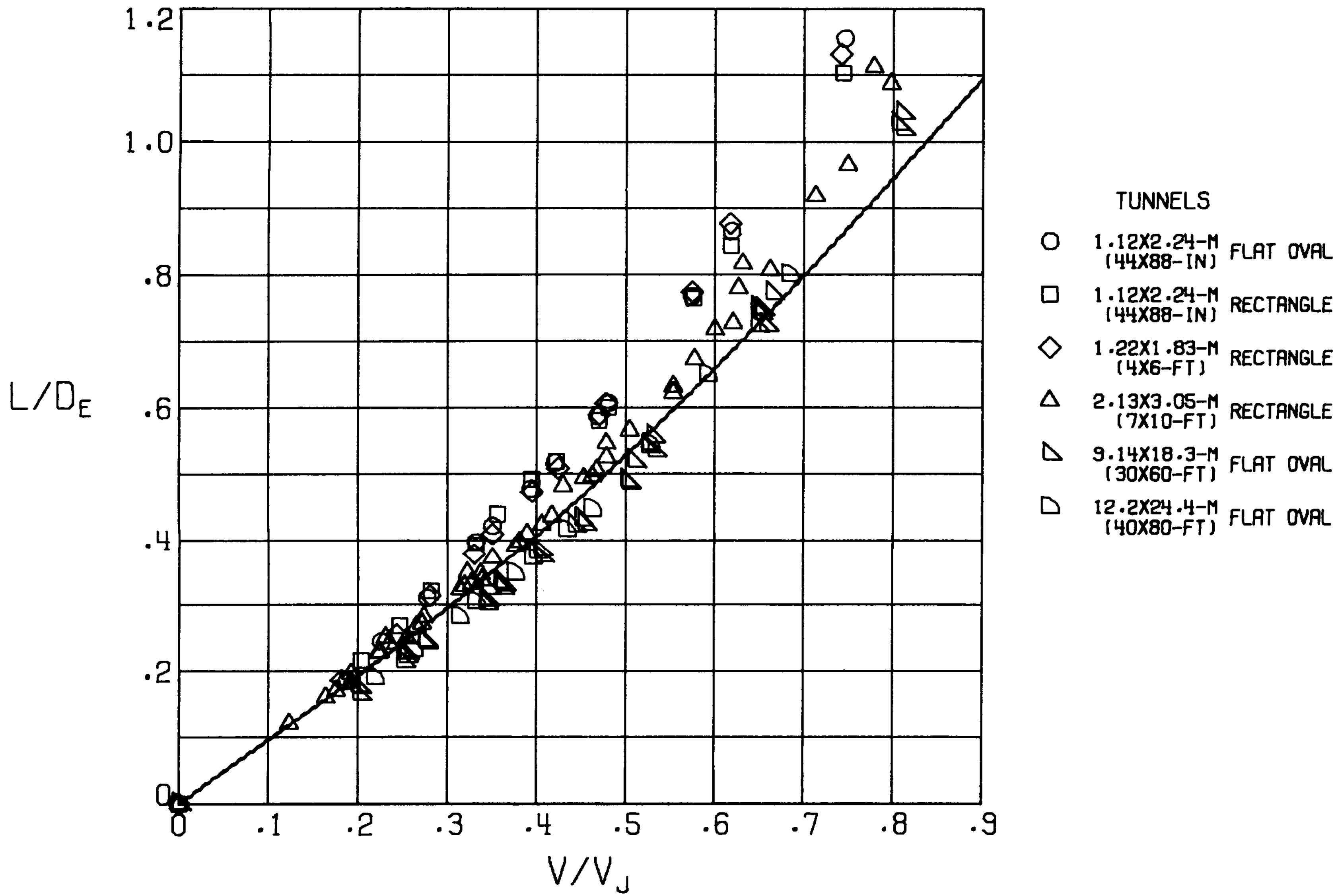

(d) $\alpha = 10^{o}$.

Figure 17.- Continued.

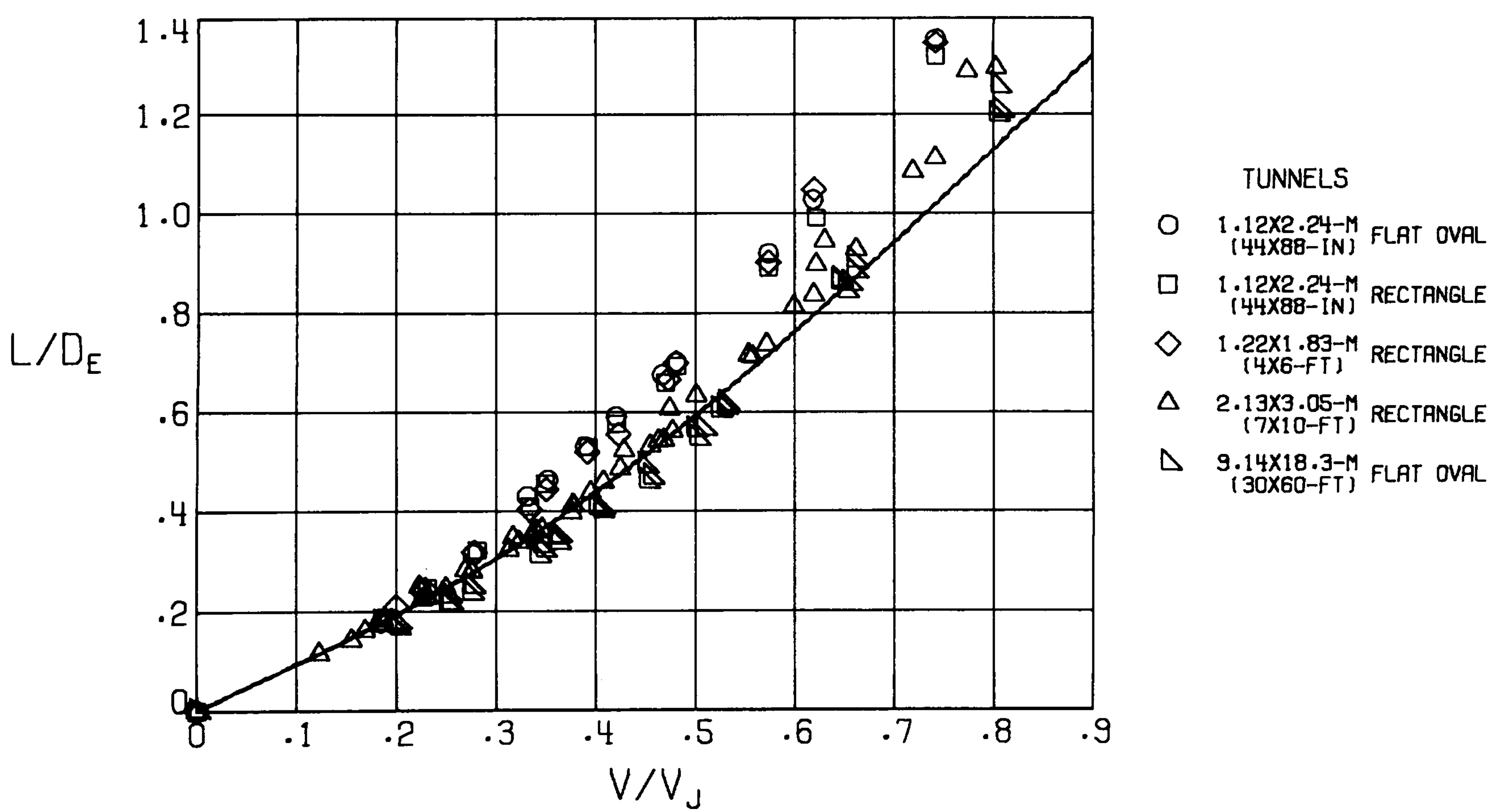

(e) $\alpha = 16^{o}$.

Figure 17.- Concluded.

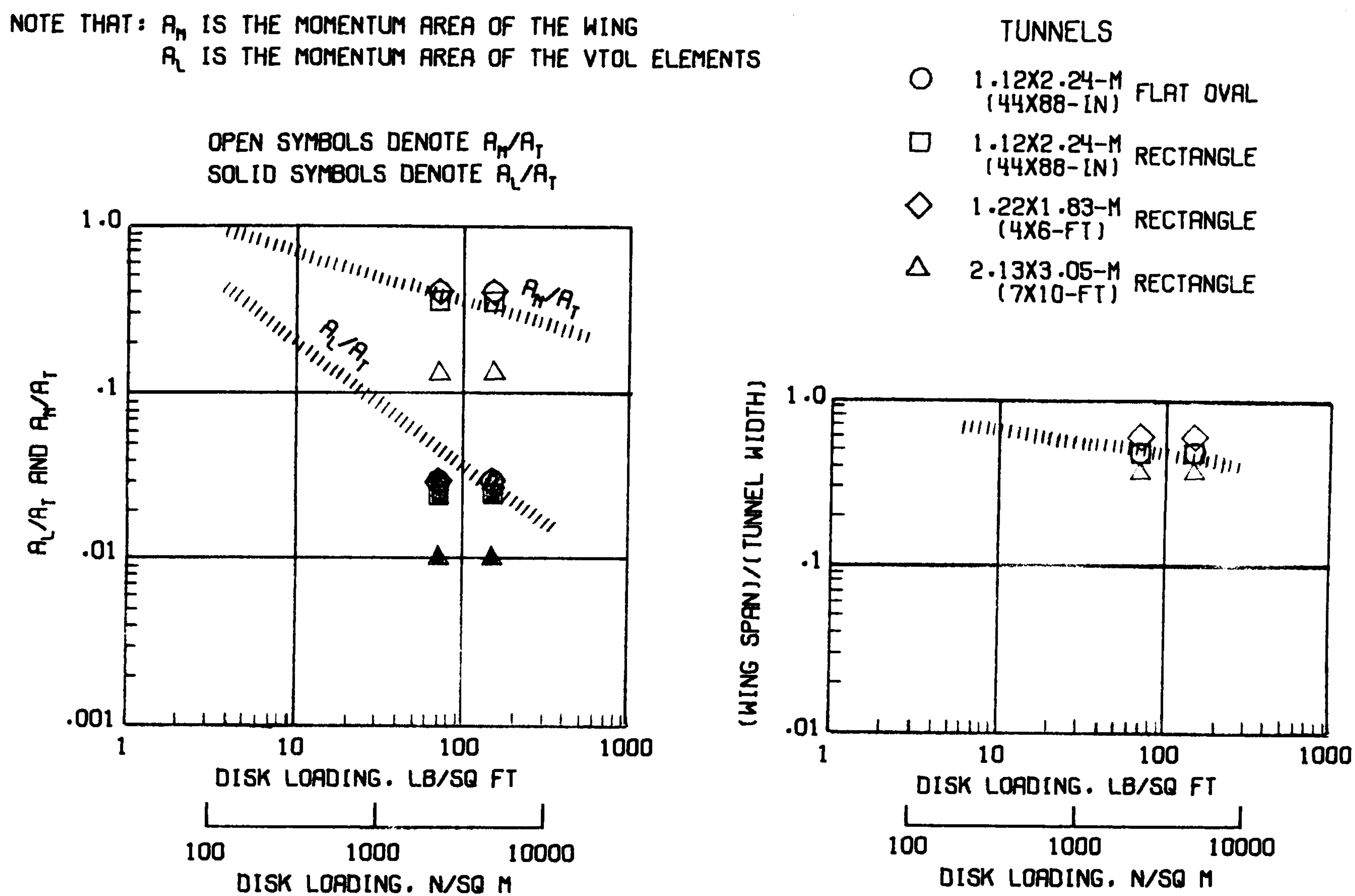

Figure 18.- Relationship between the present model and test sections and the model sizes determined by reference 7 to have negligible wall effects.

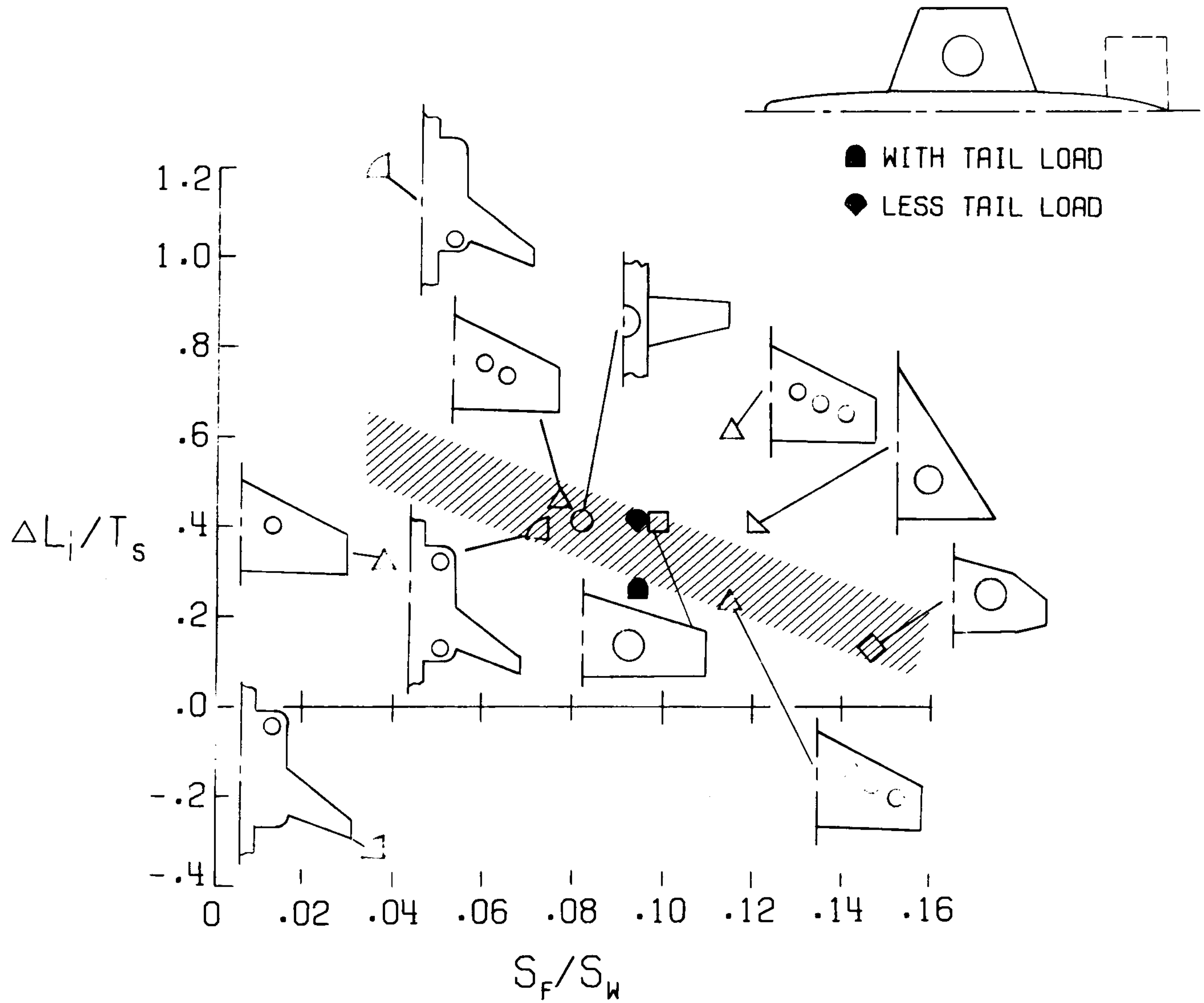

Figure 19.- Influence of the ratio of fan area to wing area on "fan-induced" lift (from ref. 19). The solid symbols show the values measured during the present tests in the 1.12- by 2.24-m (44- by 88-in.) flat-oval test section. $\alpha = 0^o$; $V/V_j = 0.4$.

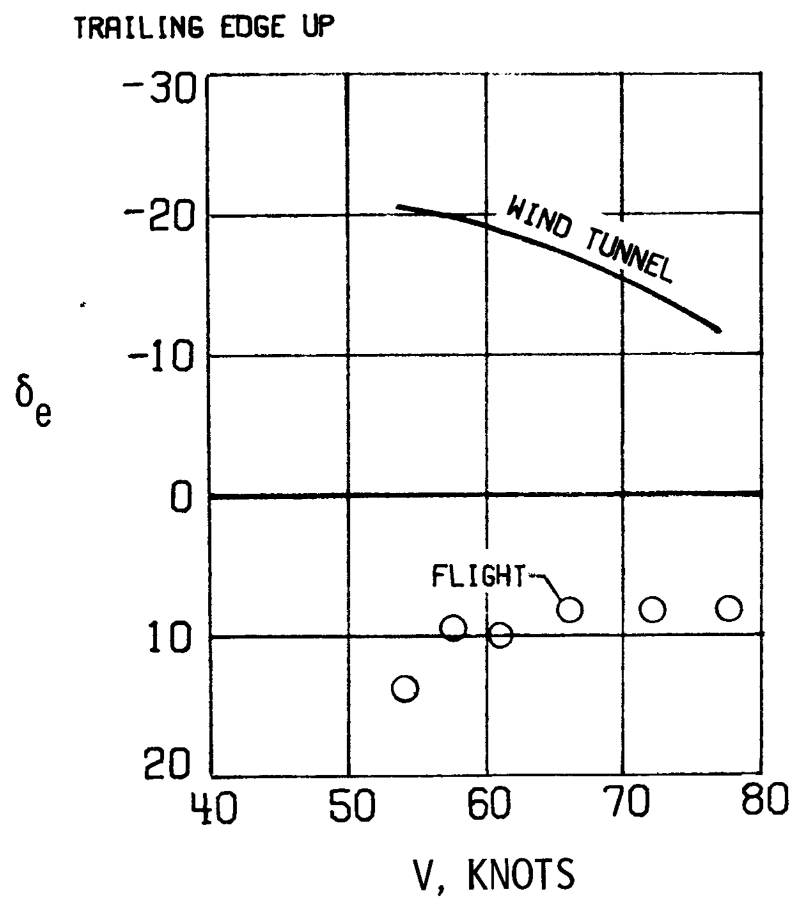

Figure 20.- Comparison between flight test and uncorrected wind-tunnel test (Ames test 388) measurements of the elevator deflection required to trim the YOV-10 aircraft when fitted with a rotating-cylinder flap (ref. 20). Flap set at $60^{\circ}/30^{\circ}$; c.g. at 0.219c.

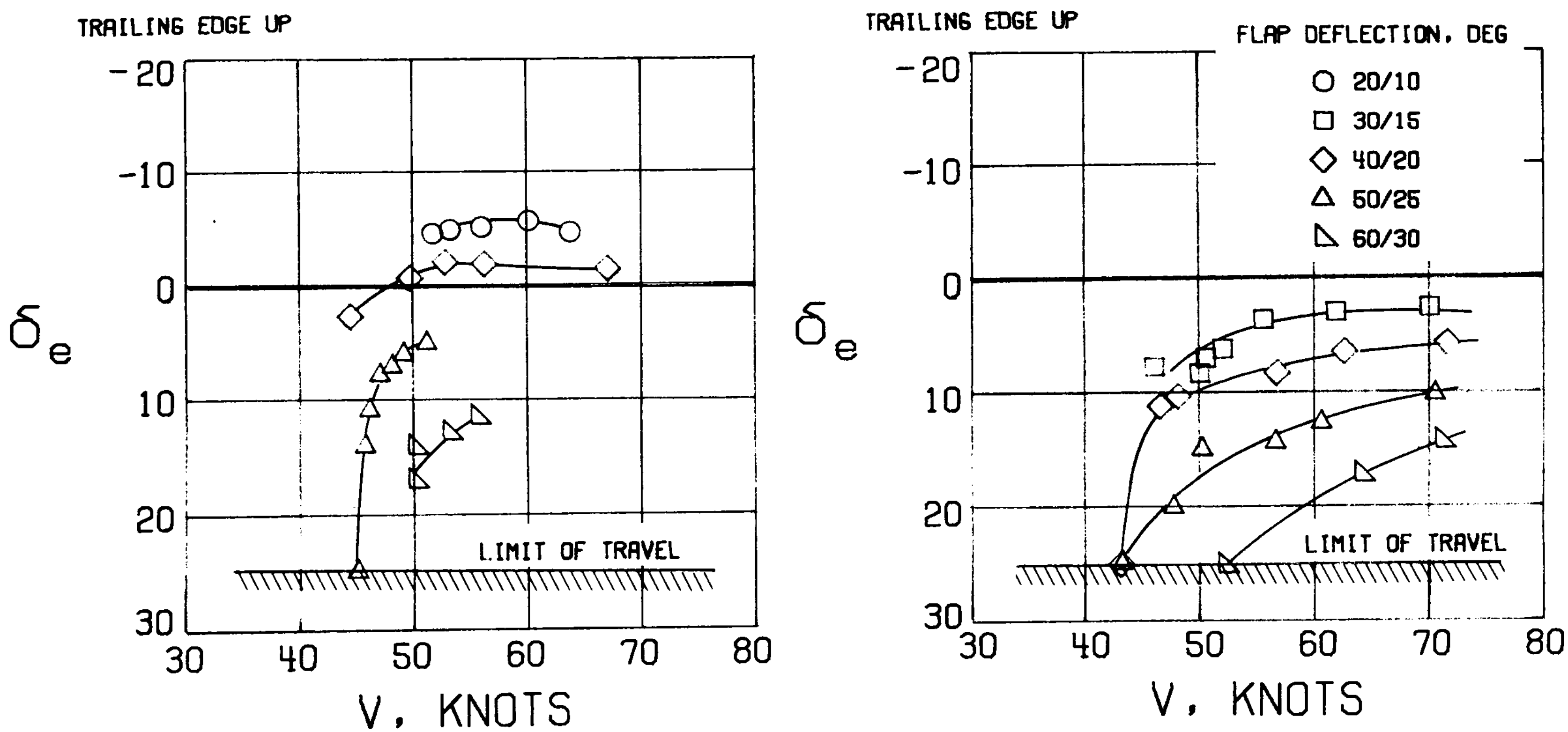

(a) c.g. at 0.246c.

(b) c.g. at 0.219c.

Figure 21.- Additional flight-test measurements of the elevator deflection required to trim the YOV-10 aircraft when fitted with a rotating-cylinder flap (ref. 20).

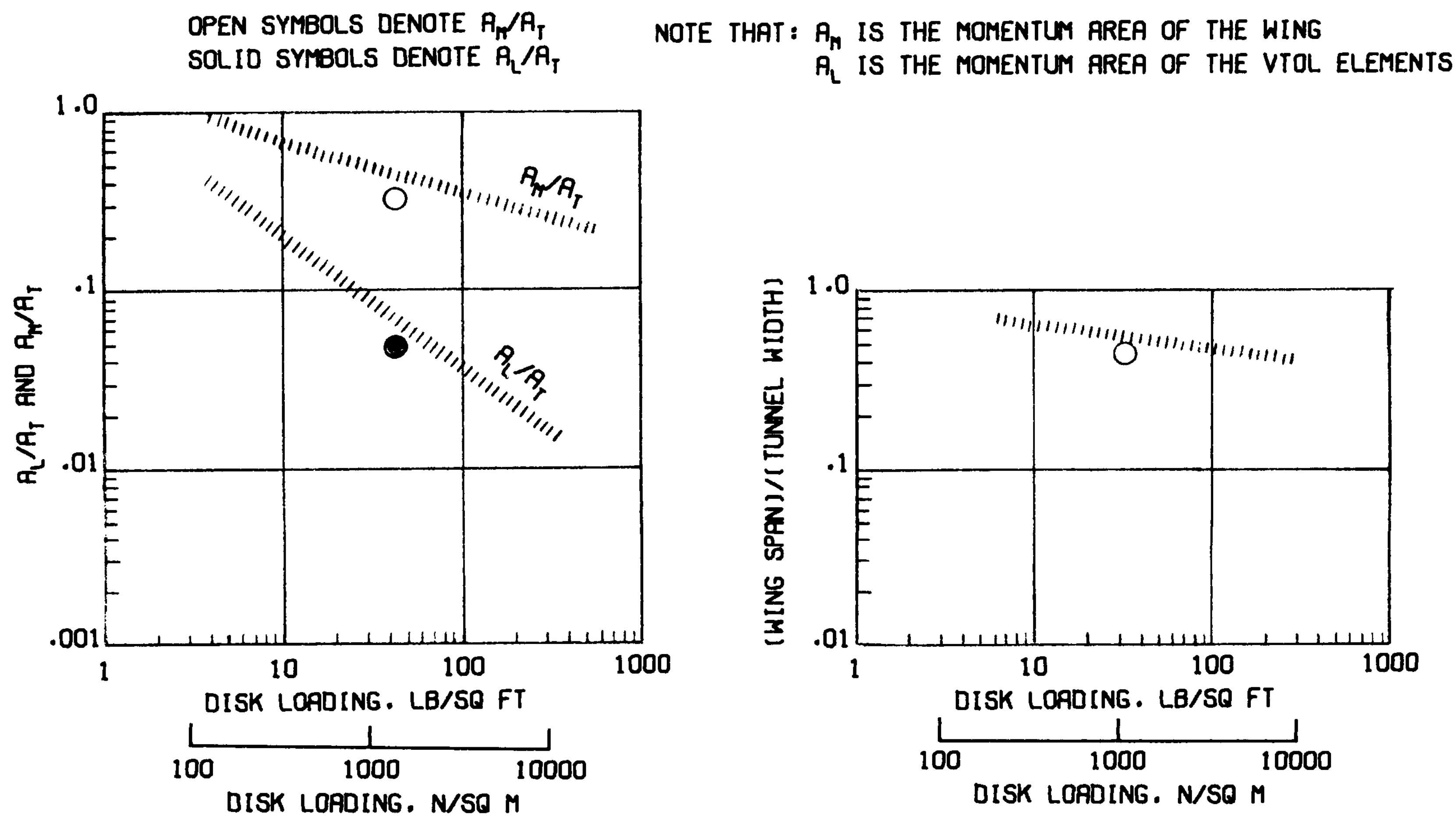

Figure 22.- Location of the YOV-10 aircraft with relation to the model sizes determined by reference 7 to have negligible wall effects.

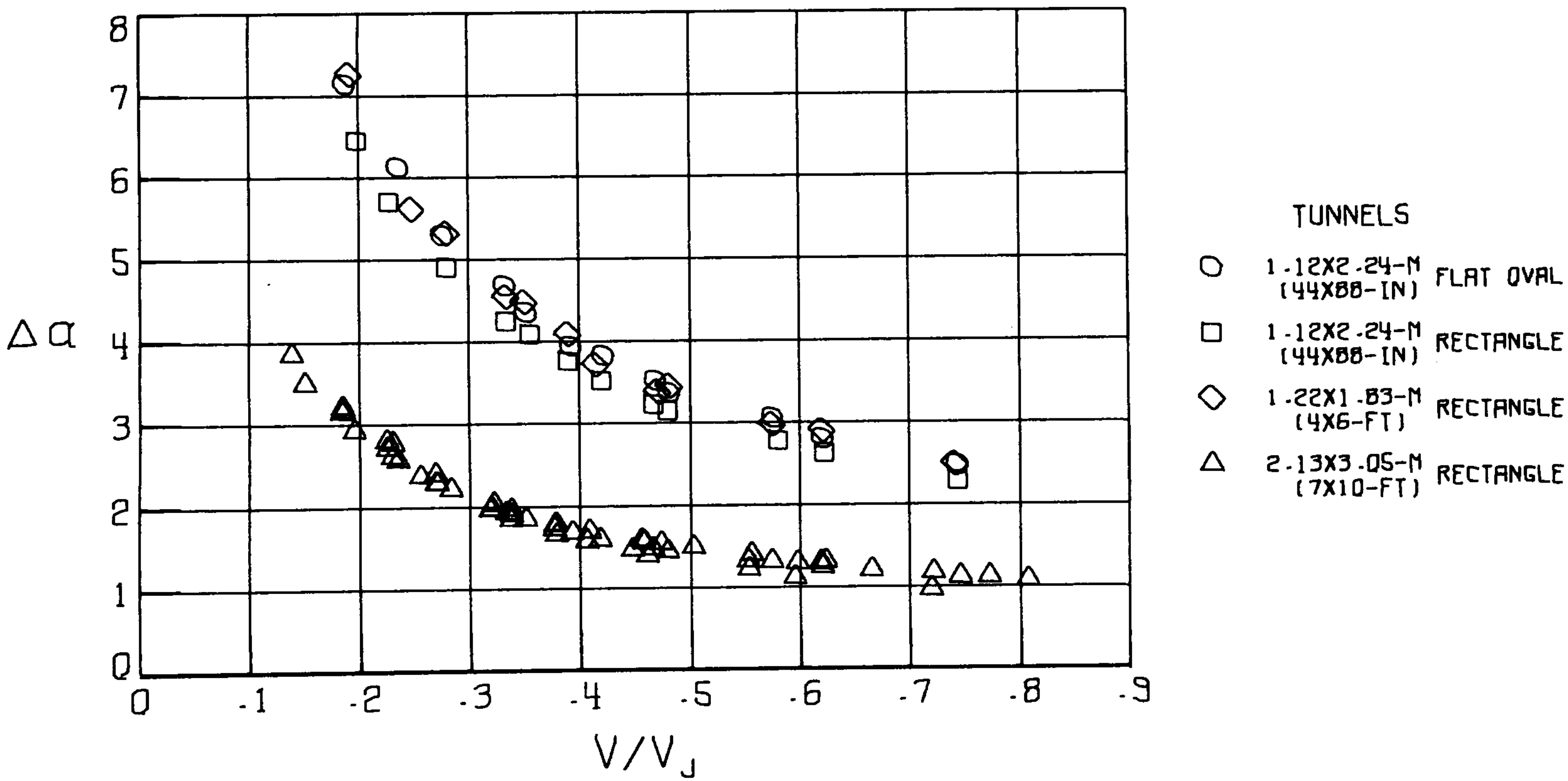

(a) $\alpha = -5^{\circ}$.

Figure 23.- Wall-induced angle of attack $\Delta\alpha$ in the uncorrected data from the fan-in-wing model as a function of V/V_j in several different wind tunnels.

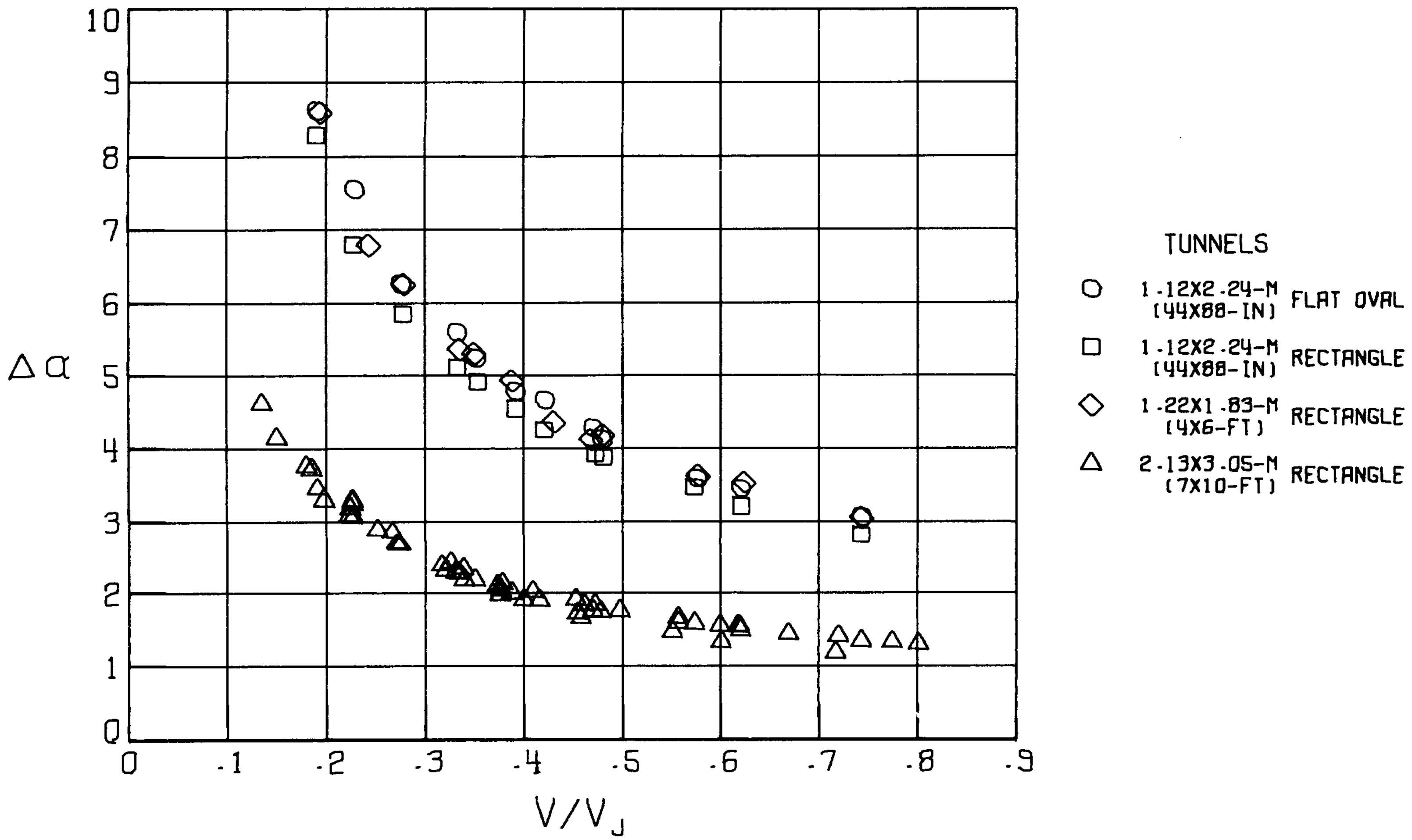

(b) $\alpha = 0^{o}$.

Figure 23.- Continued.

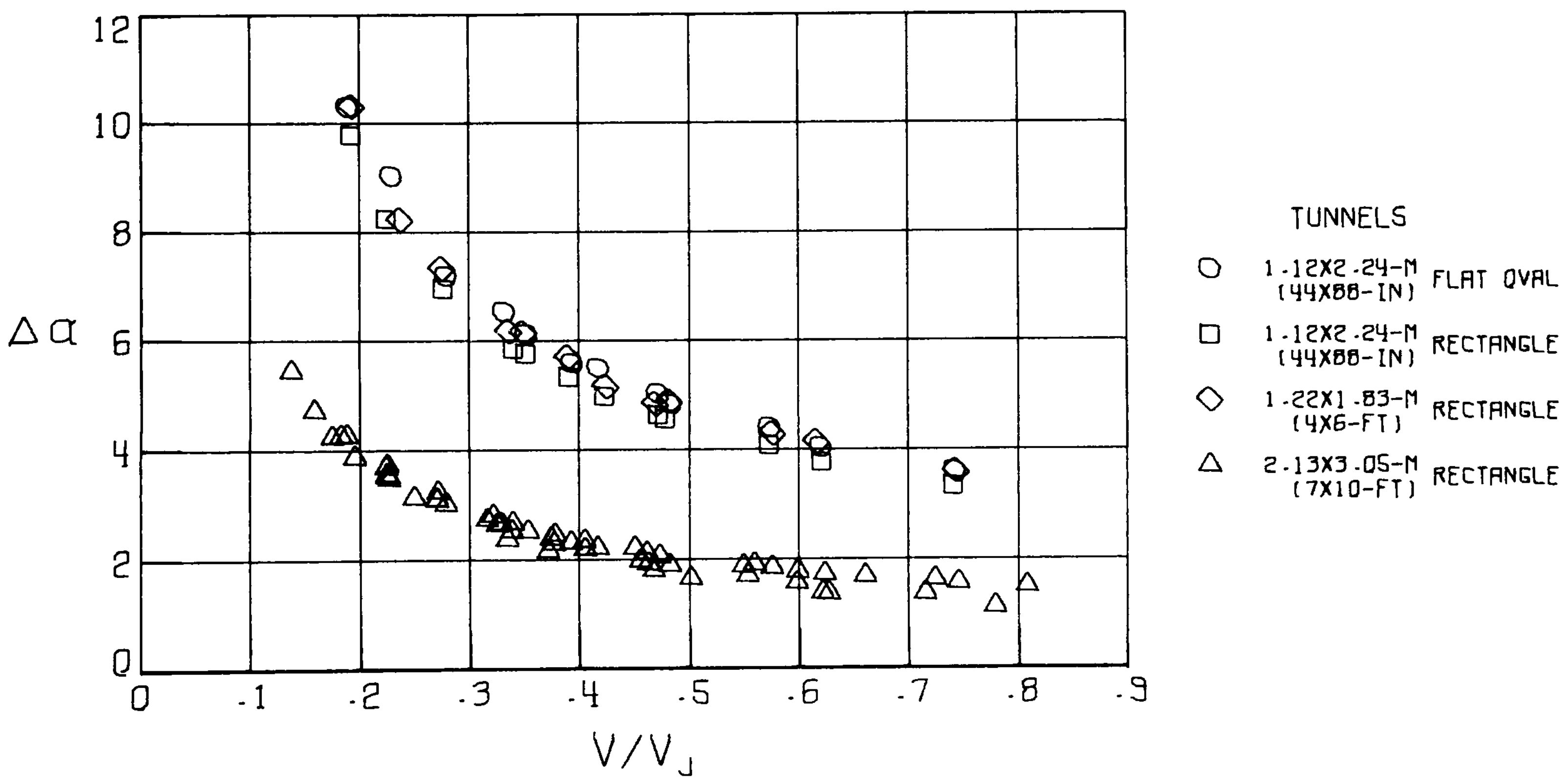

(c) $\alpha = 5^{\circ}$.

Figure 23.- Continued.

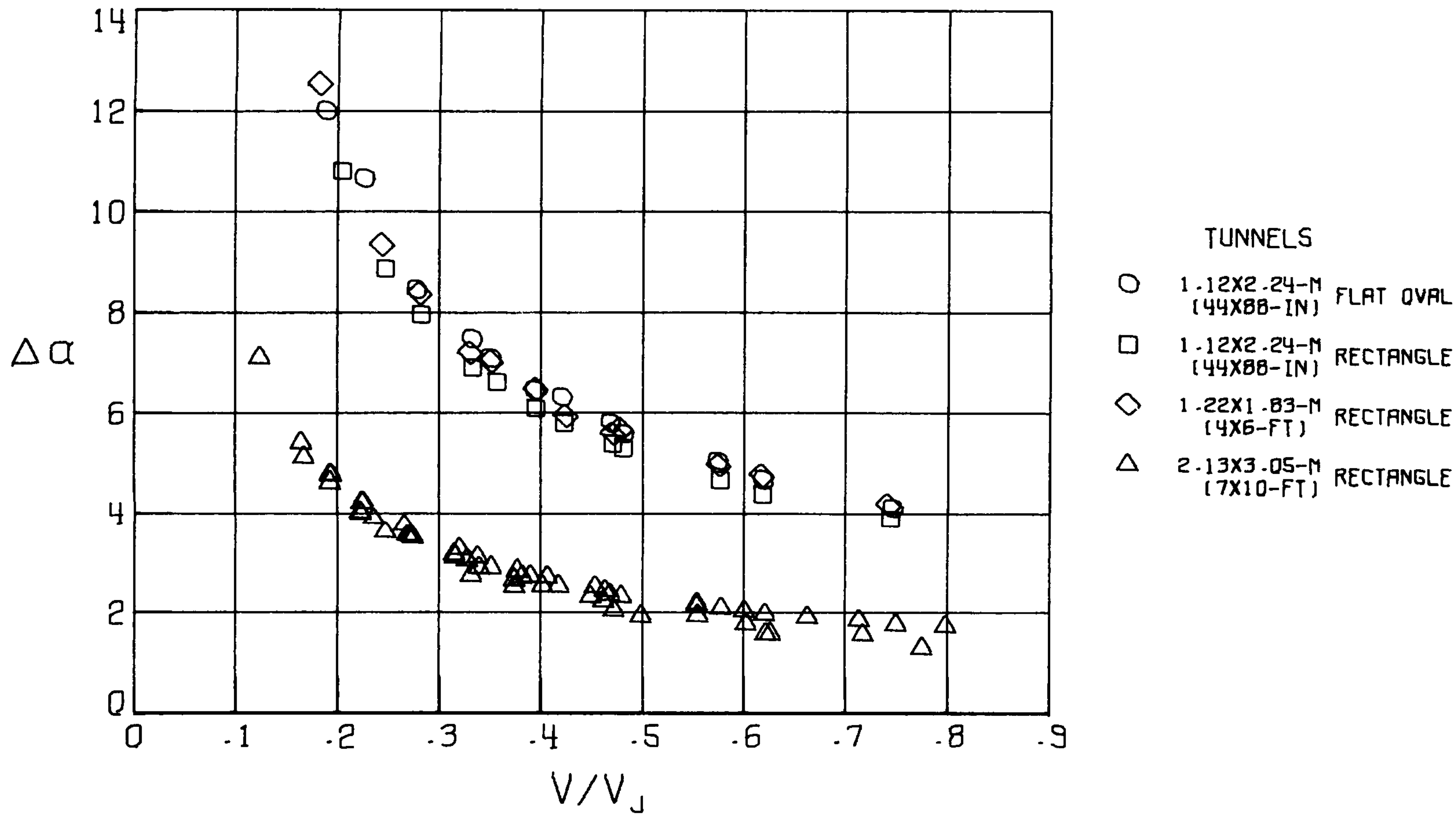

(d) $\alpha = 10^{\circ}$.

Figure 23.- Continued.

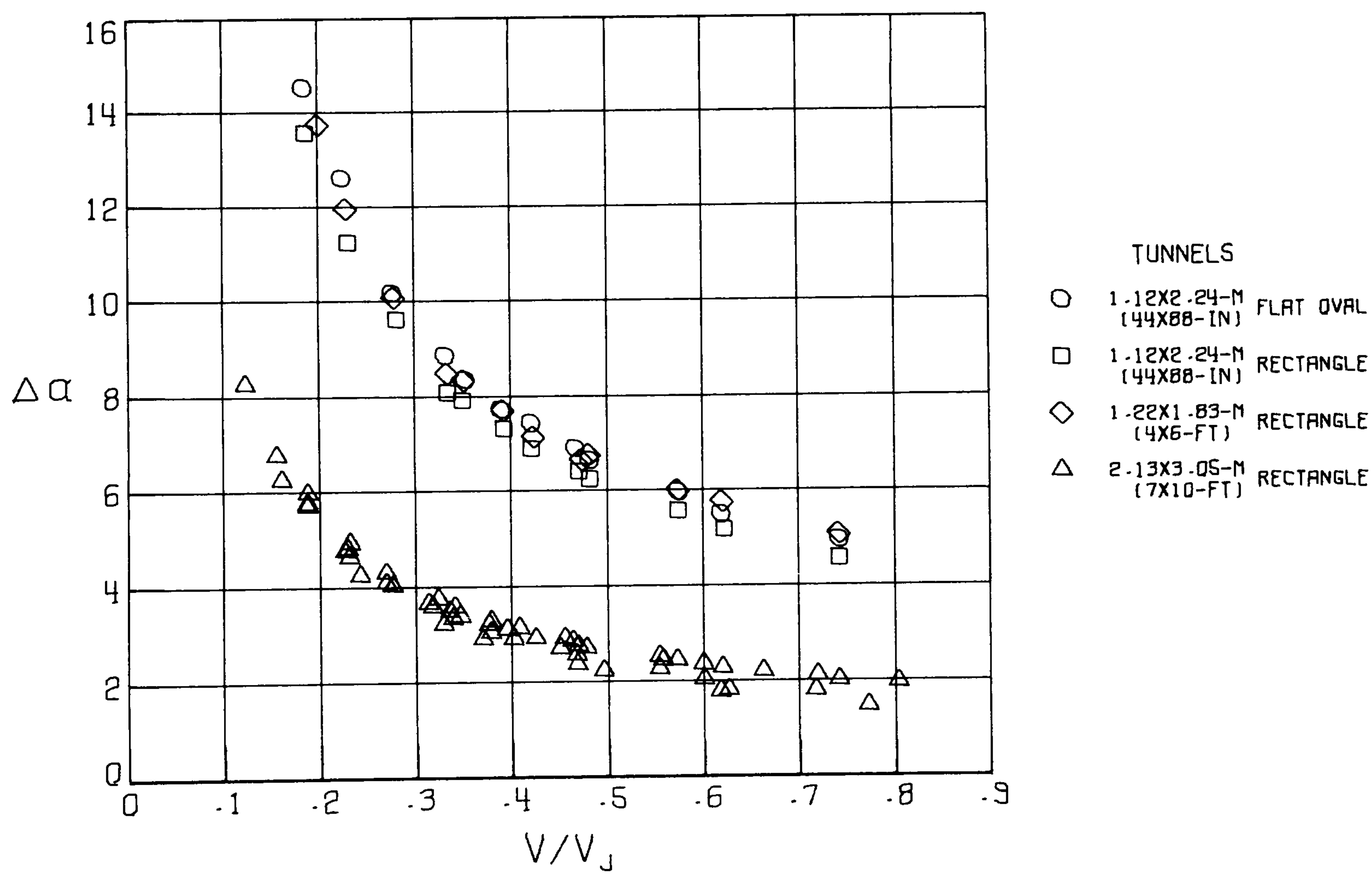

(e) $\alpha = 16^{o}$.

Figure 23.- Concluded.

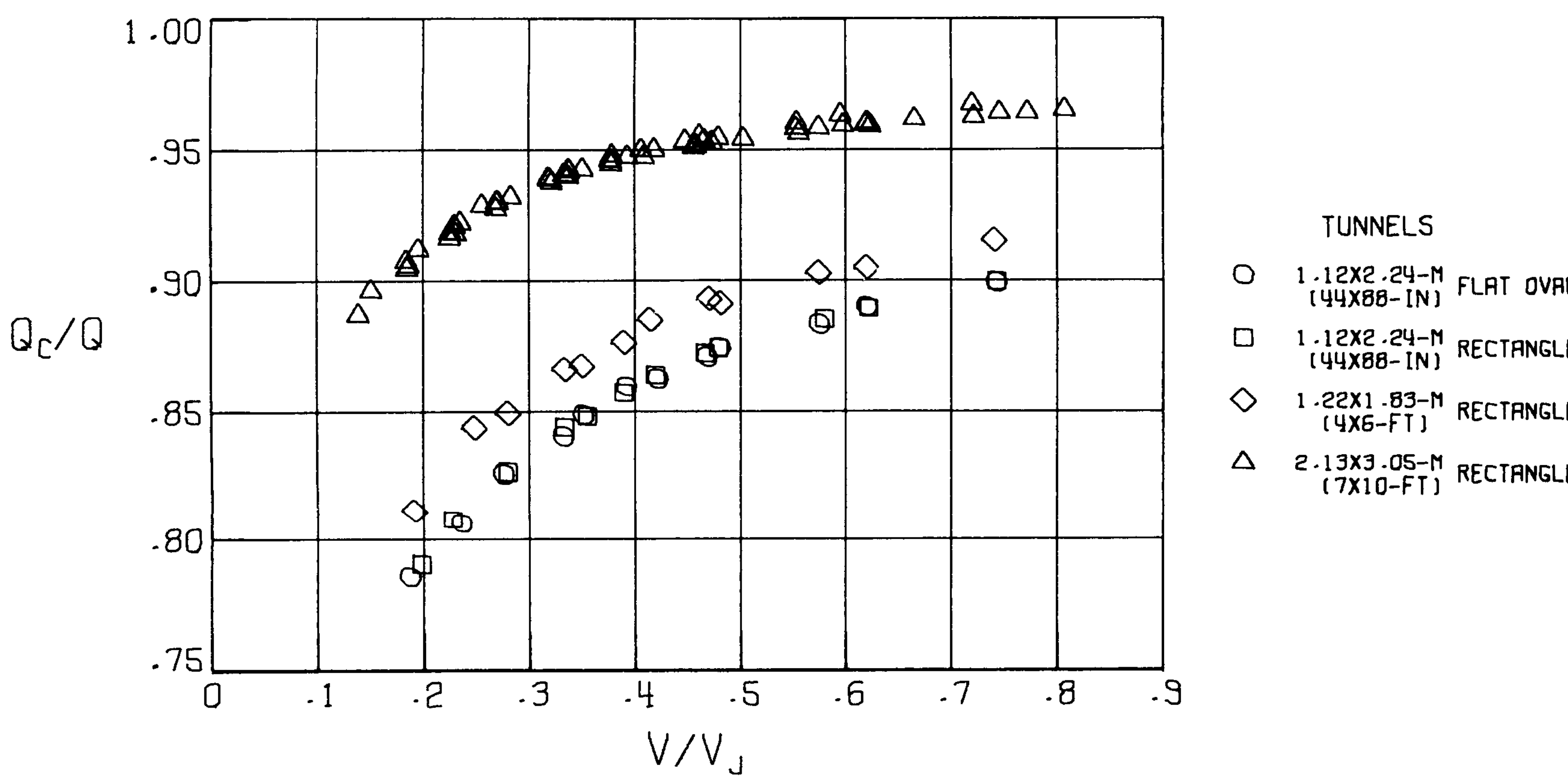

(a) $\alpha = -5^{o}$.

Figure 24.- Wall-induced values of q_c/q in the uncorrected data from the fan-in-wing model as a function of V/V_j in several different wind tunnels.

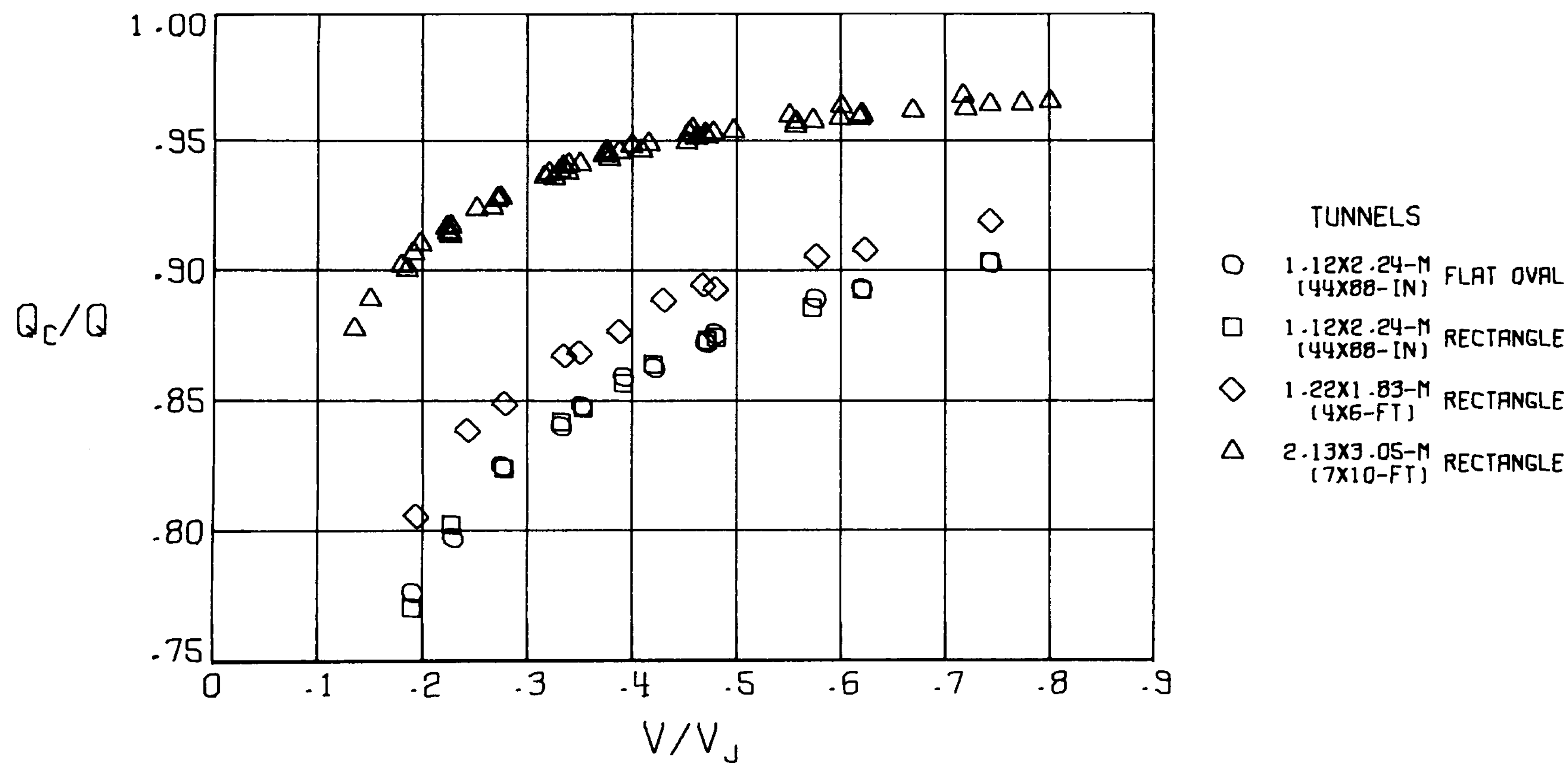

(b) $\alpha = 0^{\circ}$.

Figure 24.- Continued.

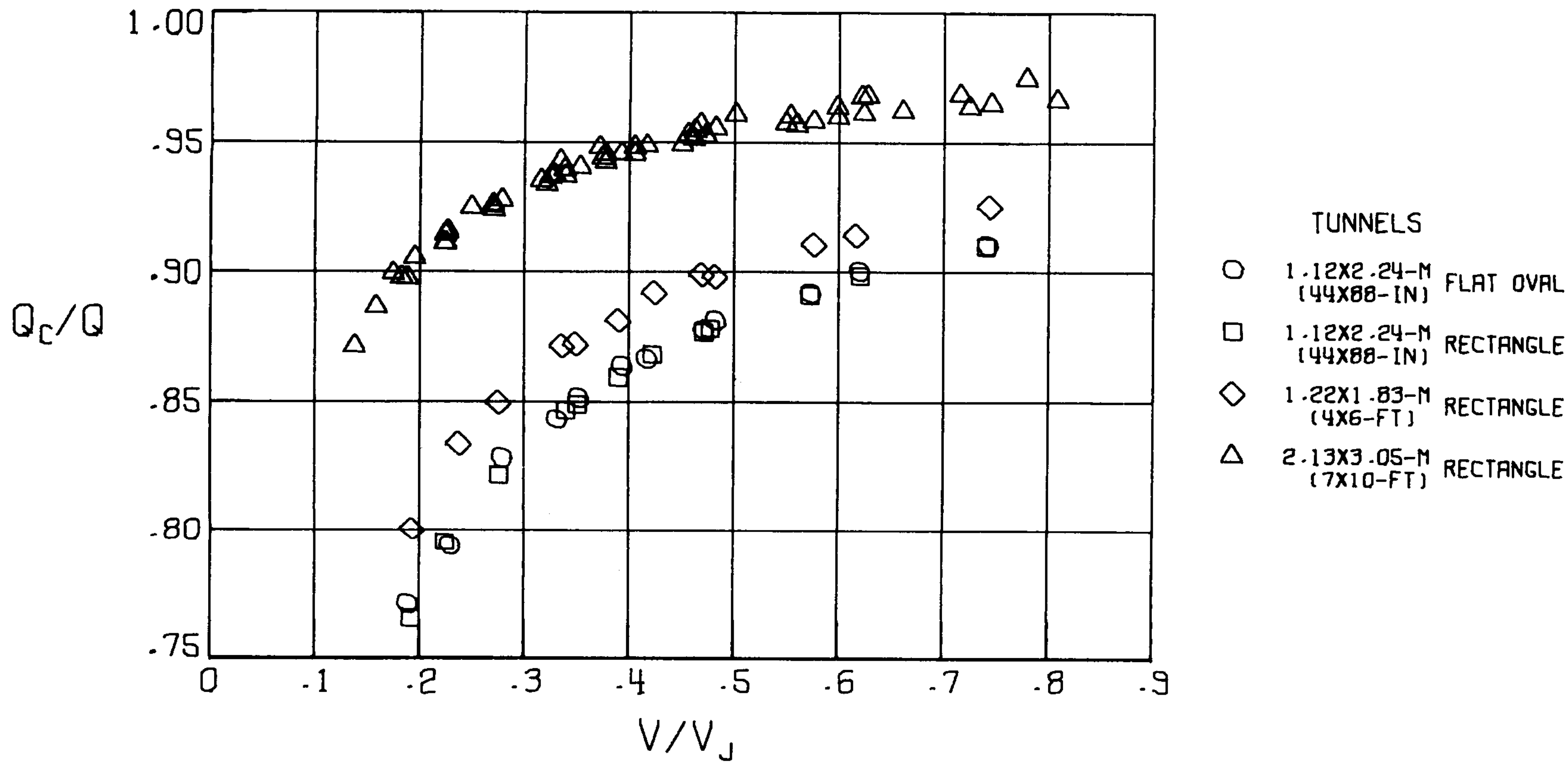

(c) $\alpha = 5^{\circ}$.

Figure 24.- Continued.

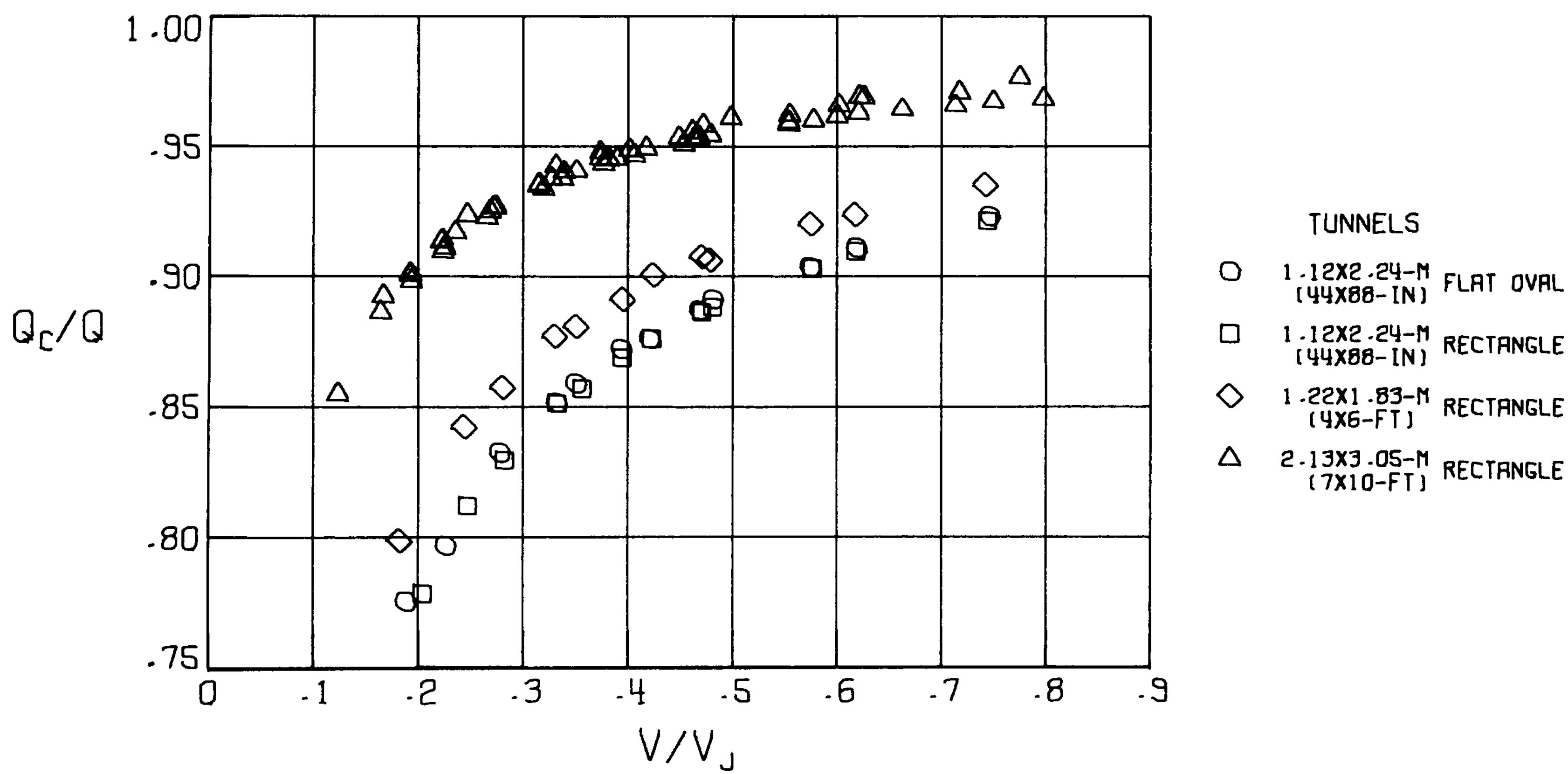

(d) $\alpha = 10^{\circ}$.

Figure 24.- Continued.

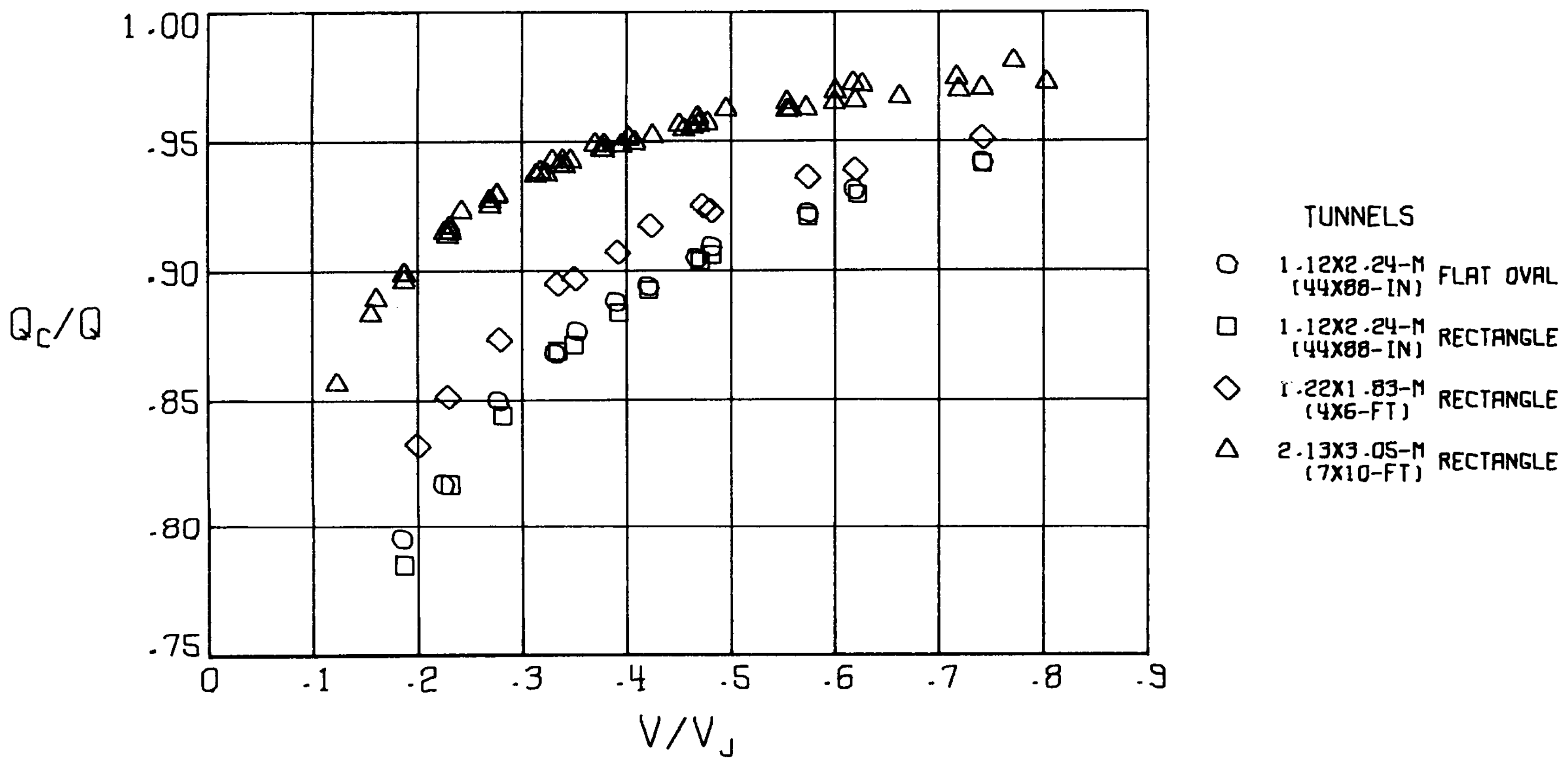

(e) $\alpha = 16^{o}$.

Figure 24.- Concluded.

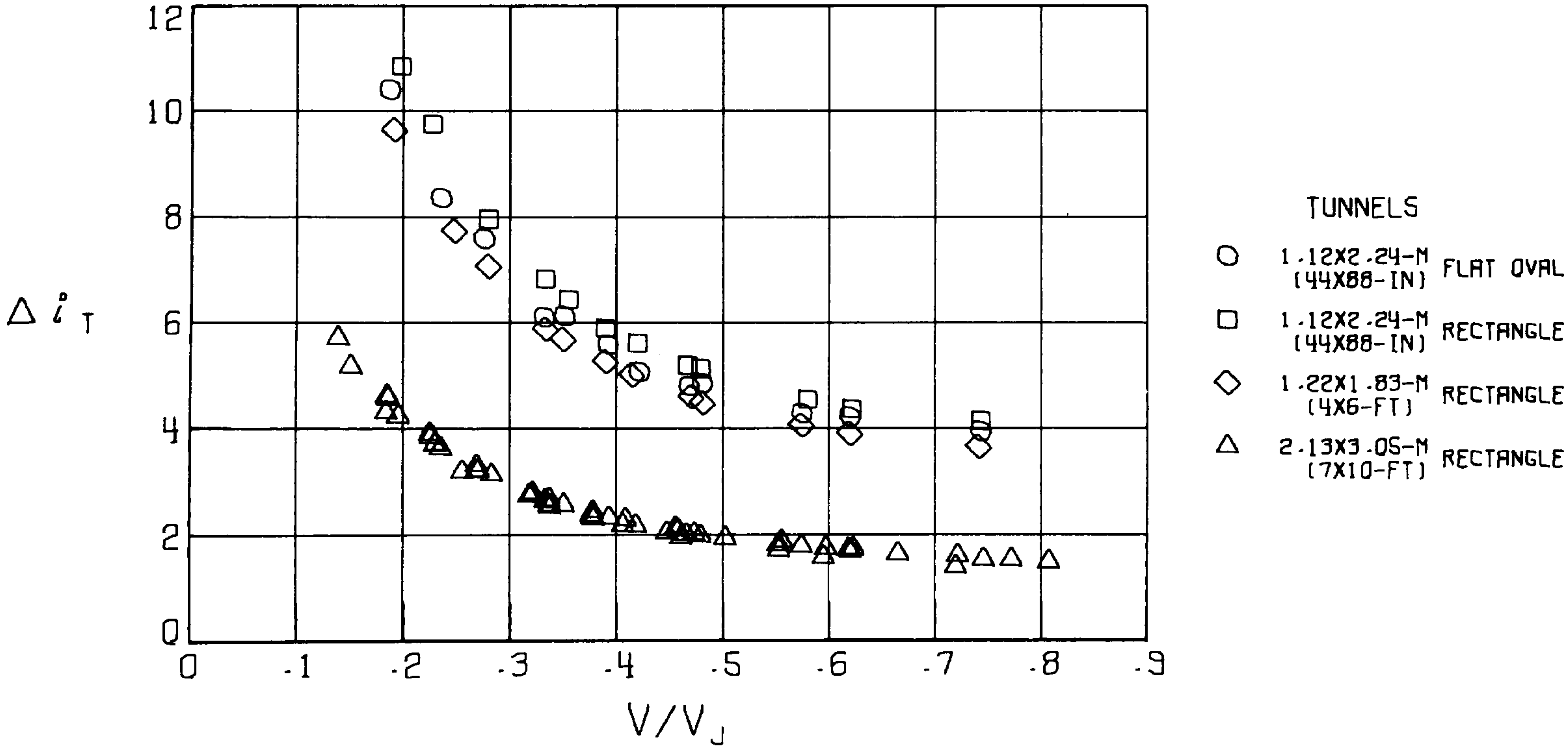

(a) $\alpha = -5^{o}$.

Figure 25.- Wall-induced tail incidence Δi_T in the uncorrected data from the fan-in-wing model as a function of V/V_j in several different wind tunnels.

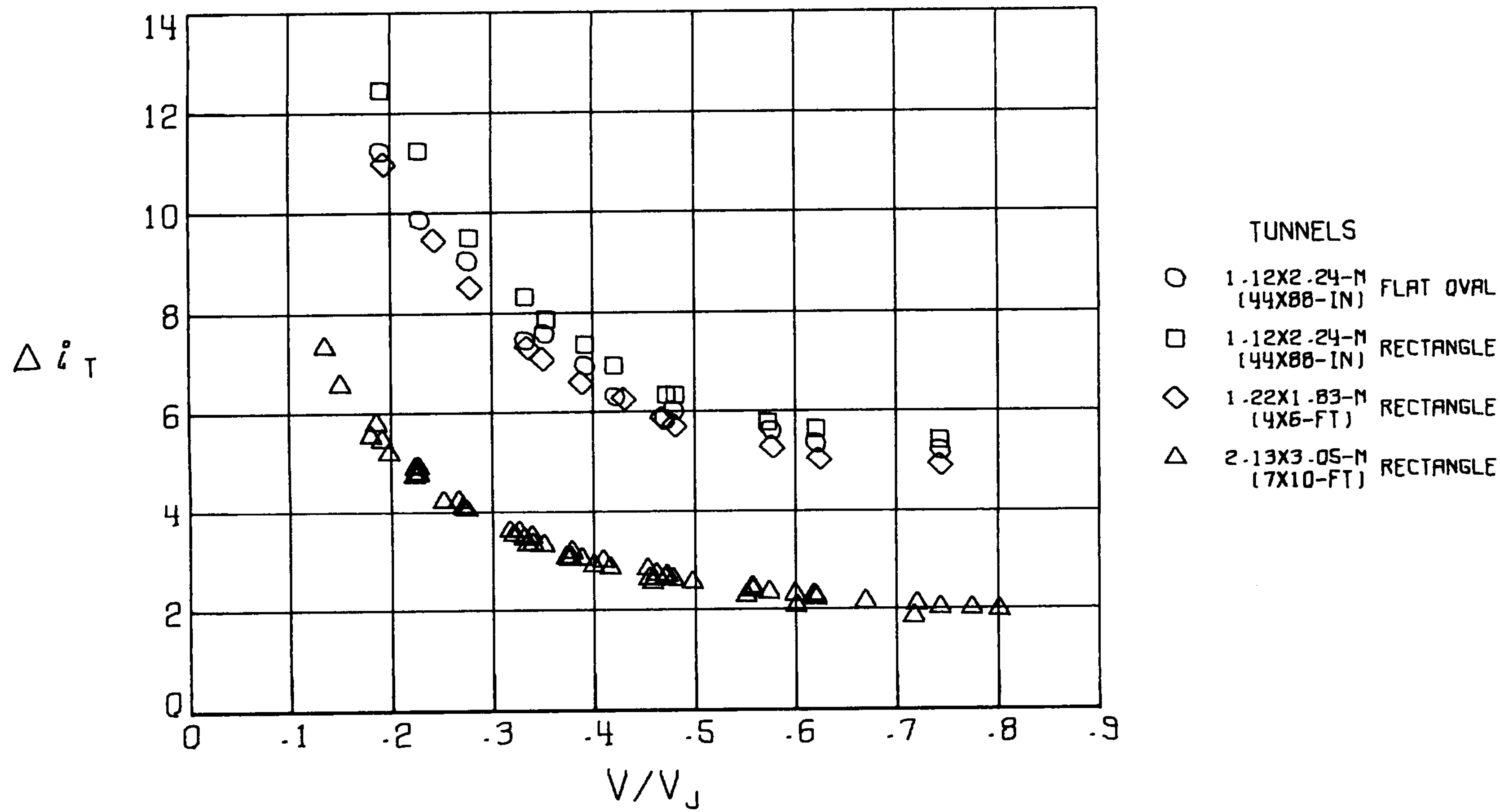

(b) $\alpha = 0^{\circ}$.

Figure 25.- Continued.

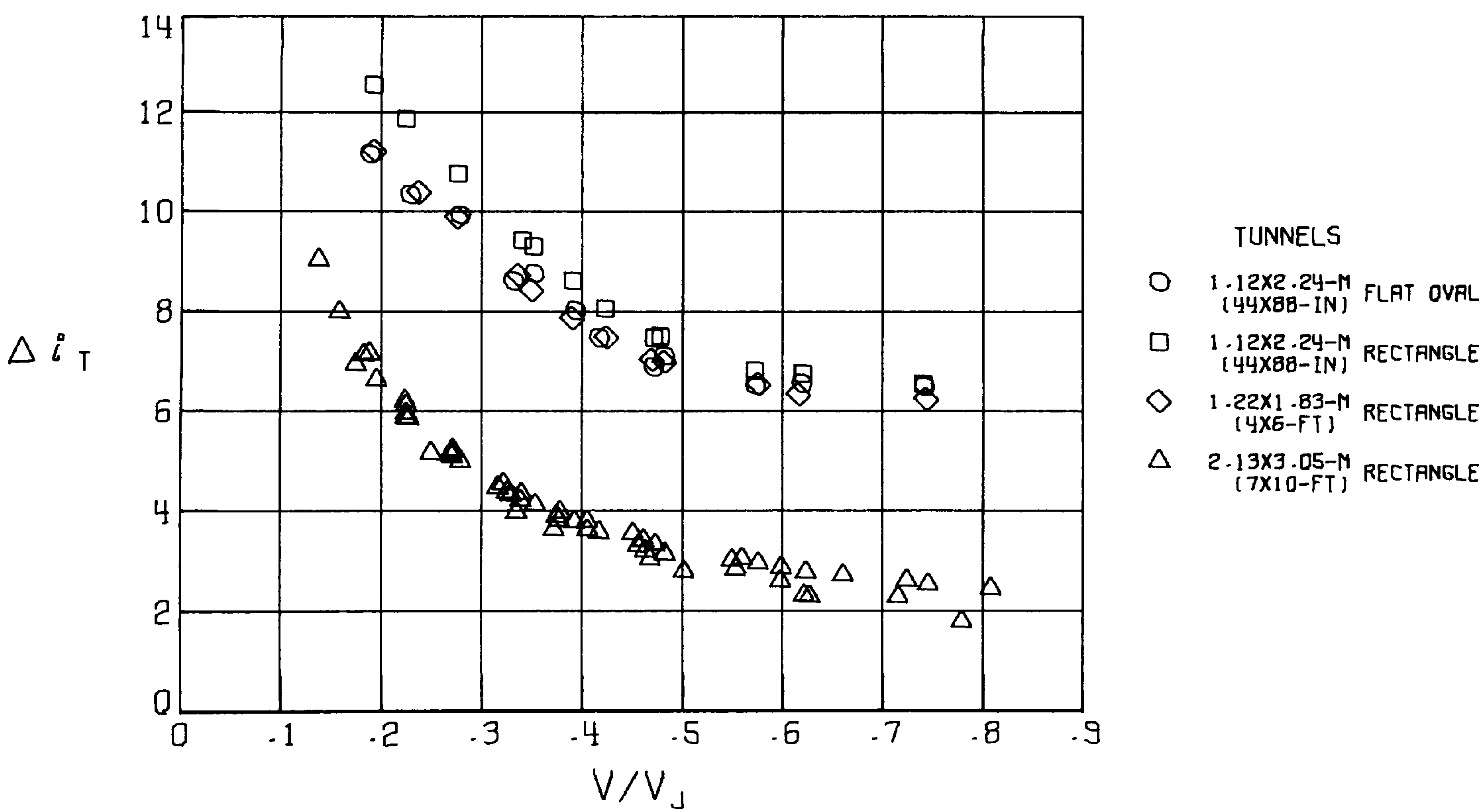

(c) $\alpha = 5^{\circ}$.

Figure 25.- Continued.

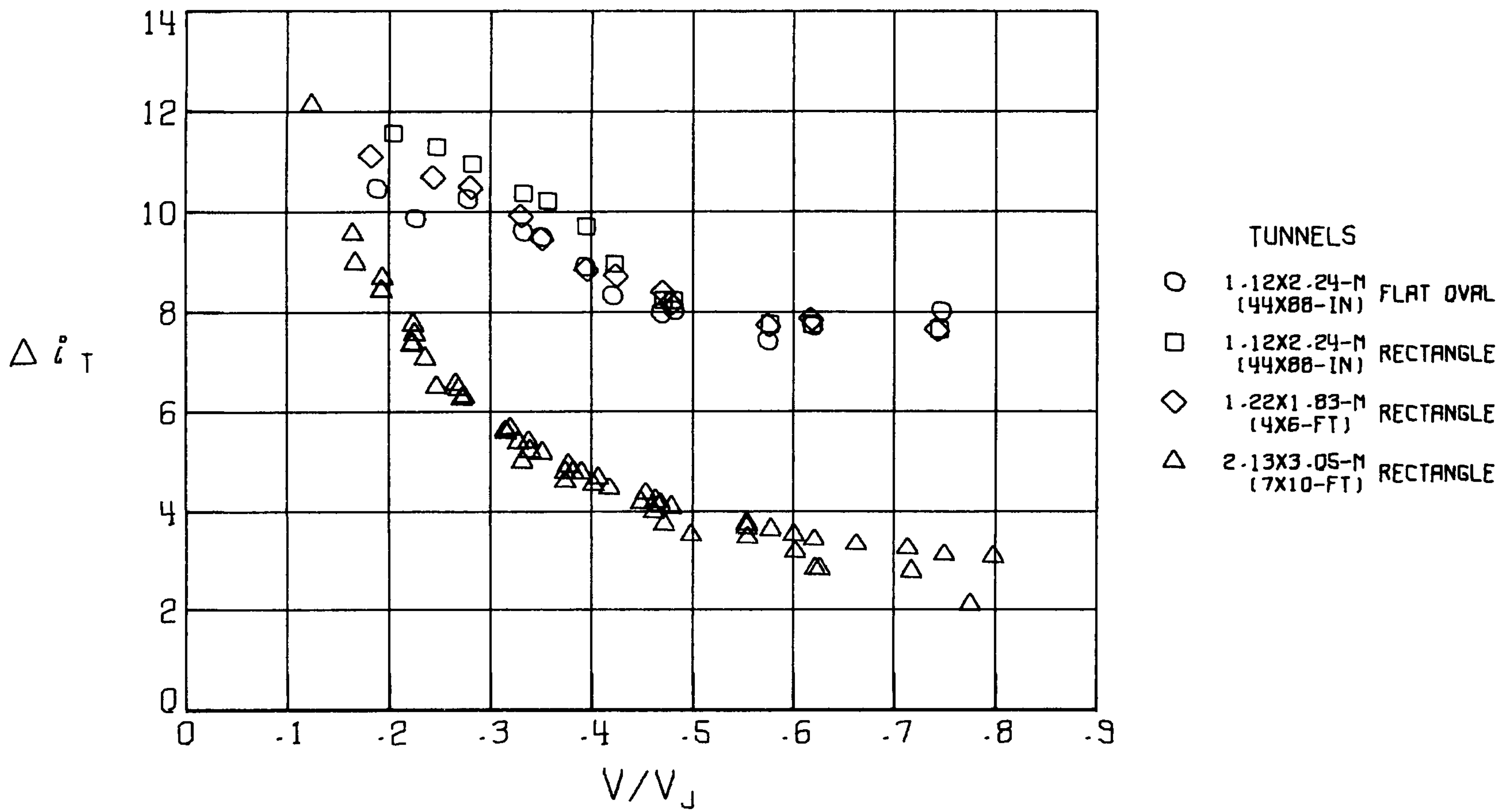

(d) $\alpha = 10^{\circ}$.

Figure 25.- Continued.

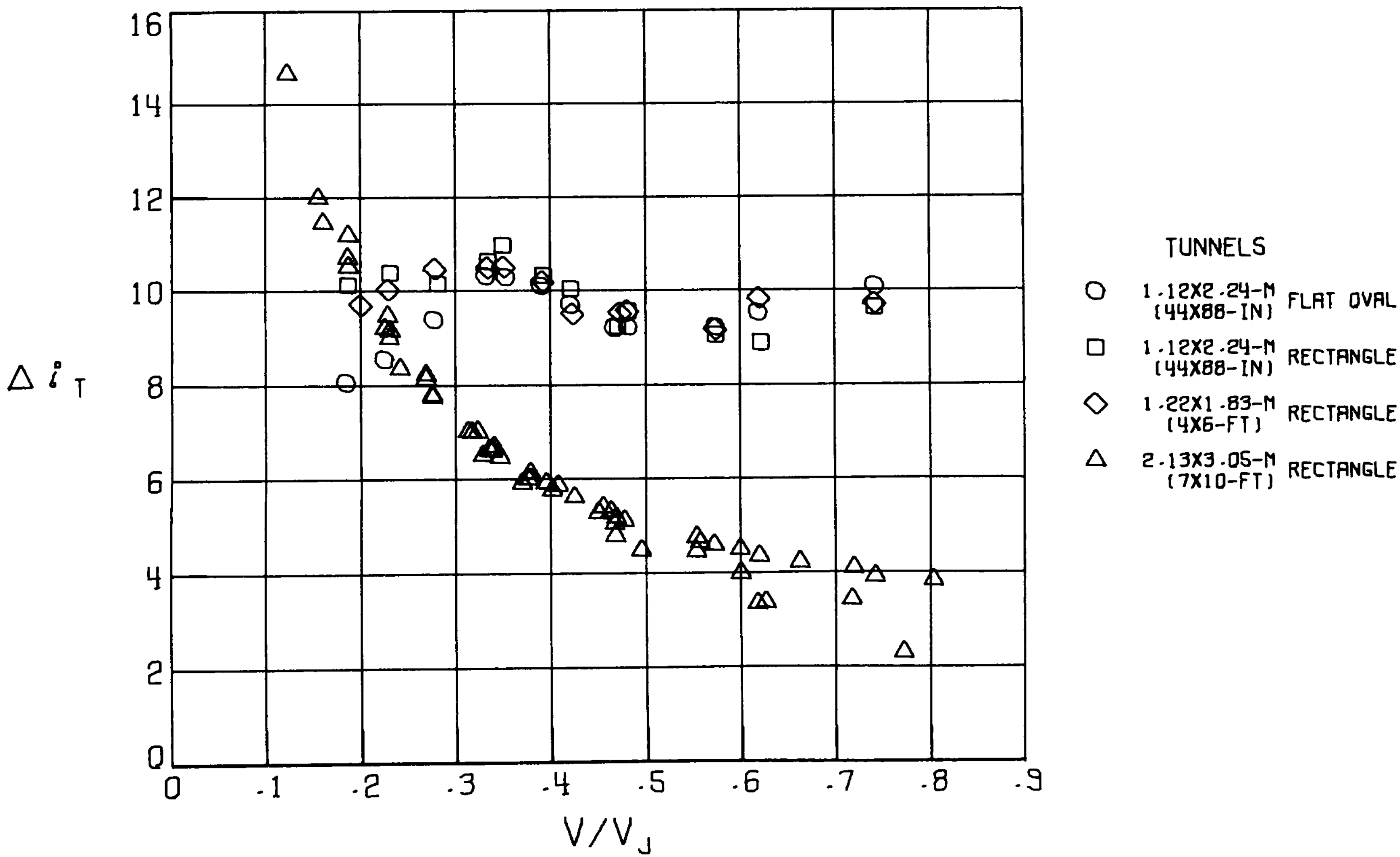

(e) $\alpha = 16^{\circ}$.

Figure 25.- Concluded.

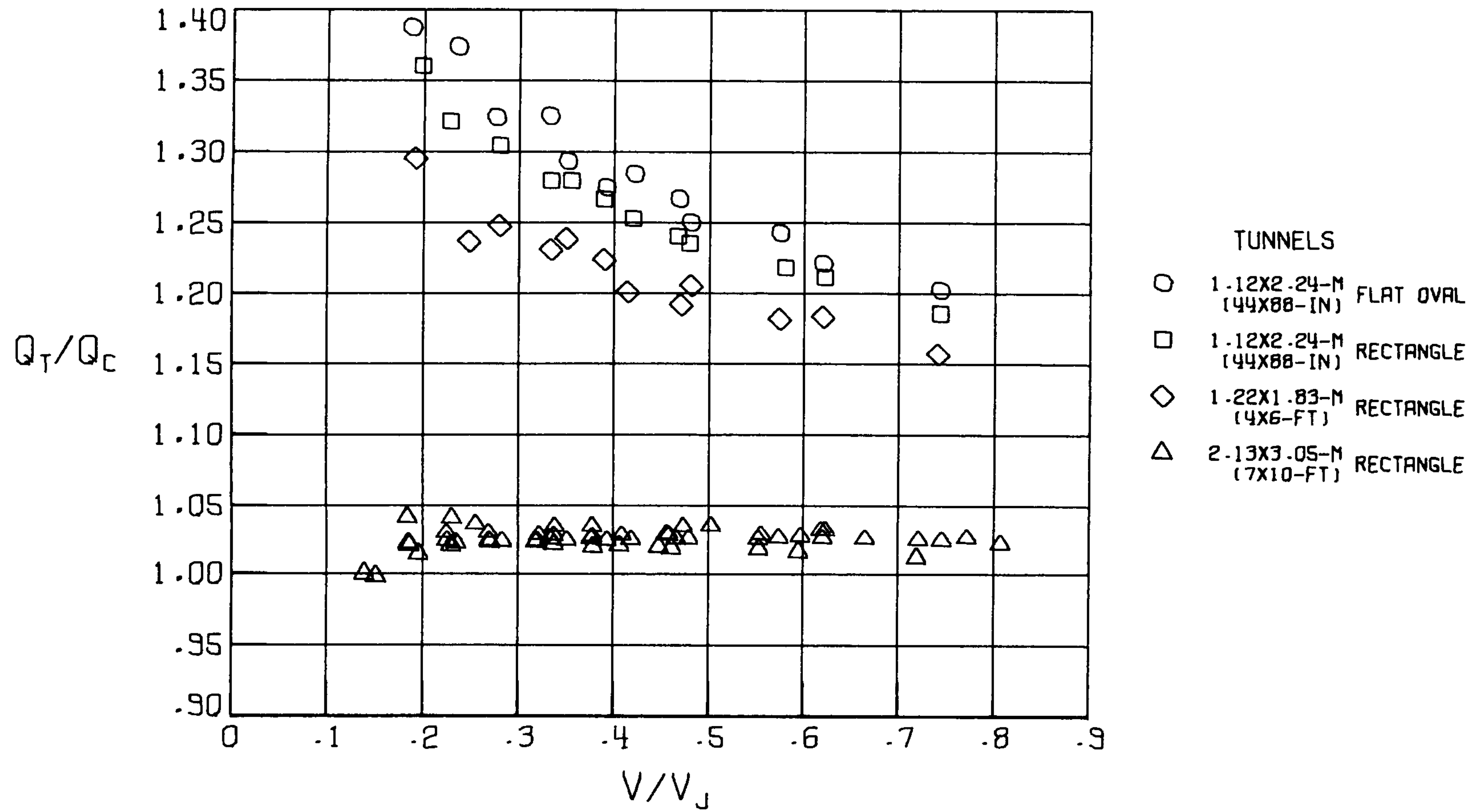

(a) $\alpha = -5^{\circ}$.

Figure 26.- Wall-induced values of q_T/q_c in the uncorrected data from the fan-in-wing model as a function of V/V_j in several different wind tunnels.

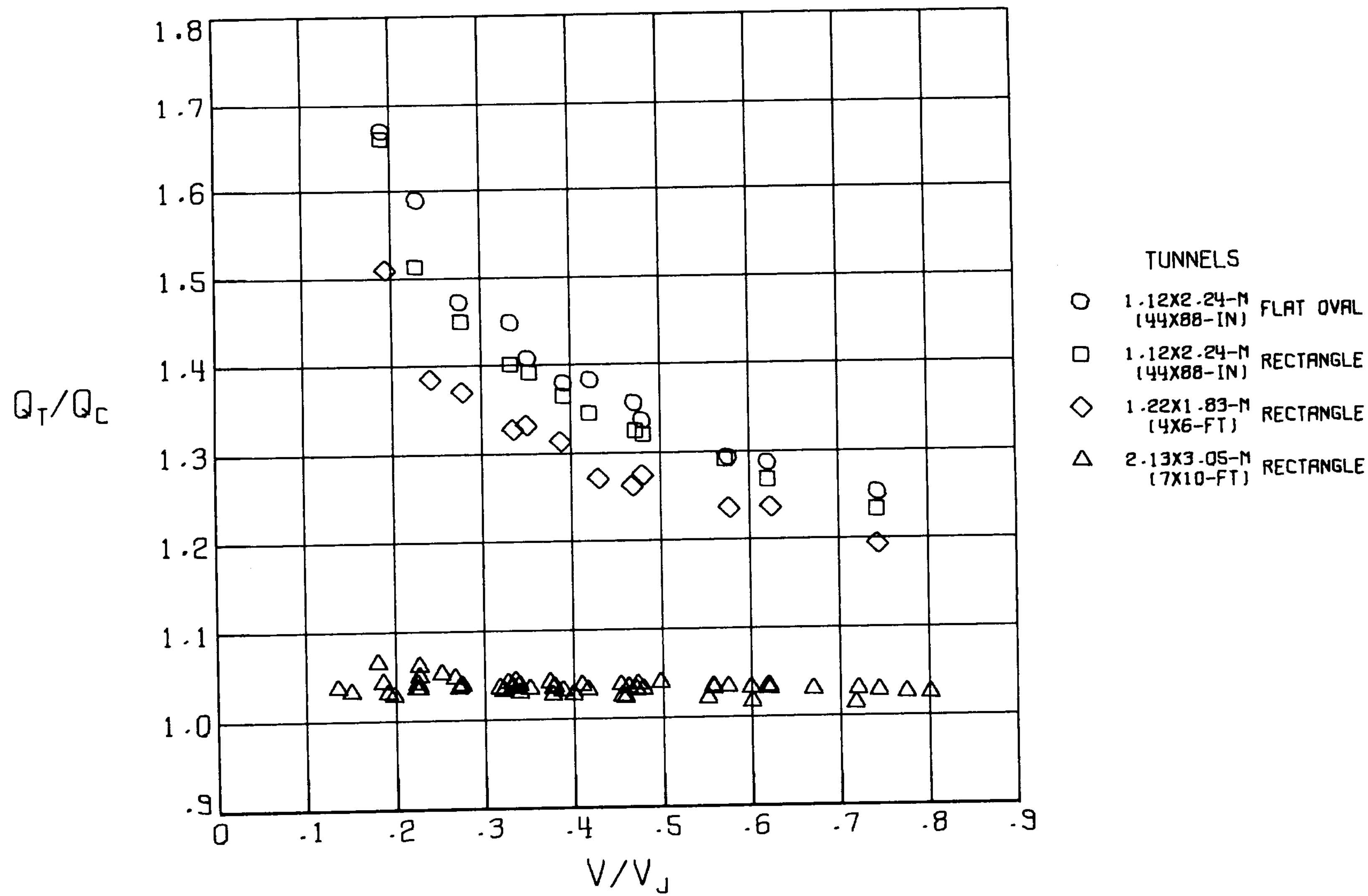

(b) $\alpha = 0^{\circ}$.

Figure 26.- Continued.

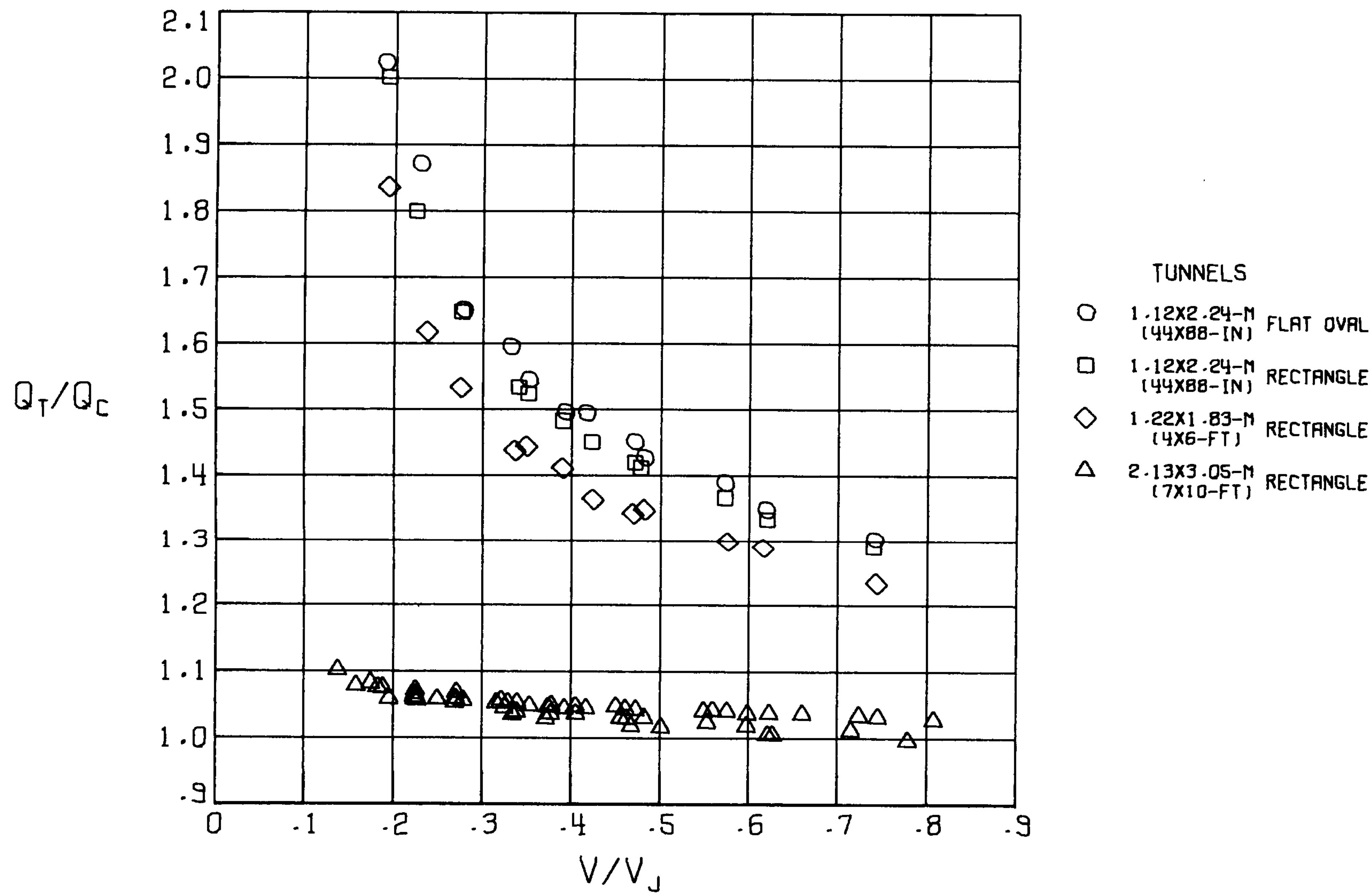

(c) $\alpha = 5^{o}$.

Figure 26.- Continued.

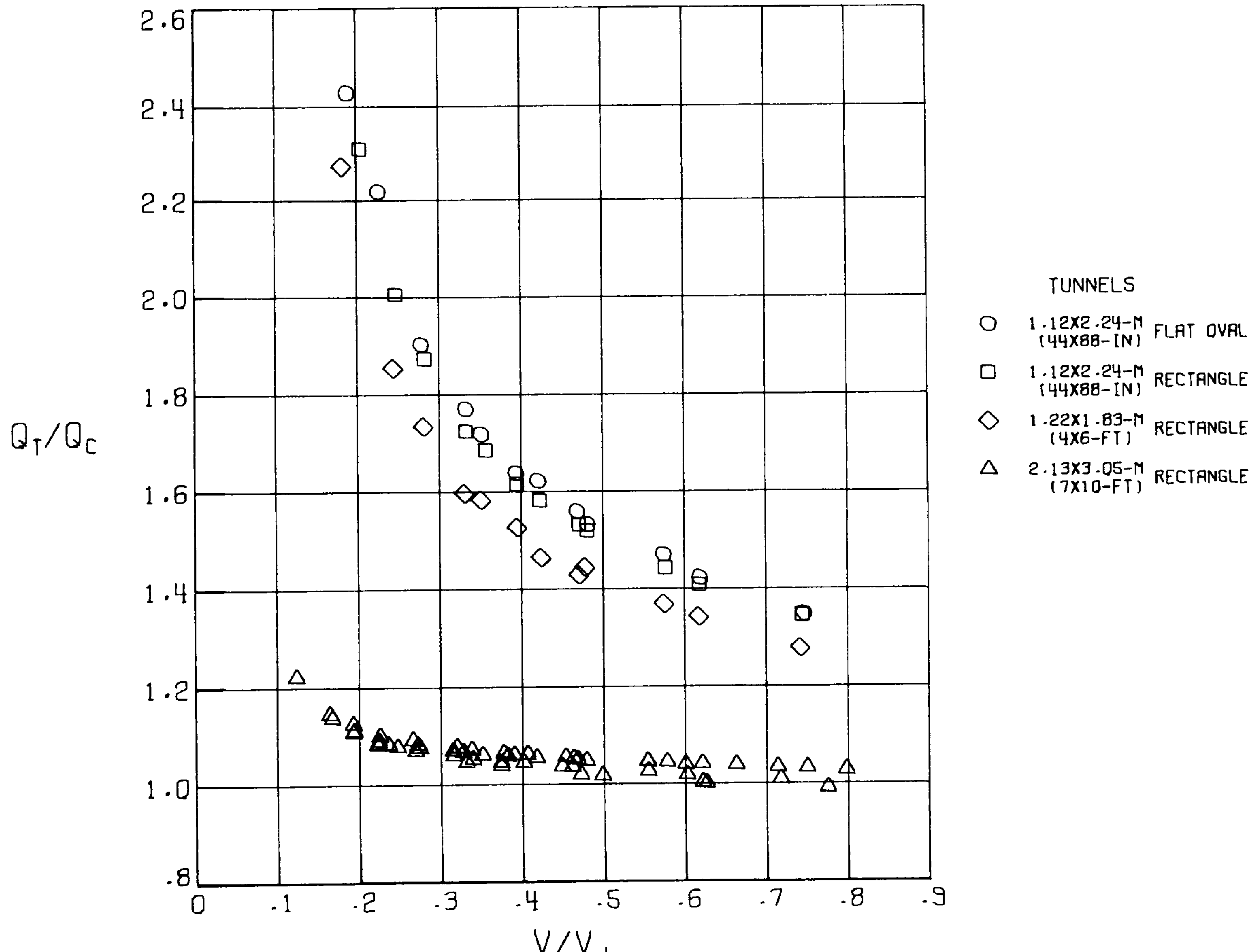

(d) $\alpha = 10^{o}$.

Figure 26.- Continued.

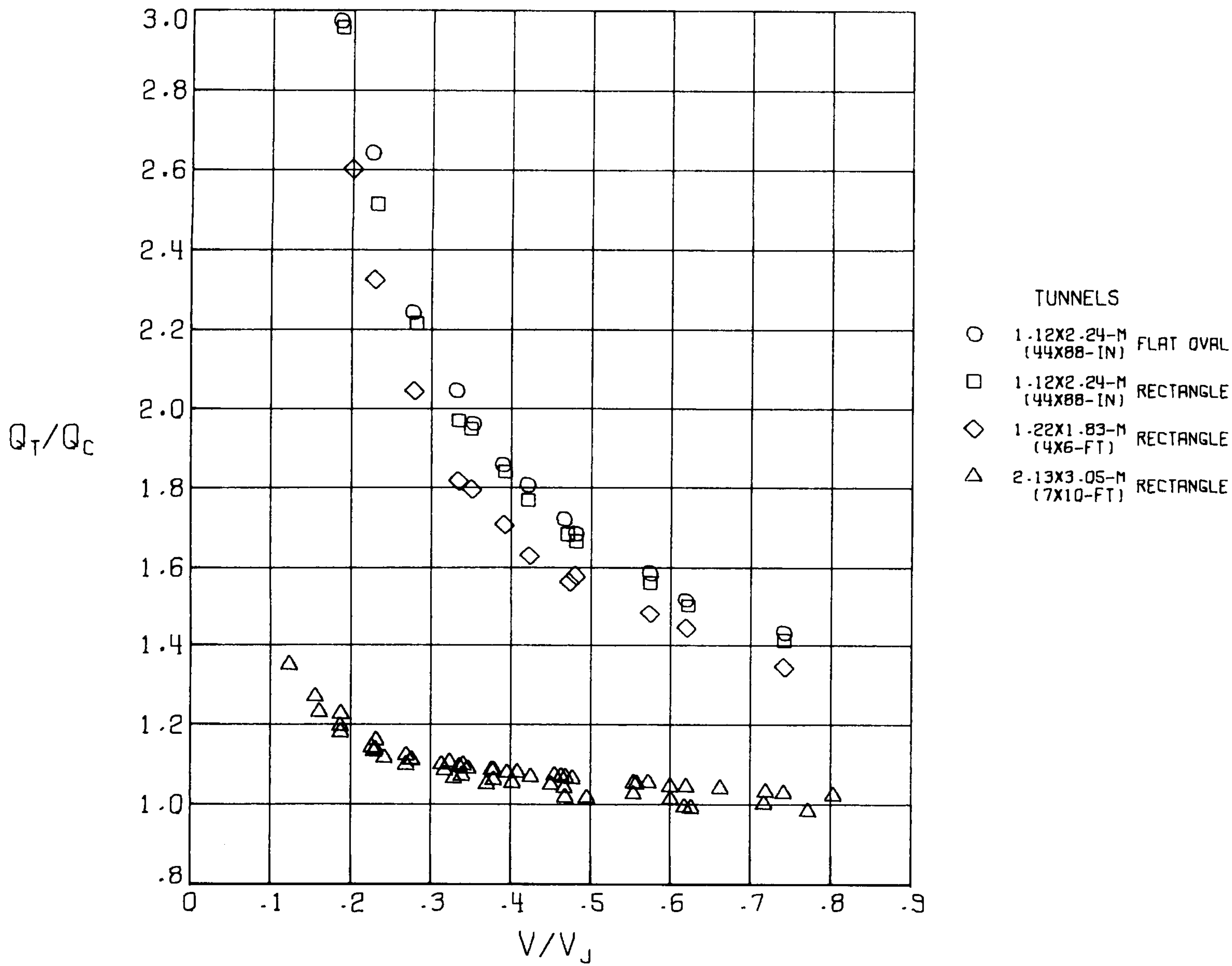

(e) $\alpha = 16^{o}$.

Figure 26.- Concluded.

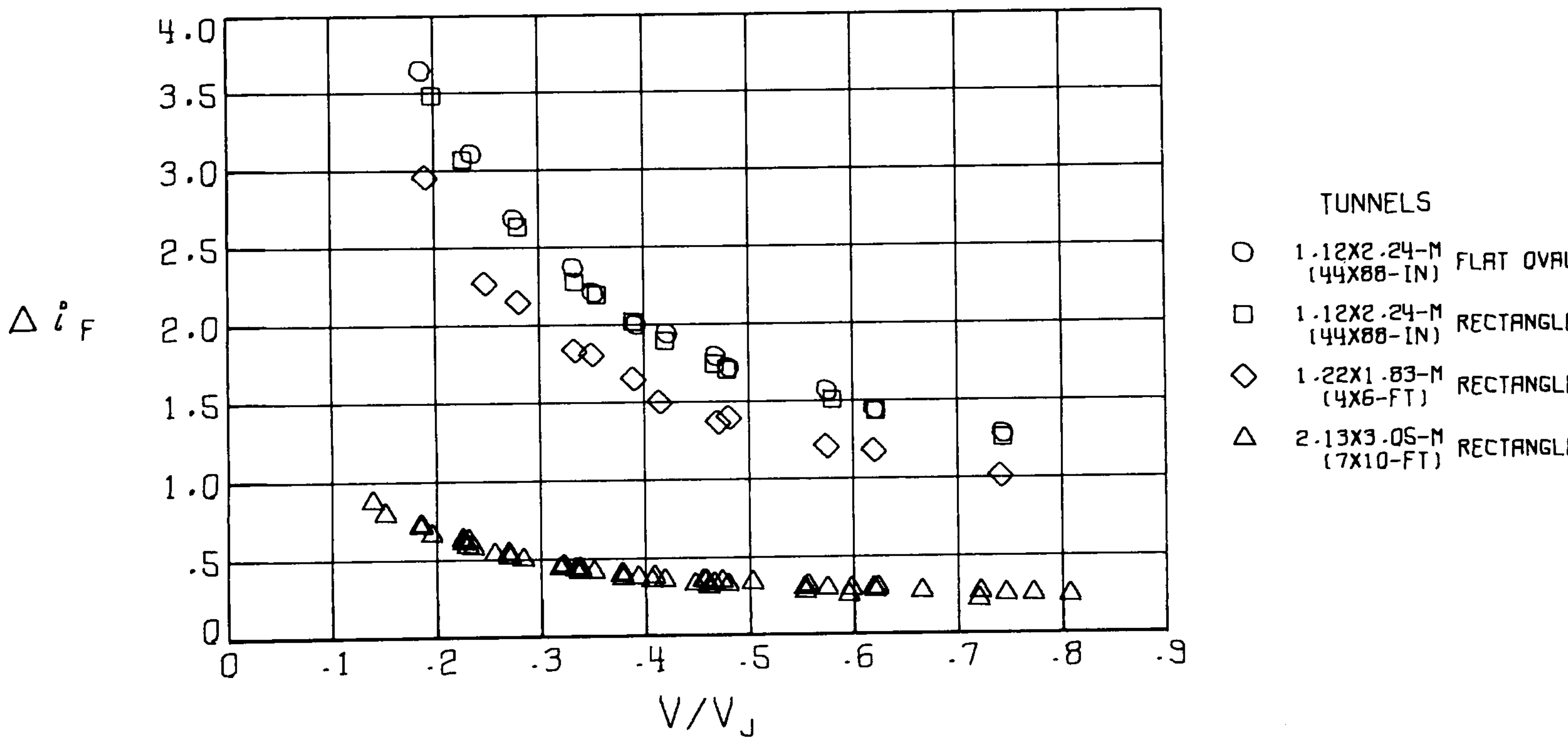

(a) $\alpha = -5^{o}$.

Figure 27.- Wall-induced fan incidence Δi_F in the uncorrected data from the fan-in-wing model as a function of V/V_j in several different wind tunnels.

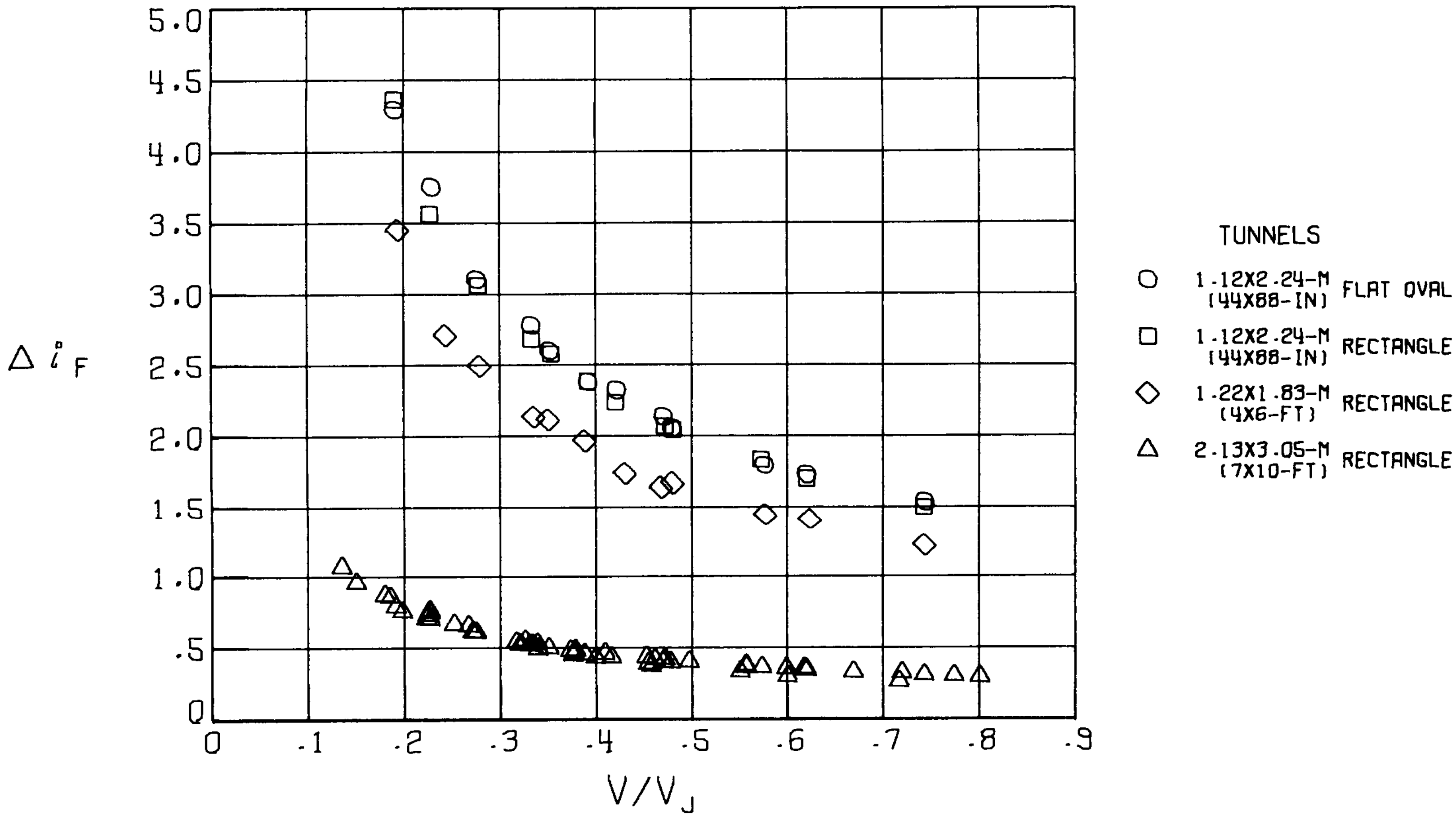

(b) $\alpha = 0^{o}$.

Figure 27.- Continued.

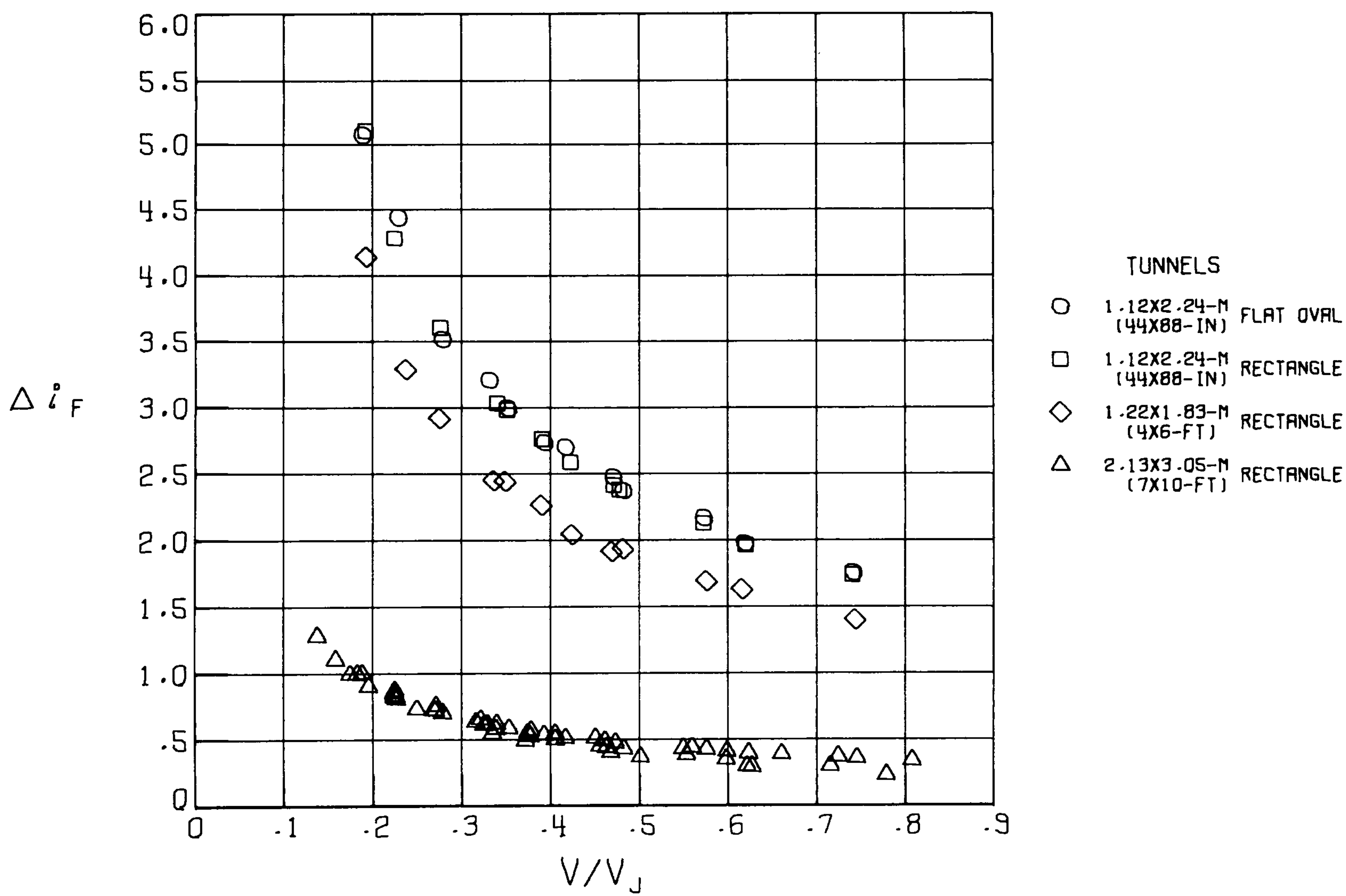

(c) $\alpha = 5^o$.

Figure 27.- Continued.

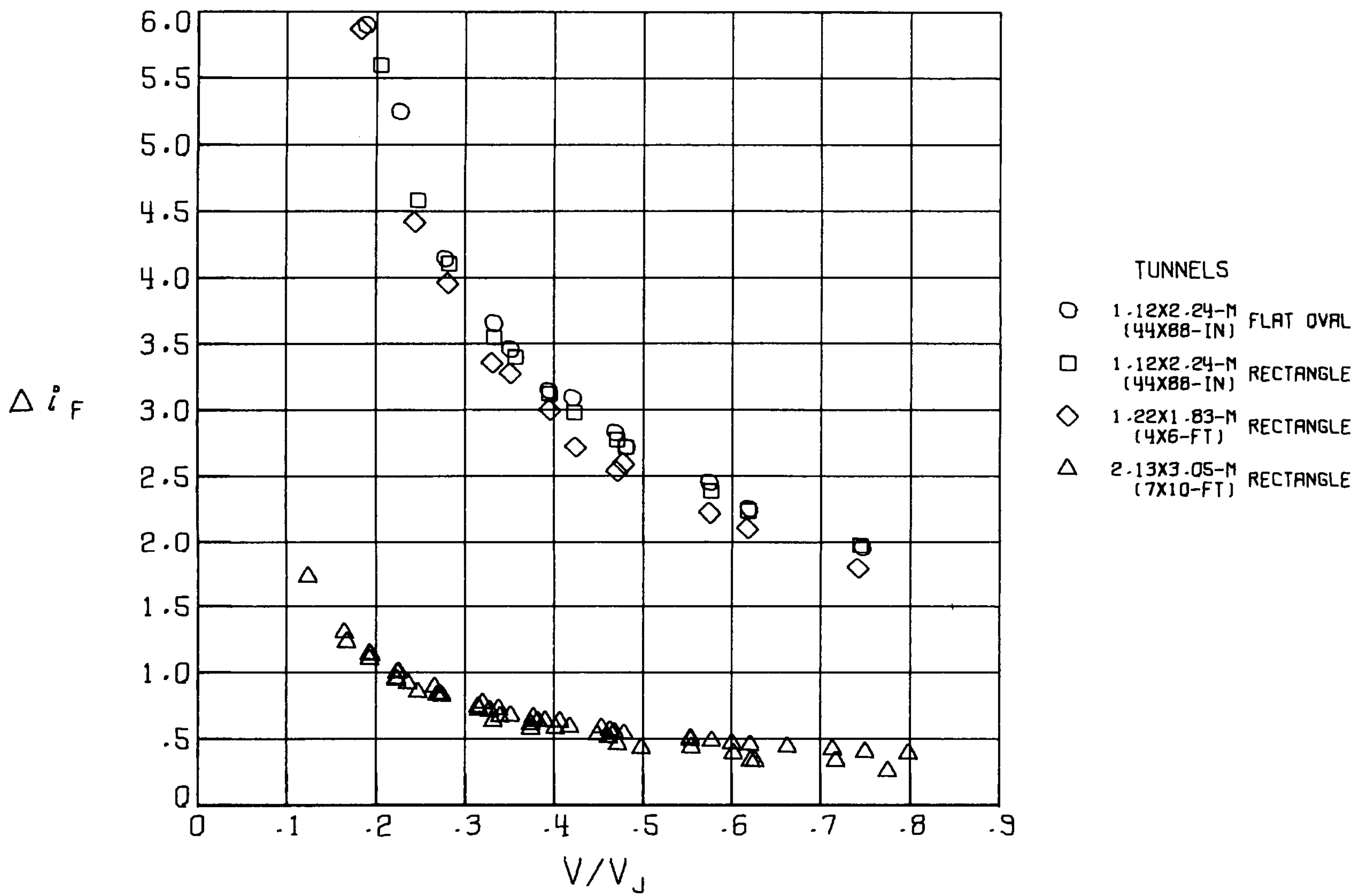

(d) $\alpha = 10^{o}$.

Figure 27.- Continued.

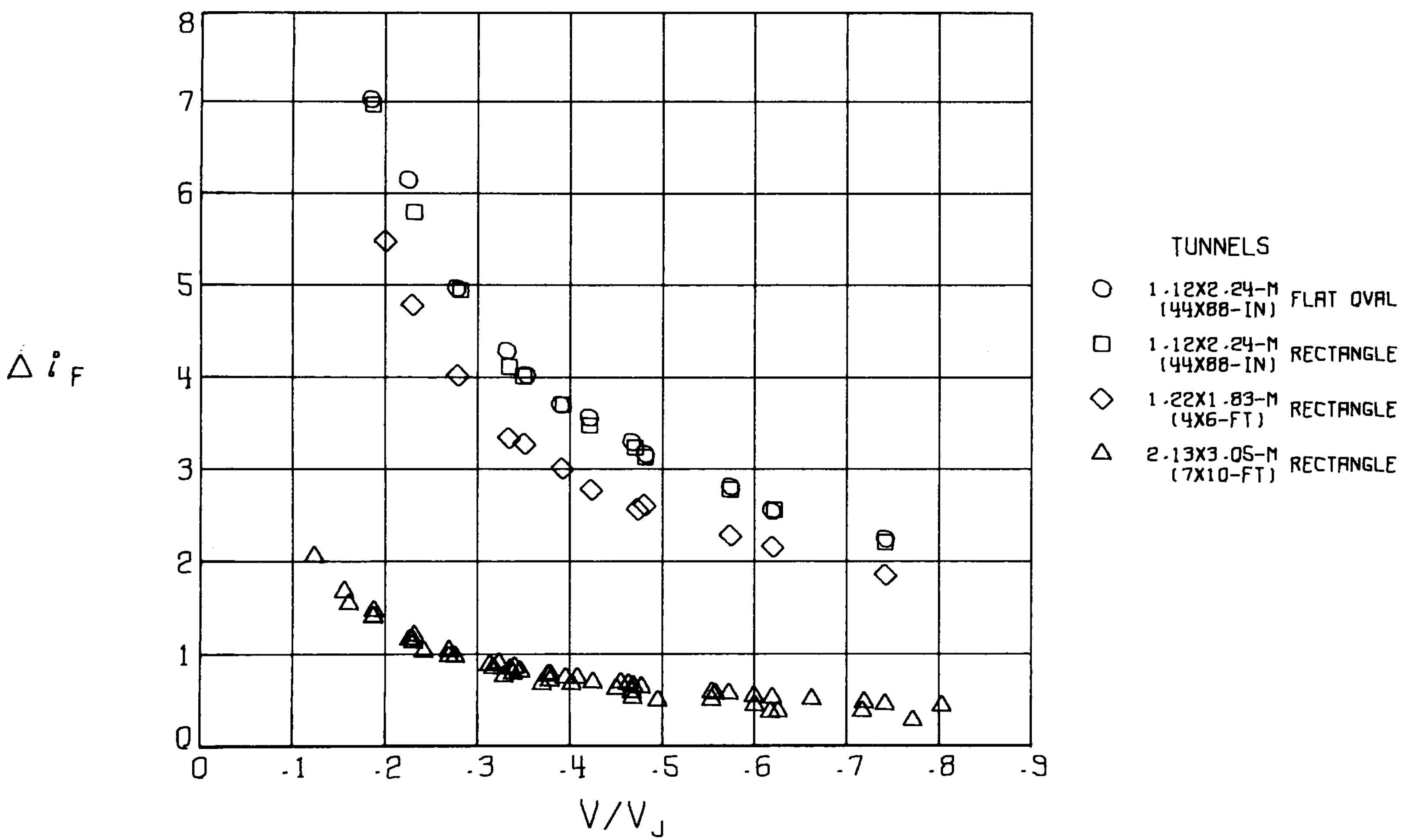

(e) $\alpha = 16^{o}$.

Figure 27.- Concluded.

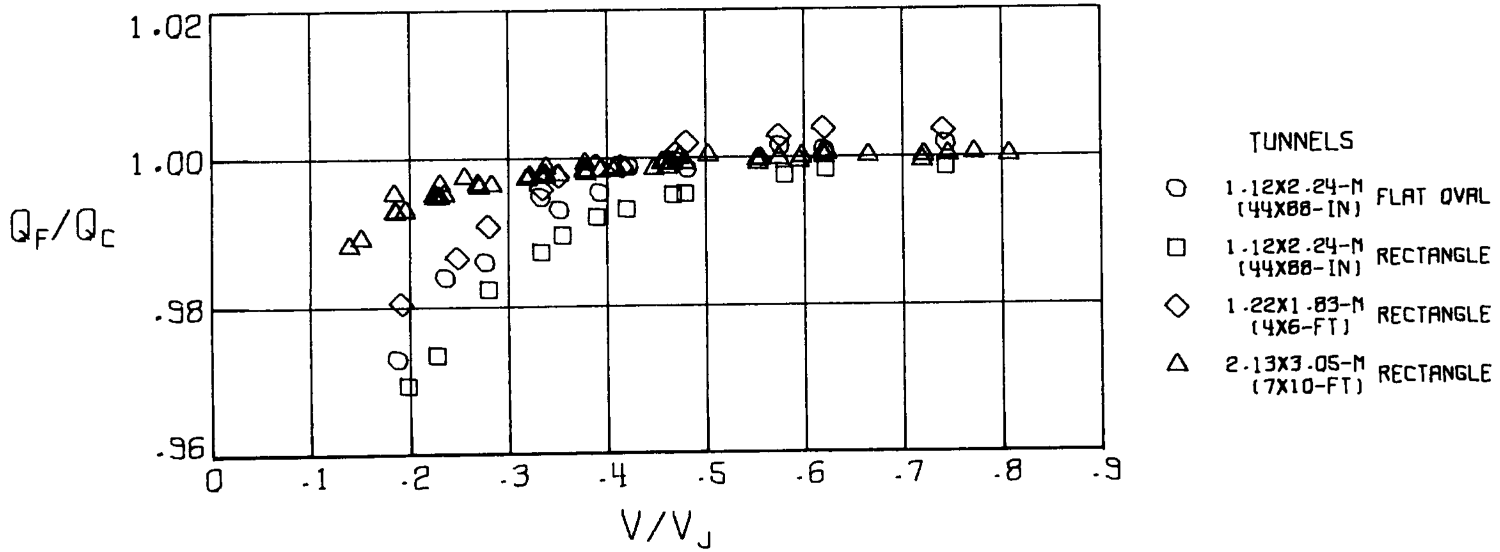

(a) $\alpha = -5^{\circ}$.

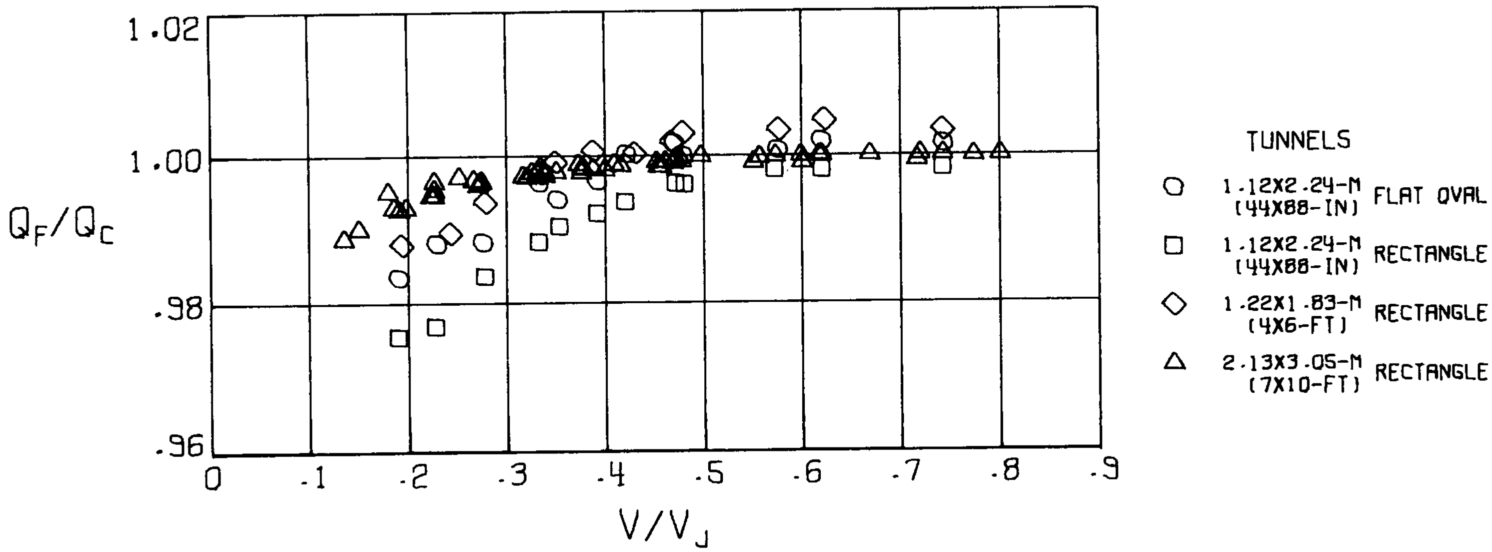

(b) $\alpha = 0^{\circ}$.

Figure 28.- Wall-induced values of q_F/q_c in the uncorrected data from the fan-in-wing model as a function of V/V_j in several different wind tunnels.

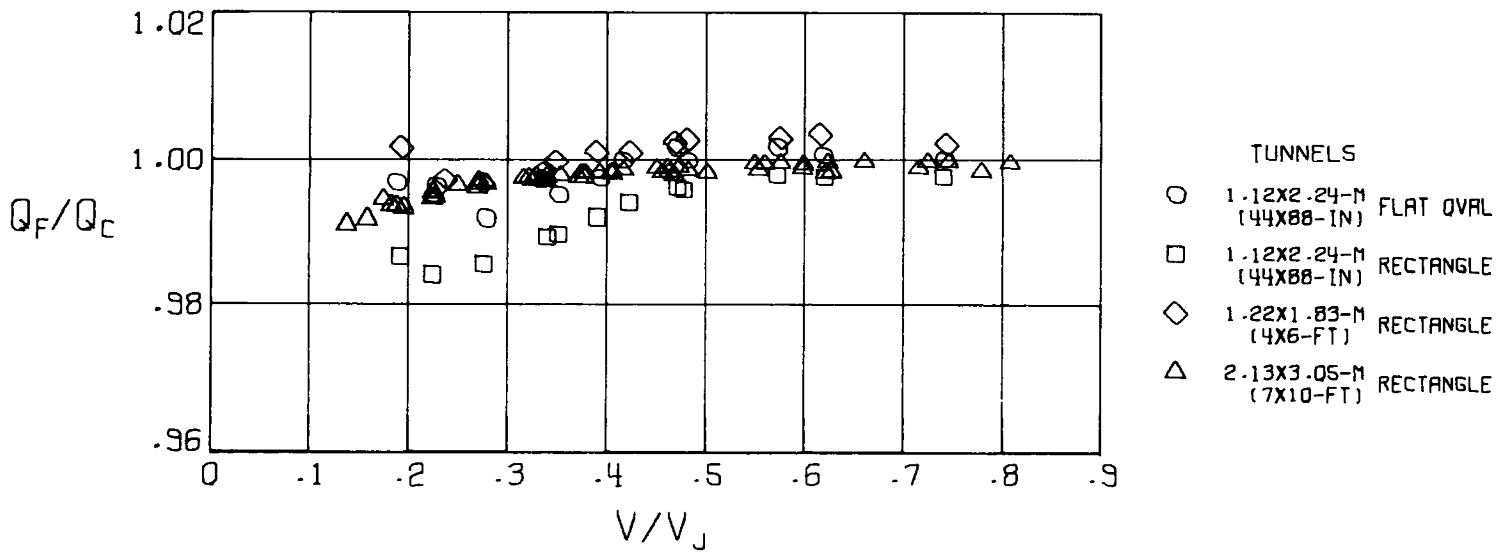

(c) α = 5°.

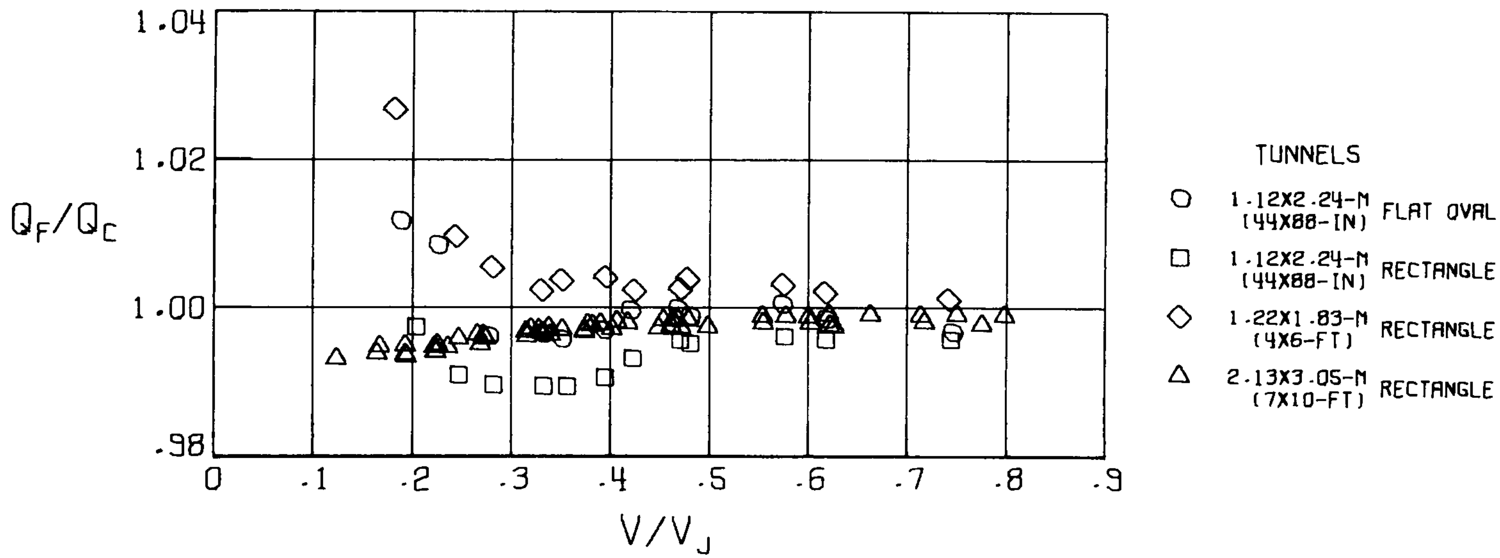

(d) α = 10°.

Figure 28.- Continued.

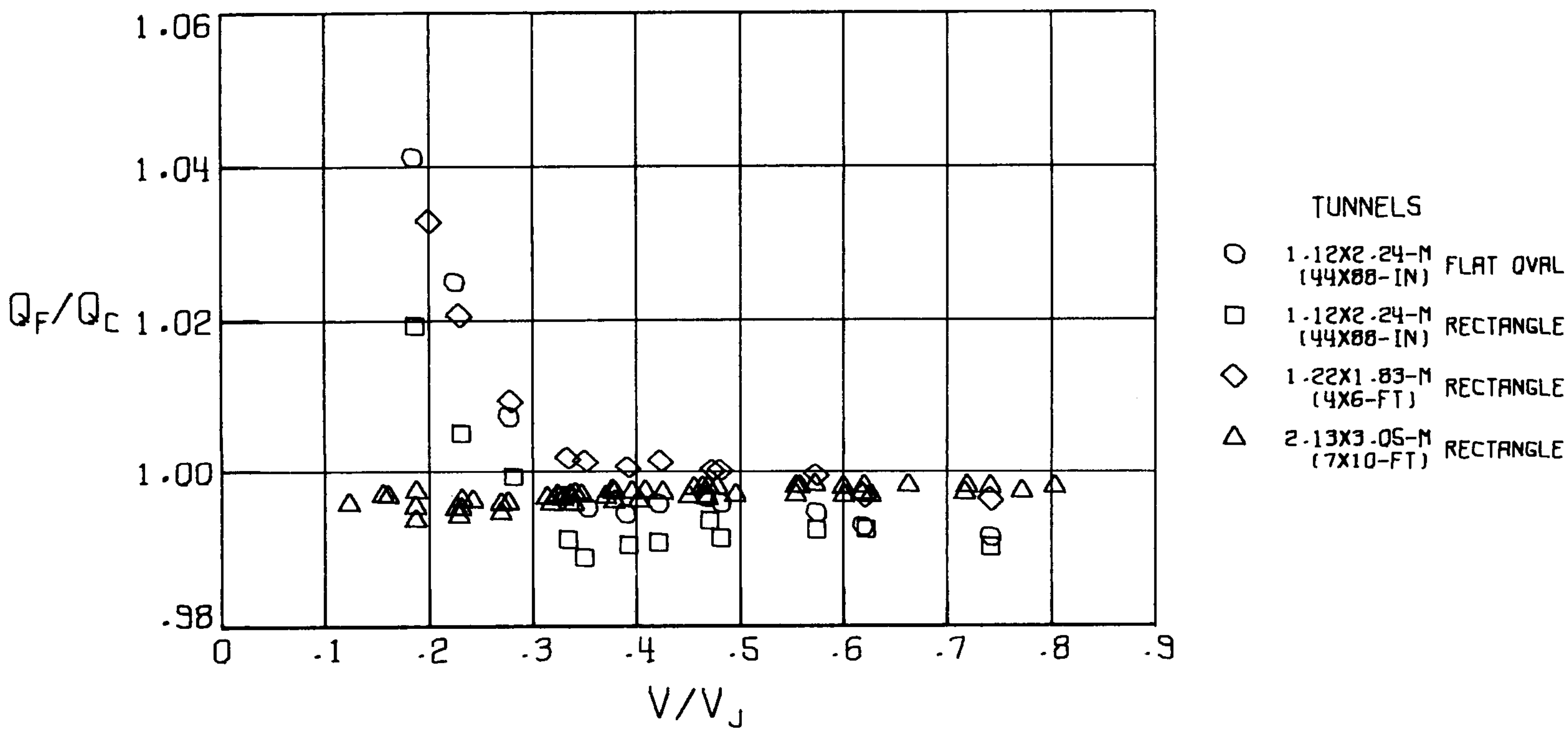

(e) $\alpha = 16^{\circ}$.

Figure 28.- Concluded.

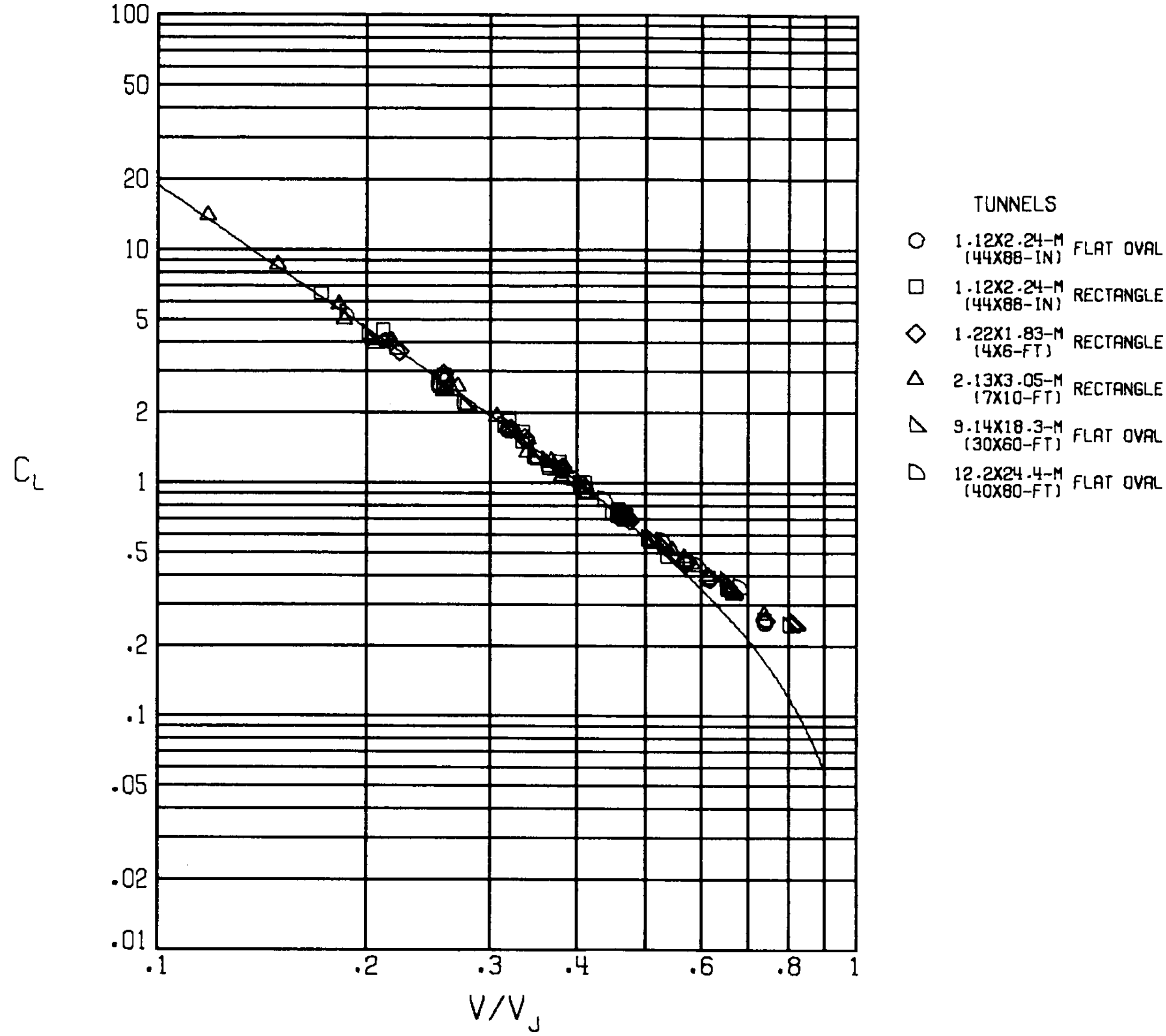

(a) $\alpha = -5^{\circ}$.

Figure 29.- Corrected values of lift coefficient as a function of V/V_j. The solid curve represents the sum of the vertical component of the static thrust and the lift of the wing expressed in coefficient form. It is assumed that there is no interference between the wing and the fans.

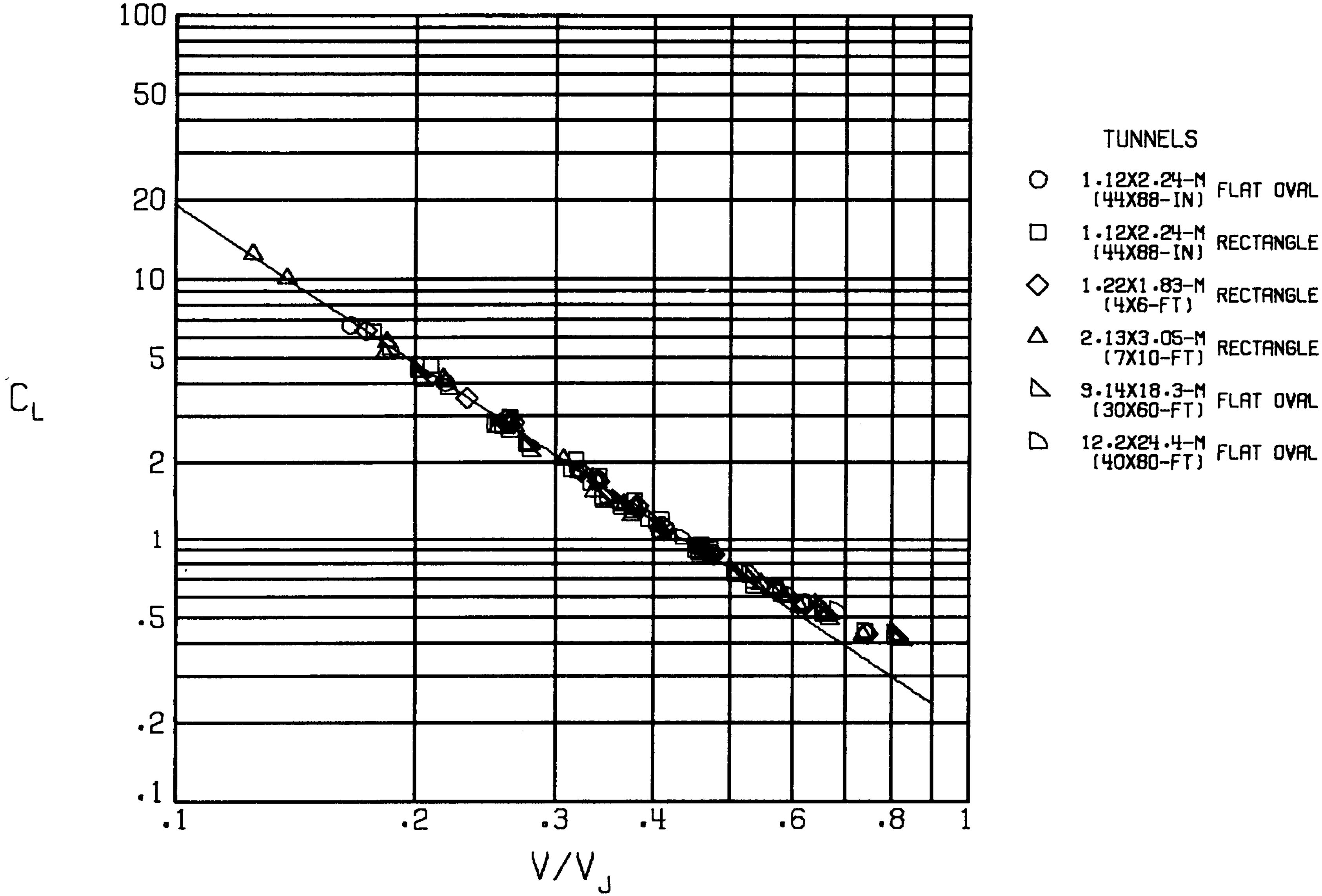

(b) $\alpha = 0^{o}$.

Figure 29.- Continued.

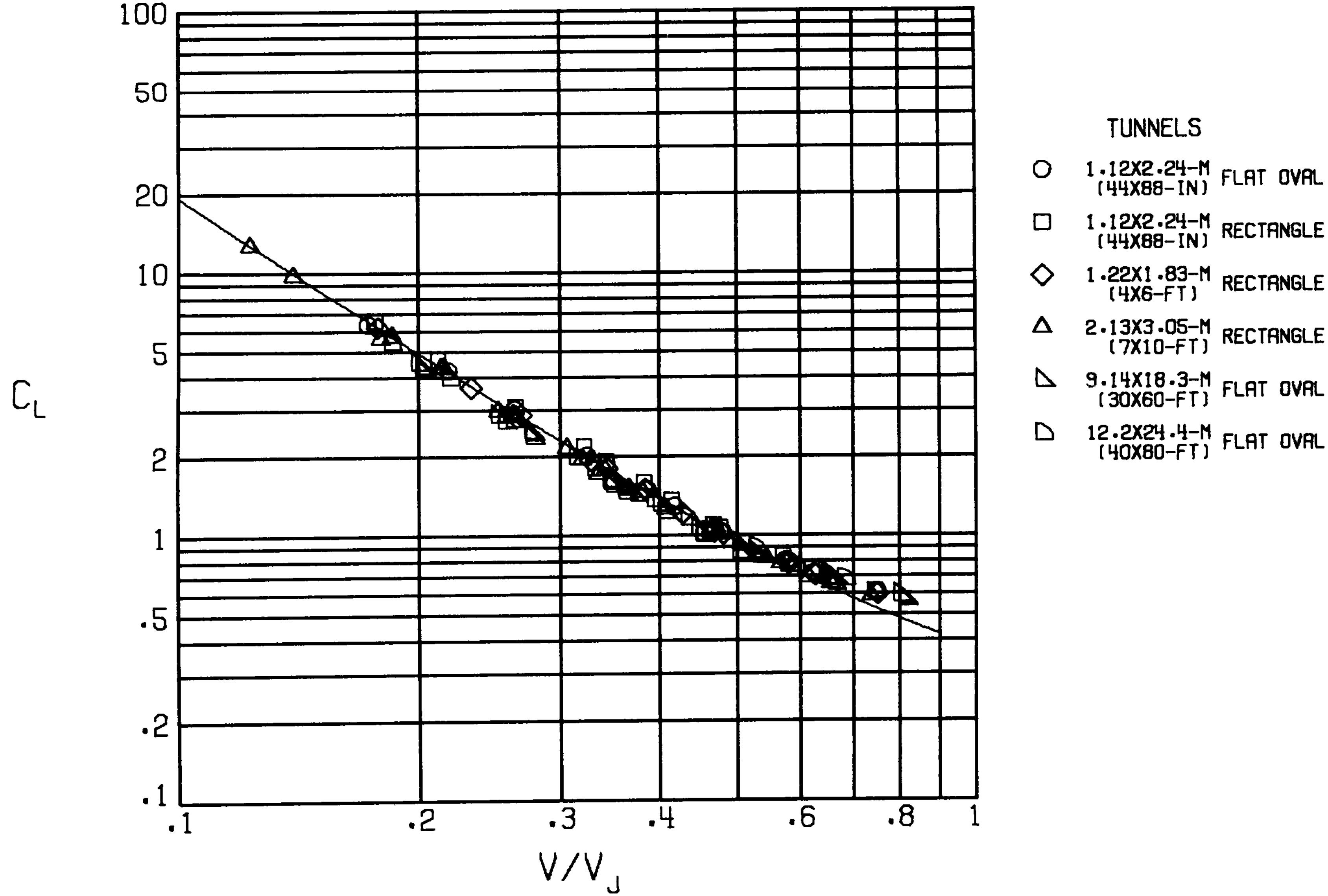

(c) $\alpha = 5^{o}$.

Figure 29.- Continued.

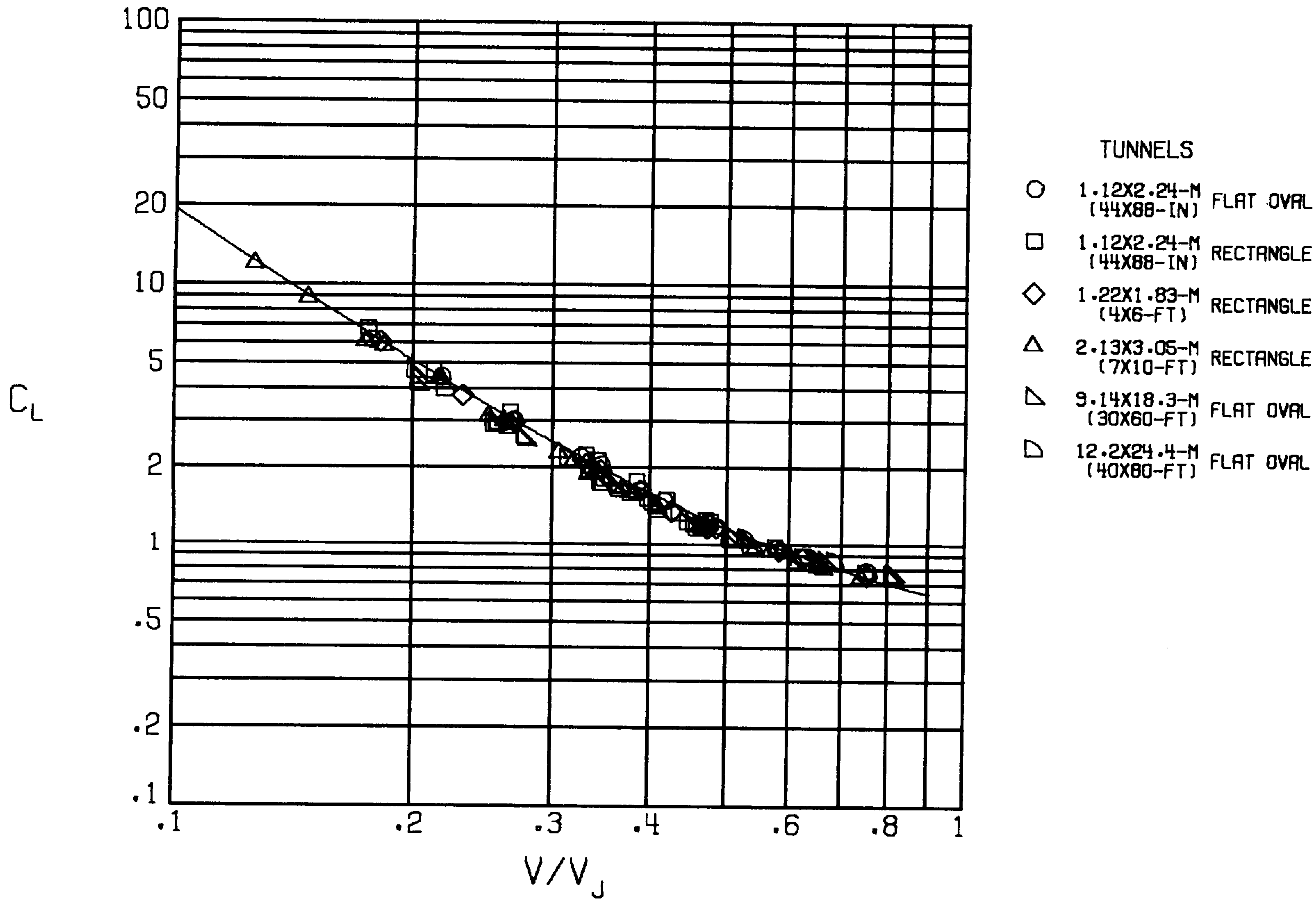

(d) $\alpha = 10^{o}$.

Figure 29.- Continued.

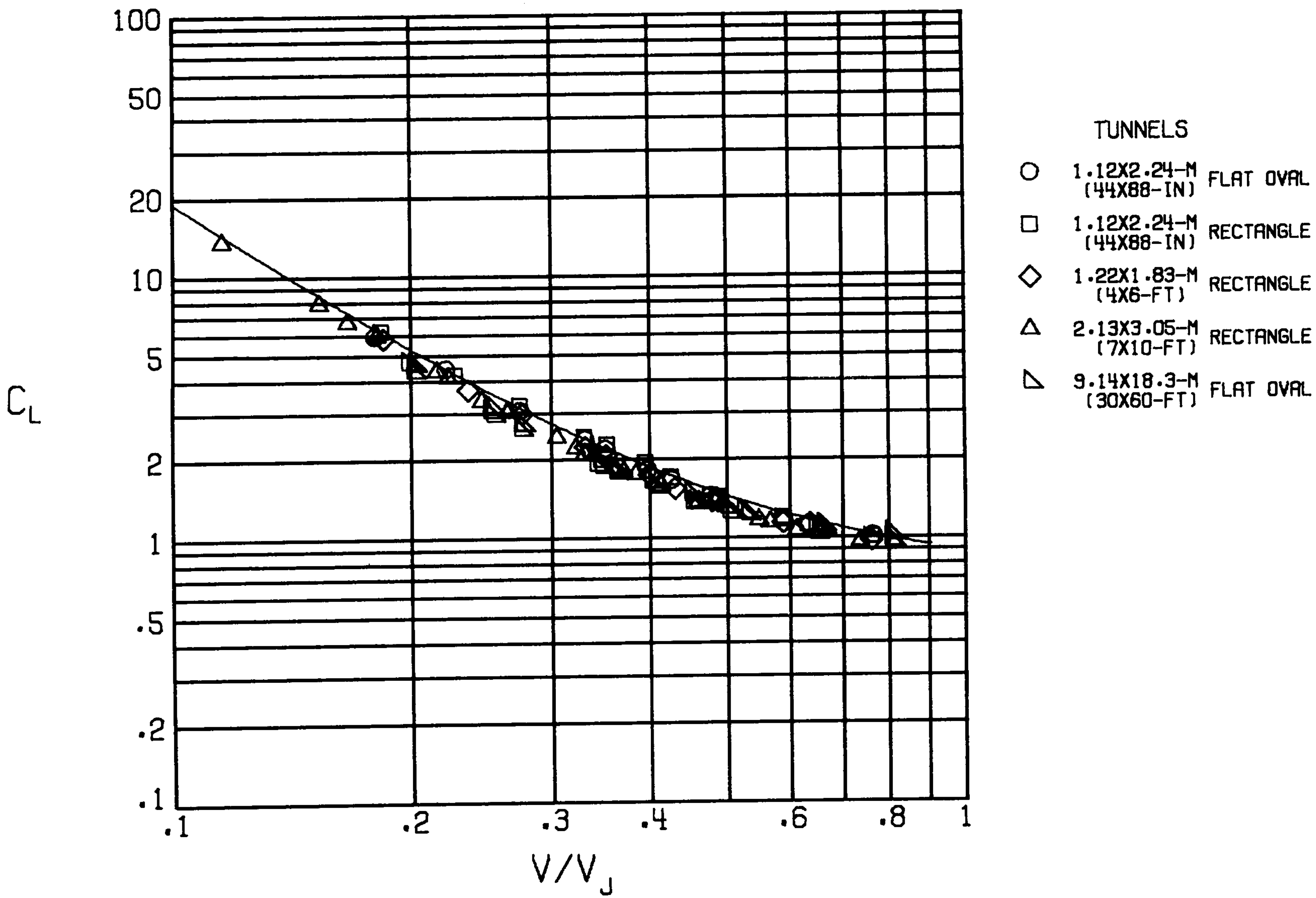

(e) $\alpha = 16^{o}$.

Figure 29.- Concluded.

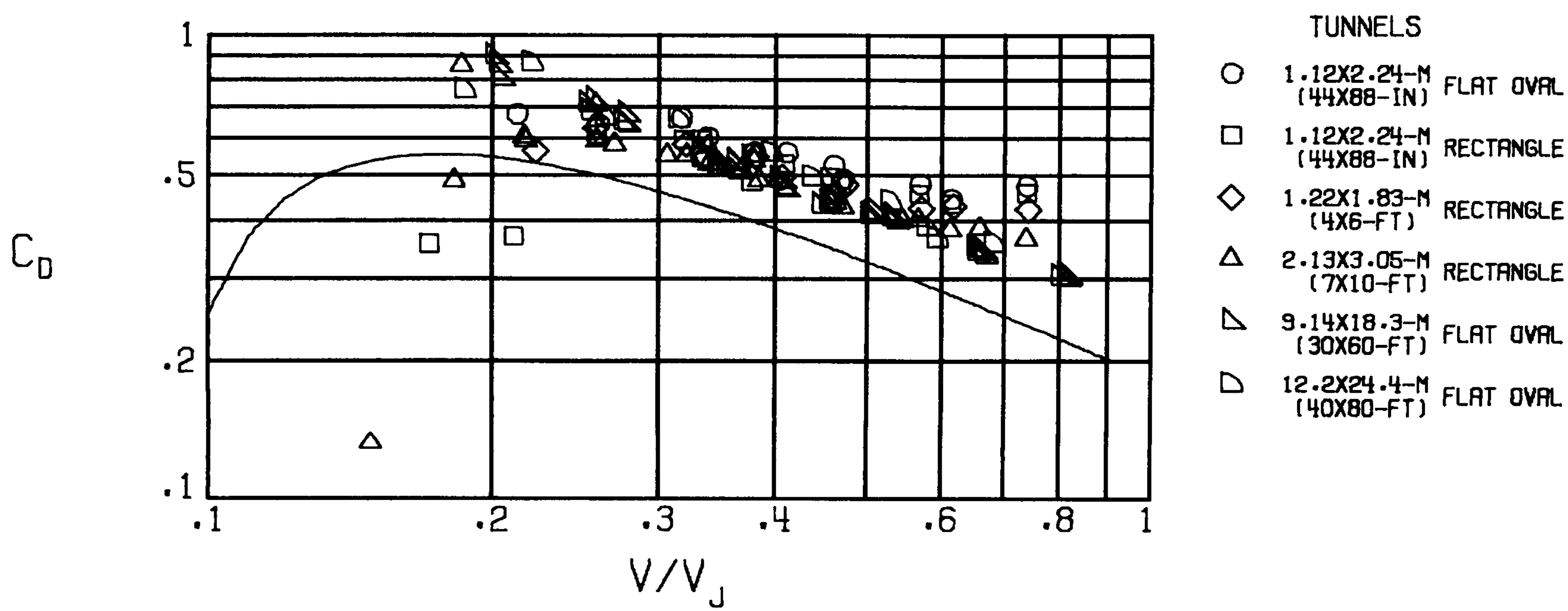

(a) $\alpha = -5^{\circ}$.

Figure 30.- Corrected values of drag coefficient as a function of V/V_j. The solid curve represents the sum of the momentum-theory value of fan drag and the drag of the wing expressed in coefficient form. It is assumed that there is no interference between the wing and the fans.

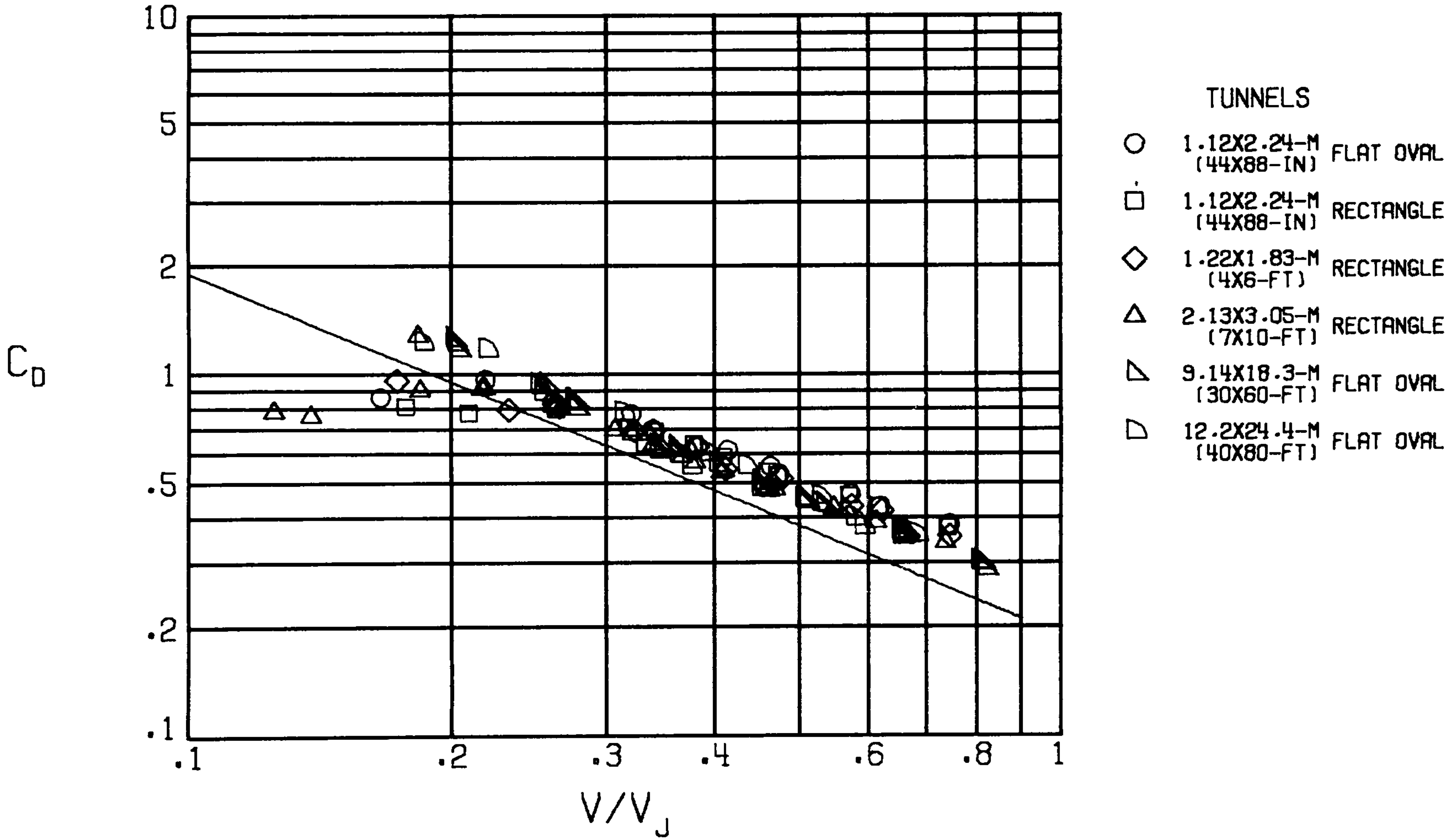

(b) $\alpha = 0^{\circ}$.

Figure 30.- Continued.

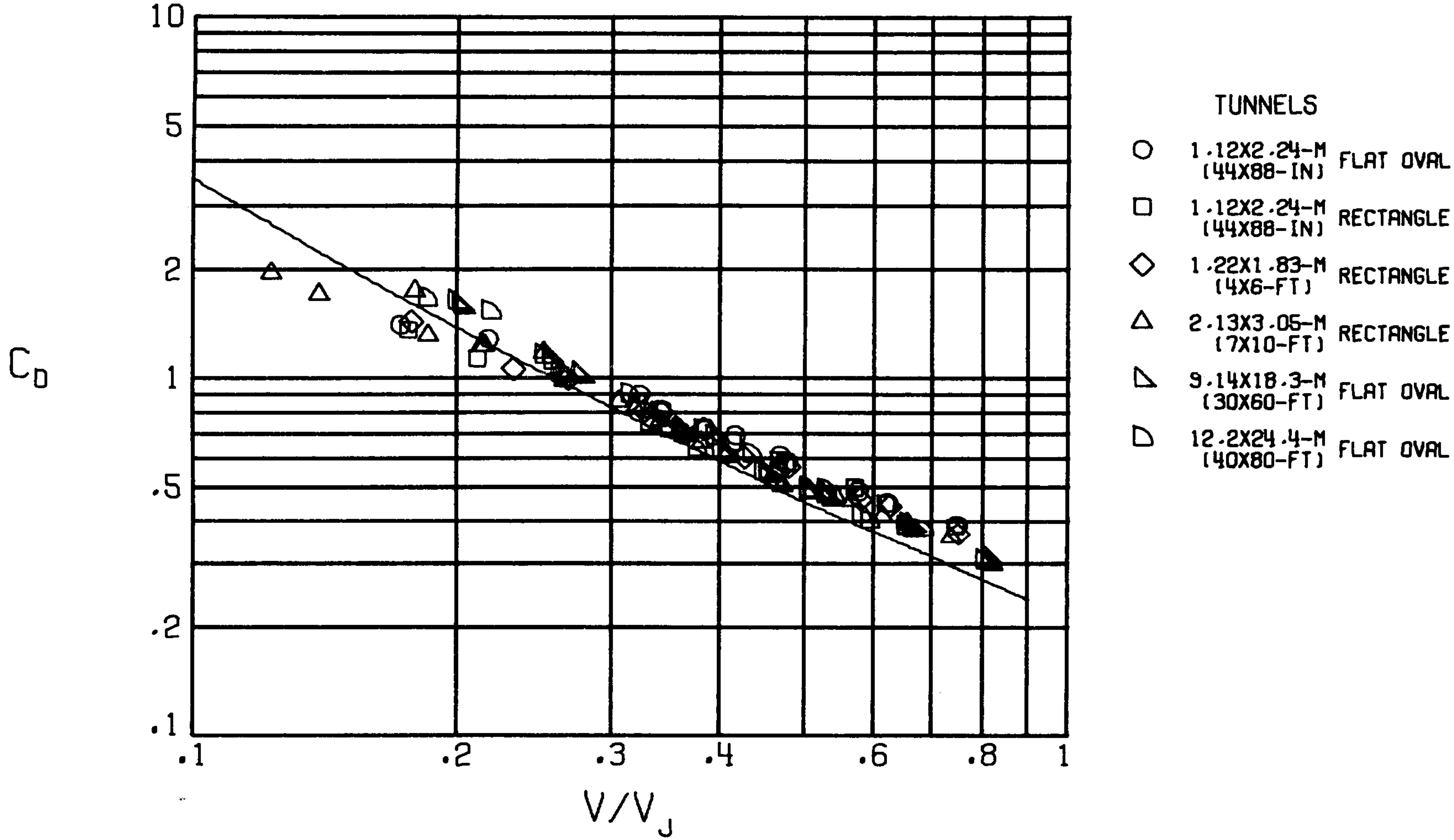

(c) $\alpha = 5^{o}$.

Figure 30.- Continued.

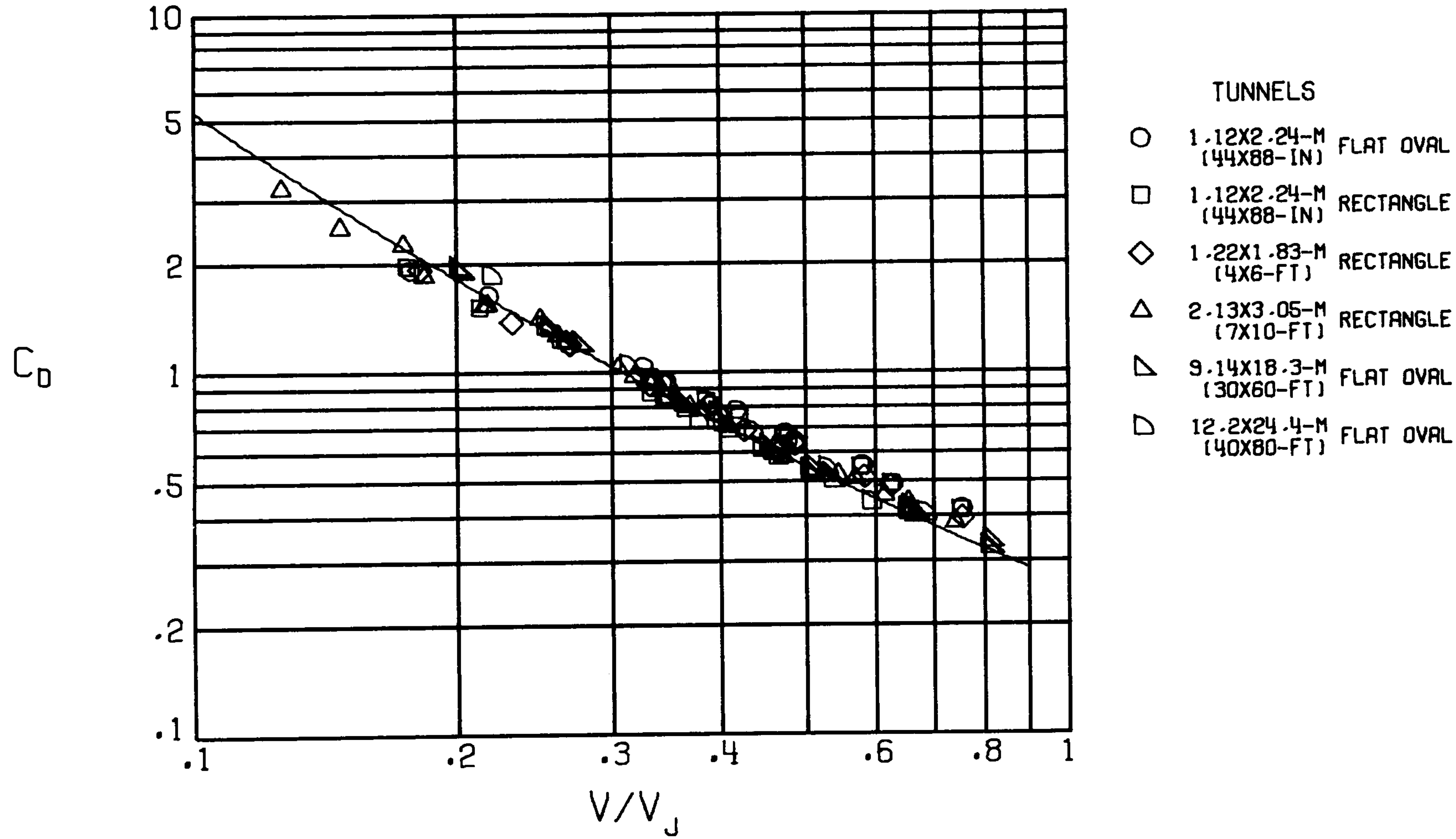

(d) $\alpha = 10^{\circ}$.

Figure 30.- Continued.

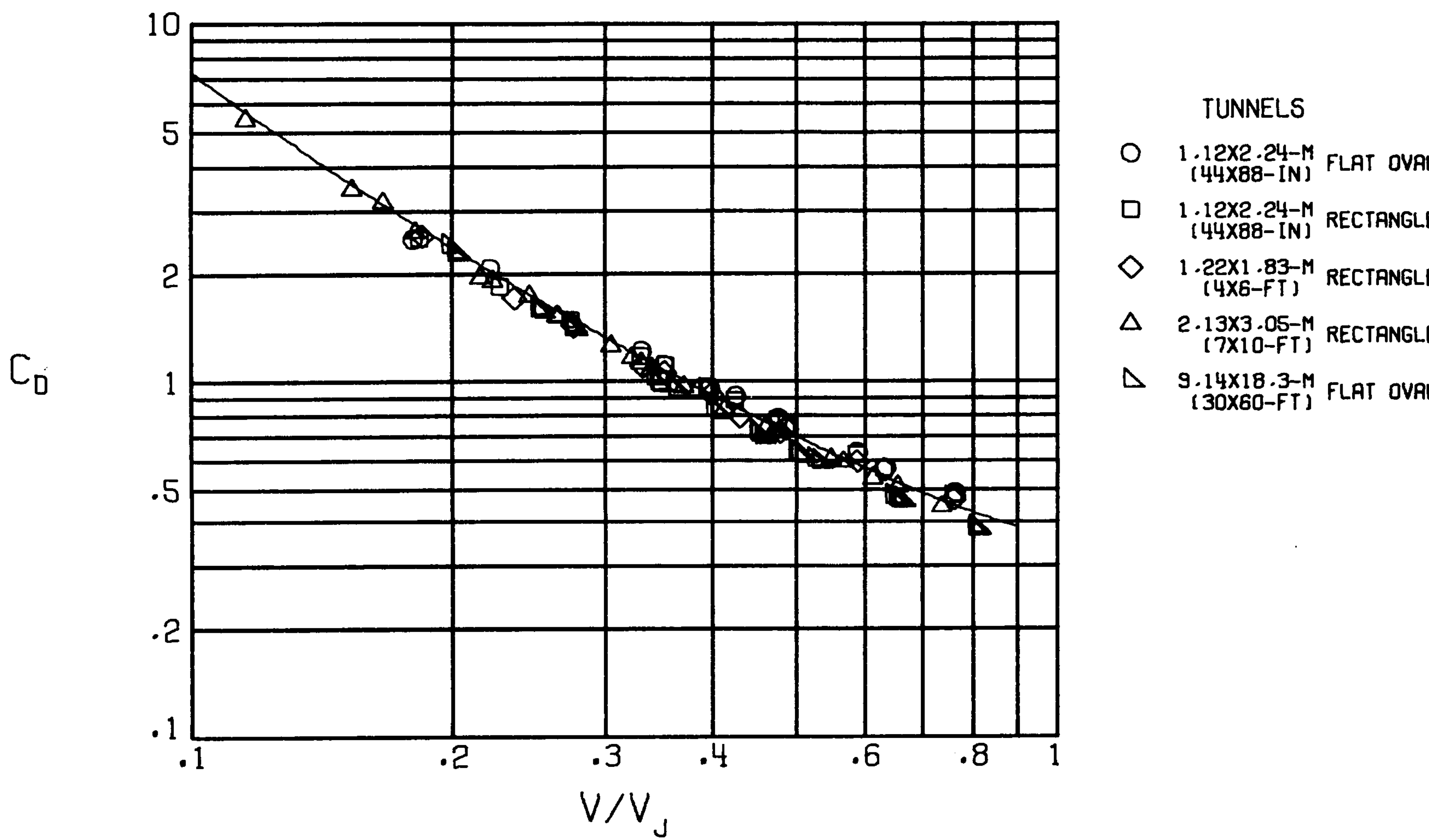

(e) $\alpha = 16^{\circ}$.

Figure 30.- Concluded.

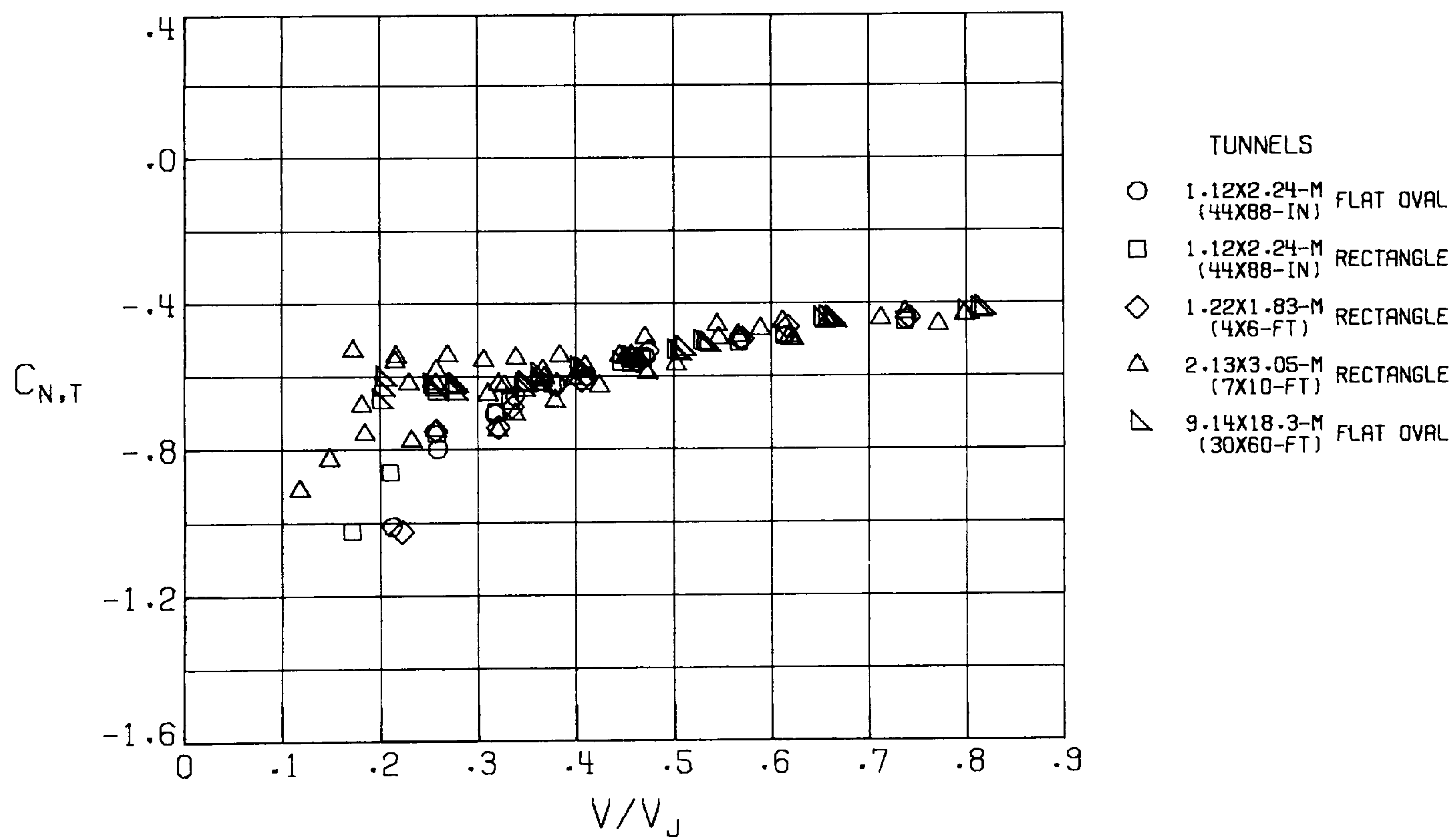

(a) $\alpha = -5^{o}$.

Figure 31.- Corrected values of tail normal-force coefficient as a function of V/V_j.

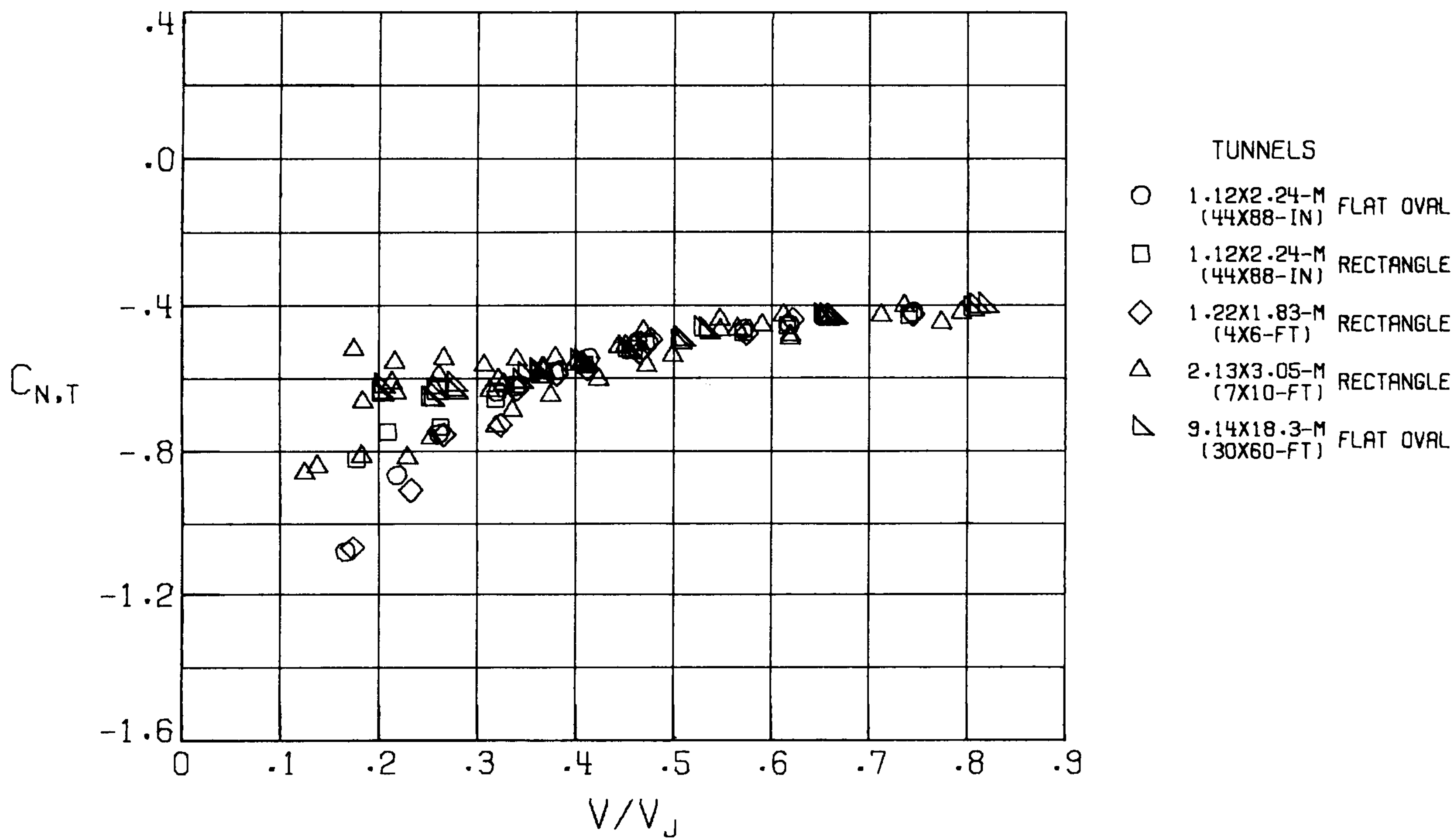

(b) $\alpha = 0^{o}$.

Figure 31.- Continued.

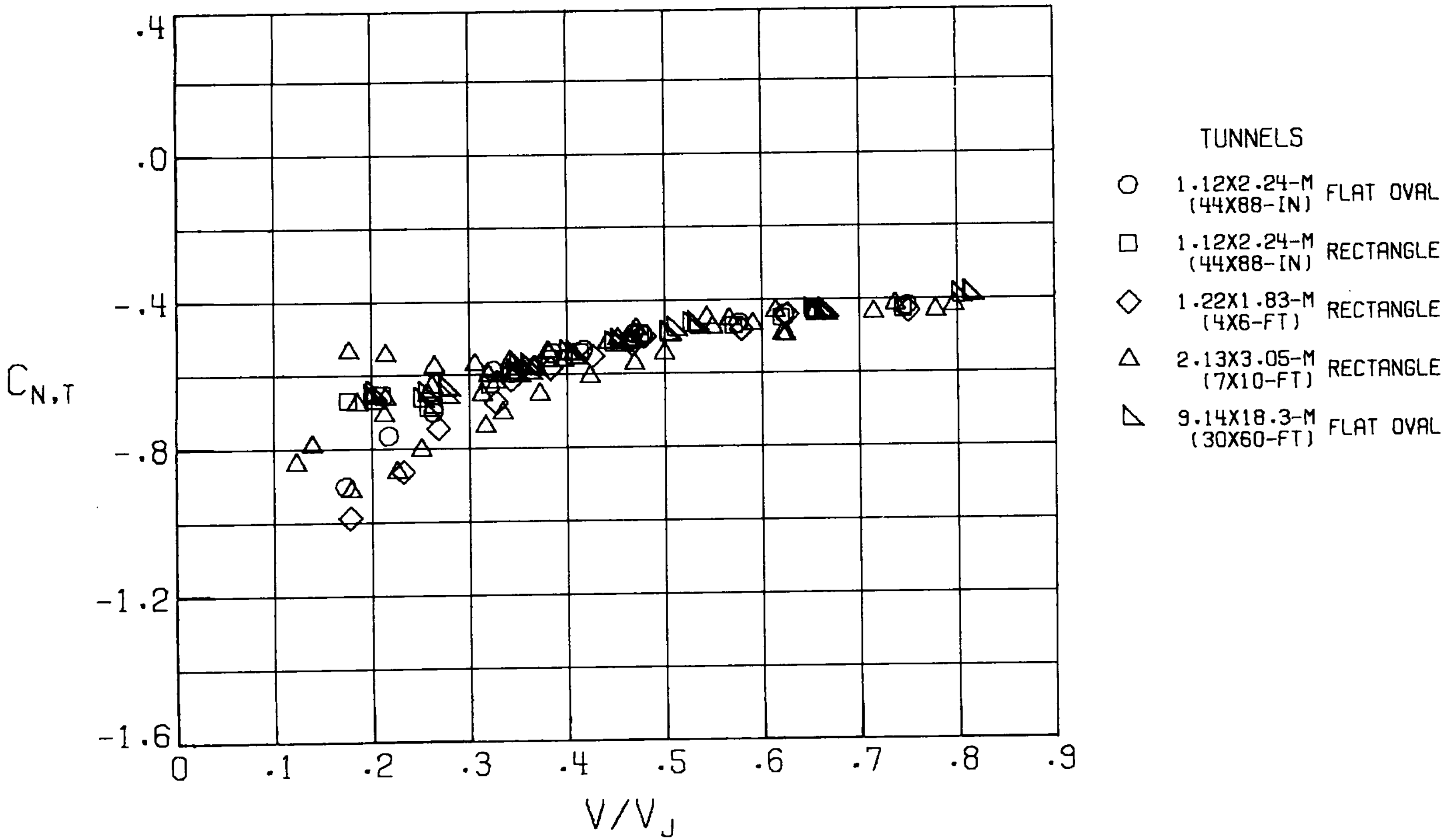

(c) $\alpha = 5^{\circ}$.

Figure 31.- Continued.

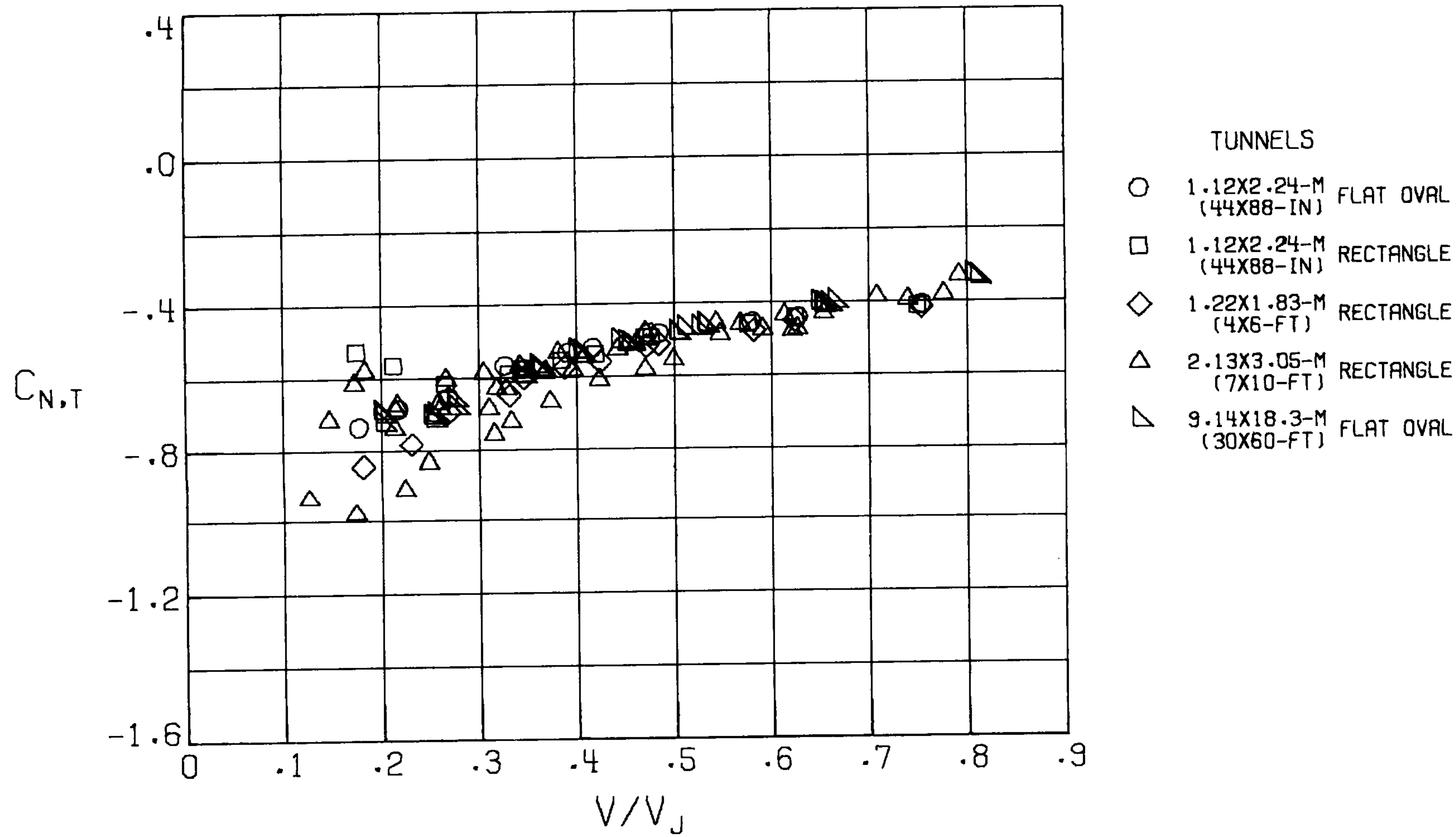

(d) $\alpha = 10^{o}$.

Figure 31.- Continued.

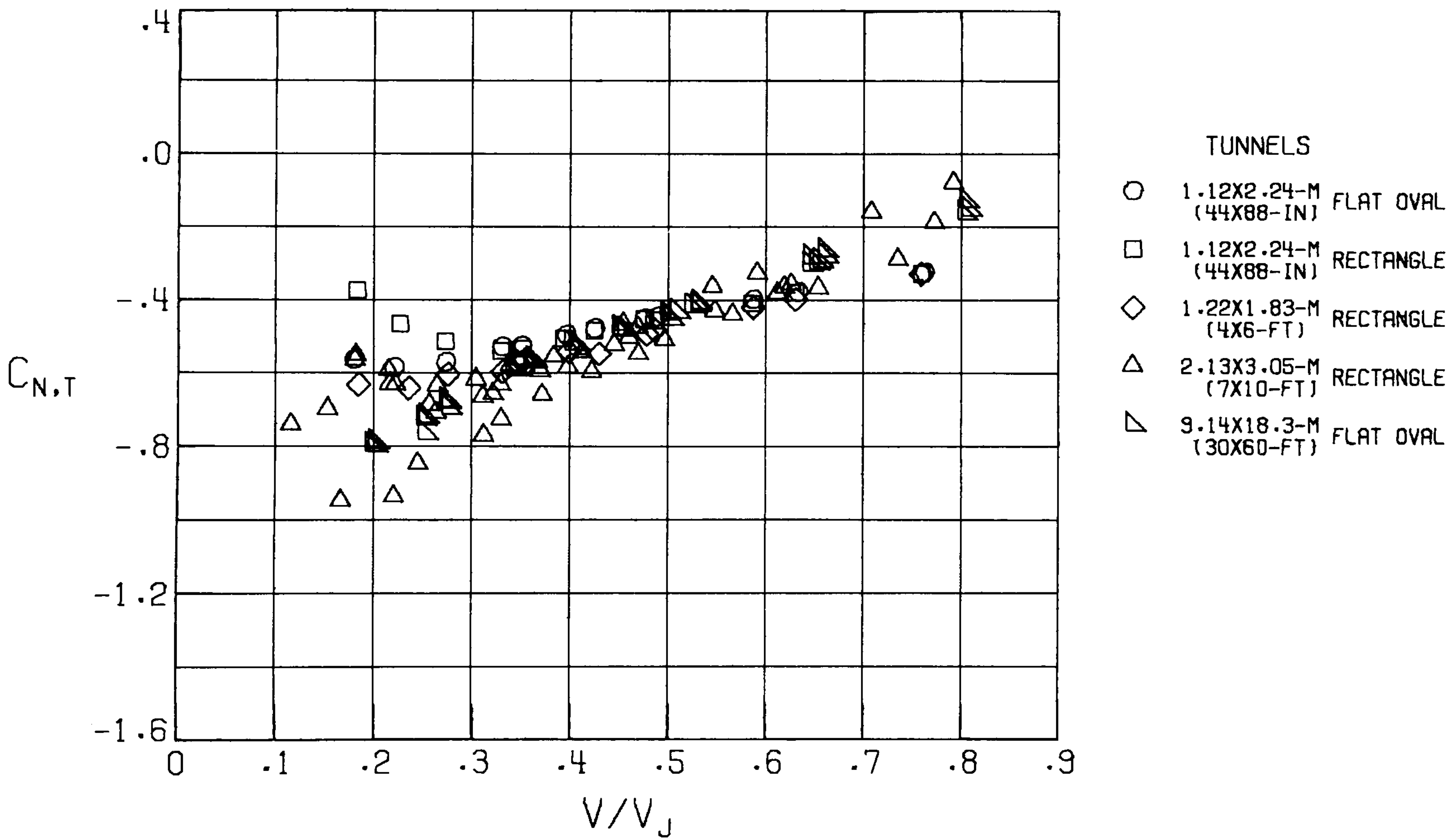

(e) $\alpha = 16^{\circ}$.

Figure 31.- Concluded.

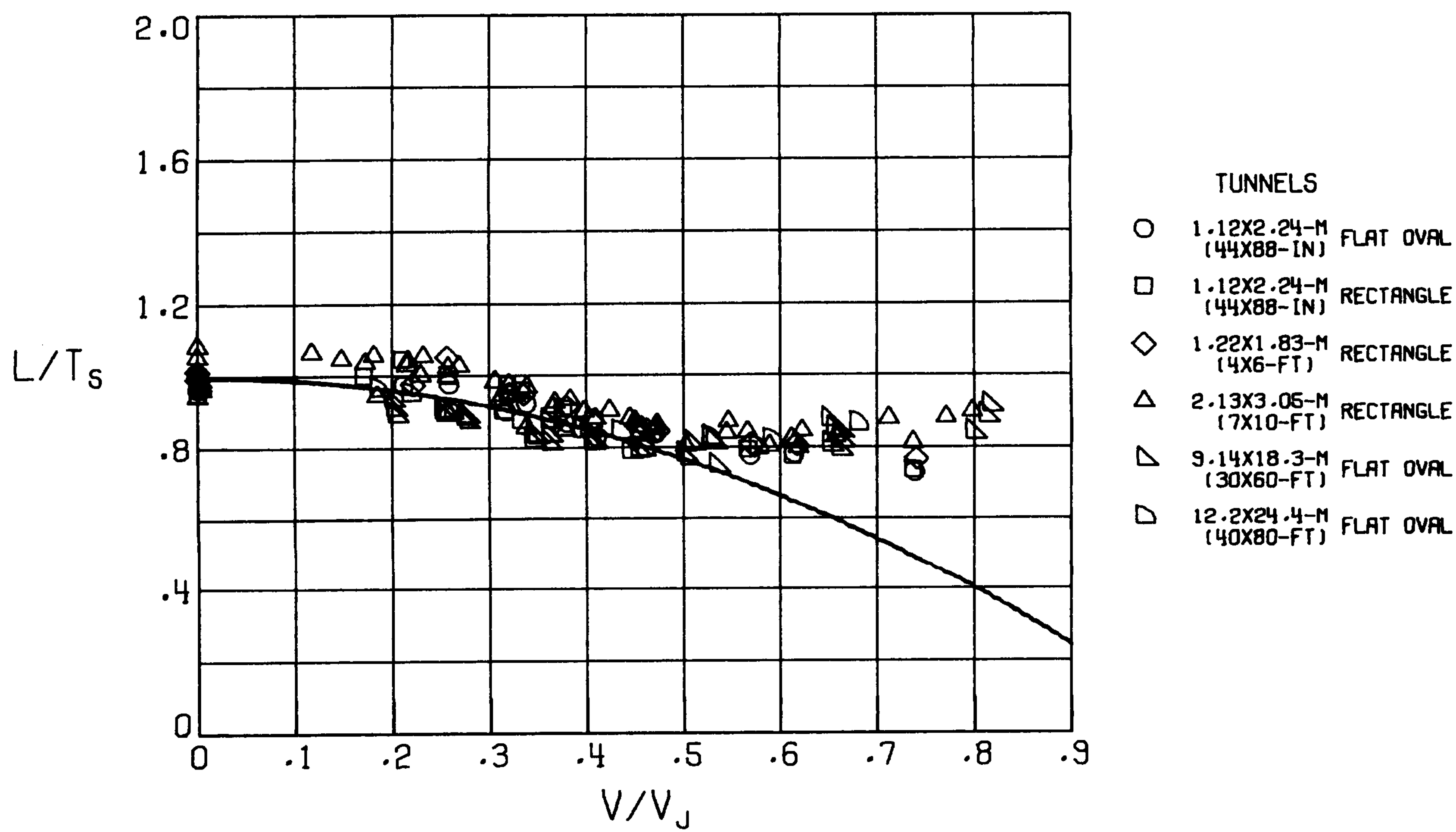

(a) $\alpha = -5^{o}$.

Figure 32.- Corrected values of ratios of lift to static thrust as a function of V/V_j. The curve is the sum of the vertical component of static thrust and the lift of the wing. It is assumed that there is no interference between the fans and the wing.

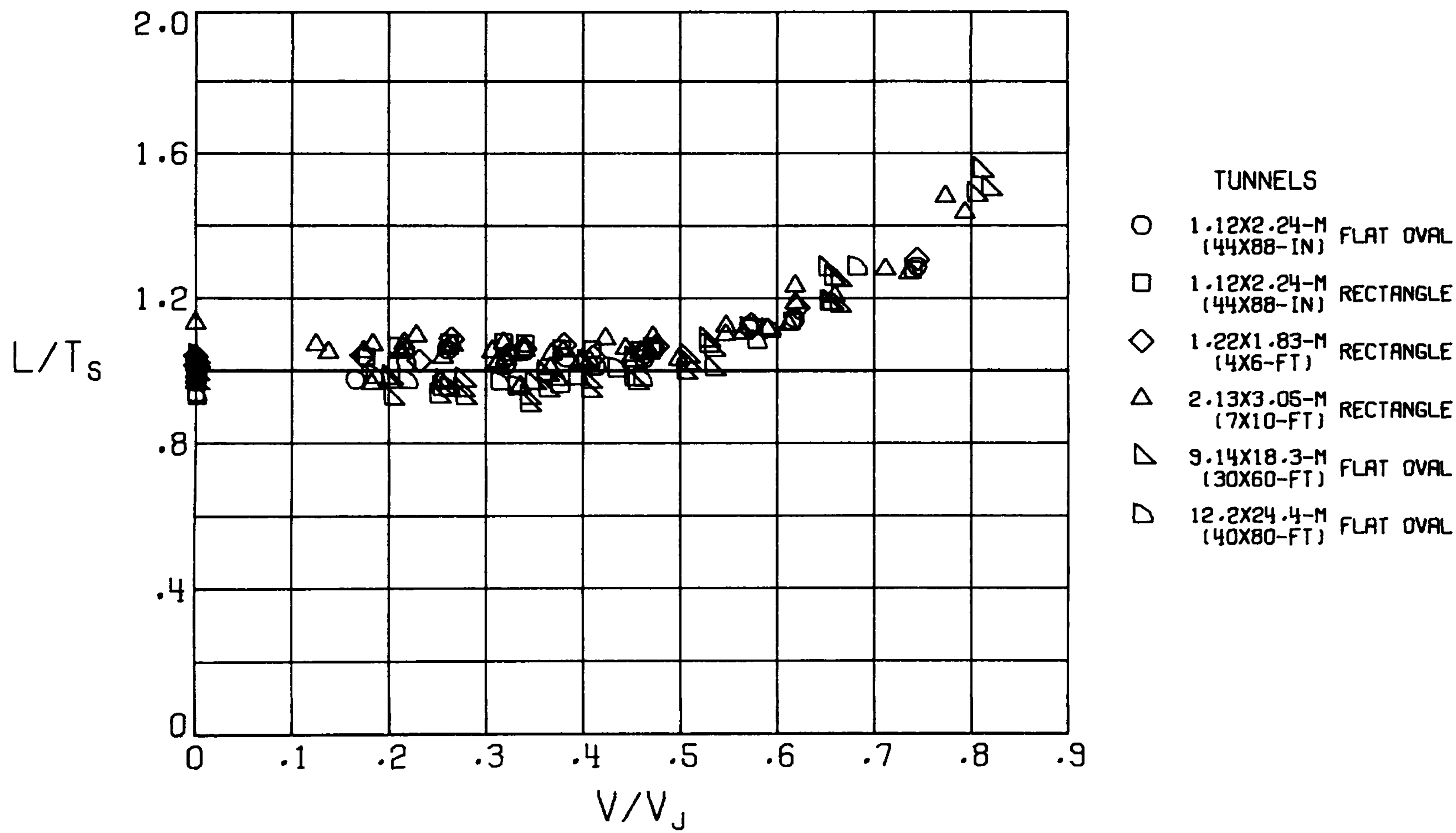

(b) $\alpha = 0^{o}$.

Figure 32.- Continued.

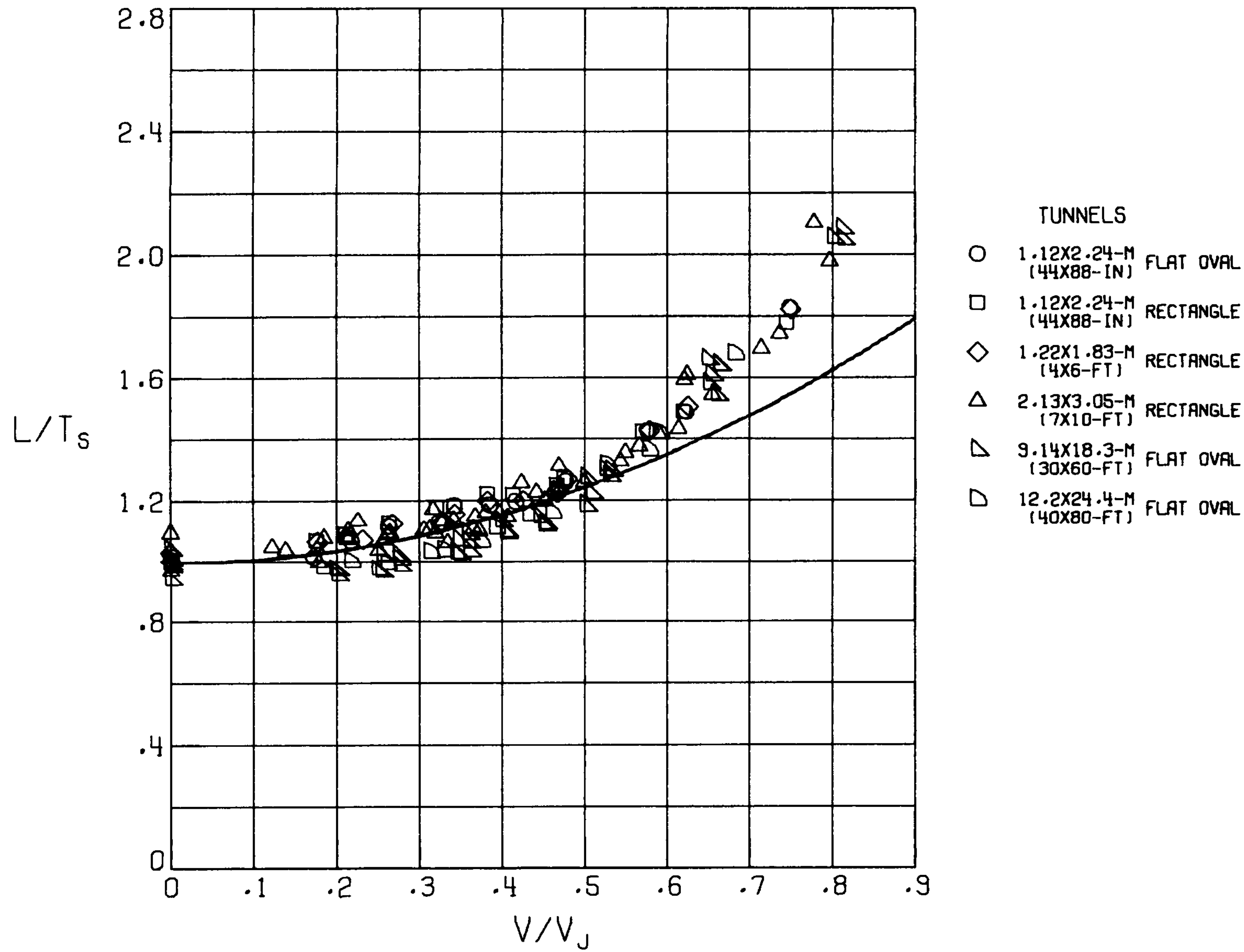

(c) $\alpha = 5^{o}$.

Figure 32.- Continued.

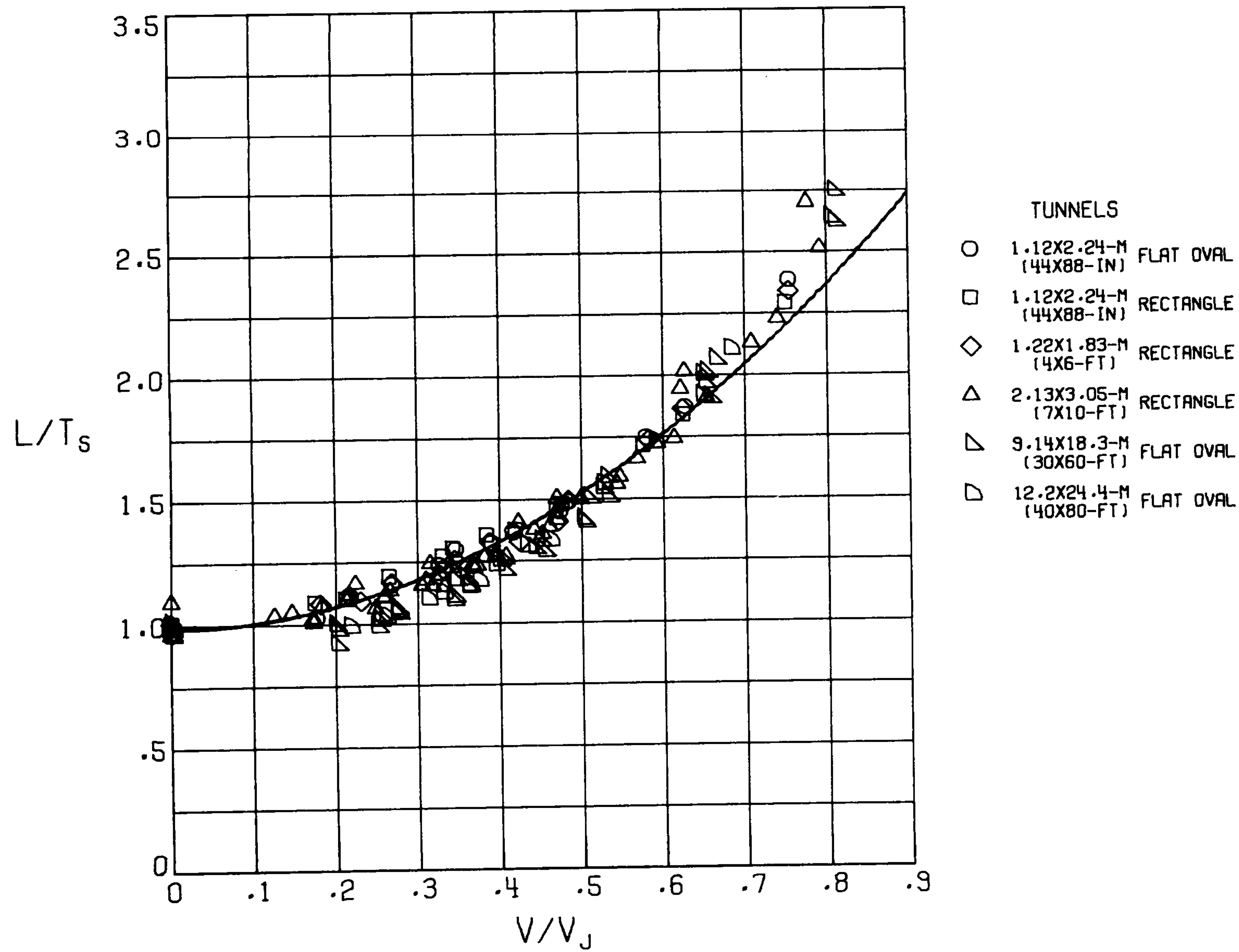

(d) $\alpha = 10^{o}$.

Figure 32.- Continued.

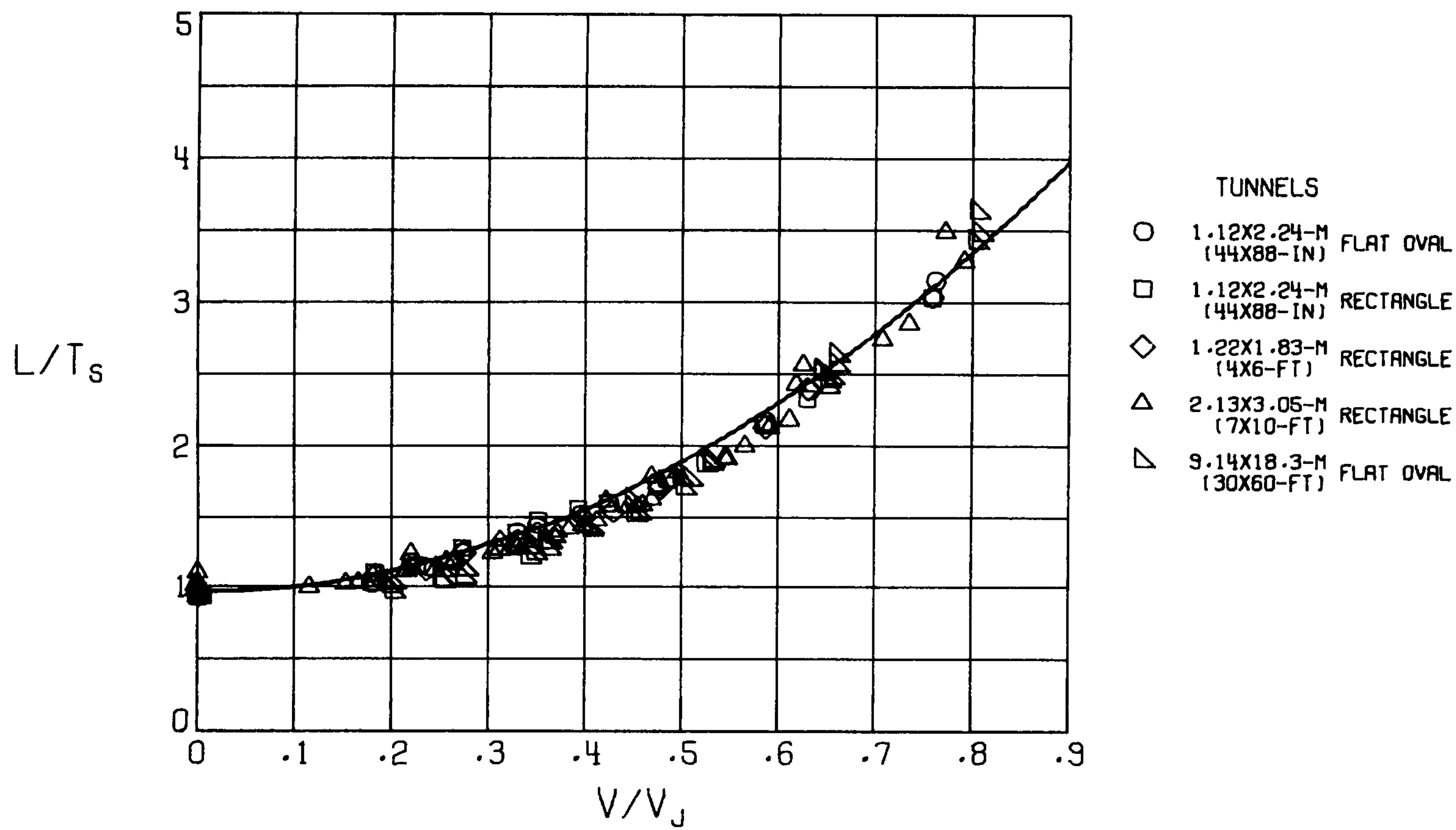

(e) $\alpha = 16^{\circ}$.

Figure 32.- Concluded.

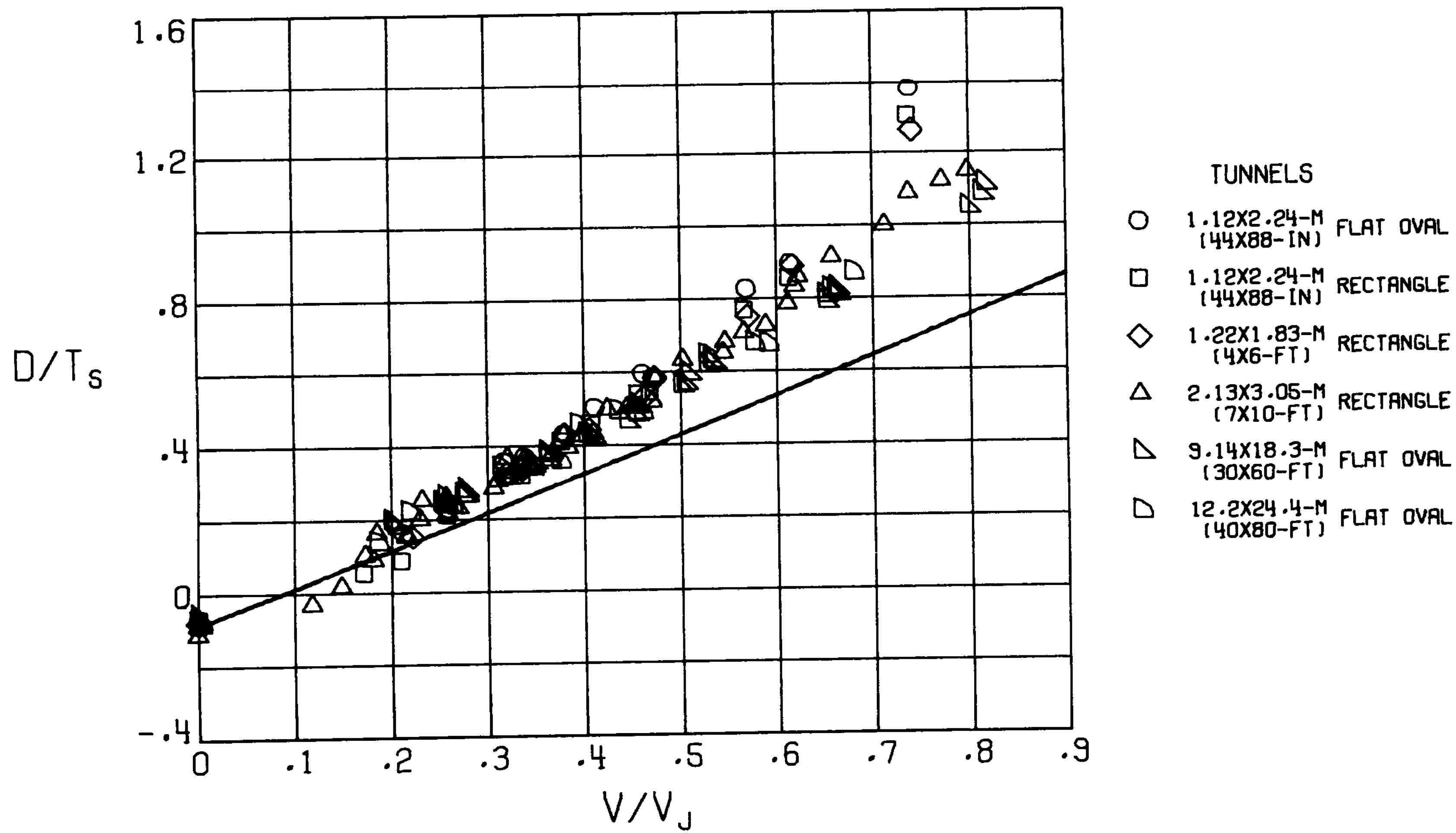

(a) $\alpha = -5^{\circ}$.

Figure 33.- Corrected values of ratios of drag to static thrust as a function of V/V_j. The curve is calculated from the momentum-theory values of the fan forces and the lift and drag of the wing. It is assumed that there is no interference between the fans and the wing.

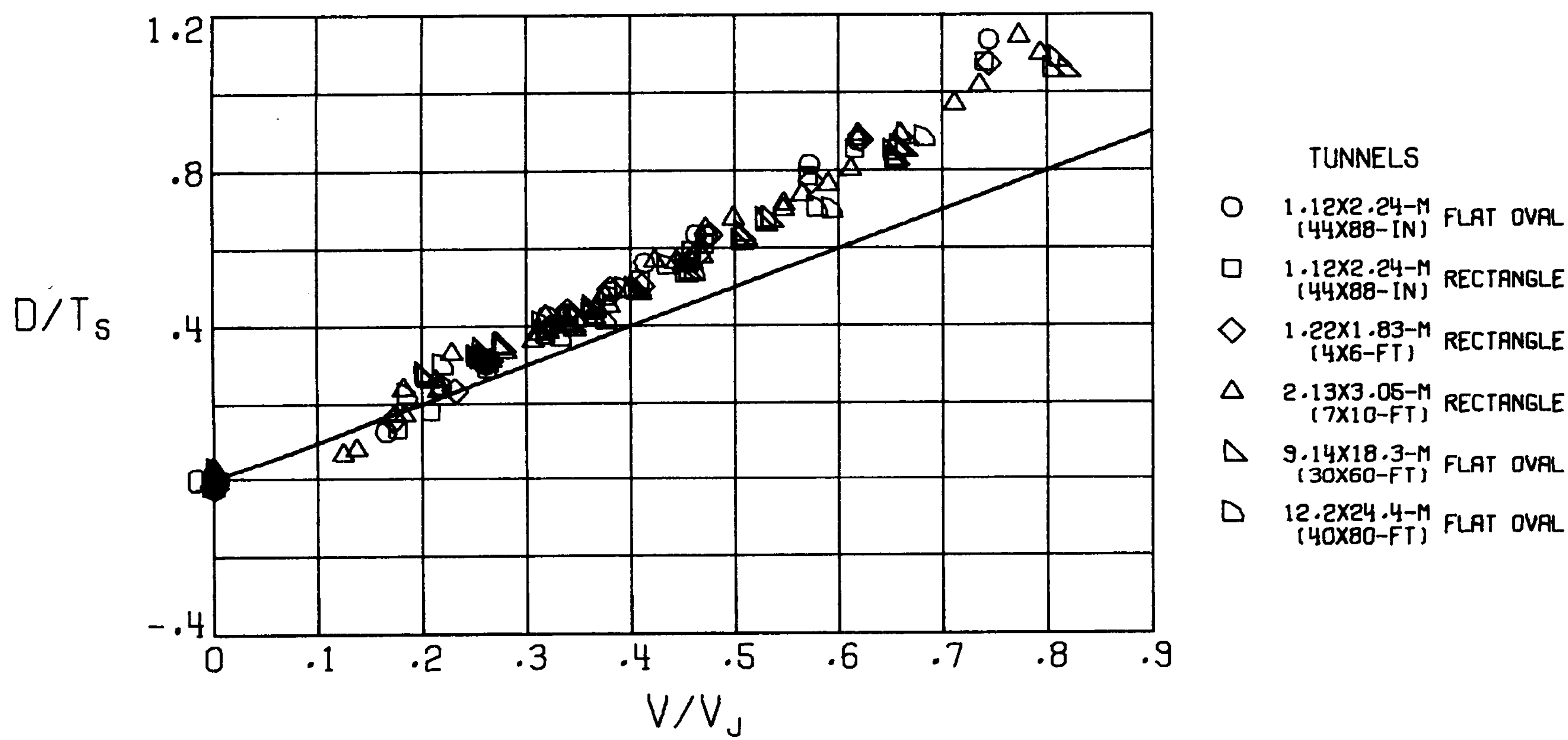

(b) $\alpha = 0^{o}$.

Figure 33.- Continued.

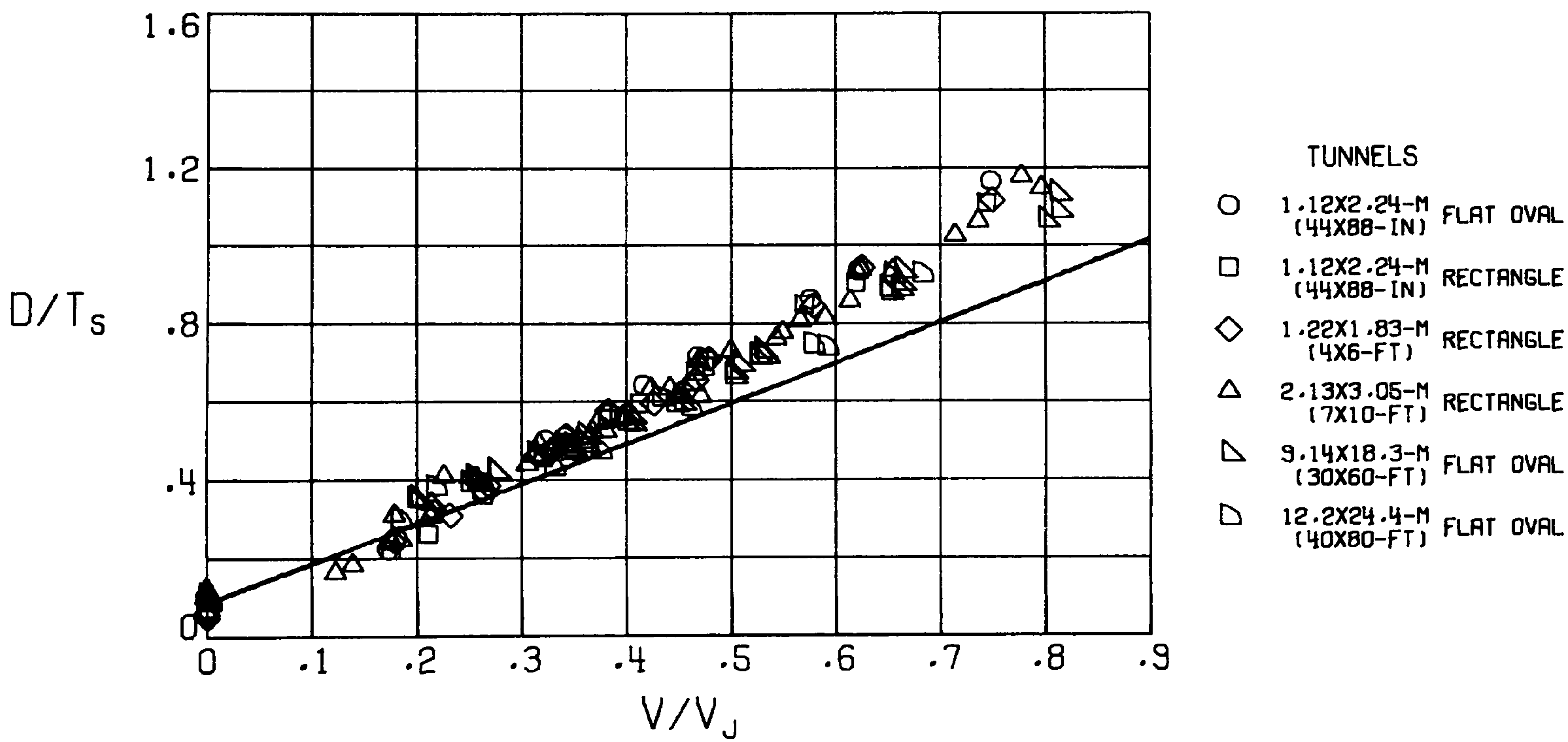

(c) $\alpha = 5^{o}$.

Figure 33.- Continued.

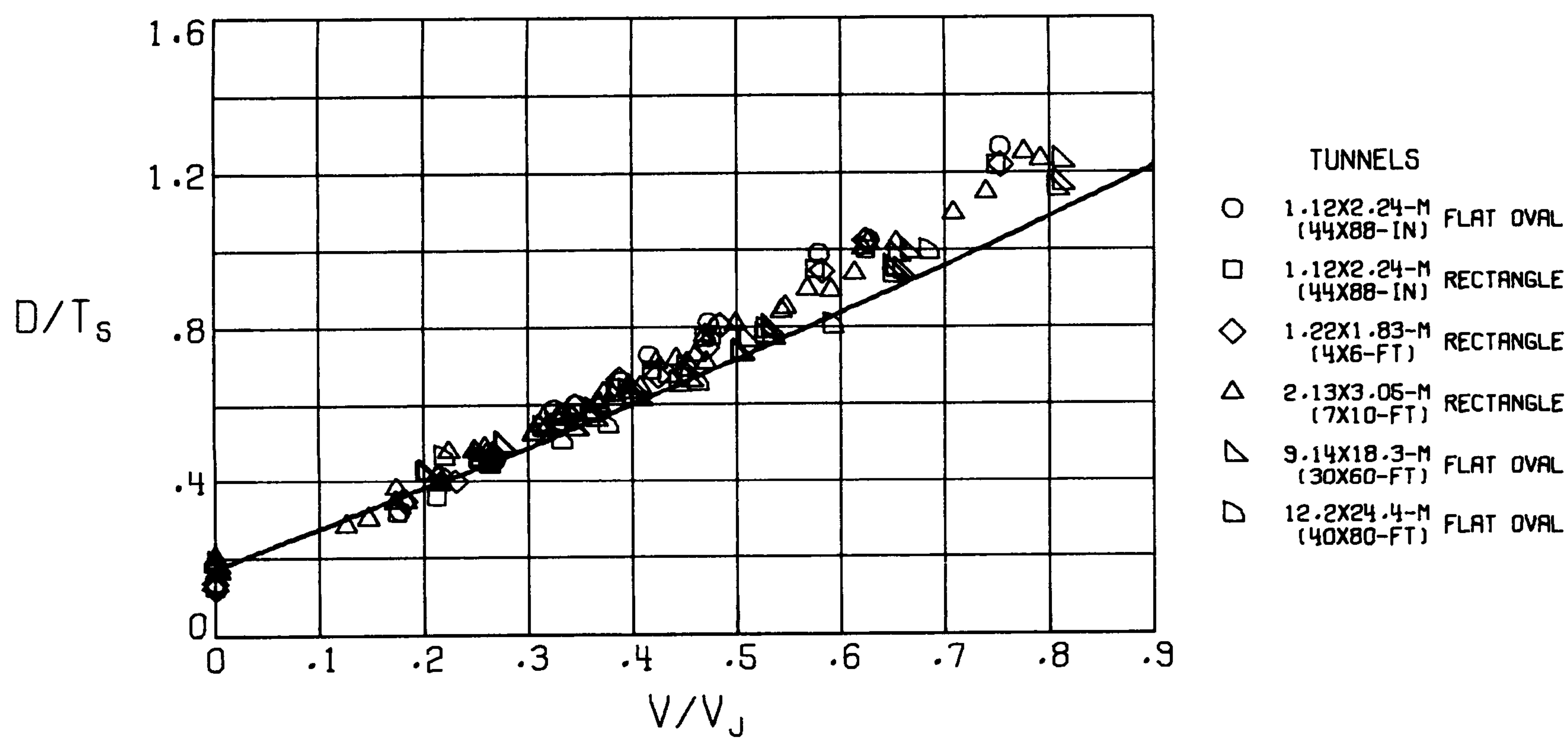

(d) $\alpha = 10^{\circ}$.

Figure 33.- Continued.

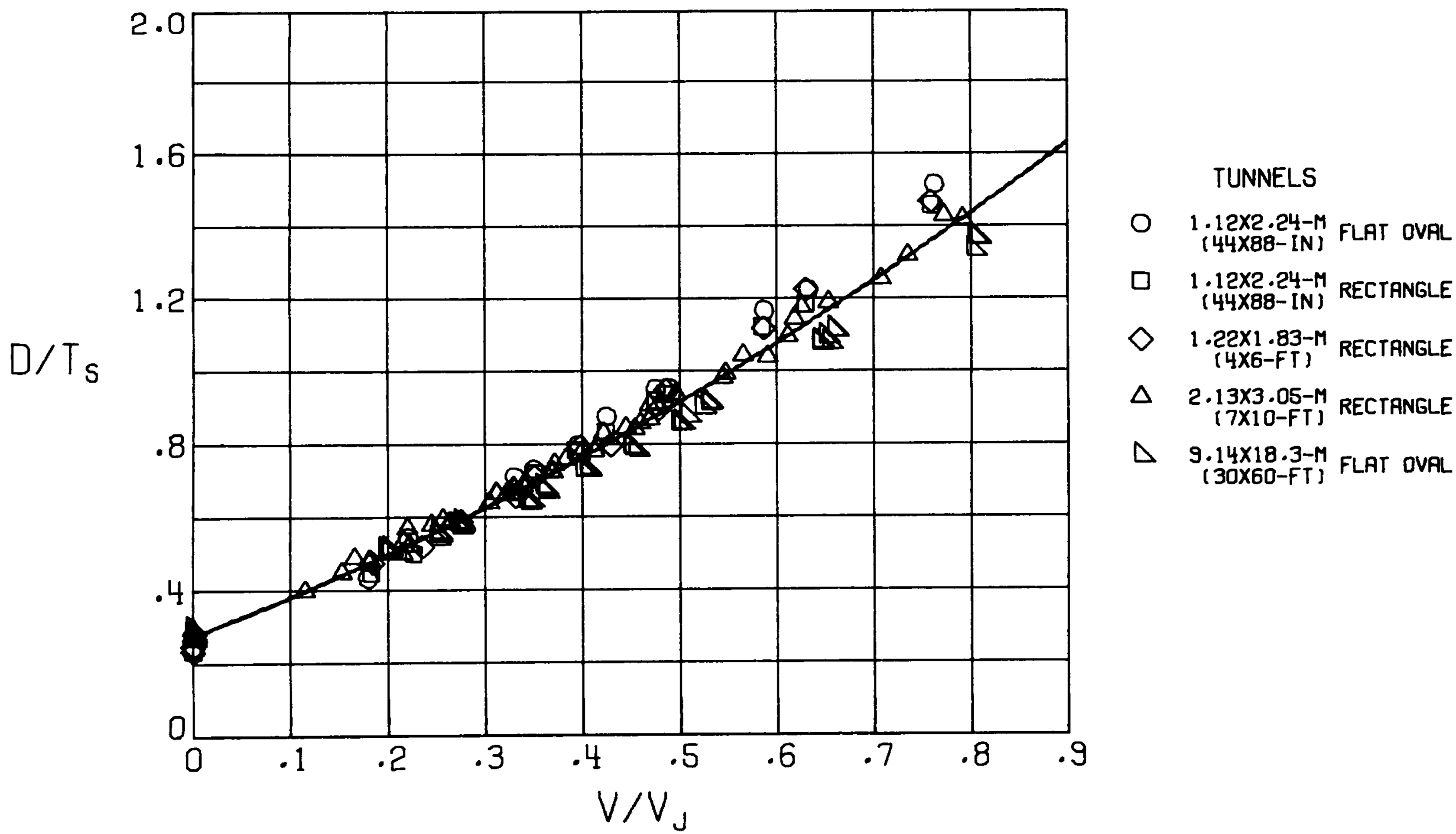

(e) $\alpha = 16^{o}$.

Figure 33.- Concluded.

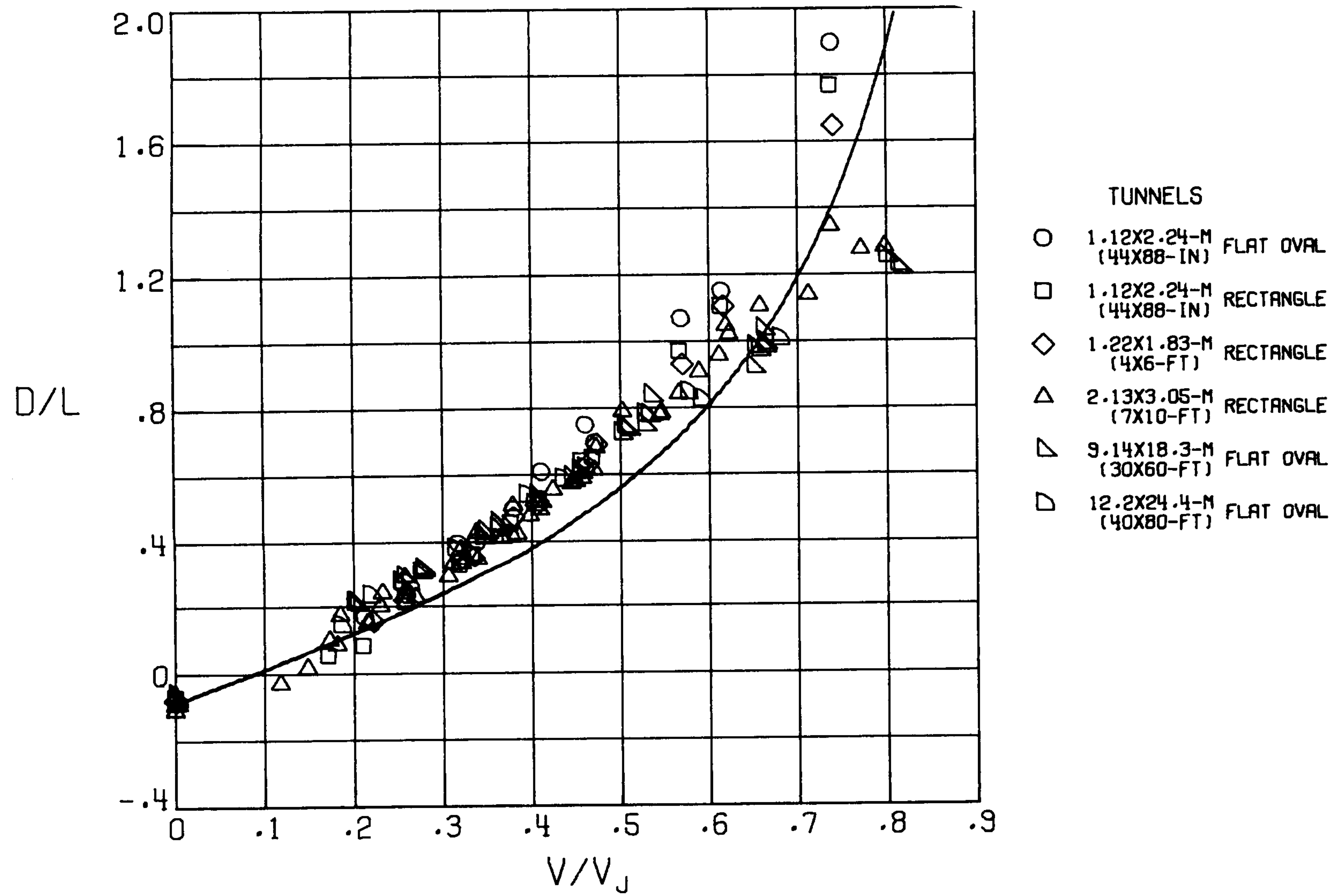

(a) $\alpha = -5^{\circ}$.

Figure 34.- Corrected values of external drag-lift ratios as a function of V/V_j. The curve is calculated from the momentum-theory values of the fan forces and the lift and drag of the wing. It is assumed that there is no interference between the fans and the wing.

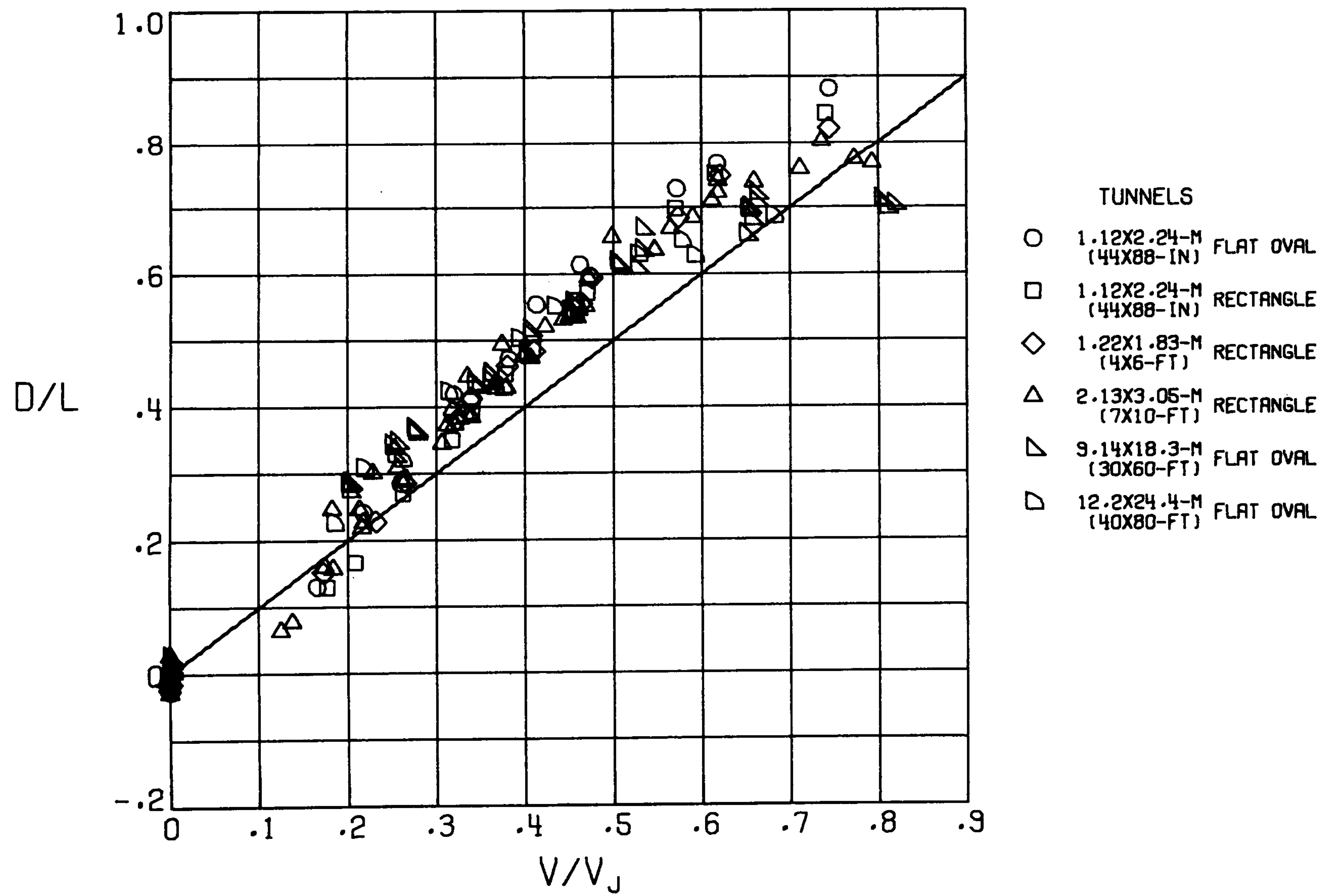

(b) $\alpha = 0^{o}$.

Figure 34.- Continued.

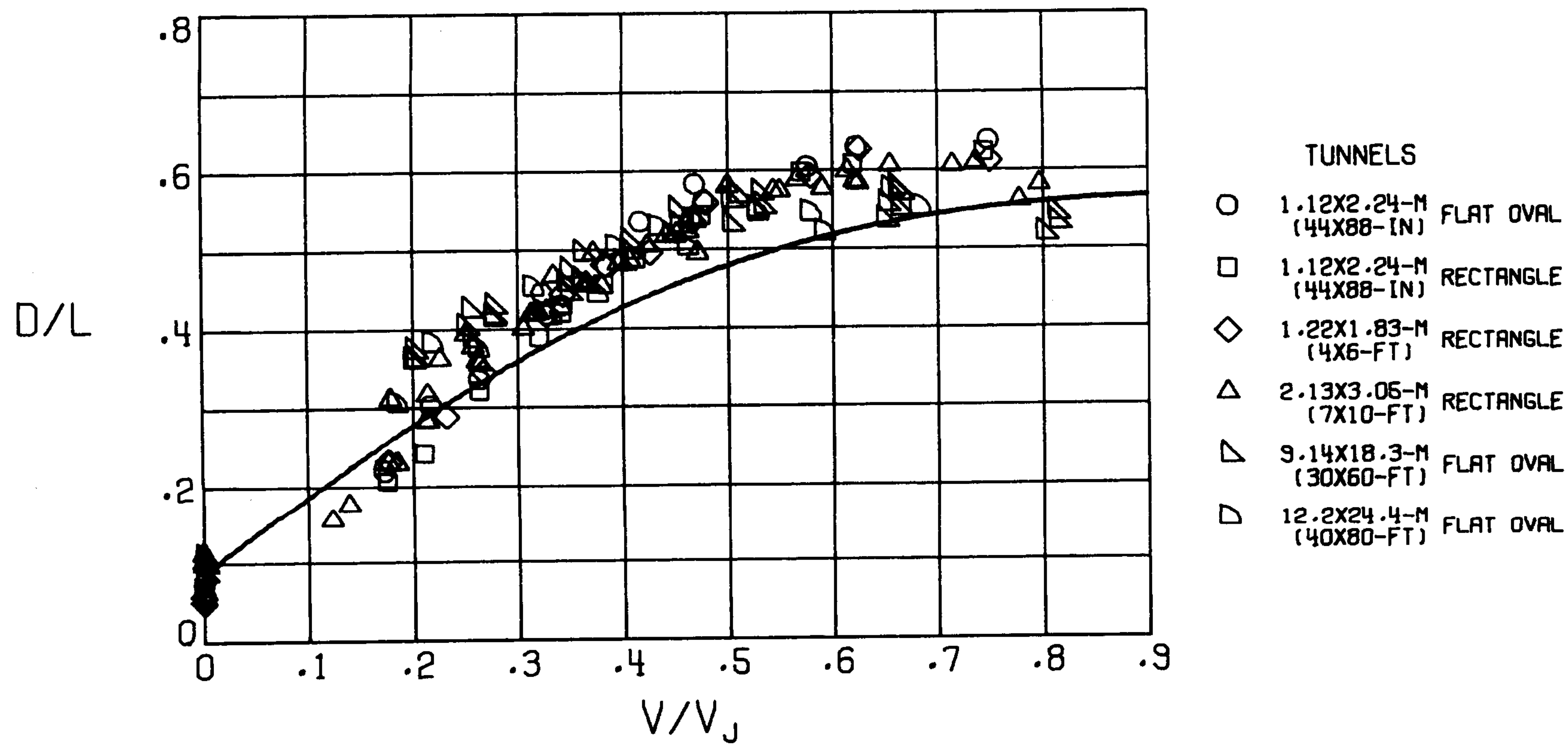

(c) $\alpha = 5^{o}$.

Figure 34.- Continued.

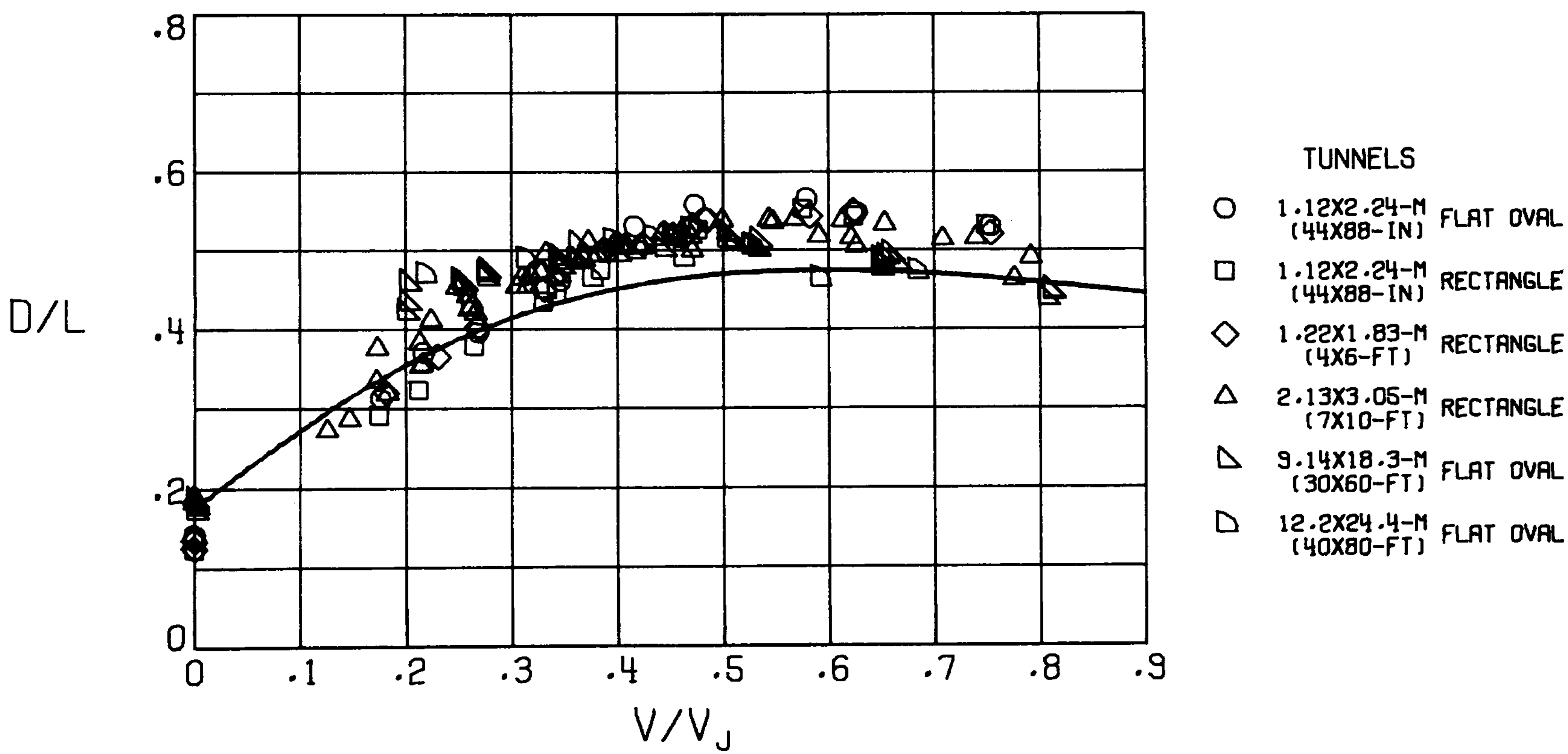

(d) $\alpha = 10^{o}$.

Figure 34.- Continued.

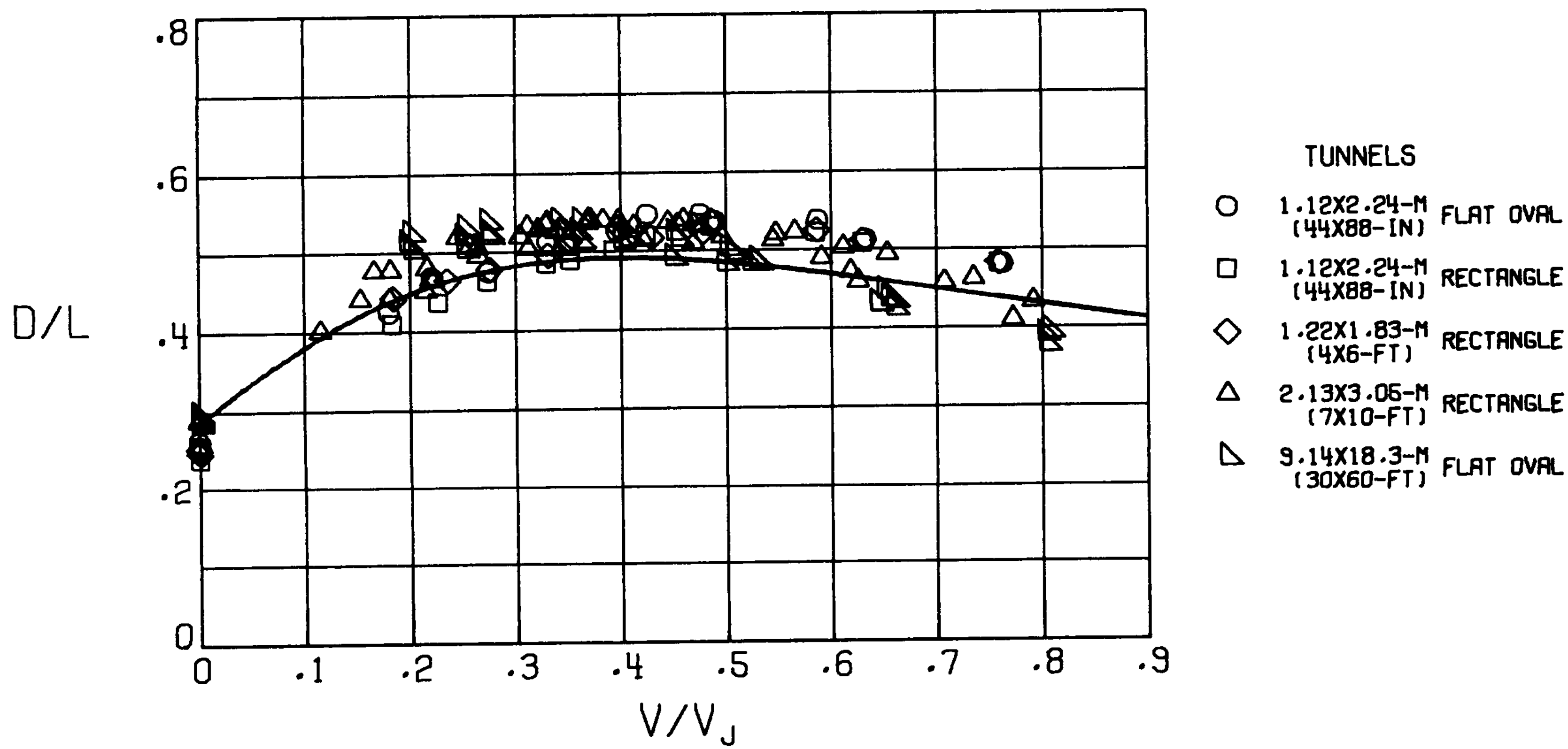

(e) $\alpha = 16^{o}$.

Figure 34.- Concluded.

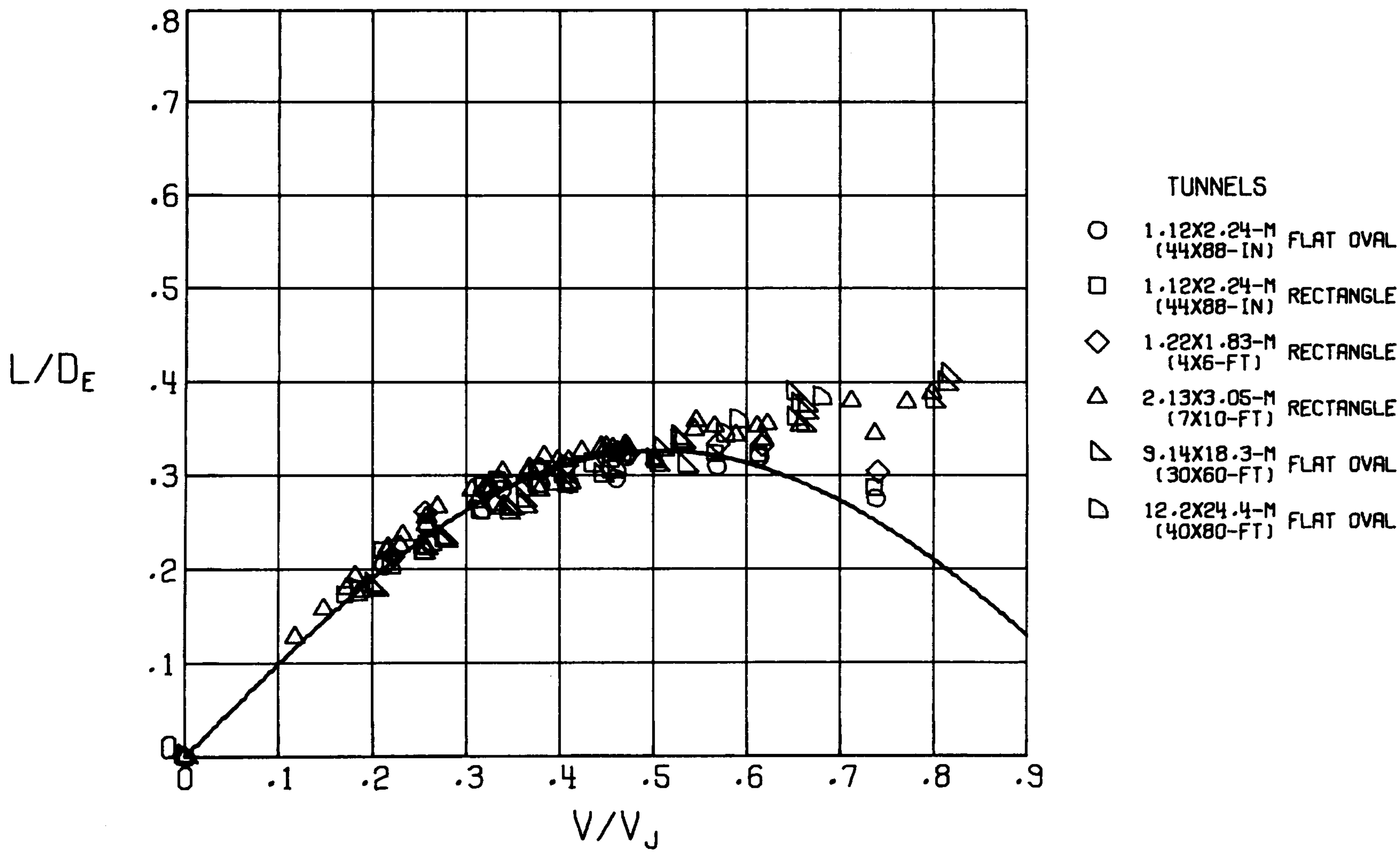

(a) $\alpha = -5^{o}$.

Figure 35.- Corrected values of equivalent lift-drag ratios as a function of V/V_j. The curve is calculated from the momentum-theory values of the fan lift, drag, and shaft power together with the lift and drag of the wing. It is assumed that there is no interference between the fans and the wing.

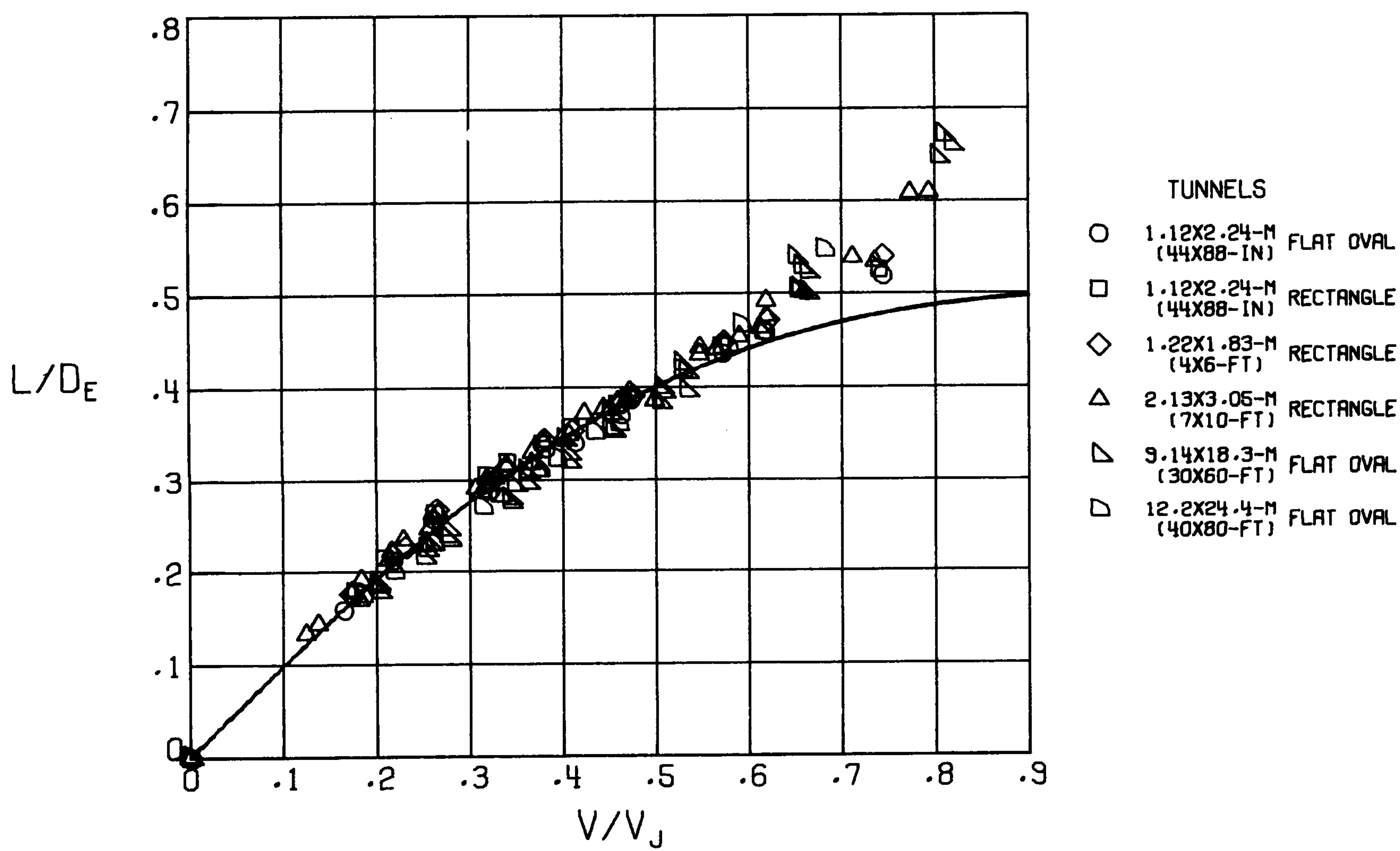

(b) $\alpha = 0^{o}$.

Figure 35.- Continued.

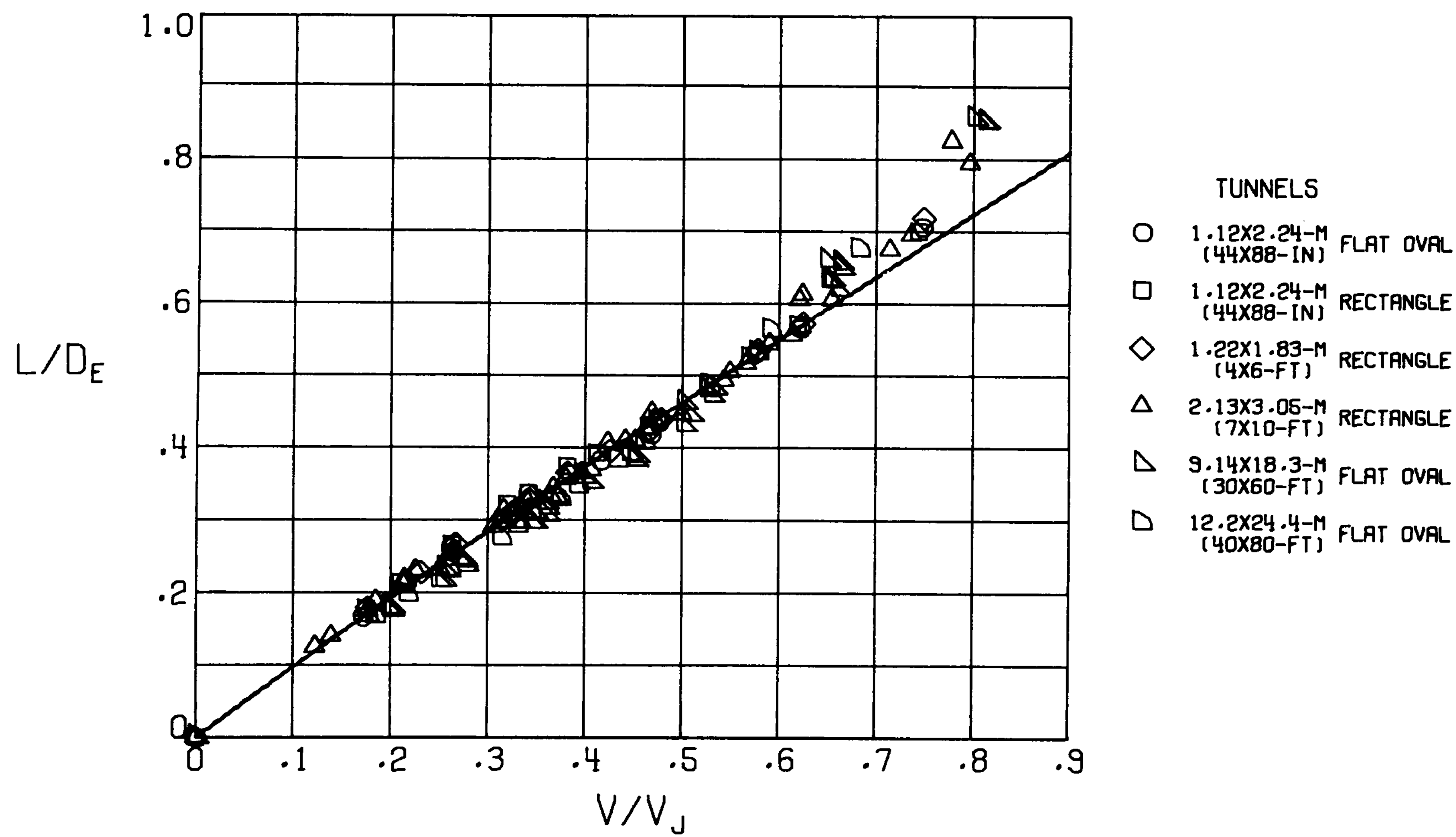

(c) $\alpha = 5^{o}$.

Figure 35.- Continued.

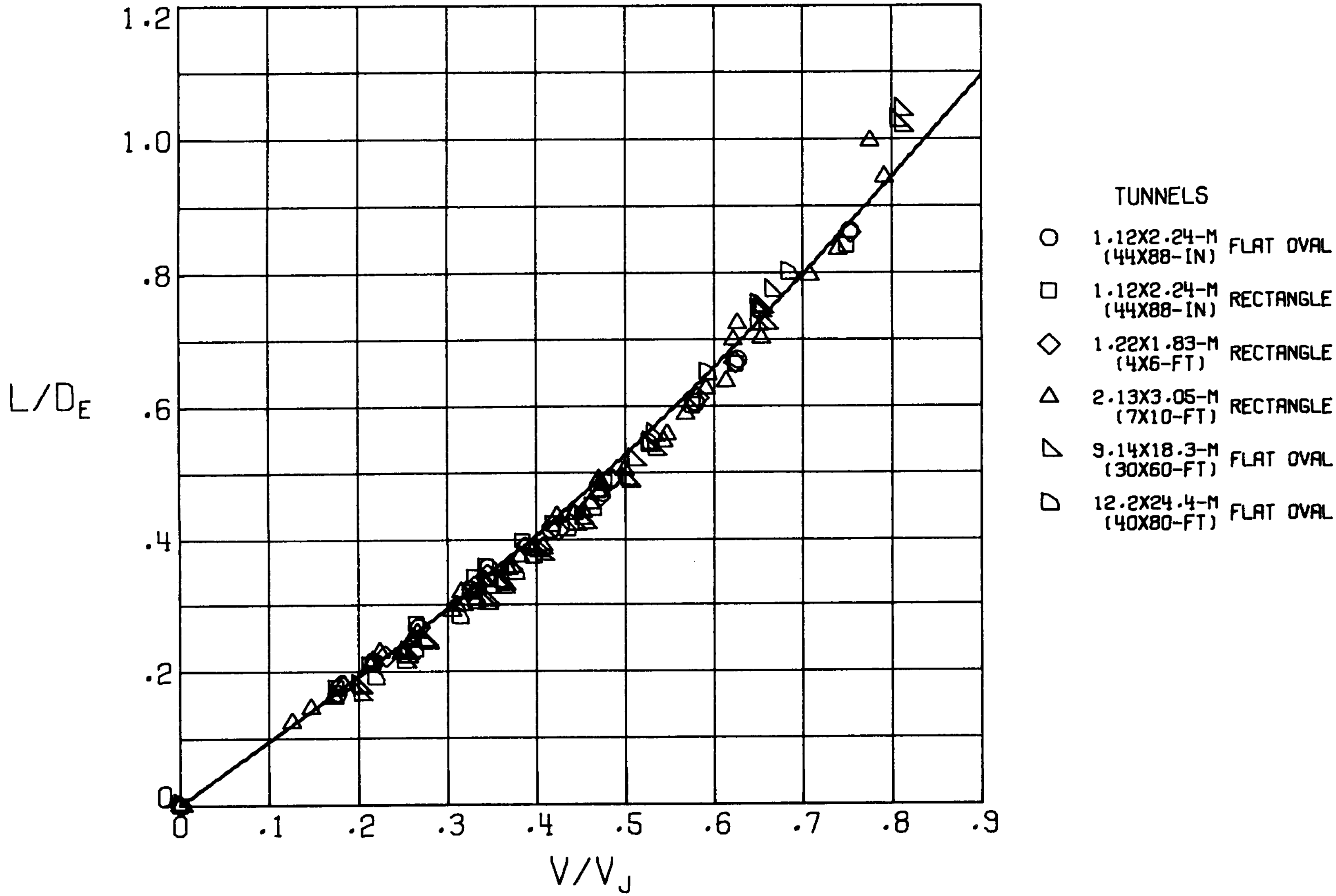

(d) $\alpha = 10^{o}$.

Figure 35.- Continued.

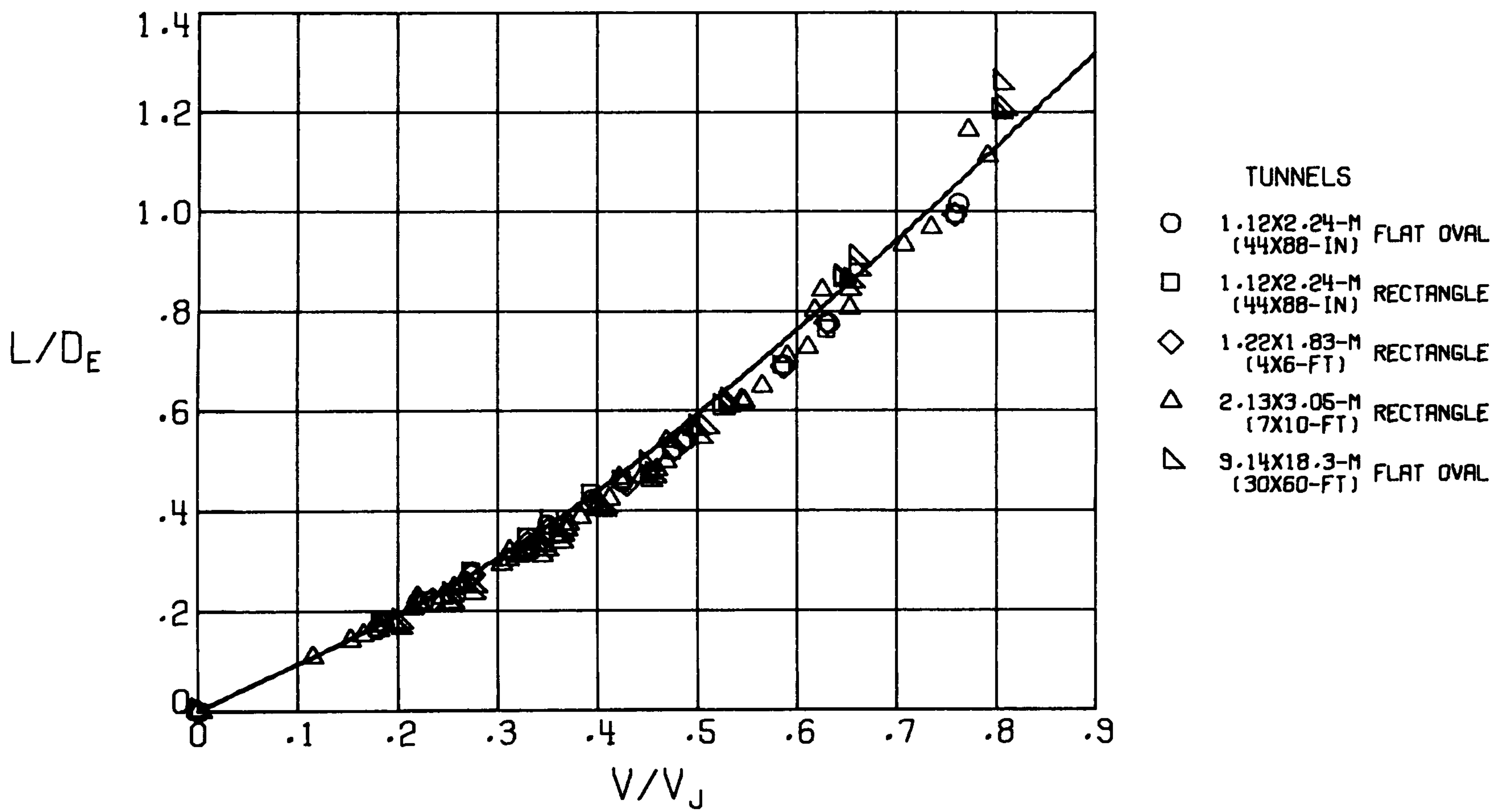

(e) $\alpha = 16^{o}$.

Figure 35.- Concluded.

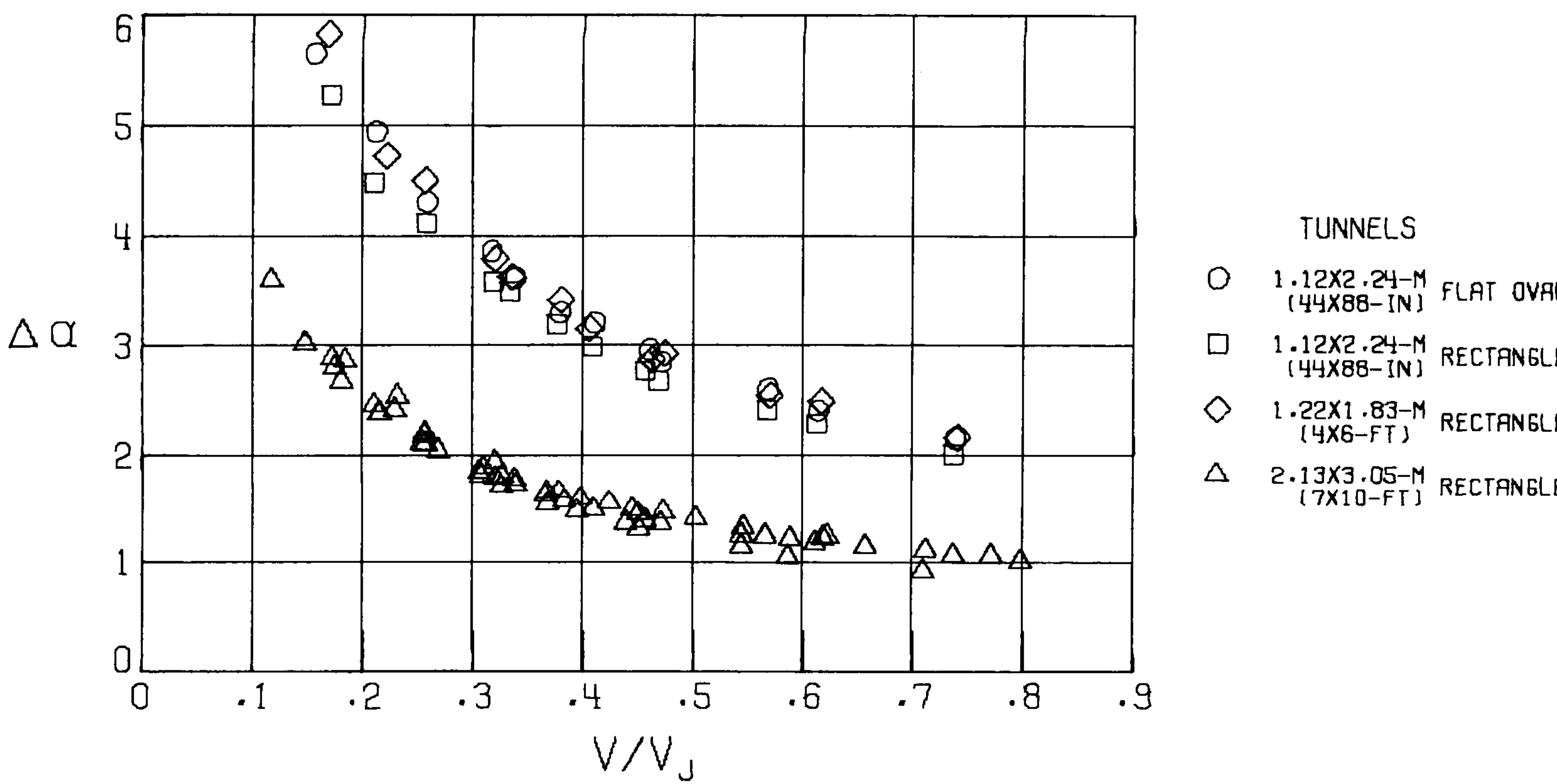

(a) $\alpha = -5^{o}$.

Figure 36.- Wall-induced angle of attack $\Delta\alpha$ in the corrected data from the fan-in-wing model as a function of V/V_j in several different wind tunnels.

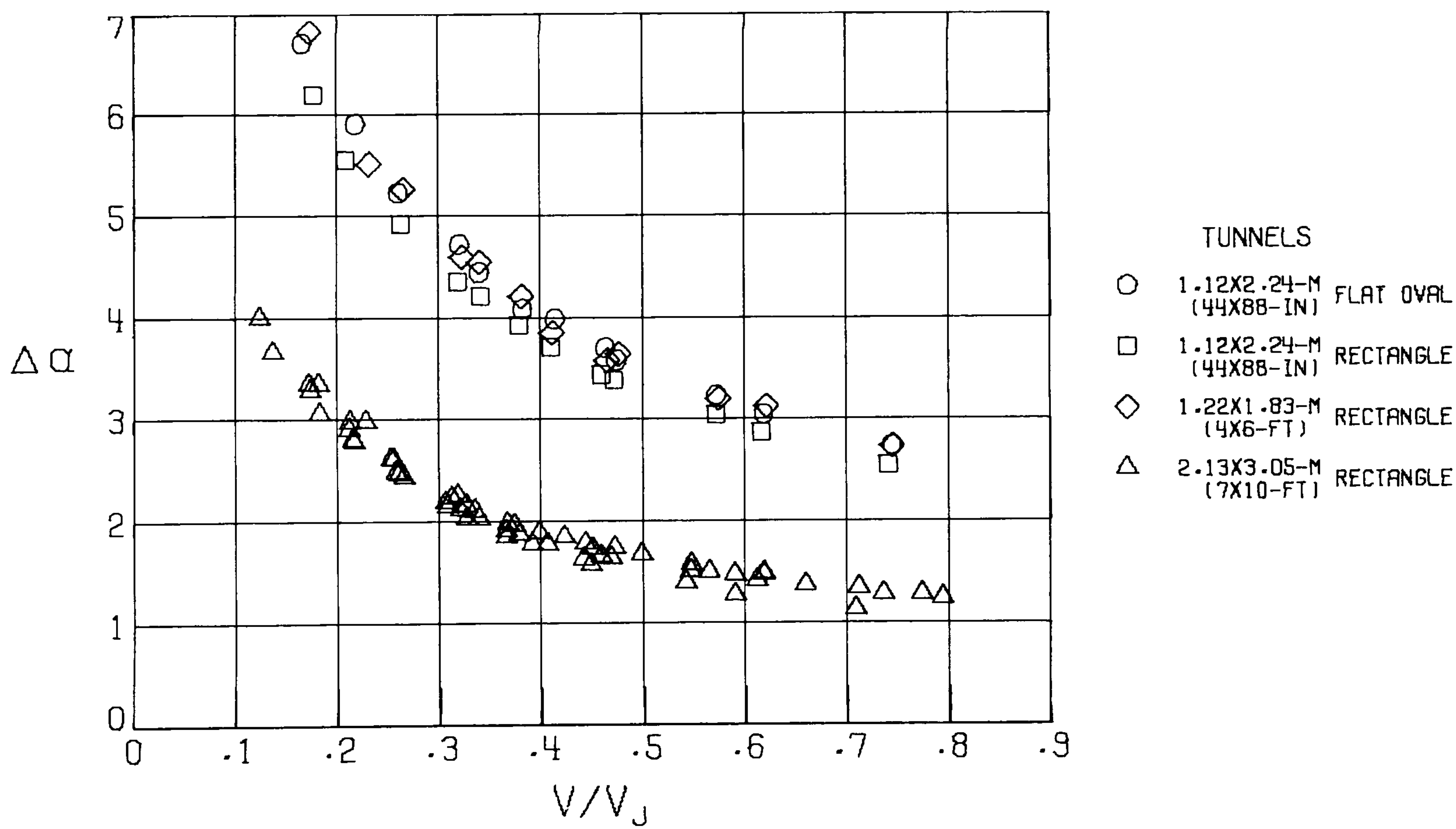

(b) $\alpha = 0^{o}$.

Figure 36.- Continued.

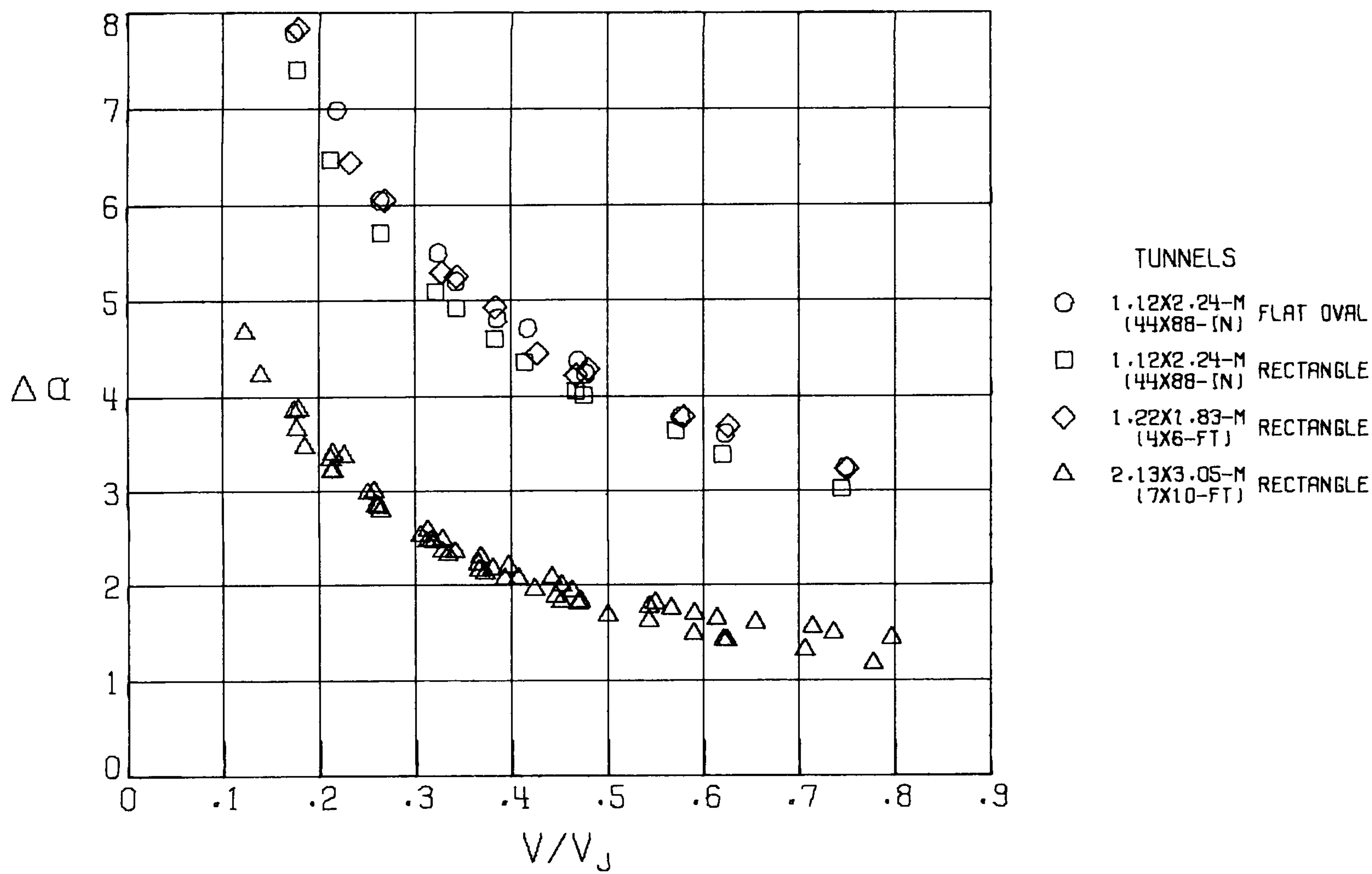

(c) $\alpha = 5^{\circ}$.

Figure 36.- Continued.

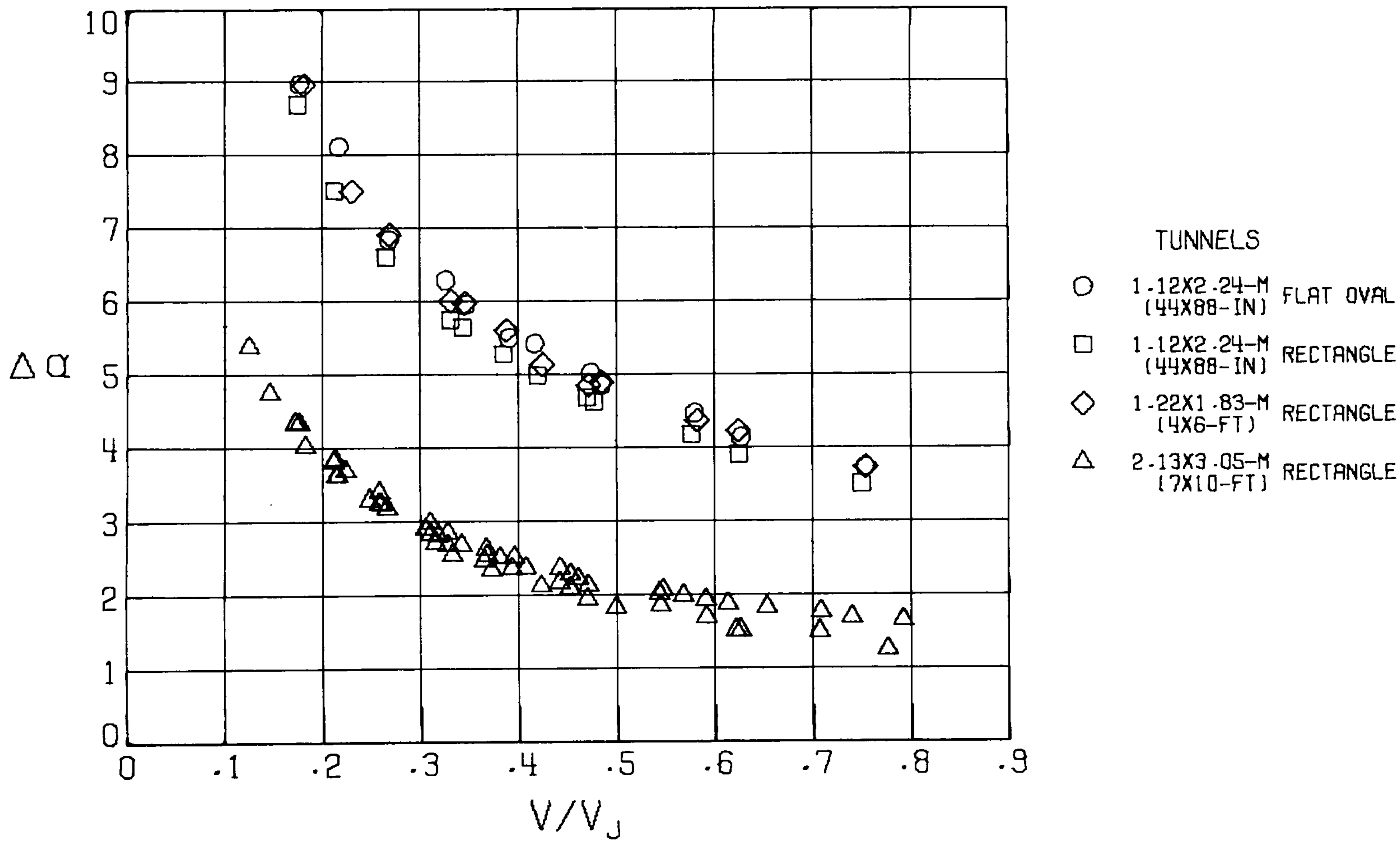

(d) $\alpha = 10^{o}$.

Figure 36.- Continued.

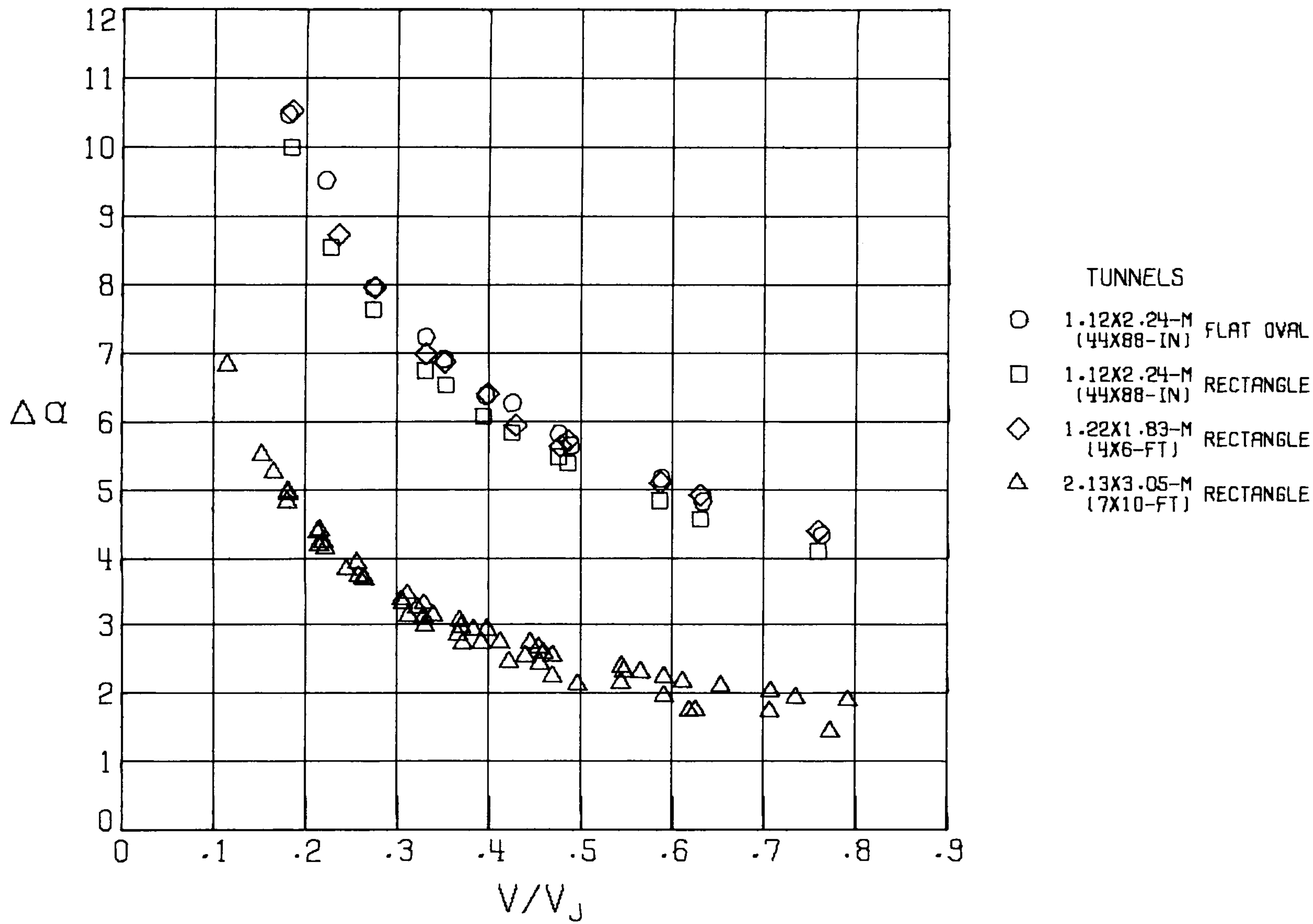

(e) $\alpha = 16^{o}$.

Figure 36.- Concluded.

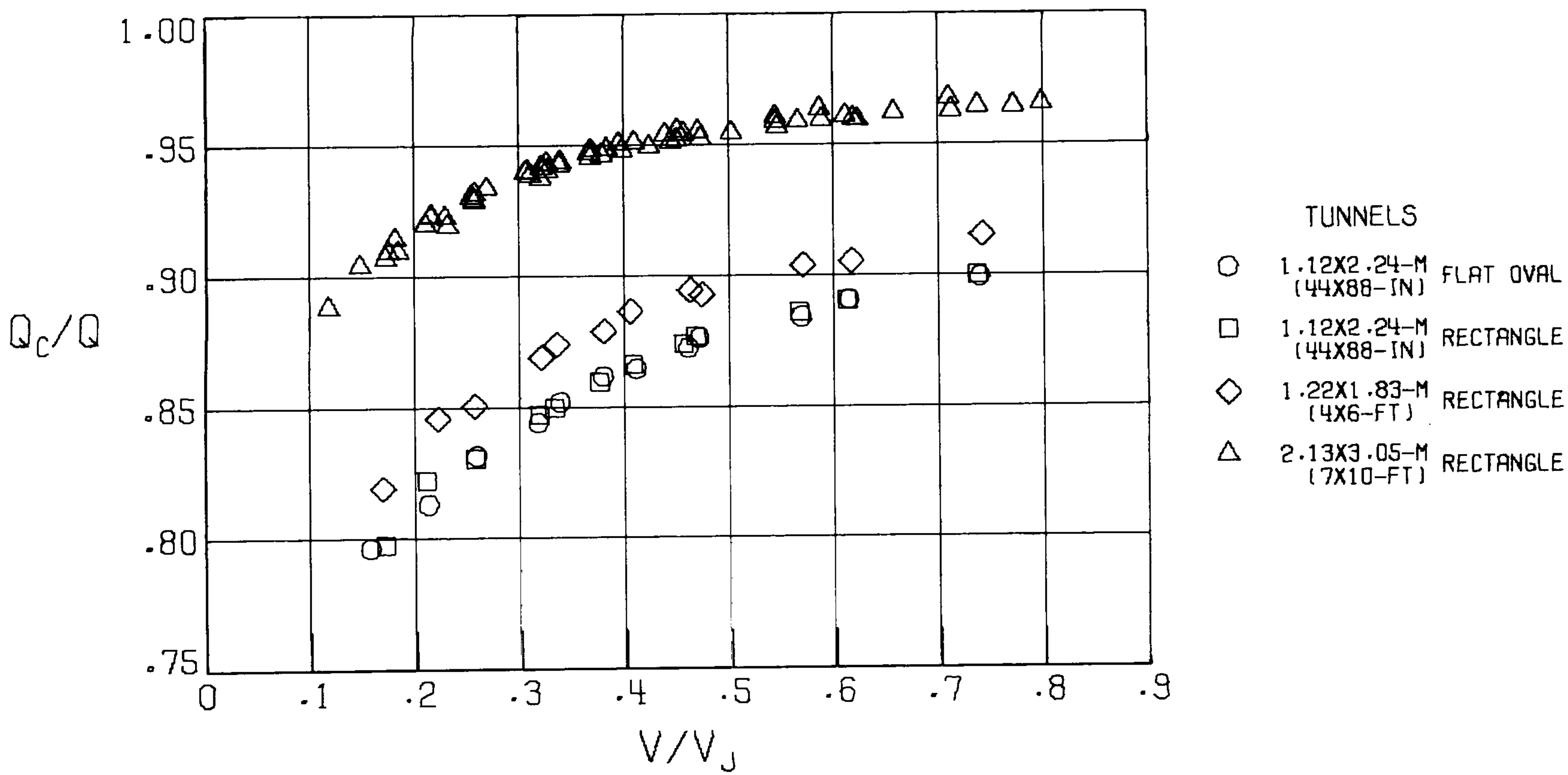

(a) $\alpha = -5^{\circ}$.

Figure 37.- Wall-induced values of q_c/q in the corrected data from the fan-in-wing model as a function of V/V_j in several different wind tunnels.

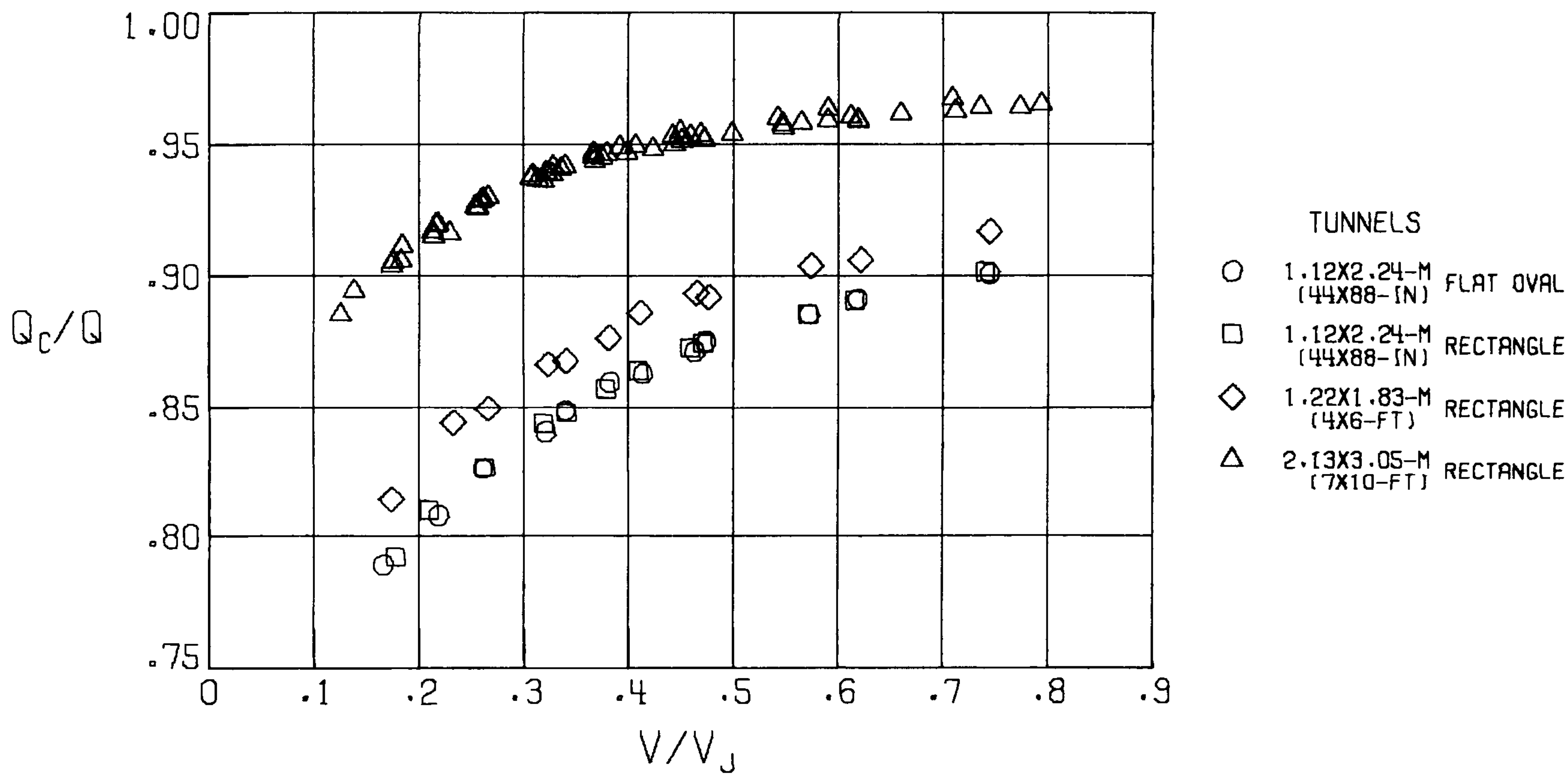

(b) $\alpha = 0^{\circ}$.

Figure 37.- Continued.

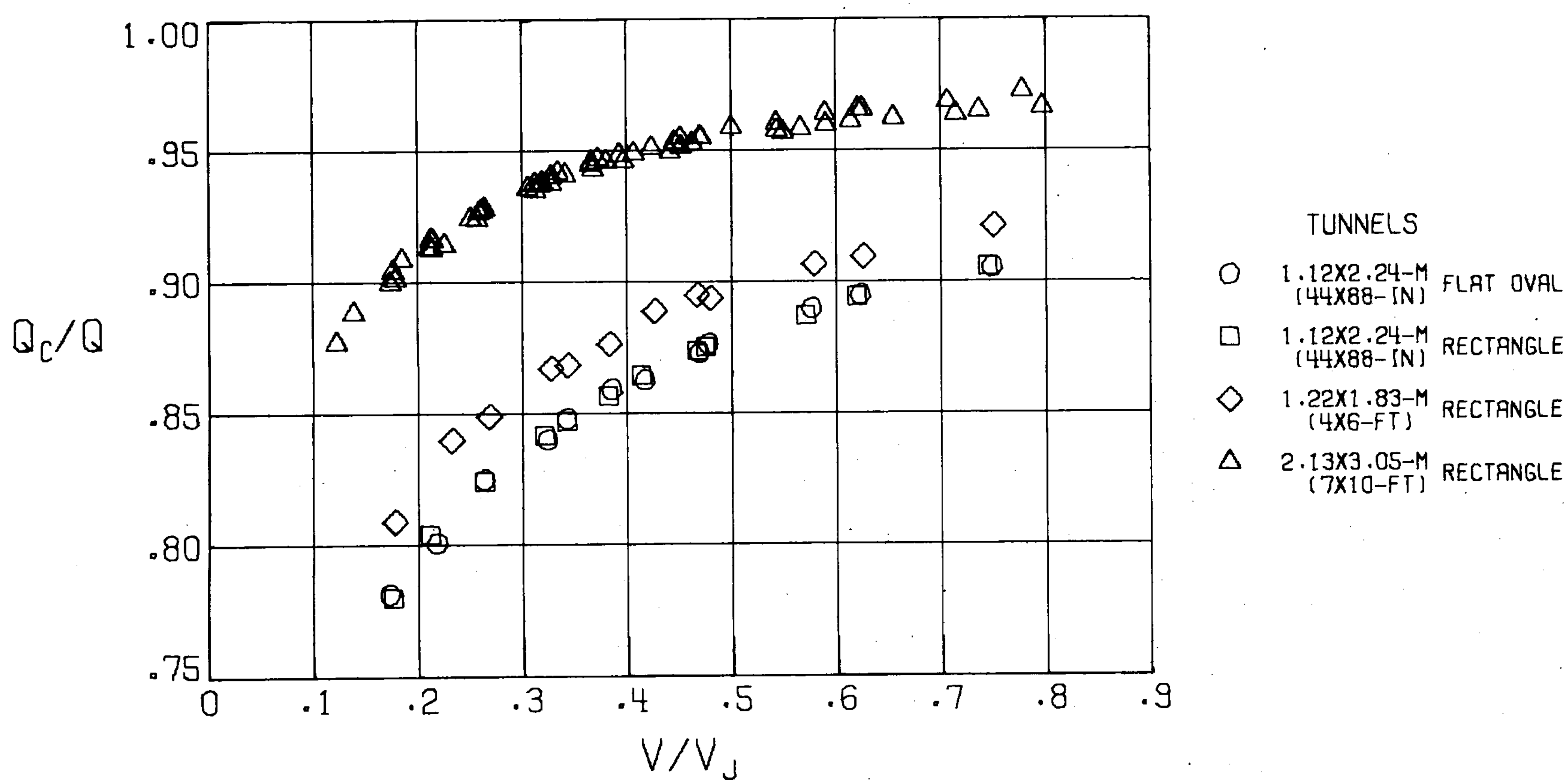

(c) $\alpha = 5^{\circ}$.

Figure 37.- Continued.

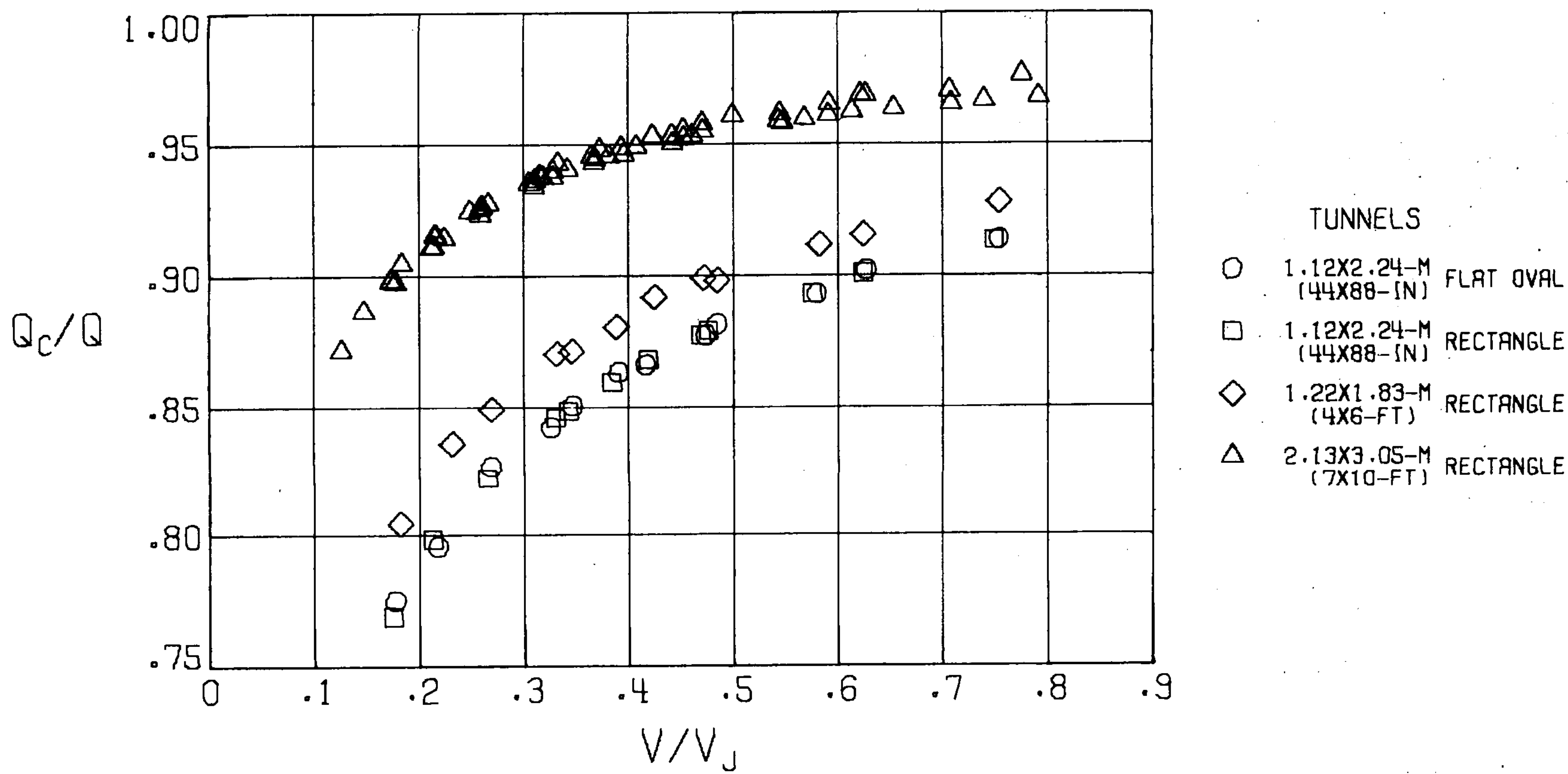

(d) $\alpha = 10^{\circ}$.

Figure 37.- Continued.

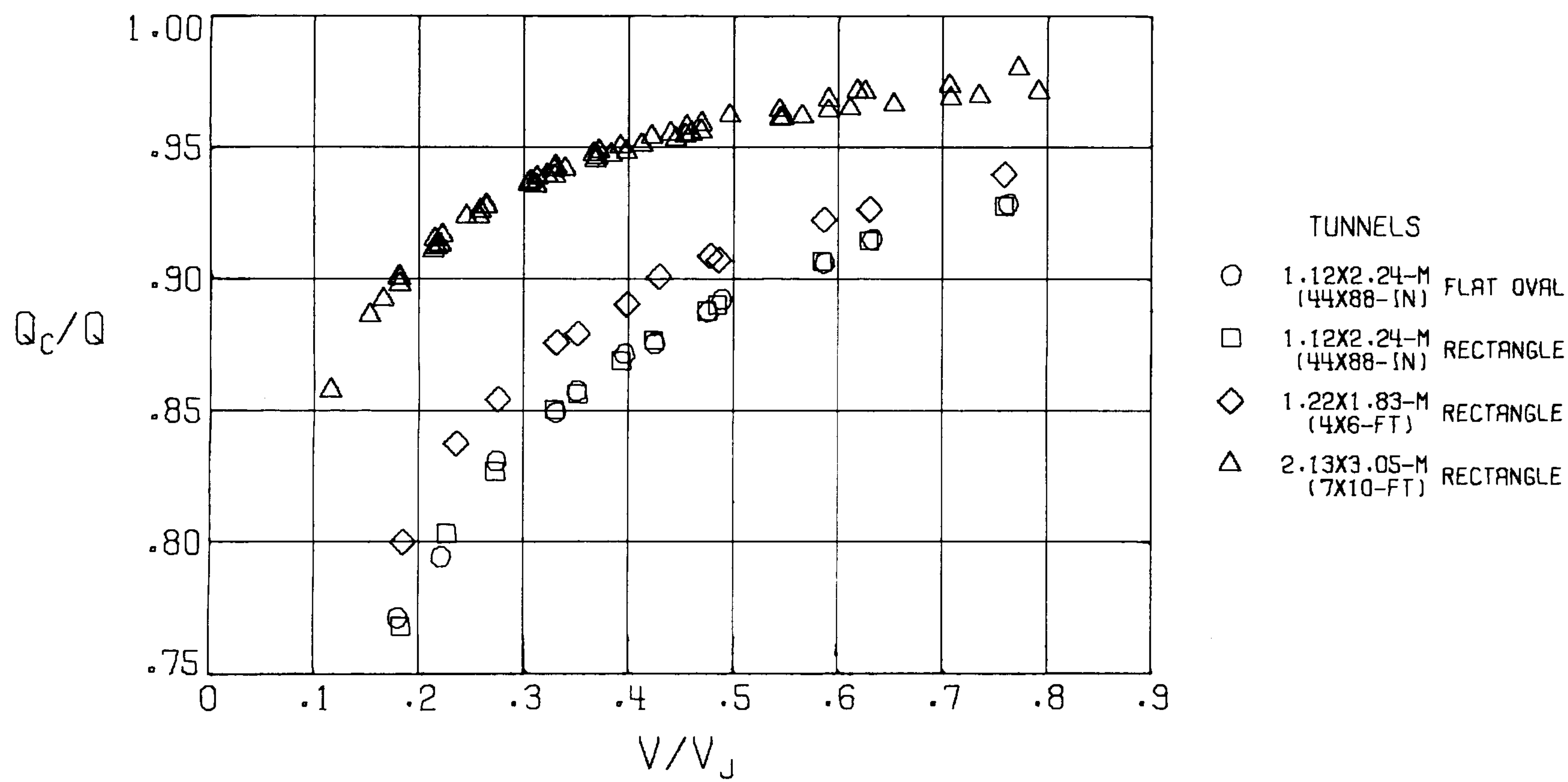

(e) $\alpha = 16^{o}$.

Figure 37.- Concluded.

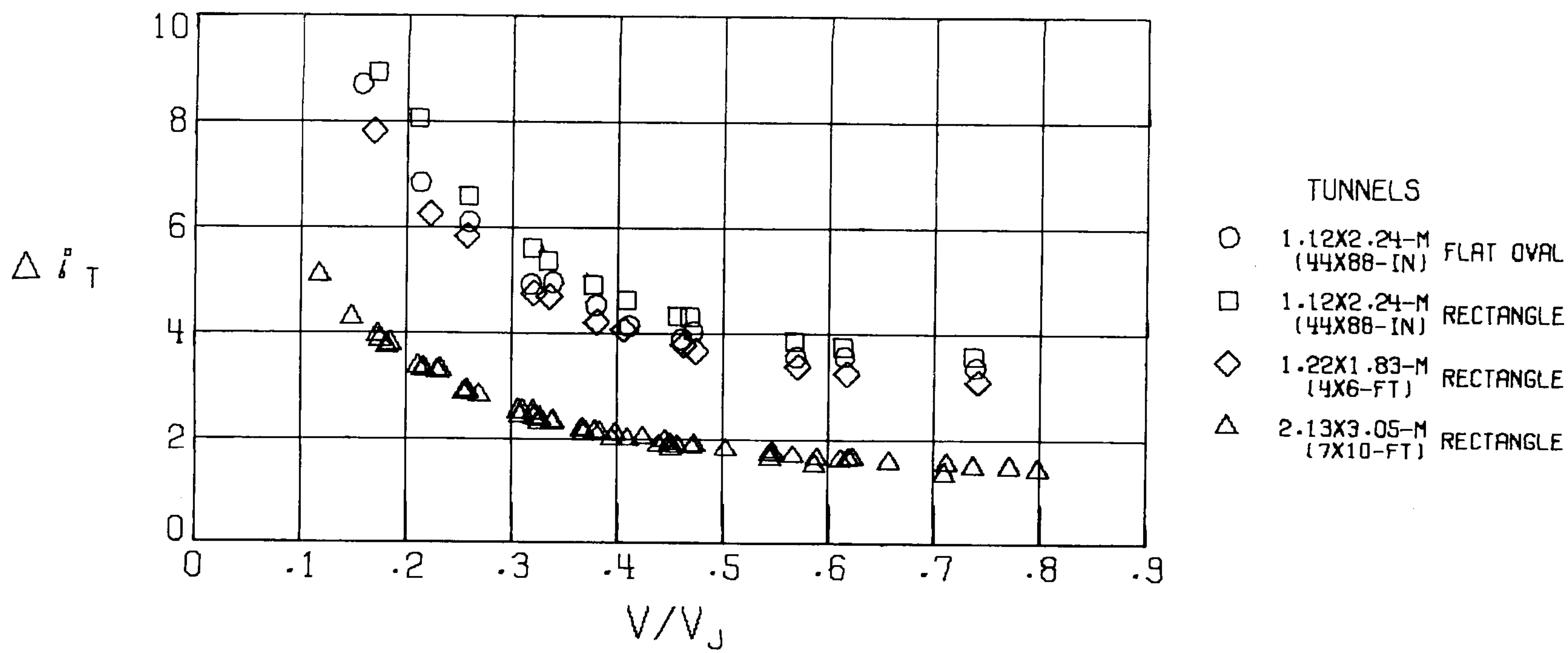

(a) $\alpha = -5^{\circ}$.

Figure 38.- Wall-induced tail incidence Δi_T in the corrected data from the fan-in-wing model as a function of V/V_j in several different wind tunnels.

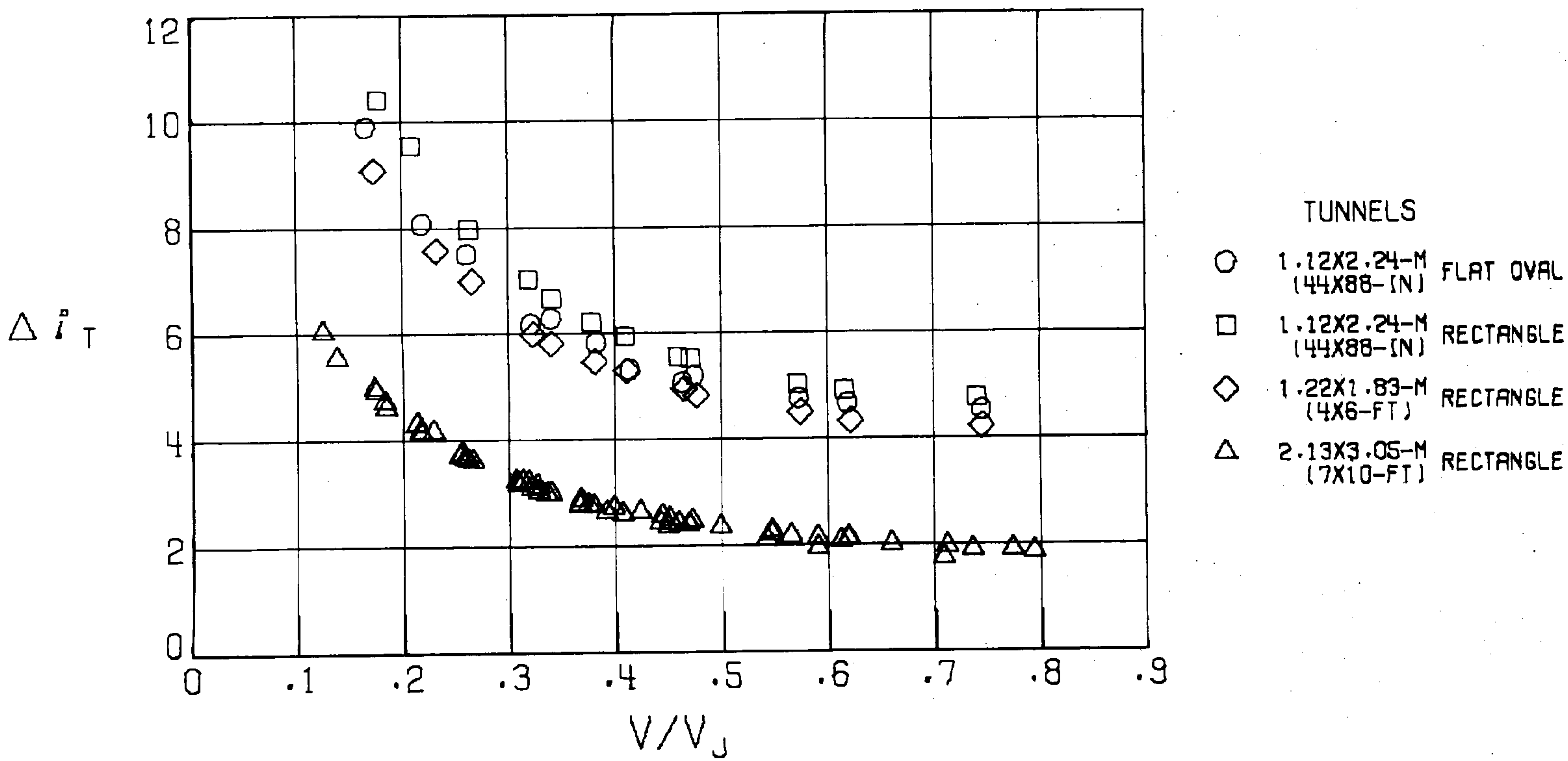

(b) $\alpha = 0^{o}$.

Figure 38.- Continued.

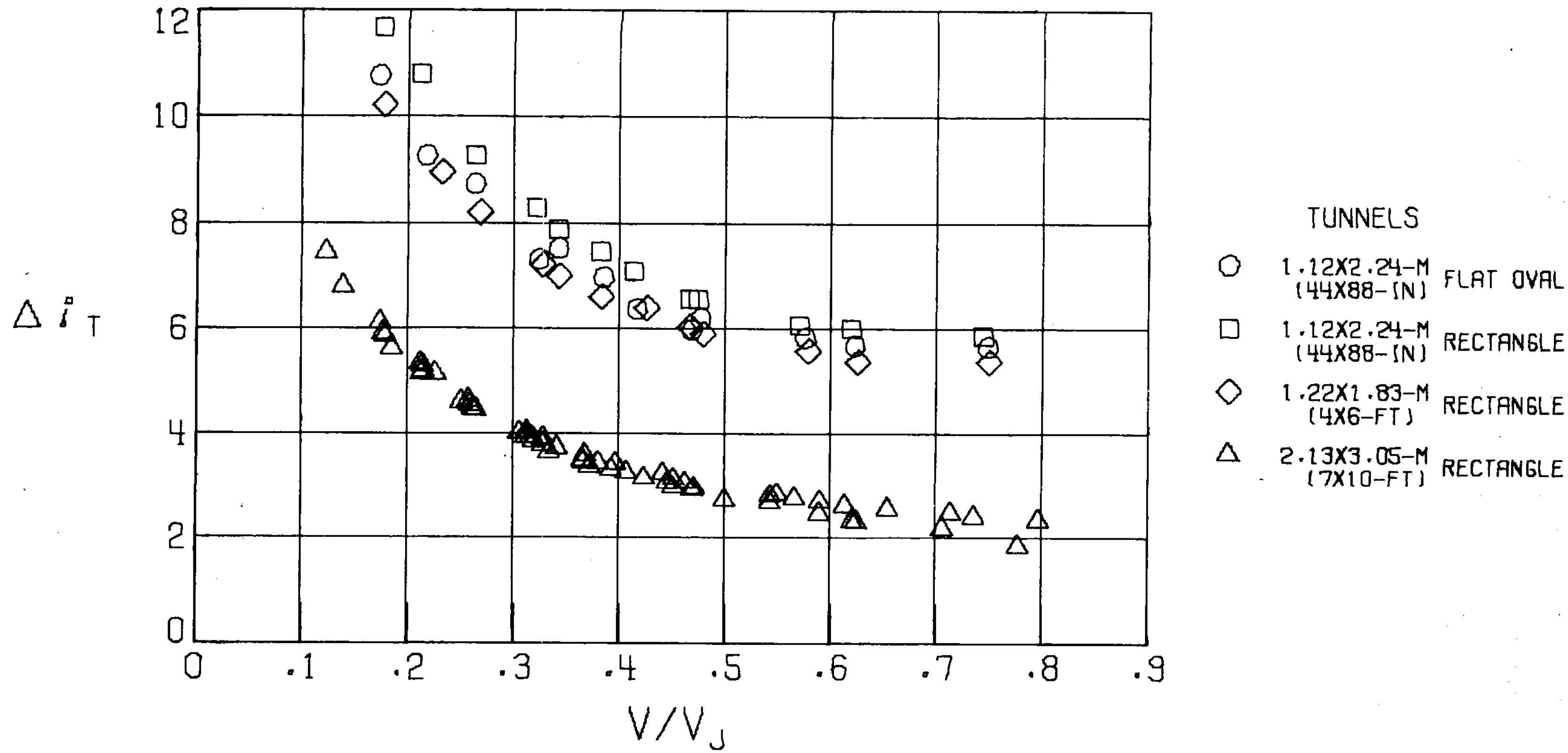

(c) $\alpha = 5^{o}$.

Figure 38.- Continued.

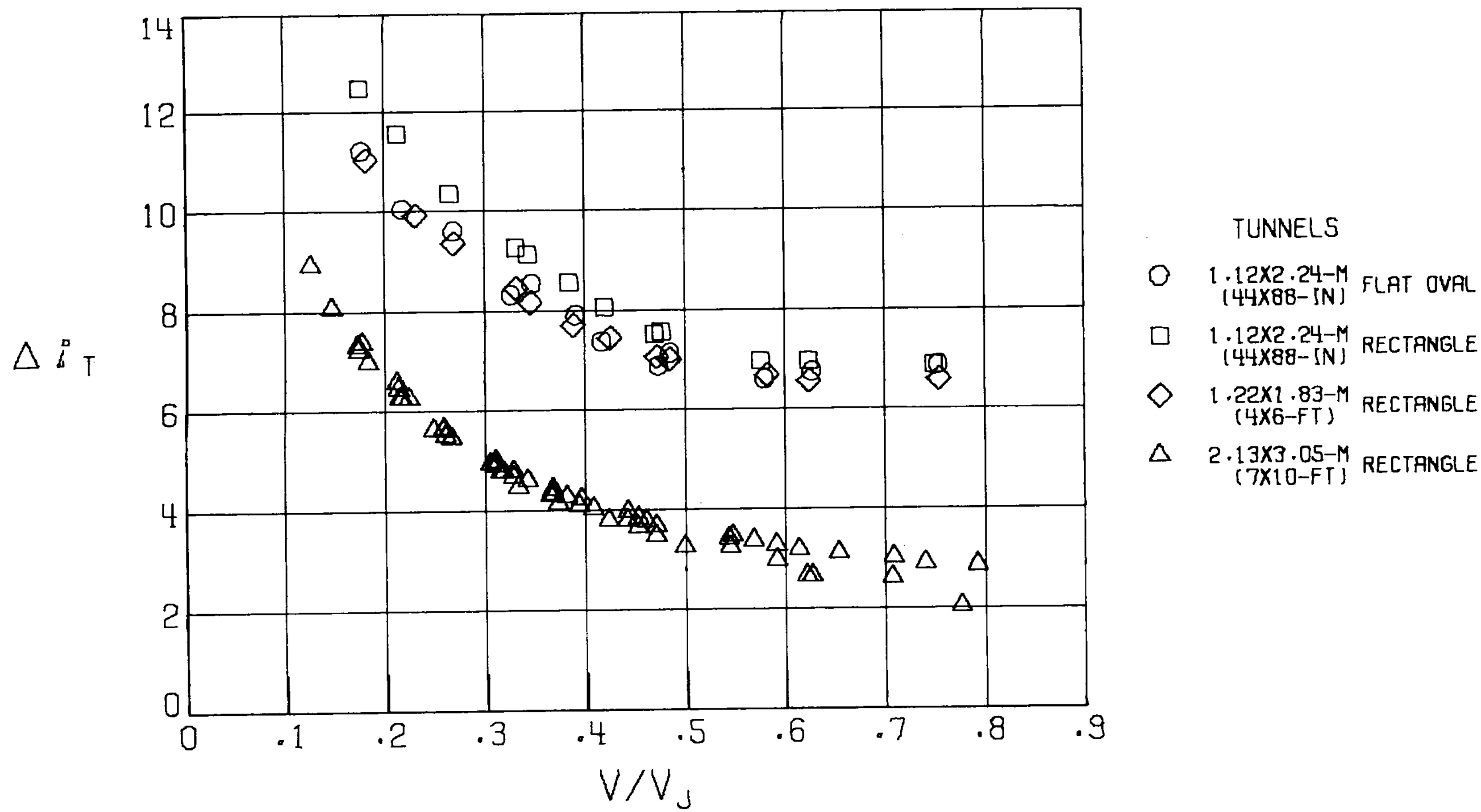

(d) $\alpha = 10^{o}$.

Figure 38.- Continued.

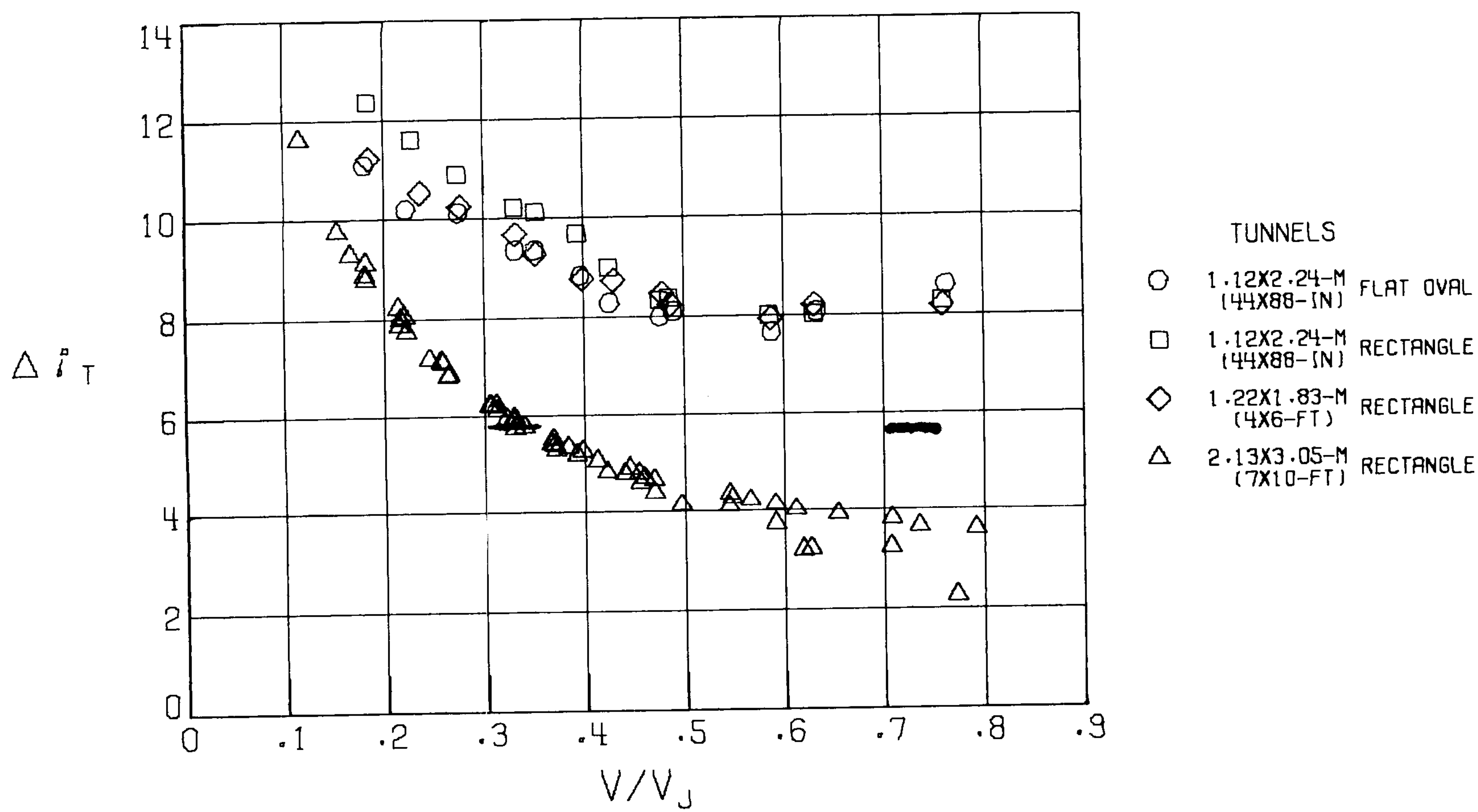

(e) $\alpha = 16^o$.

Figure 38.- Concluded.

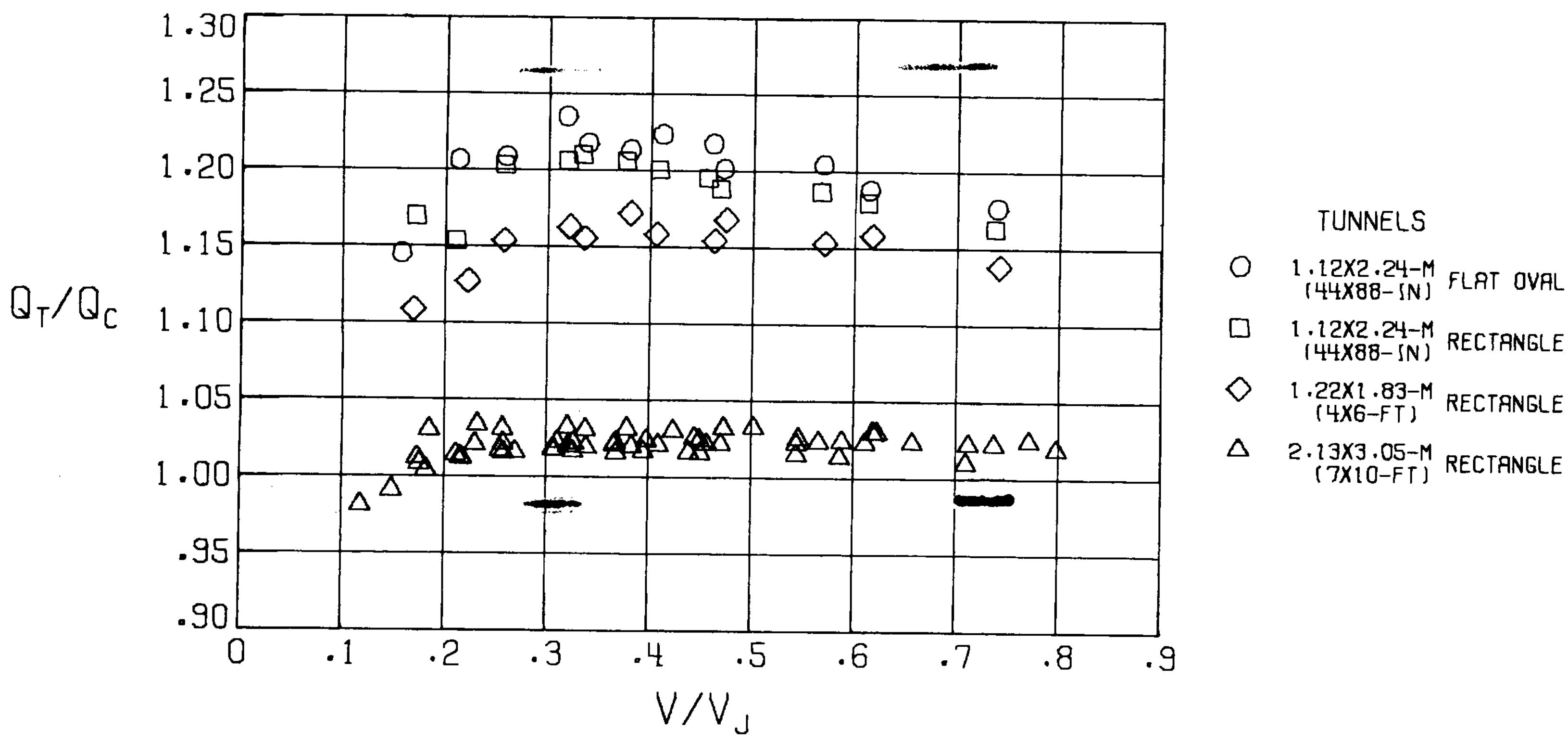

(a) $\alpha = -5^{o}$.

Figure 39.- Wall-induced values of q_T/q_c in the corrected data from the fan-in-wing model as a function of V/V_j in several different wind tunnels.

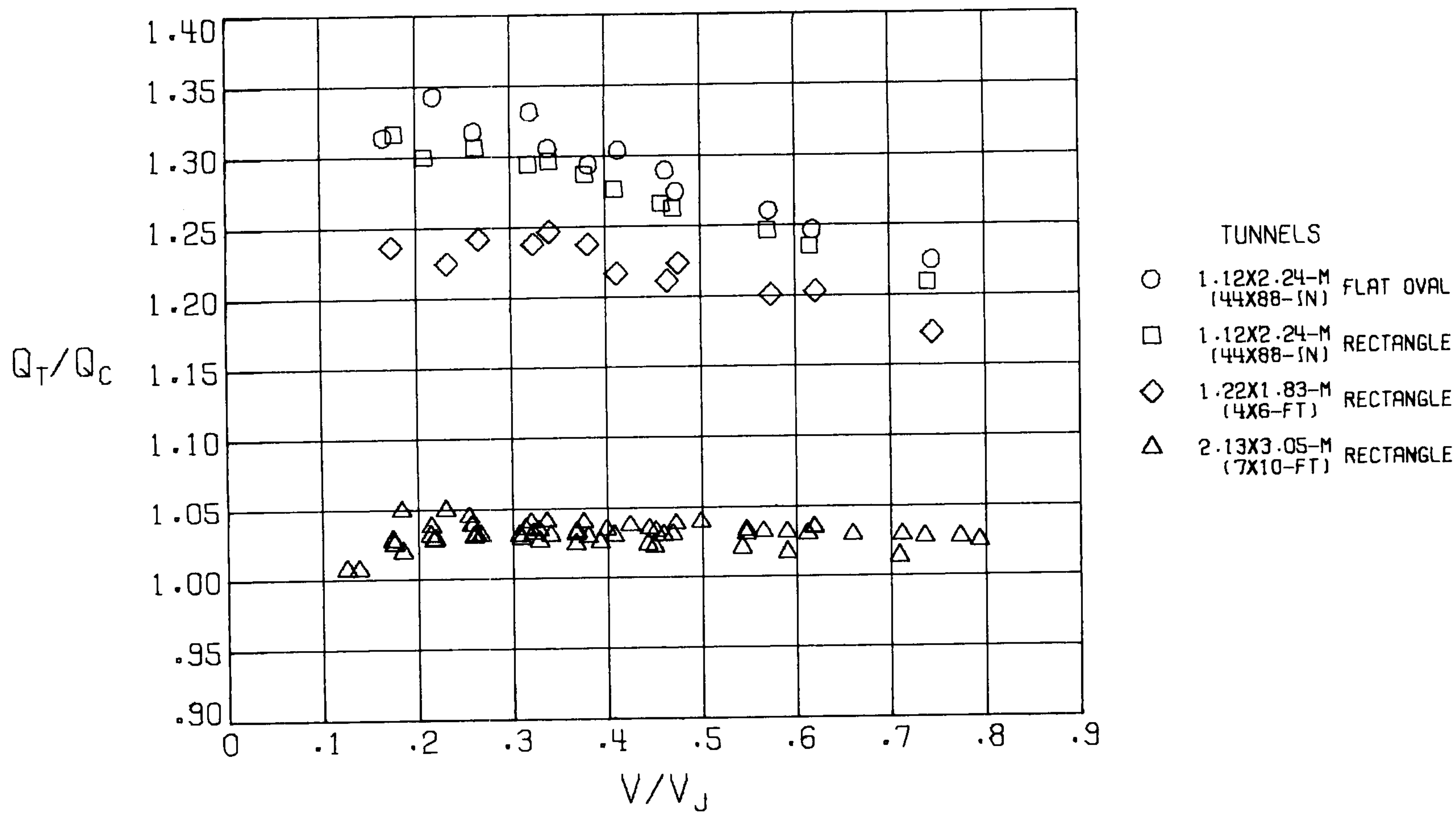

(b) $\alpha = 0^{o}$.

Figure 39.- Continued.

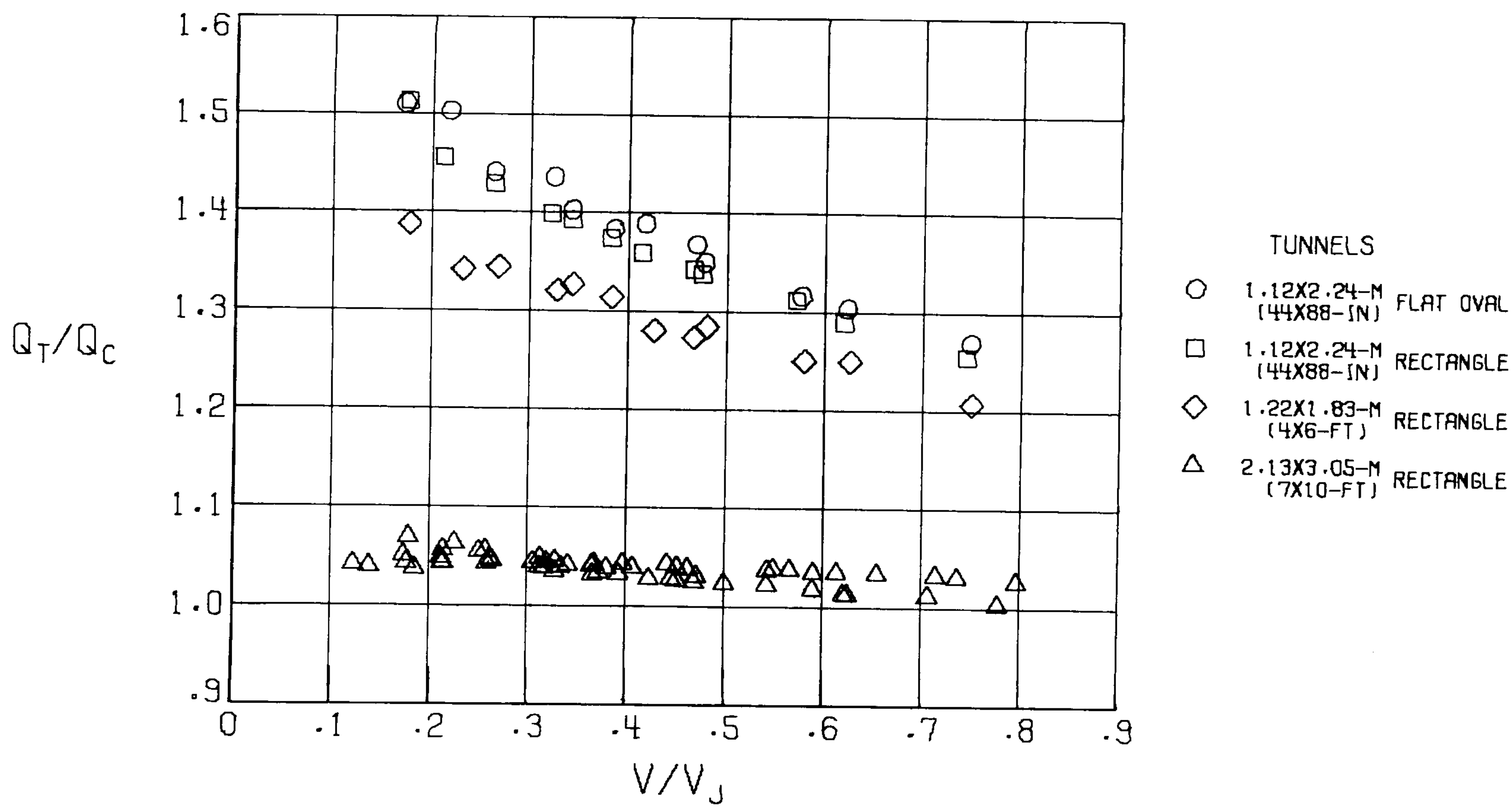

(c) $\alpha = 5^{\circ}$.

Figure 39.- Continued.

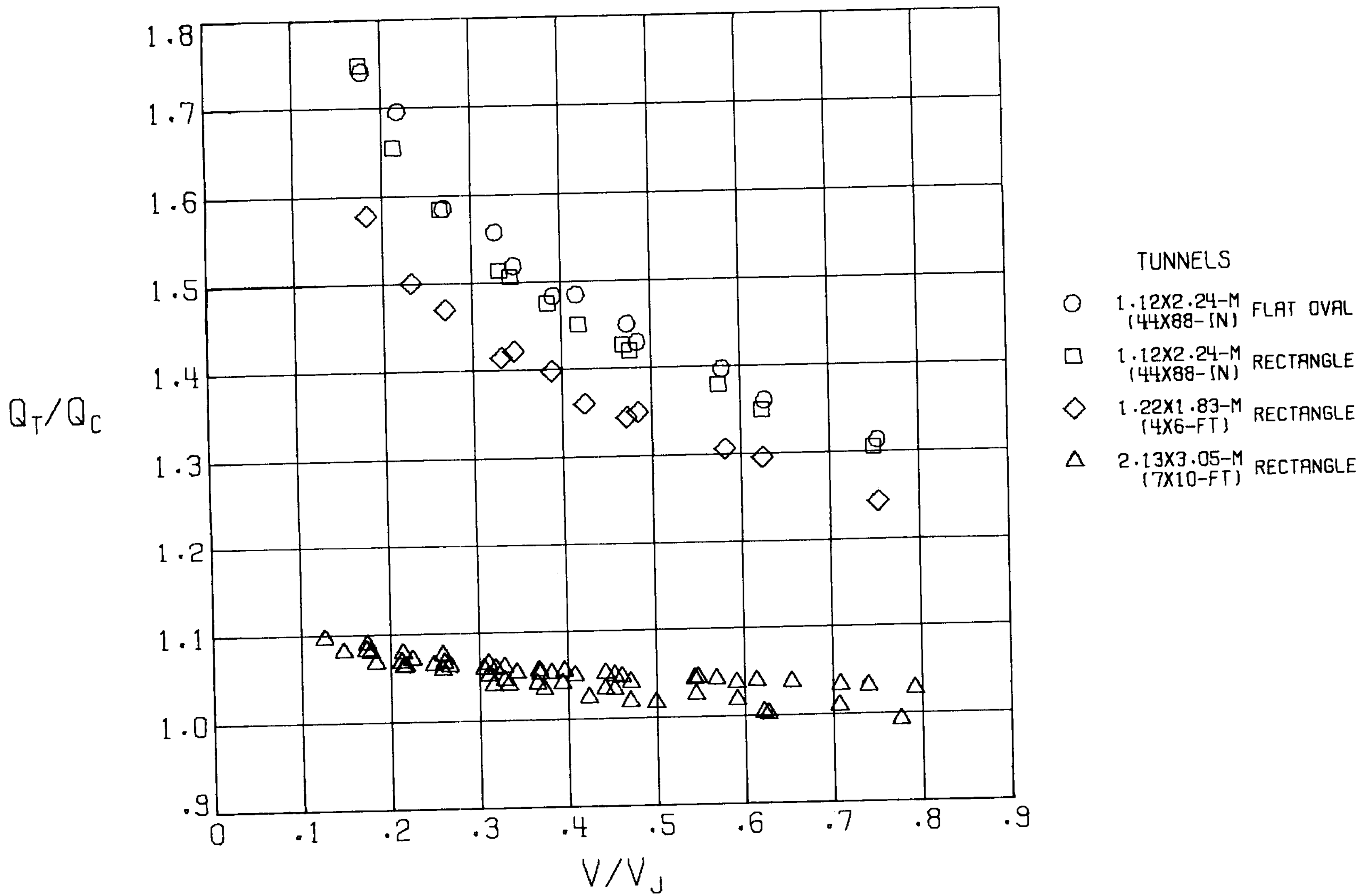

(d) $\alpha = 10^{\circ}$.

Figure 39.- Continued.

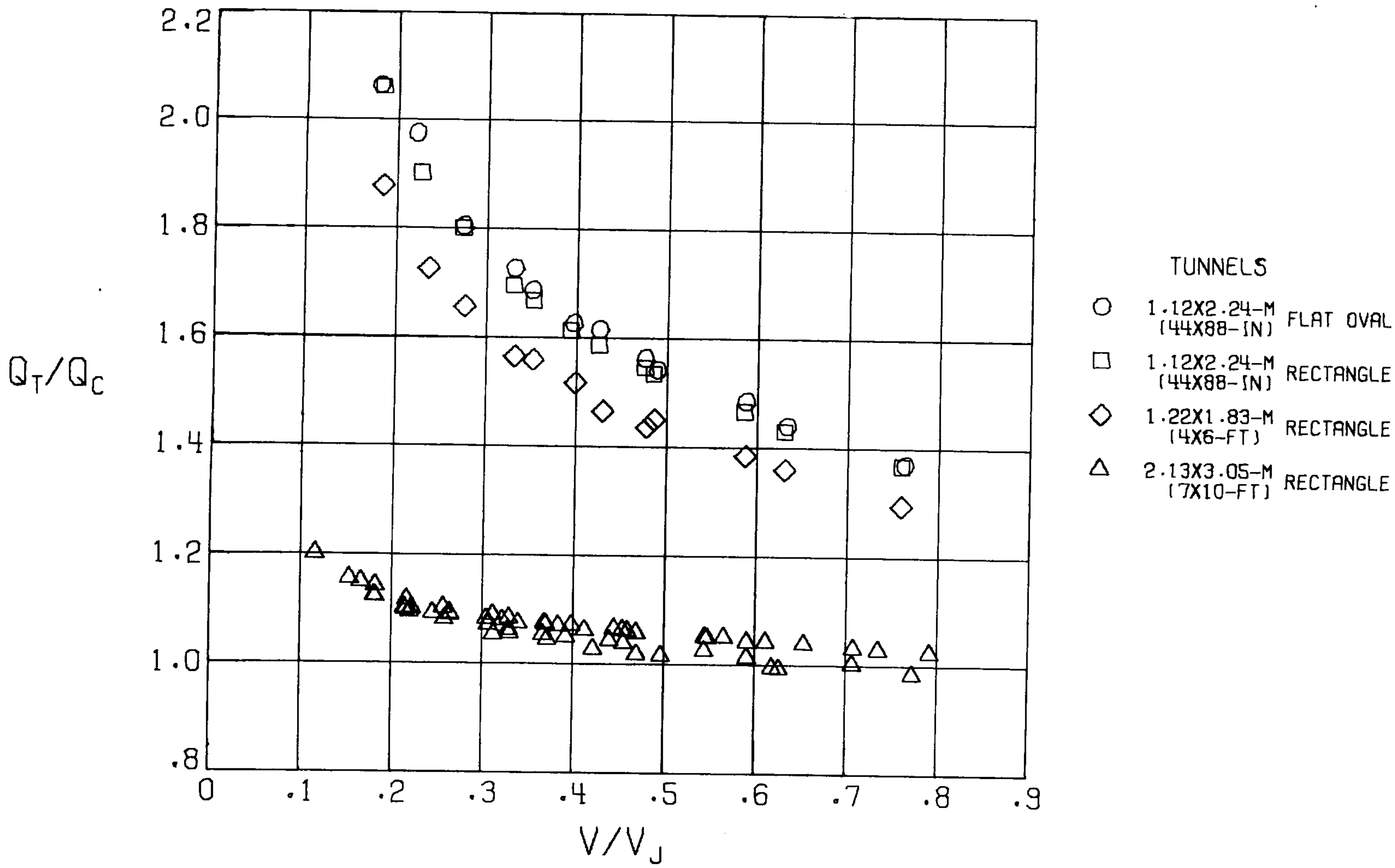

(e) $\alpha = 16^o$.

Figure 39.- Concluded.

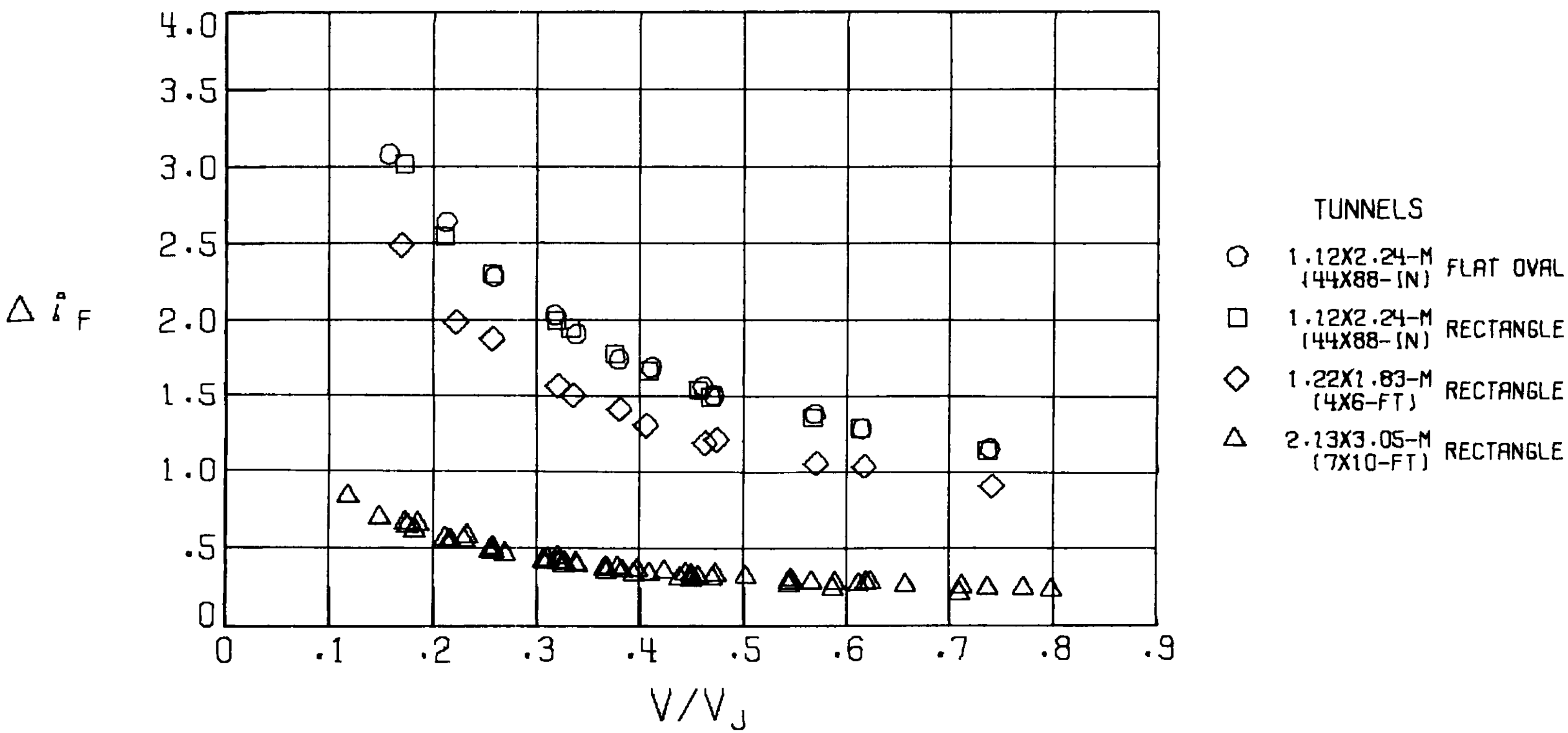

(a) $\alpha = -5^{o}$.

Figure 40.- Wall-induced fan incidence Δi_F in the corrected data from the fan-in-wing model as a function of V/V_j in several different wind tunnels.

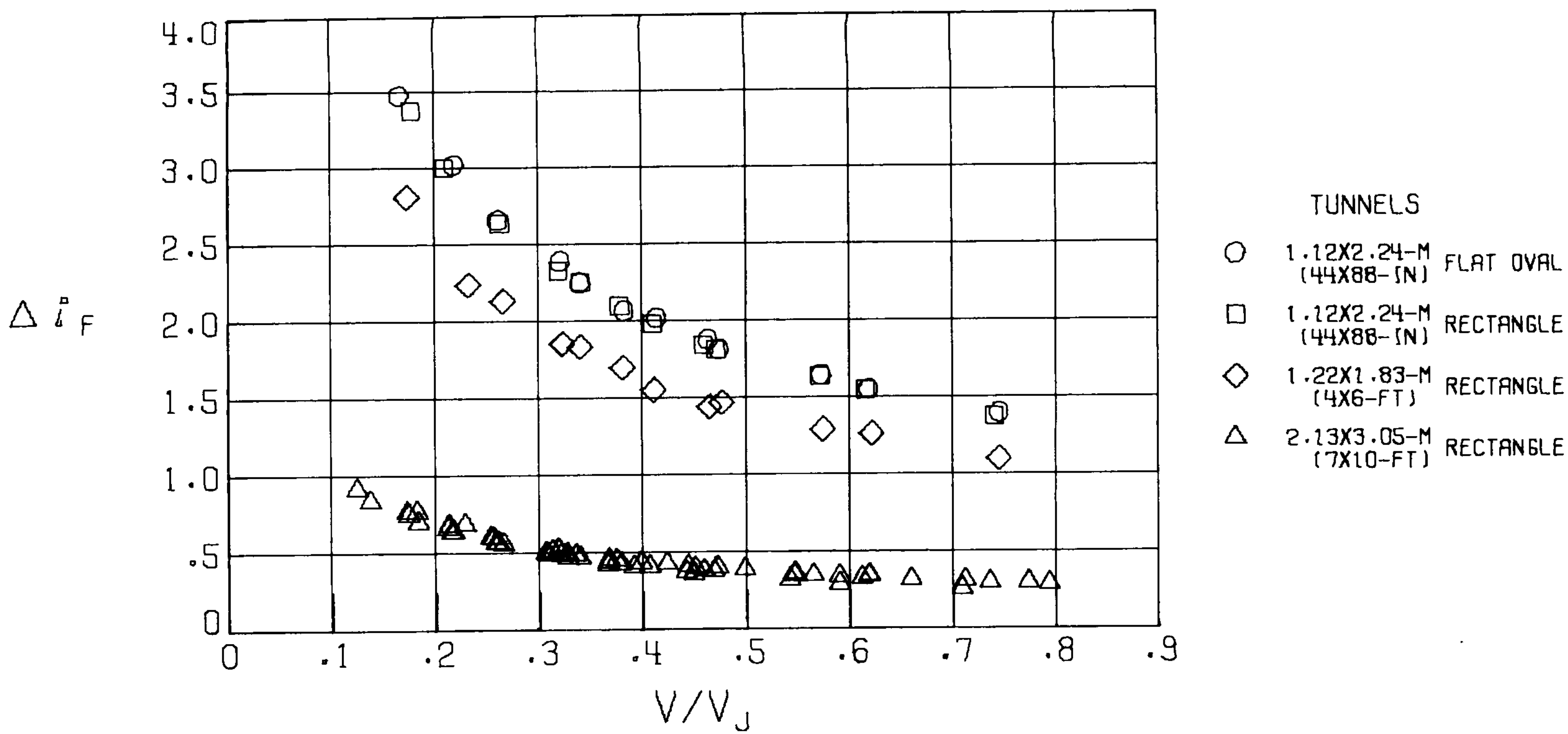

(b) $\alpha = 0^{o}$.

Figure 40.- Continued.

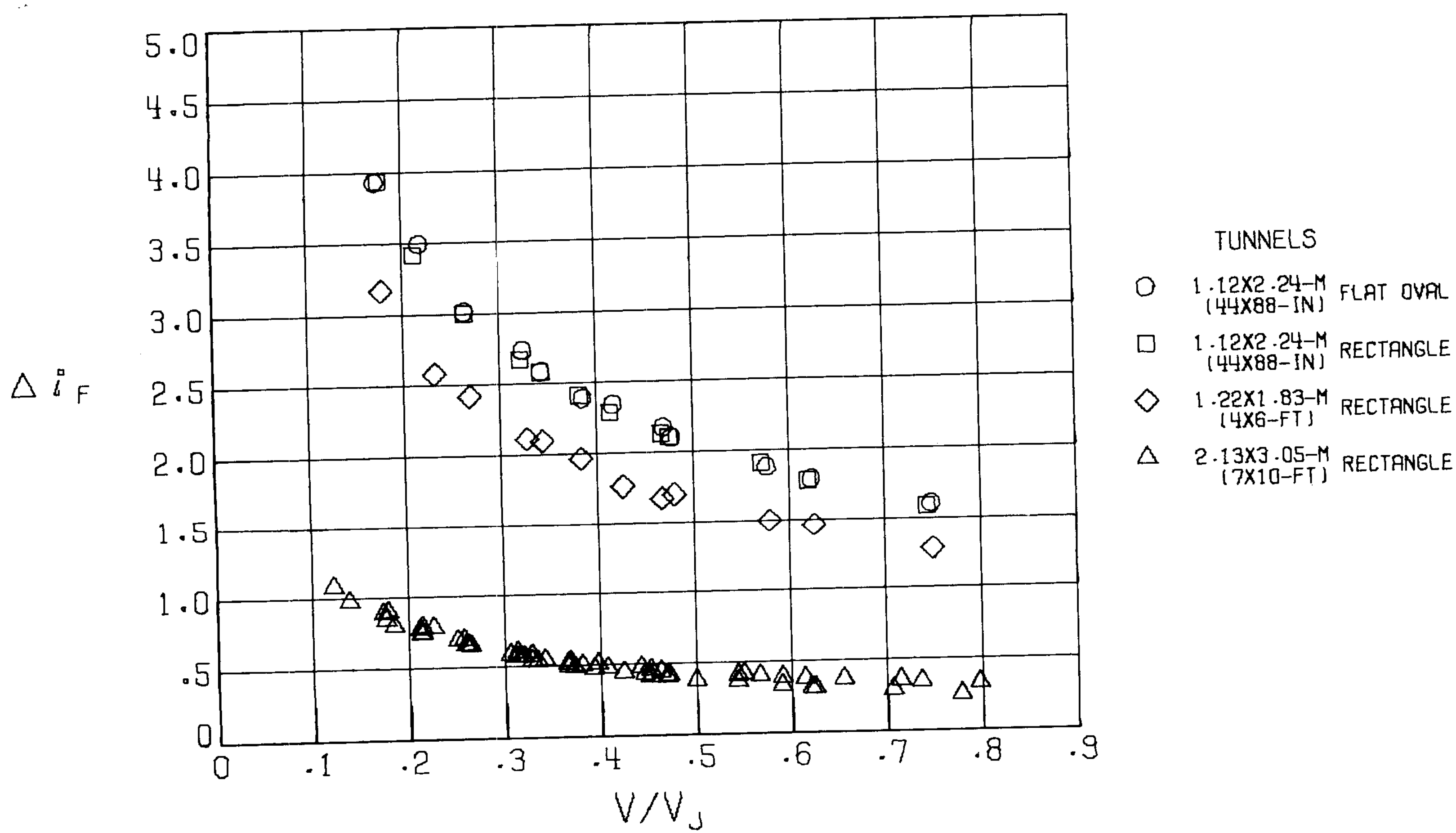

(c) $\alpha = 5^{\circ}$.

Figure 40.- Continued.

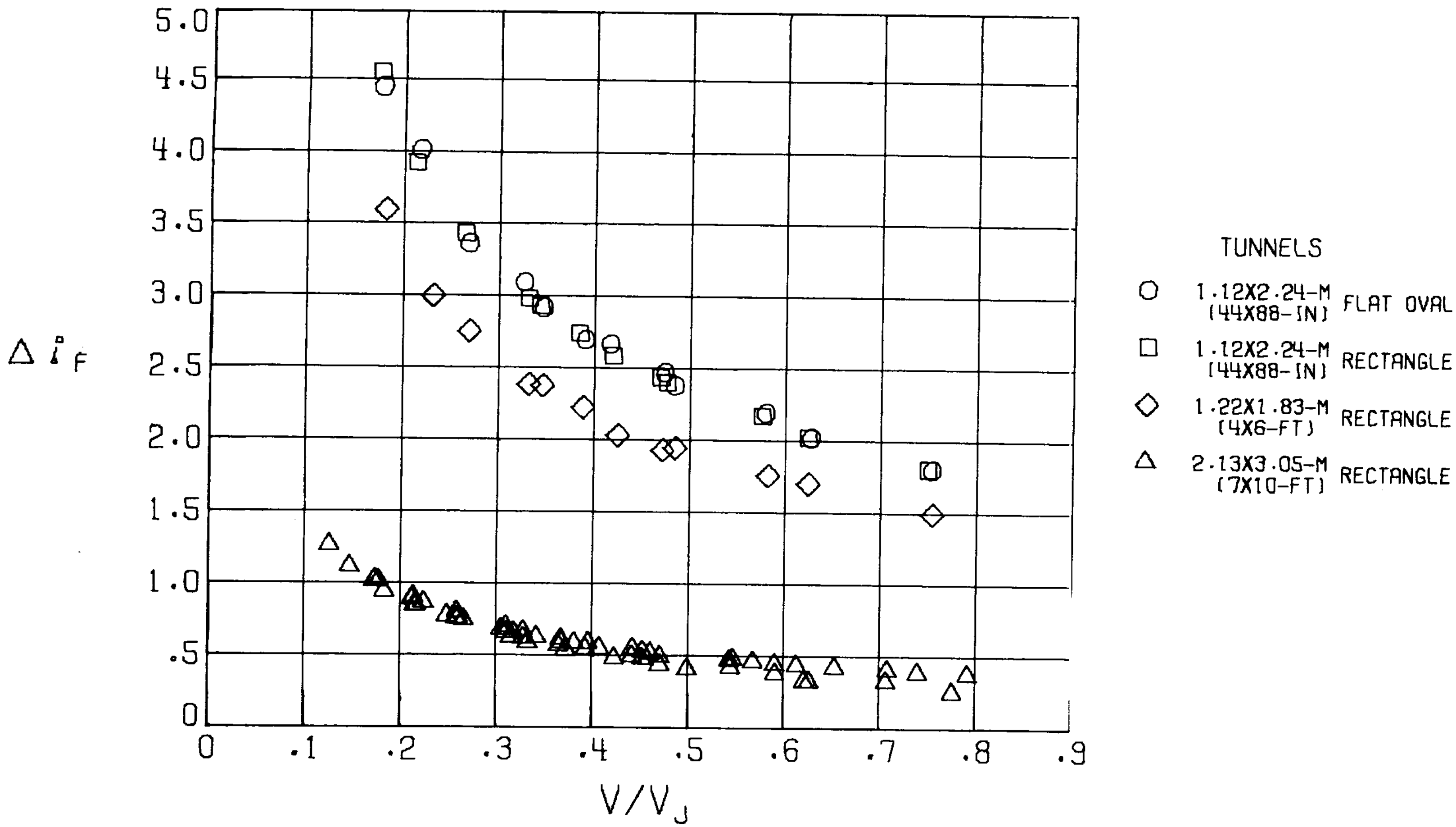

(d) $\alpha = 10^{\circ}$.

Figure 40.- Continued.

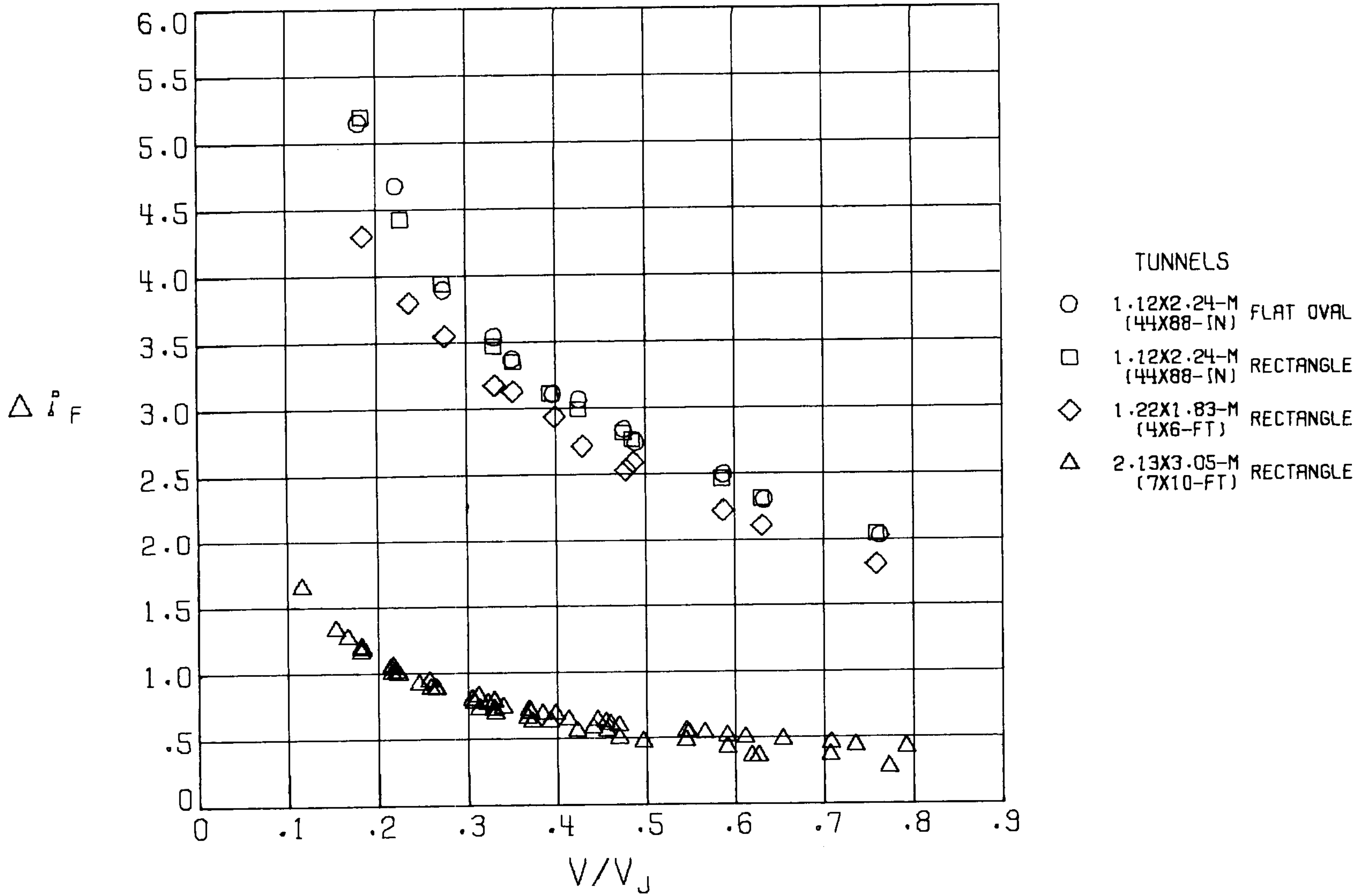

(e) $\alpha = 16^{o}$.

Figure 40.- Concluded.

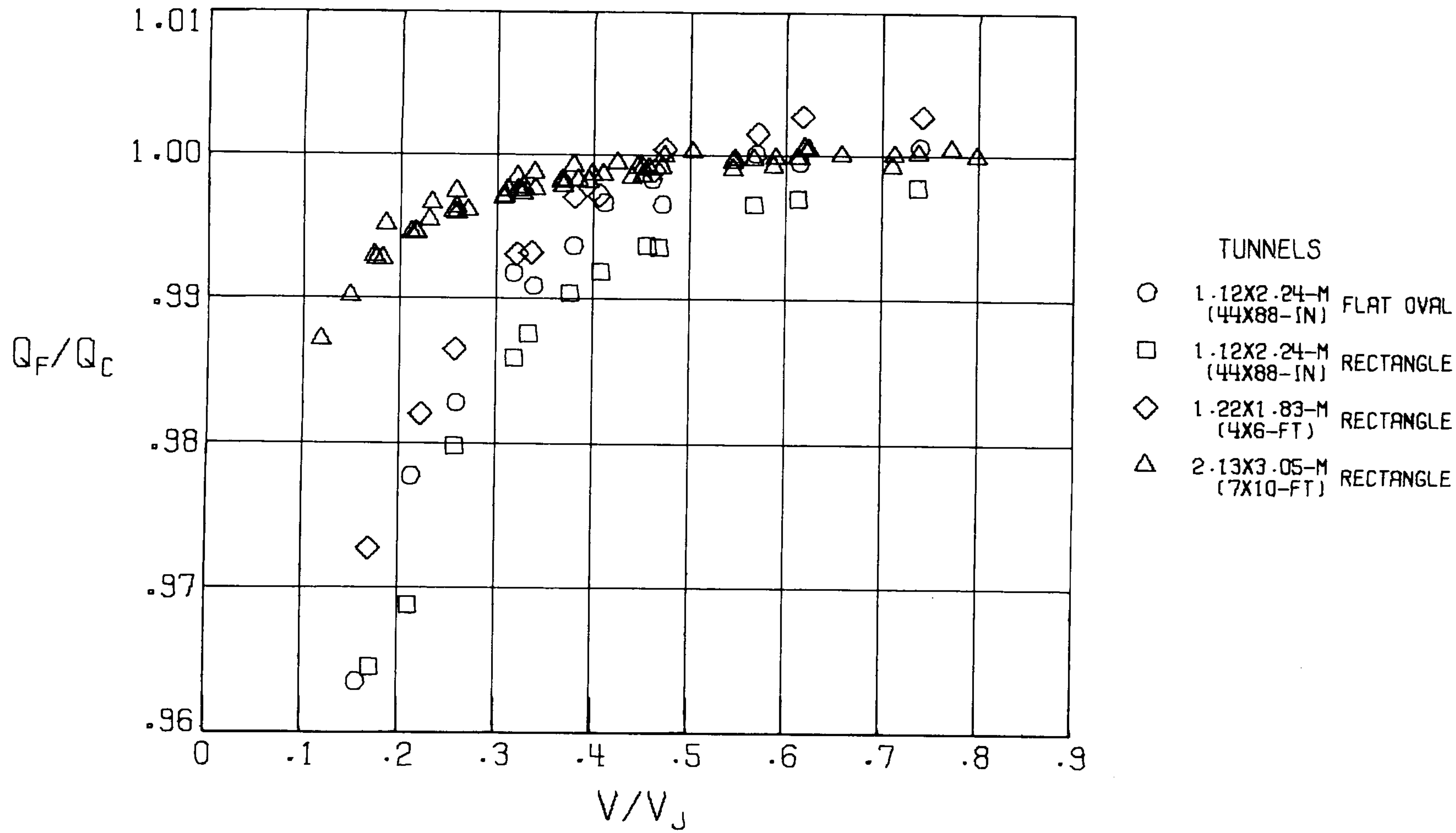

(a) $\alpha = -5^{\circ}$.

Figure 41.- Wall-induced values of q_F/q_c in the corrected data from the fan-in-wing model as a function of V/V_j in several different wind tunnels.

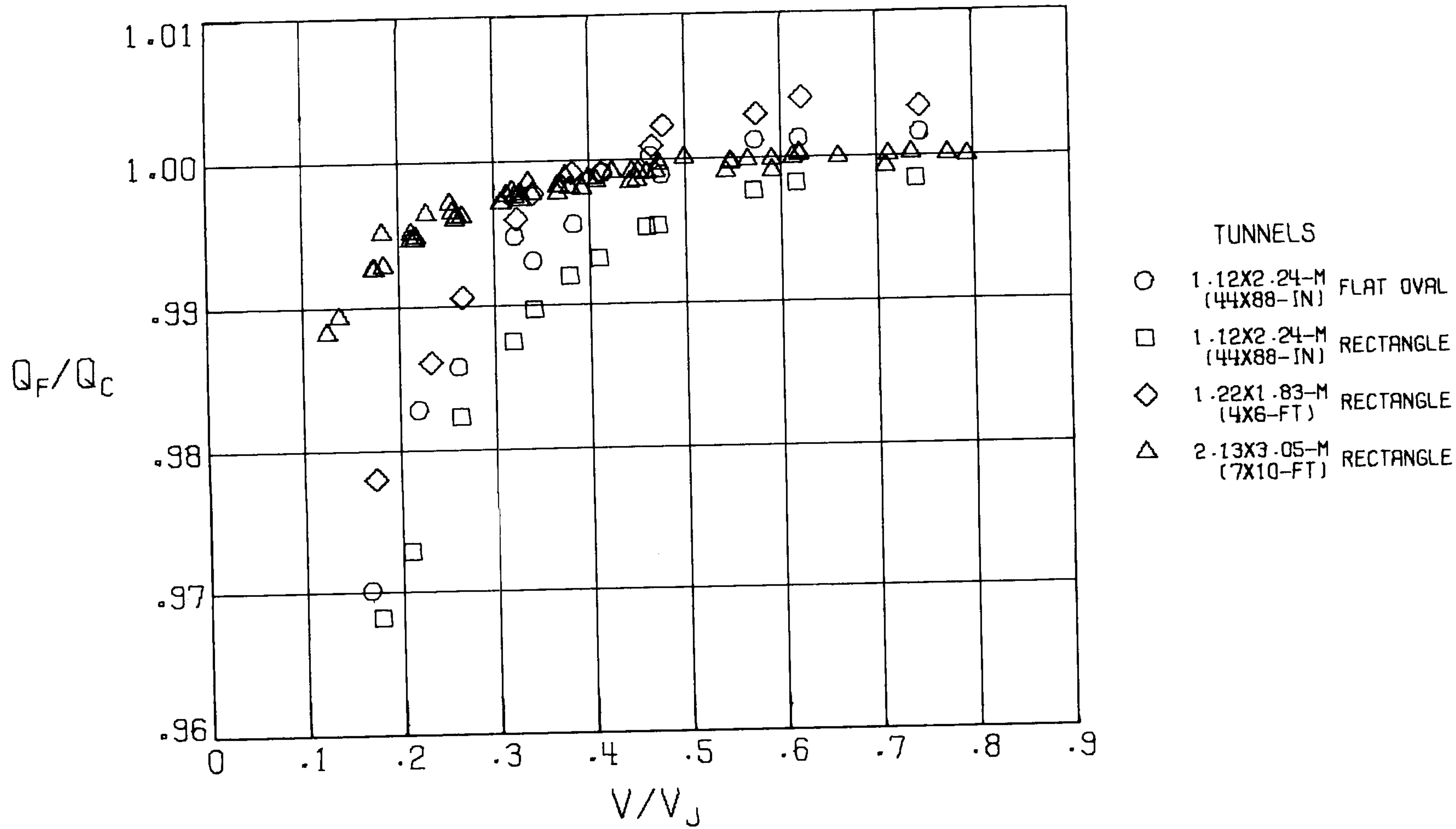

(b) $\alpha = 0^{o}$.

Figure 41.- Continued.

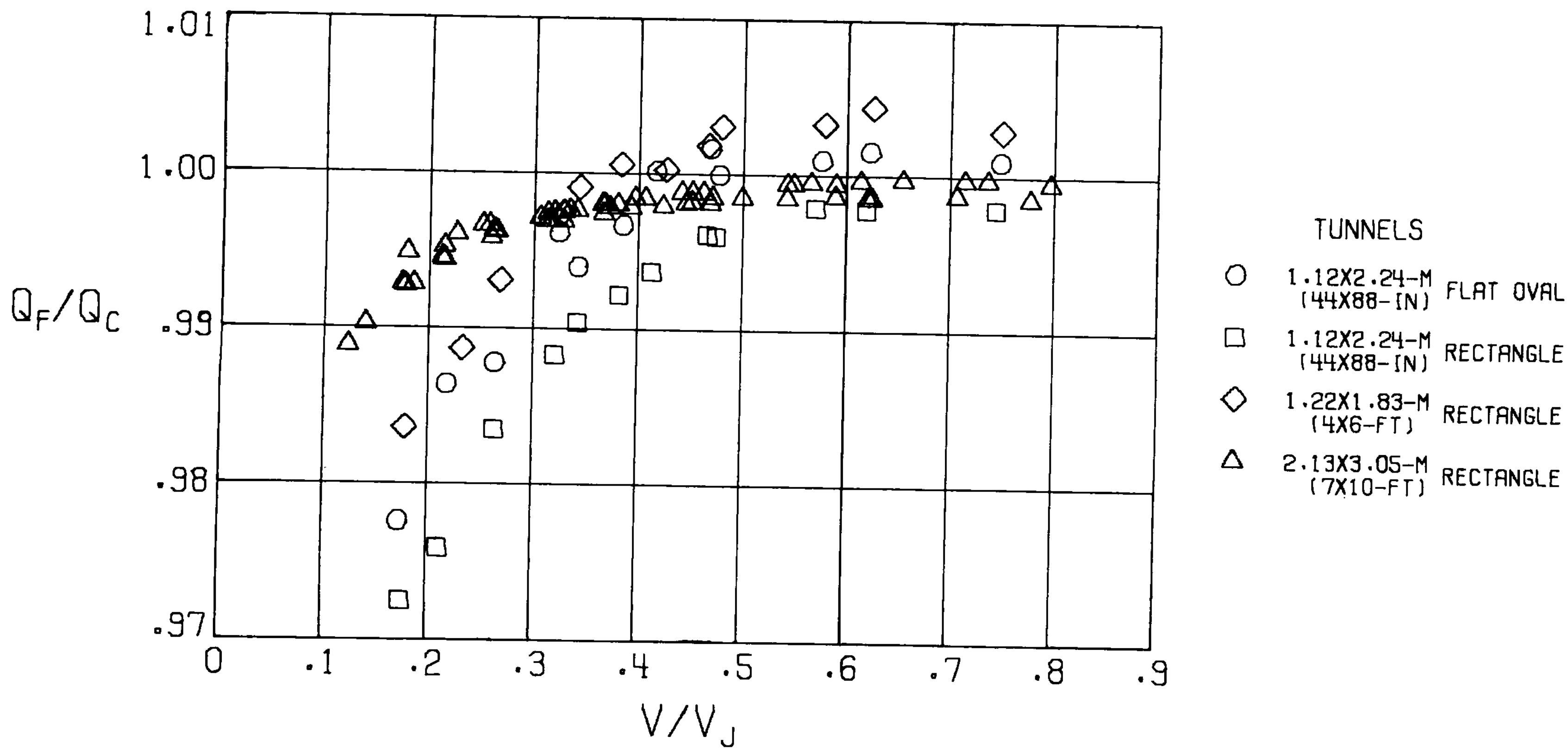

(c) $\alpha = 5^{\circ}$.

Figure 41.- Continued.

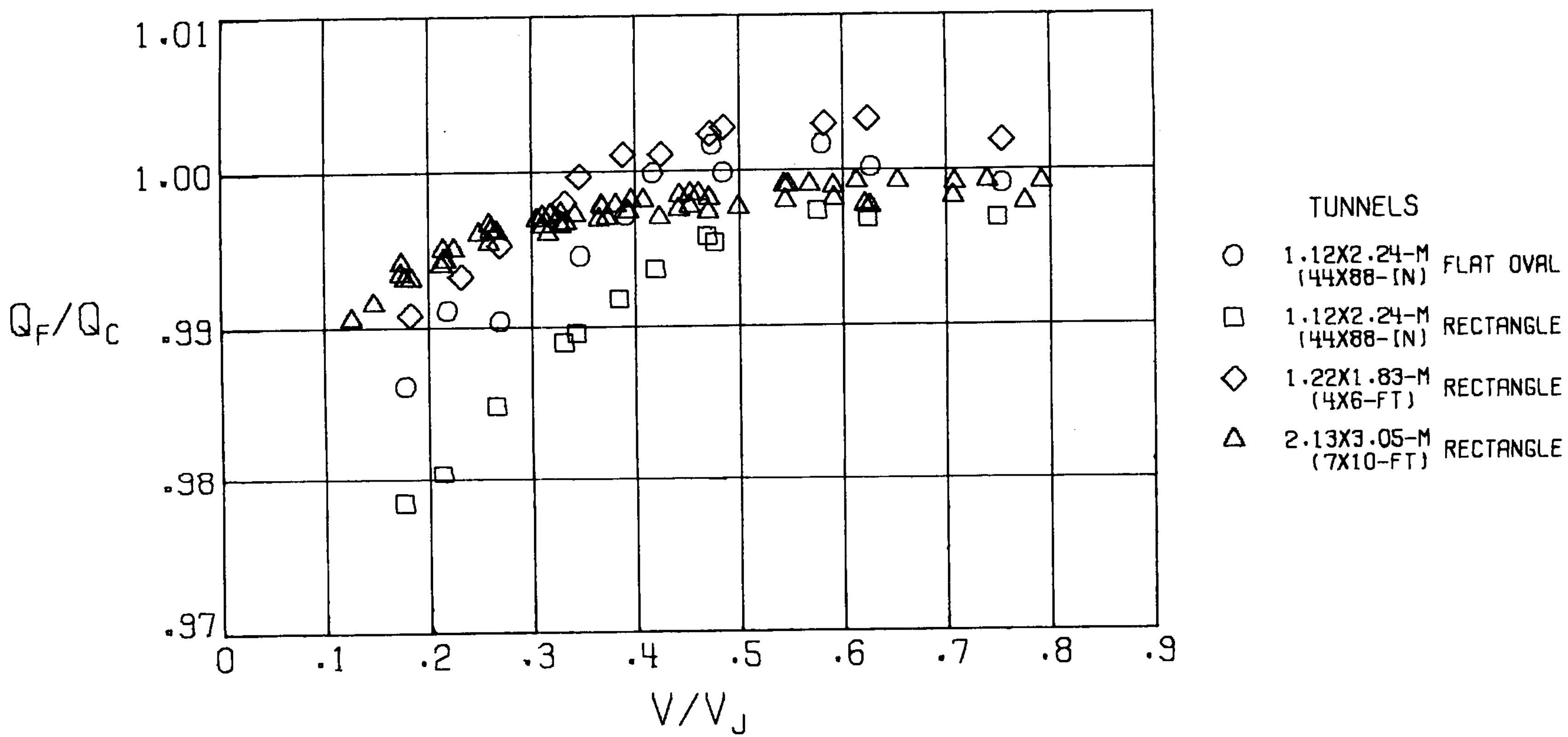

(d) $\alpha = 10^{\circ}$.

Figure 41.- Continued.

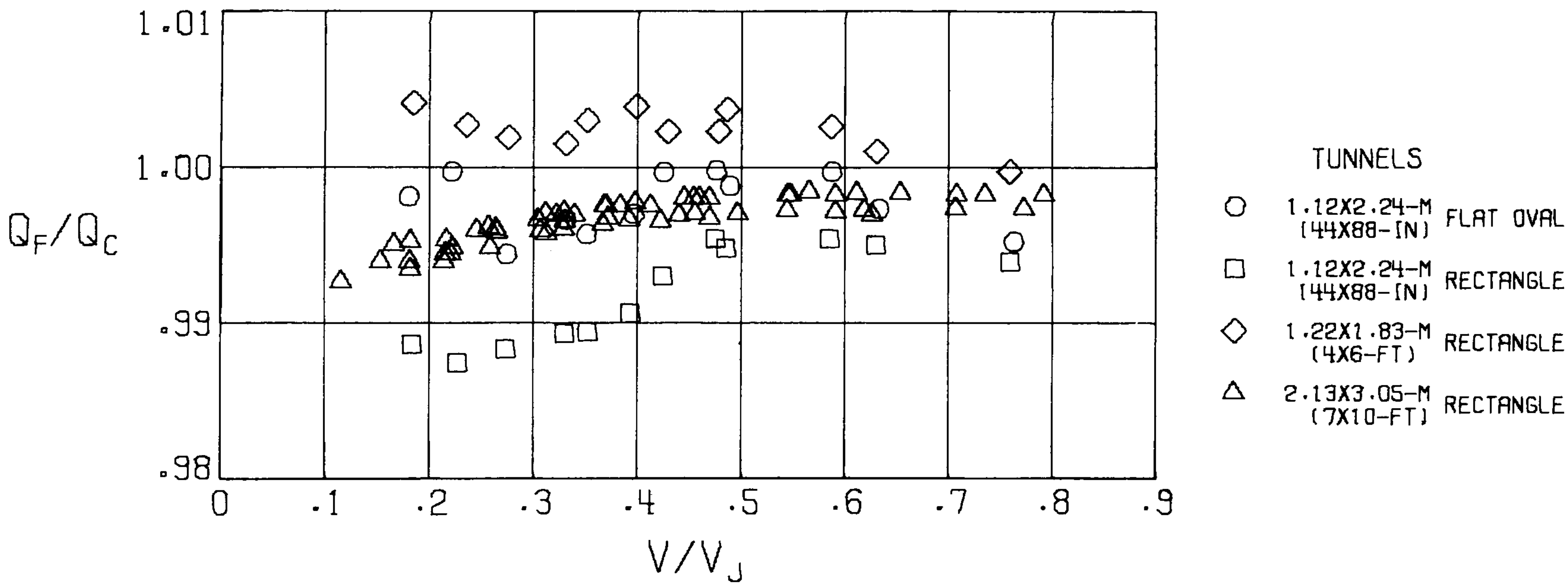

(e) $\alpha = 16^{\circ}$.

Figure 41.- Concluded.

NASA-Langley, 1974 L-9202